ISSN: 2687 - 4539

CHAOS

THEORY AND APPLICATIONS

IN APPLIED SCIENCES AND ENGINEERING

VOLUME 7, ISSUE 2, JULY 2025

AN INTERDISCIPLINARY JOURNAL OF NONLINEAR SCIENCE

ISSN: 2687 - 4539

CHAOS

THEORY AND APPLICATIONS

IN APPLIED SCIENCES AND ENGINEERING

Chaos Theory and Applications (CHTA)
Volume:7 – Issue No: 2 (July 2025)
https://dergipark.org.tr/en/pub/chaos/issue/91901

Editorial Advisory Board Members

Language Editors

Technical Coordinator

ISSN: 2687 - 4539

CHAOS

THEORY AND APPLICATIONS

IN APPLIED SCIENCES AND ENGINEERING

Chaos Theory and Applications (CHTA)
Volume: 7– Issue No:2 (July 2025)
https://dergipark.org.tr/en/pub/chaos/issue/91901

Contents

CHAOS
Theory and Applications
in Applied Sciences and Engineering

e-ISSN: 2687-4539
RESEARCH ARTICLE
Vol.7 / No.2 / 2025 / pp.99-106
https://doi.org/10.51537/chaos.1621182

On the Synchronization of Bidirectionally Coupled Nonidentical Systems via Output Feedback

Juan Gonzalo Barajas-Ramírez [α,1] **and Hugo G. Gonzalez-Hernandez** [*,2]

[α] Instituto Potosino de Investigación Científica y Tecnológica, División de Control y Sistemas Dinámicos, Camino a la Presa San José 2055, SLP, México,
[*] Tecnológico de Monterrey, Escuela de Ingeniería y Ciencias, Monterrey, C.P. 64849, N. L., México.

ABSTRACT

We investigate the synchronization of bidirectionally coupled nonidentical chaotic systems, addressing a critical challenge in nonlinear dynamics. Unlike traditional master-slave or unidirectional synchronization approaches, we propose a novel synchronization scheme based on output feedback linearization that ensures identical synchronization even in the presence of parameter mismatches and structural differences between systems. Our approach incorporates a nonlinear switching feedback law, which enhances stability and robustness in bidirectionally coupled configurations. We analyze the synchronization conditions using Lyapunov stability theory and illustrate our results through numerical simulations on well-known benchmark chaotic systems, including the Lorenz and Sprott systems. Our findings demonstrate that the proposed method can achieve stable synchronization in both identical and nonidentical configurations, even when the systems exhibit piecewise nonlinearities. These results extend the applicability of synchronization techniques to a broader class of chaotic systems and lay the groundwork for future research in networked dynamical systems.

KEYWORDS

Synchronization
Bidirectional coupling
Piece-wise linear systems
Relative degree

INTRODUCTION

Significant progress has been made since Pecora and Carroll introduced a synchronization scheme in their groundbreaking work (Pecora and Carroll 1990). In that study, they addressed the synchronization problem using a master-slave configuration, where a signal from the master system drives a slave system with an identical structure. Since its introduction, this methodology has seen broad adoption. For instance, Alvarez (1996) established formal synchronizability conditions and demonstrated their application using the Lorenz system (Lorenz 1963). Similarly, Zhu and Zhou (2008) employed this framework in the context of dual inverted pendulum systems. Research has also explored non-forced synchronization, including bifurcation patterns in non-identical Duffing oscillators (Vincent and Kenfack 2008). Over time, numerous synchronization strategies have emerged to address various aspects of the problem. One key challenge is achieving synchronization in chaotic systems without relying on a master-slave setup.

Manuscript received: 16 January 2025,
Revised: 28 March 2025,
Accepted: 1 April 2025.

[1] jgbarajas@ipicyt.edu.mx
[2] hgonz@tec.mx (**Corresponding author**)

Hong *et al.* (2001) presented an adaptive synchronization method in this context, and Sarasola *et al.* (2003) proposed a technique based on linear feedback coupling. A robust approach using sliding mode control was introduced by (Alvarez *et al.* 2010). More recently, the scope of synchronization has expanded to encompass complex networks (Duan *et al.* 2007), with notable examples including consensus and pinning strategies (Olfati-Saber *et al.* 2007).

In the most general sense, two or more dynamical systems are said to be synchronized if through a subtle interaction their states become correlated in time Rulkov *et al.* (1995). From this point of view, many different types of synchronized behavior can be defined, including identical, phase, and generalized synchronization to mention but a few (Pikovsky *et al.* 2001; Boccaletti *et al.* 2002). In the simplest case, two systems are *unidirectionally* connected, which is usually called *drive-response* configuration (Pecora and Carroll 1990). Designing the interaction between these systems poses a significant challenge, particularly in formulating the coupling term within the response subsystem. This term is typically developed using diverse control techniques such as robust control (Almeida *et al.* 2006), adaptive schemes (Hong *et al.* 2001), and optimal control approaches (Pan and Yin 1997). Another approach involves establishing a bidirectional coupling between the two systems. In this setup, synchronization becomes more intricate,

as both subsystems mutually influence one another through their dynamic interplay (Boccaletti *et al.* 2002). Research in this area has naturally progressed toward the study of dynamical networks (Boccaletti *et al.* 2006), giving rise to prominent challenges such as consensus achievement and pinning control (Su and Wang 2013).

The study of synchronization in dynamical systems has evolved significantly in the last decade, with a growing focus on nonidentical systems, bidirectional coupling, and networked dynamics. Recent works have explored more complex configurations. In Arreola-Delgado and Barajas-Ramírez (2021), they investigated the controllability of networks with nonidentical linear nodes, providing theoretical conditions under which heterogeneous systems can be synchronized. Their findings highlight the impact of network topology on synchronization feasibility, offering insights into designing control strategies for complex networks. Bidirectional coupling presents additional challenges, particularly when systems exhibit multistability. In (Ruiz-Silva *et al.* 2022), they analyzed bidirectionally coupled multistable systems, showing that synchronization depends on initial conditions and parameter mismatches. This work builds on previous research by (Ruiz-Silva *et al.* 2021), which explored the emergence of synchronous behavior in chaotic multistable systems. Their results emphasize the role of dynamical stability and bifurcation structures in determining synchronization outcomes, suggesting that synchronization can be highly sensitive to system parameters.

The influence of network topology on synchronization patterns has also been studied in the context of network motifs, Uriostegui-Legorreta *et al.* (2024) examined the synchronization of three piecewise Rössler systems coupled in a ring configuration. Their study demonstrates that different coupling configurations can lead to phase-locking, generalized synchronization, or desynchronization, depending on the system parameters and interaction strengths. These findings highlight the importance of structural connectivity in determining collective dynamics. Time delays in coupling can significantly affect synchronization behavior, either facilitating or disrupting synchronization. In (Serrano and Ghosh 2022), they proposed a robust stabilization and synchronization strategy for chaotic systems with time-varying delays, showing that adaptive control techniques can mitigate the negative effects of delays. Their approach is particularly relevant for applications where communication constraints or biological rhythms introduce inherent time-dependent perturbations.

Beyond classical integer-order systems, synchronization in fractional-order and neural networks has gained attention as can be observed in (Jahanshahi *et al.* 2022); they studied the synchronization of variable-order fractional Hopfield-like neural networks, revealing that parameter adaptation techniques can effectively synchronize such systems. Their work suggests that fractional dynamics introduce additional flexibility in synchronization, making them applicable to biological and artificial neural networks.These studies collectively emphasize the significance of bidirectional interactions, network topology, and system heterogeneity in synchronization dynamics. While recent advances have provided a deeper understanding of these factors, challenges remain in achieving robust synchronization in complex networks, particularly in the presence of uncertainties and structural mismatches. Future research may explore hybrid synchronization strategies, integrate learning-based approaches, and extend these concepts to multi-agent and cyber-physical systems.

This work addresses the synchronization challenge in nonidentical dynamical systems configured both in *drive-response* form (Assali 2021) and through *bidirectional* coupling. Our focus is directed toward chaotic systems characterized by simple quadratic dynamics, as well as more tractable chaotic models incorporating piecewise linear (PWL) elements (Delgado-Aranda *et al.* 2020; Escalante-González and Campos 2021). To achieve asymptotic identical synchronization, we develop an interconnection framework based on output feedback control. Nonetheless, attaining synchronized behavior in non-identical systems remains nontrivial due to potential amplitude suppression arising from the coupling effects. To address this, we introduce a synchronization strategy tailored for bidirectionally coupled, piecewise smooth nonlinear systems exhibiting full relative degree. The approach relies on a nonlinear switching feedback mechanism capable of handling parameter mismatches and structural disparities, including nonsmooth components.

The remainder of this paper is organized as follows. In Section 2, we define the synchronization problem for both *drive-response* and *bidirectional* coupling scenarios, and introduce an output feedback-based design methodology. Section 3 details the proposed synchronization scheme, and Section 4 showcases numerical simulations that validate our findings. The paper concludes with a summary of key insights and suggestions for future research directions.

PROBLEM FORMULATION

In this contribution, we consider two nonidentical systems bidirectionally coupled, that is,

$$\begin{aligned} \dot{x}_1(t) &= f_1(x_1(t)) + \mathcal{G}_{12}(y_1(t), y_2(t)), \\ y_1(t) &= h_1(x_1(t)), \end{aligned} \tag{1}$$

$$\begin{aligned} \dot{x}_2(t) &= f_2(x_2(t)) + \mathcal{G}_{21}(y_1(t), y_2(t)), \\ y_2(t) &= h_2(x_2(t)), \end{aligned} \tag{2}$$

where $x_1(t), x_2(t) \in \mathbf{R}^n$ are the state variables, $y_1(t), y_2(t) \in \mathbf{R}^m$ $(m \leq n)$ are output variables with measurement functions $h_1(\cdot), h_2(\cdot) : \mathbf{R}^n \to \mathbf{R}^m$, and $f_1(\cdot), f_2(\cdot) : \mathbf{R}^n \to \mathbf{R}^n$ describe the dynamics of each isolated system, respectively. The coupling functions of system 2 to 1; $\mathcal{G}_{12}(\cdot,\cdot) : \mathbf{R}^{2m} \to \mathbf{R}^n$, and system 1 to 2; $\mathcal{G}_{21}(\cdot,\cdot) : \mathbf{R}^{2m} \to \mathbf{R}^n$ are to be designed.

For simplicity, we consider both systems to be three-dimensional, the outputs scalar, and their measurement functions linear ($h_1(x_1(t)) = C_1 x_1(t)$, $h_2(x_2(t)) = C_2 x_2(t)$ with $C_1, C_2 \in \mathbf{R}^{1\times 3}$). Furthermore, the systems are interconnected through a linear function based on the difference in their outputs, that is, diffusive output coupling:

$$\begin{aligned} \mathcal{G}_{12}(y_1(t), y_2(t)) &= K_{12}(C_2 x_2(t) - C_1 x_1(t)), \\ \mathcal{G}_{21}(y_1(t), y_2(t)) &= K_{21}(C_1 x_1(t) - C_2 x_2(t)), \end{aligned} \tag{3}$$

where the coupling gains $K_{12} \in \mathbf{R}^{3\times 1}$ and $K_{21} \in \mathbf{R}^{3\times 1}$ are chosen such that *identical synchronization* is achieved, that is, the following conditions are satisfied:

$$\lim_{t\to\infty} x_1(t) - x_2(t) = 0, \text{ and } \lim_{t\to\infty} x_2(t) - x_1(t) = 0. \tag{4}$$

To assess whether *identical synchronization* occurs in systems (1)-(3), as described by the condition in (4), we introduce the corresponding error variables:

$$e_{12}(t) = x_2(t) - x_1(t),$$
$$e_{21}(t) = x_1(t) - x_2(t). \tag{5}$$

Then, the error dynamics are given by

$$\begin{aligned} \dot{e}_{12}(t) &= f_{12}(t) + K_{12}(C_2x_2(t) - C_1x_1(t)) \\ &\quad -K_{21}(C_1x_1(t) - C_2x_2(t)), \\ \dot{e}_{21}(t) &= f_{21}(t) + K_{21}(C_1x_1(t) - C_2x_2(t)) \\ &\quad -K_{12}(C_2x_2(t) - C_1x_1(t)), \end{aligned} \tag{6}$$

where $f_{12}(t) = f_2(x_2(t)) - f_1(x_1(t))$ and $f_{21}(t) = f_1(x_1(t)) - f_2(x_2(t))$. Letting the output functions be identical ($C = C_1 = C_2 \in \mathbf{R}^{1\times 3}$), the error dynamics can be rewritten as:

$$\begin{aligned} \dot{e}_{12}(t) &= f_{12}(t) + K_{12}Ce_{12}(t) - K_{21}Ce_{21}(t), \\ \dot{e}_{21}(t) &= f_{21}(t) - K_{12}Ce_{12}(t) + K_{21}Ce_{21}(t). \end{aligned} \tag{7}$$

Let the coupling gains be chosen as: $K_{12} = K_{21} = k\,[1,1,1]^\top \in \mathbf{R}^3$, then the error dynamics in vector form becomes:

$$\dot{\mathbf{e}}(t) = \mathbf{f}(t) + k\,[\mathbf{1}(6,2) \otimes C]\,\mathbf{e}(t), \tag{8}$$

where $\mathbf{e}(t) = [e_{12}(t), e_{21}(t)]^\top \in \mathbf{R}^6$, $\mathbf{f}(t) = [f_{12}(t), f_{21}(t)]^\top \in \mathbf{R}^6$, $\mathbf{1}(6,2)$ is matrix of one entries with six rows and two columns, and $\otimes$ represents the Kronecker product.

Finding a coupling gain k such that (8) has zero as its asymptotically stable equilibrium point can be very difficult. In general, when $f_1(\cdot) \neq f_2(\cdot)$ the *identical synchronization* solution for (1)-(3) can not be stabilized by a choice of k. An alternative way to describe the conditions in (4) is to assume that an identical synchronization solution exist (Duane *et al.* 2007), that is,

$$\lim_{t\to\infty} x_1(t) = x_2(t) = s(t), \tag{9}$$

where $s(t) \in \mathbf{R}^3$ is the identical synchronization solution. Further, we assume that the dynamics of $s(t)$ are also known, such that we have:

$$\dot{s}(t) = f_s(s(t)), \tag{10}$$

with $f_s(\cdot) : \mathbf{R}^3 \to \mathbf{R}^3$.

In the case of identical dynamics the synchronized solution $s(t)$ is realized since the differential coupling term vanish. Therefore, $s()t$ is actually the dynamics of either node in isolation. Furthermore, identical synchronization can be achieved by an appropriately chosen constant gain k. For the case of non-identical nodes, the diffusive coupling does not vanishes so $s(t)$ is not exactly the dynamics of an isolated node. Yet if the coupling function forces the nodes to synchronize to the same behavior as in (10), the synchronization solution, either impose as desired behavior $\dot{s}(t) = f_s(s(t))$, or as the average dynamics of the nodes $\dot{s}(t) = f_s(s(t)) = (\frac{1}{2})(f_1(s(t)) + f_2(s(t)))$, can be assume to exit. Additionally, it can only be made stable by an appropriate design of the coupling function, which as describe in the remainder of this contribution it will require nonlinear terms to guaranty its stability. From the above, we do not argue that $\dot{s}(t) = f_1(s(t))$ nor $\dot{s}(t) = f_2(s(t))$, but that $s(t)$ is a solution where the coupled nodes are synchronized despite their differences, therefore $\dot{s}(t) = f_s(s(t))$ is our control objective dynamics. In this sense, we are solving a controlled synchronization problem that becomes a bit more interesting since the systems are bidirectionally coupled.

In terms of this desired synchronization solution the errors are:

$$e_1(t) = x_2(t) - s(t),$$
$$e_2(t) = x_1(t) - s(t). \tag{11}$$

Then, the error dynamics are found from (1)-(10) to be:

$$\begin{aligned} \dot{e}_1(t) &= f_{1s}(t) + \mathcal{G}_{12}(y_1(t), y_2(t)), \\ \dot{e}_2(t) &= f_{2s}(t) + \mathcal{G}_{21}(y_1(t), y_2(t)), \end{aligned} \tag{12}$$

where $f_{1s}(t) = f_1(x_1(t)) - f_s(s(t))$ and $f_{2s}(t) = f_2(x_2(t)) - f_s(s(t))$.

In this contribution, instead of using a purely linear component for the coupling function, like (3), we propose to add a nonlinear component $\mathcal{F}_i(\cdot)$, $(i = 1, 2)$, such that:

$$\begin{aligned} \mathcal{G}_{12}(y_1(t), y_2(t)) &= KC(e_2(t) - e_1(t)) + \mathcal{F}_1(y_1(t), y_2(t)), \\ \mathcal{G}_{21}(y_1(t), y_2(t)) &= KC(e_1(t) - e_2(t)) + \mathcal{F}_2(y_1(t), y_2(t)), \end{aligned} \tag{13}$$

with $K \in \mathbf{R}^{3\times 1}$, $\mathcal{F}_1$ and $\mathcal{F}_2$ are designed to have

$$\lim_{t\to\infty} e_1(t) = 0, \text{ and } \lim_{t\to\infty} e_2(t) = 0. \tag{14}$$

Again, a general solution for the design problem described above is very complex. However, since the error and output functions in (13) can be expressed in terms of the state variable $x(t)$, each system (1) and (2) may be rewritten as a control-input/affine system. Using this notation will allow a better design for inputs. Therefore, we consider three-dimensional systems of the form:

$$\begin{aligned} \dot{x}(t) &= F(x(t)) + G(x(t))u(t), \\ y(t) &= H(x(t)), \end{aligned} \tag{15}$$

with $F(\cdot)$ used to represent functions like $f_1(\cdot)$ and $f_2(\cdot)$ in (1) and (2) and the control-input/affine function $G(\cdot)u(t)$ represent functions $\mathcal{G}_{12}(\cdot,\cdot)$ and $\mathcal{G}_{21}(\cdot,\cdot)$. Also, $x(t) \in \mathbf{R}^3$ and $u(t) \in \mathbf{R}$ are the state variables and input to the system, respectively. In particular, we focus on the case of vector fields $F(x(t))$ and $G(x(t))$ such that (15) has *full relative degree*. That is, the following conditions are satisfied (Isidori 1985):

i) $L_G L_F^k H(x) = 0, k = 0, 1,$
ii) $L_G L_F^2 H(x) \neq 0,$

where $L_F H(x) = \frac{\partial H(x)}{\partial x} F(x)$ represents the Lie derivative of $H(x)$ along the vector field $F(x)$, where $L_F^0 H(x) = H(x)$ by definition.

Using a coordinate transformation $z_1(t) = H(x(t))$, $z_2(t) = L_F H(x(t))$, $z_3(t) = L_F^2 H(x(t))$. The system in (15) can be rewritten in its normal form:

$$\begin{aligned} \dot{z}_1(t) &= z_2(t), \\ \dot{z}_2(t) &= z_3(t), \\ \dot{z}_3(t) &= L_F^3 H(x(t)) + L_G L_F^2 H(x(t))u(t), \\ y_z(t) &= z_1(t). \end{aligned} \tag{16}$$

Different three-dimensional chaotic systems may have a full relative degree.

We also consider, dynamical systems with an structure based on the Jerk equation

$$\dddot{x}(t) = a_1\ddot{x}(t) + a_2\dot{x}^2(t) + a_3 x(t) + NL(x(t)). \tag{17}$$

Using $x_1(t) = x(t)$, $x_2(t) = \dot{x}(t)$, and $x_3(t) = \ddot{x}(t)$ in vector form of (17) is rewritten as:

$$\begin{aligned} \dot{x}_1(t) &= x_2(t), \\ \dot{x}_2(t) &= x_3(t), \\ \dot{x}_3(t) &= a_1 x_3(t) + a_2 x_2^2(t) + a_3 x_1(t) + NL(x(t)), \\ y_x(t) &= x_1(t). \end{aligned} \tag{18}$$

As shown in (Sprott 2000), for many different choices of parameters and nonlinear function $NL(x(t))$, the system (18) exhibits chaotic behavior.

In the following Section, we propose a design for the bidirectional coupling of systems in the form of (16) and (18), such that identical synchronization is achieved in the sense of (14).

SYNCHRONIZATION STRATEGY

In this Section the controlled synchronization problem is addressed departing form the version of theproblem formulated above, in our proposed strategy the error dynamics are described under the assumption that a known desired synchronization solution exist, that is, instead of solving for the errors $x_1(t) - x_2(t)$ as the problem is originally formulated, we focus on the reformulated errors as $x_1(t) - s(t)$ and $x_2(t) - s(t)$. In this way, the *bidirectionally* coupled systems have the error dynamics:

$$\begin{aligned} \dot{e}_1(t) &= F_1 + \kappa_1 C e_2(t) - \kappa_2 C e_1(t), \\ \dot{e}_2(t) &= F_2 + \kappa_2 C e_1(t) - \kappa_1 C e_2(t), \end{aligned} \tag{19}$$

for $F_2 = F(y(t)) - F(x(t))$. For simplicity, we assume $\kappa_1 = \kappa_2 = \kappa \in \mathbf{R}^3$. Under successful synchronization, the coupled systems admit a common solution of the form:

$$x(t) = y(t) = s(t). \tag{20}$$

This implies that when the systems are synchronized, the coupling terms in (11) vanish, and each node evolves according to:

$$\dot{s}(t) = F(s(t)). \tag{21}$$

To characterize the deviation from this synchronized behavior, we define the following error variables:

$$\begin{aligned} \epsilon_1(t) &= x(t) - s(t), \\ \epsilon_2(t) &= y(t) - s(t). \end{aligned} \tag{22}$$

The dynamics of these error variables are then given by:

$$\begin{aligned} \dot{\epsilon}_1(t) &= F_{1s} + \kappa C \epsilon_2(t) - \kappa C \epsilon_1(t), \\ \dot{\epsilon}_2(t) &= F_{2s} + \kappa C \epsilon_1(t) - \kappa C \epsilon_2(t), \end{aligned} \tag{23}$$

where $F_{1s} = F(x(t)) - F(s(t))$ and $F_{2s} = F(y(t)) - F(s(t))$. In vector form, these equations can be rewritten as:

$$\dot{E}(t) = \mathbf{F} + (A \otimes \kappa C)E(t), \tag{24}$$

with $E(t) = \begin{bmatrix} \epsilon_1(t) \\ \epsilon_2(t) \end{bmatrix} \in \mathbf{R}^6$, $\mathbf{F} = \begin{bmatrix} F_{1s} \\ F_{2s} \end{bmatrix} : \mathbf{R}^6 \to \mathbf{R}^6$, $A = \begin{bmatrix} -1 & 1 \\ 1 & -1 \end{bmatrix}$ representing the Laplacian matrix associated with the *bidirectional* coupling. The symbol $\otimes$ denotes the Kronecker product.

Bidirectional synchronization of the coupled systems described by (1)-(3) is achieved if the error dynamics in (24) is, at least, locally asymptotically stable at the origin.

To analyze stability, we linearize equation (24) at the zero solution, yielding:

$$\dot{E}(t) = \left[D\mathbf{F}(s(t)) + (A \otimes \kappa C)\right] E(t), \tag{25}$$

where $D\mathbf{F}(s(t)) = [DF(s(t)), DF(s(t))]^\top$ and $DF(\cdot)$ the Jacobian of the nonlinear dynamics. Given that A is a Laplacian matrix, a change of coordinates $E(t) = \Phi[\nu_1(t), \nu_2(t)]^\top$, where Φ built with eigenvectors of A, allows us to decouple the linearized error dynamics into:

$$\begin{aligned} \dot{\nu}_1(t) &= \left[DF(s(t)) + \lambda_1 \kappa C\right] \nu_1(t), \\ \dot{\nu}_2(t) &= \left[DF(s(t)) + \lambda_2 \kappa C\right] \nu_2(t), \end{aligned} \tag{26}$$

where $\lambda_1 = 0$ and $\lambda_2 = -2$ are the eigenvalues of A. Since λ_1 corresponds to the synchronized motion $x(t) = y(t)$ it suffices to ensure that $\dot{\nu}_2(t) = [DF(s(t)) + \lambda_2 \kappa C]\, \nu_2(t)$ is asymptotically stable. This can be established using the Lypaunov function

$$V(\nu_2(t)) = \nu_2(t)^\top \Pi \nu_2(t), \tag{27}$$

where $\Pi = \Pi^\top > 0$ is a positive definite matrix of suitable dimension. The derivative of this function along the trajectories of the second equation in (26) yields:

$$\begin{aligned} \dot{V}(\nu_2(t)) = \nu_2(t)^\top &\left([DF(s(t)) + \lambda_2 \kappa C]^\top \Pi \right. \\ &\left. + \Pi \left[DF(s(t)) + \lambda_2 \kappa C\right]\right) \nu_2(t). \end{aligned} \tag{28}$$

The function $\dot{V}(\nu_2(t))$ is strictly negative if the following inequality holds:

$$[DF(s(t)) + \lambda_2 \kappa C]^\top \Pi + \Pi [DF(s(t)) + \lambda_2 \kappa C] \leq -\tau_2 I_3, \quad (29)$$

for some $\tau_2 > 0$. Therefore, selecting κ such that the aforementioned inequality (29) is satisfied, ensures that the coupled system (1)-(3) will achieve bidirectionally synchronization.

To identically synchronize the systems (16) and (18) with a bidirectional coupling in the form of (13). We start by defining the desired synchronization solution to have the structure of (18), that is:

$$\begin{aligned} \dot{s}_1(t) &= s_2(t), \\ \dot{s}_2(t) &= s_3(t), \\ \dot{s}_3(t) &= a_1 s_3(t) + a_2 s_2(t) + a_3 s_1(t) + NL(s(t)), \end{aligned} \quad (30)$$

$$y_s(t) = s_1(t).$$

The errors are defined as:

$$\begin{aligned} e_z(t) &= z(t) - s(t). \\ e_x(t) &= x(t) - s(t). \end{aligned} \quad (31)$$

Thus:

$$\begin{aligned} \dot{e}_{z1}(t) &= e_{z2}(t) + \mathcal{G}_{zs1}(y_z(t), y_s(t)), \\ \dot{e}_{z2}(t) &= e_{z3}(t) + \mathcal{G}_{zs2}(y_z(t), y_s(t)), \\ \dot{e}_{z3}(t) &= L_F^3 H(x(t)) + L_G L_F^2 H(x(t)) u(t) \\ &\quad -[a_1 s_3(t) + a_2 s_2(t) + a_3 s_1(t) + NL(s(t))] \\ &\quad +\mathcal{G}_{zs3}(y_z(t), y_s(t)), \\ \dot{e}_{x1}(t) &= e_{x2} + \mathcal{G}_{xs1}(y_x(t), y_s(t)), \\ \dot{e}_{x2}(t) &= e_{x3} + \mathcal{G}_{xs2}(y_x(t), y_s(t)), \\ \dot{e}_{x3}(t) &= a_1 x_3(t) + a_2 x_2(t) + a_3 x_1(t) + NL(x(t)), \\ &\quad -[a_1 s_3(t) + a_2 s_2(t) + a_3 s_1(t) + NL(s(t))], \\ &\quad +\mathcal{G}_{xs3}(y_x(t), y_s(t)). \end{aligned} \quad (32)$$

With:

$$\begin{aligned} \mathcal{G}_{zs3}(y_1(t), y_2(t)) &= [0, 0, K_{z3}]^\top C(e_x(t) - e_z(t)), \\ &\quad +\mathcal{F}_z(y_z(t), y_x(t)) \\ \mathcal{G}_{xs3}(y_1(t), y_2(t)) &= [0, 0, K_{x3}]^\top C(e_z(t) - e_x(t)), \\ &\quad +\mathcal{F}_x(y_z(t), y_x(t)). \end{aligned} \quad (33)$$

Then, by property designing the coupling gains K_{z3}, K_{z3} and the nonlinear functions $\mathcal{F}_z(y_z(t), y_x(t))$, or $\mathcal{F}_x(y_z(t), y_x(t))$ we can make the error dynamics asymptotically stable.

SIMULATION RESULTS

In the following subsections, we present simulation results demonstrating the application of the proposed synchronization law to several well-known chaotic systems.

Example 1

For the simulations, we employed a slightly adapted variant of a circuit originally introduced by Sprott (2000), known to exhibit chaotic dynamics for specific parameter values. The structure of the selected circuit is given by:

$$\dddot{x} = -\mu \ddot{x} + \dot{x}^2 - x + \beta u, \quad (34)$$

The system shows chaotic dynamics for $\mu = -2.017$ and $\beta = 0$, with Lyapunov exponents of $(0.055, 0, -2.072)$. By selecting the output $y = x$, it is straightforward to show that equation (34) has full relative degree. Consequently, a pair of Sprott-like circuits can be described as follows:

$$\begin{aligned} \dot{x}_1^j &= x_2^j, \\ \dot{x}_2^j &= x_3^j, \\ \dot{x}_3^j &= -x_1^j + (x_2^j)^2 + \mu_j x_3^j + \beta_j u, \\ y_j &= x_1^j, \end{aligned} \quad (35)$$

for $j = 1, 2$. We define the synchronization error as $e_1 = x_1^1 - x_1^2 = y_1 - y_2$, leading to the following error dynamics:

$$\begin{aligned} \dot{e}_1 &= e_2, \\ \dot{e}_2 &= e_3, \\ \dot{e}_3 &= -e_1 + e_2(e_2 + 2x_2^2) + \mu_1 x_3^1 - \mu_2 x_3^2 + \tilde{\beta} u, \end{aligned} \quad (36)$$

with $\tilde{\beta} = \beta_1 - \beta_2$ and $\beta_1 \neq \beta_2$. The systems described in (35) exhibit chaotic dynamics for parameter values $\mu_j = -2.017$, $\beta_j = 0$, $(j = 1, 2)$ and initial conditions given by $x^j(0) = \begin{bmatrix} 0 & 0 & 1 \end{bmatrix}^T$.

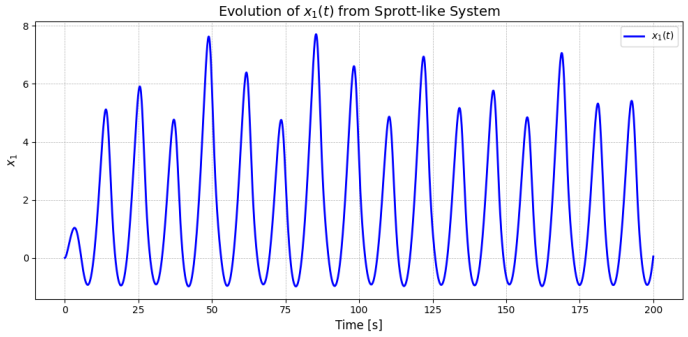

Figure 1 Temporal evolution of state variable x_1 from system (35) for parameter $\mu_1 = -2.017$

It is evident that if $\mu_1 = \mu_2$ and the initial conditions satisfy $x^1(0) = x^2(0)$, the circuits will remain perfectly synchronized. To validate our approach, we consider $\mu_1 = -2.017$ and $\mu_2 = -2.02$. Figure 1 displays the solution for x_1 in system 34. Despite the

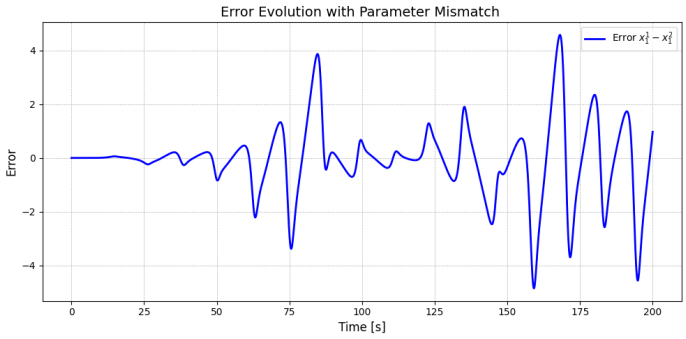

Figure 2 Time evolution for the synchronization error in state x_1 of systems (35) under parameter mismatch conditions.

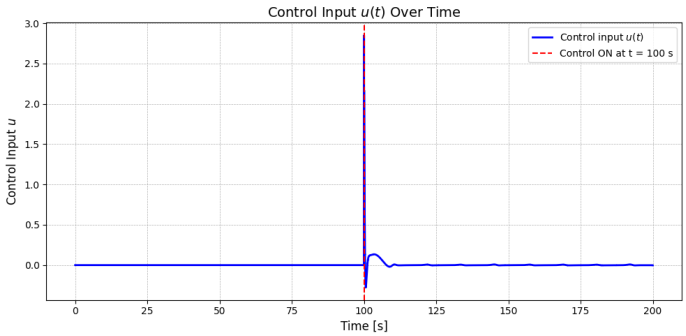

Figure 3 Time response for the synchronization law used for system (35) in Example 1.

seemingly minor parameter mismatch, the time responses of the two systems diverge significantly, as illustrated in Figure 2.

To ensure that the system states synchronize, i.e., $e \to 0$, we introduce the following synchronization control law:

$$u = \frac{1}{\tilde{\beta}}[a^T e + e_1 - e_2(e_2 + 2x_2^2) - \mu_1 x_3^1 + \mu_2 x_3^2]. \tag{37}$$

For demonstration purposes, we select $a = \begin{bmatrix} -6 & -11 & -6 \end{bmatrix}^T$, corresponding to desired pole locations at $\lambda = 1, 2, 3$. With this synchronization law, the closed-loop system is expected to exhibit an asymptotically stable equilibrium point.

The synchronization control was activated at $t = 70s$, and its time evolution is illustrated in Fig. 3. The corresponding synchronization error over time is presented in Fig. 4.

Example 2

This example focuses on synchronizing two distinct dynamical systems using the proposed approach: a normal-form Lorenz system and a Sprott system. The Lorenz system is defined by the following dynamics:

$$\begin{aligned} \dot{x}_1 &= \sigma(x_2 - x_1), \\ \dot{x}_2 &= \rho x_1 - x_2 - x_1 x_3, \\ \dot{x}_3 &= x_1 x_2 - \beta x_3 + u, \\ y &= x_1. \end{aligned} \tag{38}$$

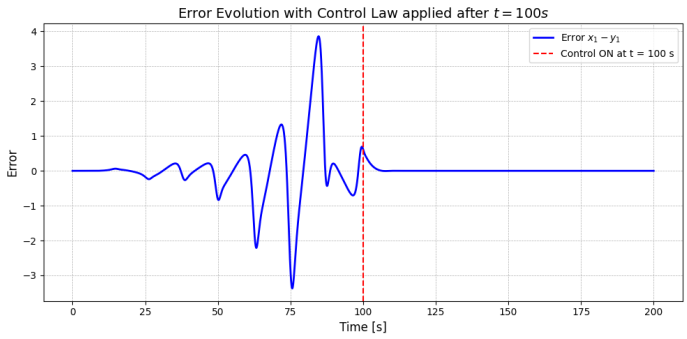

Figure 4 Time response of the synchronization error for system (35) in Example 1.

It is well known that the system exhibits chaotic behavior for the parameter values $\sigma = 10$, $\rho = 28$, and $\beta = \frac{8}{3}$ Lorenz (2017). System (38) can be expressed in normal form via the coordinate transformation defined in (16), i.e., $x^1 = \varphi(x)$. Accordingly, the new coordinates for the Lorenz system are:

$$\begin{aligned} \varphi_1(x) &= x_1, \\ \varphi_2(x) &= \sigma(x_2 - x_1), \\ \varphi_3(x) &= -\sigma^2(x_2 - x_1) + \sigma(\rho x_1 - x_2 - 20 x_1 x_3), \end{aligned} \tag{39}$$

leading to the following dynamics

$$\begin{aligned} \dot{x}_1^1 &= x_2^1, \\ \dot{x}_2^1 &= x_3^1, \\ \dot{x}_3^1 &= f^1(x^1) + g^1(x^1)u, \\ y &= x_1^1, \end{aligned} \tag{40}$$

for

$$\begin{aligned} f^1(x^1) = {} & (\rho - 1)\sigma x_2^1 - \\ & (\sigma + 1)x_3^1 - (x_1^1)^2(x_2^1 + \sigma x_1^1) - \\ & (\beta x_1^1 - x_2^1) \\ & \left[\frac{\sigma(1-\rho)x_1^1 + (\sigma+1)x_2^1 + x_3^1}{x_1^1}\right], \end{aligned} \tag{41}$$

and

$$g^1(x^1) = -\sigma x_1^1. \tag{42}$$

System (40) is now expressed in normal form. Next, we consider another system to synchronize with:

$$\dddot{x} = -\mu\ddot{x} - \dot{x} + x - x^3 + \beta u. \tag{43}$$

Equation (43) models an electronic circuit described in Sprott (2000), which exhibits chaotic behavior for $\mu = 0.7$ and $\beta = 0$. The corresponding normal form of this system is given by:

$$\begin{aligned} \dot{x}_1^2 &= x_2^2, \\ \dot{x}_2^2 &= x_3^2, \\ \dot{x}_3^2 &= -\mu x_3^2 - x_2^2 + x_1^2 - (x_1^2)^3 + \beta u, \\ y^2 &= x_1^2. \end{aligned} \tag{44}$$

The synchronization error is defined as $e_1 = y^1 - y^2 = x_1^1 - x_1^2$, which leads to the following error dynamics:

$$\begin{aligned} \dot{e}_1 &= e_2, \\ \dot{e}_2 &= e_3, \\ \dot{e}_3 &= f(x^1, x^2) + g(x^1, x^2)u, \end{aligned} \tag{45}$$

where $f(x^1, x^2) = f^1(x^1) - f^2(x^2)$ and $g(x^1, x^2) = \beta - \sigma x_1^1$. Accordingly, a synchronization law can be formulated as follows:

$$u = \frac{a^T e - f(x^1, x^2)}{g(x^1, x^2)}. \tag{46}$$

For demonstration purposes, we apply the synchronization law in $t = 100s$, Fig. 5 shows the time response for e_1.

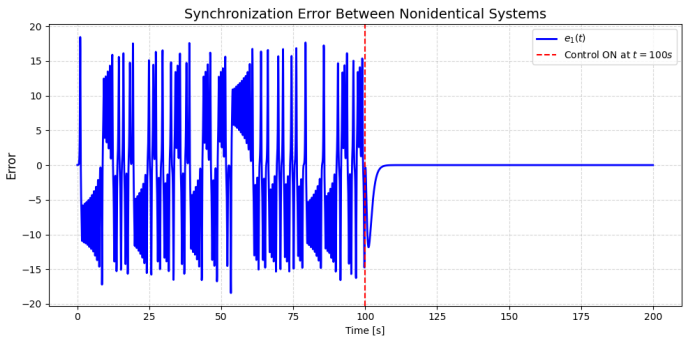

Figure 5 Error e_1 between (40) and (44) with synchronization law applied at $t = 100s$.

CONCLUSION

This work presented a synchronization strategy for bidirectionally coupled, nonidentical chaotic systems using an output feedback design framework. The approach leverages the concept of full relative degree and applies a coordinate transformation to bring the systems into normal form, enabling the design of nonlinear feedback coupling laws. Unlike traditional master-slave schemes, this method addresses mutual interactions and allows for synchronization even under structural differences and parameter mismatches. The proposed method demonstrated successful synchronization of both identical and non-identical systems, including combinations such as Lorenz and Sprott-type models. Numerical simulations confirmed the stability and convergence of the synchronization errors under the proposed coupling scheme. The inclusion of both linear and nonlinear feedback components contributes to the robustness and flexibility of the control design, making it suitable for a wide range of chaotic systems, including those with nonsmooth or piecewise linear dynamics. This contribution provides a promising direction for practical applications in engineering systems where exact matching of models is not feasible. It opens avenues for synchronization in real-world scenarios involving imperfect information, model uncertainties, and heterogeneous components.

Future research will aim to generalize the proposed method to networks with more than two nodes, including those found in complex systems and multi-agent coordination problems. Additional work will focus on the development of robust synchronization schemes by incorporating internal model control and adaptive techniques capable of handling uncertainty and external disturbances. Lastly, experimental validation will be pursued using physical platforms such as electronic circuits or robotic systems, in order to assess the real-time performance and practical feasibility of the approach under realistic conditions. Overall, this work contributes a scalable and effective strategy for the synchronization of nonidentical chaotic systems, with potential applications across a variety of fields in applied sciences and engineering.

Ethical standard

The authors have no relevant financial or non-financial interests to disclose.

Conflicts of interest

The authors declare that there is no conflict of interest regarding the publication of this paper.

Availability of data and material

Not applicable.

LITERATURE CITED

Almeida, D. I. R., J. Alvarez, and J. G. Barajas, 2006 Robust synchronization of sprott circuits using sliding mode control. Chaos, Solitons & Fractals **30**: 11–18.

Alvarez, J., 1996 Synchronization in the lorenz system: stability and robustness. Nonlinear Dynamics **10**: 89–103.

Alvarez, J., D. Rosas, D. Hernandez, and E. Alvarez, 2010 Robust synchronization of arrays of lagrangian systems. International Journal of Control, Automation and Systems **8**: 1039–1047.

Arreola-Delgado, A. and J. G. Barajas-Ramírez, 2021 On the controllability of networks with nonidentical linear nodes. IMA Journal of Mathematical Control and Information **38**: 39–53.

Assali, E. A., 2021 Predefined-time synchronization of chaotic systems with different dimensions and applications. Chaos, Solitons & Fractals **147**: 110988.

Boccaletti, S., J. Kurths, G. Osipov, D. Valladares, and C. Zhou, 2002 The synchronization of chaotic systems. Physics reports **366**: 1–101.

Boccaletti, S., V. Latora, Y. Moreno, M. Chavez, and D.-U. Hwang, 2006 Complex networks: Structure and dynamics. Physics reports **424**: 175–308.

Delgado-Aranda, F., I. Campos-Cantón, E. Tristán-Hernández, and P. Salas-Castro, 2020 Hidden attractors from the switching linear systems. Revista mexicana de física **66**: 683–691.

Duan, Z., G. Chen, and L. Huang, 2007 Complex network synchronizability: Analysis and control. Physical Review E—Statistical, Nonlinear, and Soft Matter Physics **76**: 056103.

Duane, G. S., D. Yu, and L. Kocarev, 2007 Identical synchronization, with translation invariance, implies parameter estimation. Physics Letters A **371**: 416–420.

Escalante-González, R. d. J. and E. Campos, 2021 Emergence of hidden attractors through the rupture of heteroclinic-like orbits of switched systems with self-excited attractors. Complexity **2021**: 1–24.

Hong, Y., H. Qin, and G. Chen, 2001 Adaptive synchronization of chaotic systems via state or output feedback control. International Journal of Bifurcation and Chaos **11**: 1149–1158.
Isidori, A., 1985 *Nonlinear control systems: an introduction*. Springer.
Jahanshahi, H., E. Zambrano-Serrano, S. Bekiros, Z. Wei, C. Volos, *et al.*, 2022 On the dynamical investigation and synchronization of variable-order fractional neural networks: The hopfield-like neural network model. The European Physical Journal Special Topics **231**: 1757–1769.
Lorenz, E. N., 1963 Deterministic nonperiodic flow. Journal of atmospheric sciences **20**: 130–141.
Lorenz, E. N., 2017 Deterministic nonperiodic flow 1. In *Universality in Chaos, 2nd edition*, pp. 367–378, Routledge.
Olfati-Saber, R., J. A. Fax, and R. M. Murray, 2007 Consensus and cooperation in networked multi-agent systems. Proceedings of the IEEE **95**: 215–233.
Pan, S. and F. Yin, 1997 Optimal control of chaos with synchronization. International Journal of Bifurcation and Chaos **7**: 2855–2860.
Pecora, L. M. and T. L. Carroll, 1990 Synchronization in chaotic systems. Physical review letters **64**: 821.
Pikovsky, A., M. Rosenblum, J. Kurths, and A. Synchronization, 2001 A universal concept in nonlinear sciences. Self **2**: 3.
Ruiz-Silva, A., B. B. Cassal-Quiroga, G. Huerta-Cuellar, and H. E. Gilardi-Velázquez, 2022 On the behavior of bidirectionally coupled multistable systems. The European Physical Journal Special Topics **231**: 369–379.
Ruiz-Silva, A., H. E. Gilardi-Velázquez, and E. Campos, 2021 Emergence of synchronous behavior in a network with chaotic multistable systems. Chaos, Solitons & Fractals **151**: 111263.
Rulkov, N. F., M. M. Sushchik, L. S. Tsimring, and H. D. Abarbanel, 1995 Generalized synchronization of chaos in directionally coupled chaotic systems. Physical Review E **51**: 980.
Sarasola, C., F. J. Torrealdea, A. D'ANJOU, A. Moujahid, and M. Graña, 2003 Feedback synchronization of chaotic systems. International Journal of Bifurcation and Chaos **13**: 177–191.
Serrano, F. E. and D. Ghosh, 2022 Robust stabilization and synchronization in a network of chaotic systems with time-varying delays. Chaos, Solitons & Fractals **159**: 112134.
Sprott, J. C., 2000 Simple chaotic systems and circuits. American Journal of Physics **68**: 758–763.
Su, H. and X. Wang, 2013 *Pinning control of complex networked systems: Synchronization, consensus and flocking of networked systems via pinning*. Springer Science & Business Media.
Uriostegui-Legorreta, U., J. Estevez-Delgado, and H. Pérez-Aguilar, 2024 Synchronization in network motifs of three piecewise rössler systems coupled in ring configuration. International Journal of Modern Physics C **35**: 2450084.
Vincent, U. and A. Kenfack, 2008 Synchronization and bifurcation structures in coupled periodically forced non-identical duffing oscillators. Physica Scripta **77**: 045005.
Zhu, D. and D. Zhou, 2008 Synchronization control of parallel dual inverted pendulums. In *2008 IEEE International Conference on Automation and Logistics*, pp. 1486–1490, IEEE.

How to cite this article: Barajas-Ramírez, J. G., and Gonzalez-Hernandez, H. G. On the Synchronization of Bidirectionally Coupled Nonidentical Systems via Output Feedback. *Chaos Theory and Applications*, 7(2), 99-106, 2025.

CHAOS
Theory and Applications
in Applied Sciences and Engineering

e-ISSN: 2687-4539
RESEARCH ARTICLE
Vol.7 / No.2 / 2025 / pp.107-116
https://doi.org/10.51537/chaos.1601947

Neurochaos Learning for Classification using Composition of Chaotic Maps

Akhila Henry *,1 **and Nithin Nagaraj** α,2

*Amrita Vishwa Vidyapeetham, Amritapuri Campus, 690525, India, αComplex Systems Programme, National Institute of Advanced Studies, Bengaluru, 560012, India.

ABSTRACT

In the age of increasing data availability, there is a pressing need for fast and precise algorithms that can classify datasets. Traditional methods like Support Vector Machines, Random Forest, and Neural Networks are commonly used, but a novel approach known as Neurochaos Learning (NL) has demonstrated strong classification performance across various datasets by incorporating chaos theory. However, the original NL algorithm requires tuning three hyperparameters and involves extraction of multiple features, leading to significant training time. In this study, we propose a modified NL algorithm with only a single hyperparameter and a single feature, using two distinct compositions of 1D chaotic maps, the Skew Tent map with the Logistic map, and the Skew Tent map with $sin(\pi x)$, thereby drastically reducing training time while maintaining classification performance. This study also analyses the 1D chaotic properties of composition of these chaotic maps including Lyapunov Exponent and the stability of fixed points. Testing on ten datasets including *Iris*, *Penguin*, *Haberman*, and *Bank Note Authentication*, our method yields very competitive F1 scores. The composition of the Logistic Map and Skew Tent Map yields an F1 score of 0.569 for the *Haberman* dataset and an impressive 0.968 for the *Penguin* dataset using cosine similarity. Utilizing the composition of $sin(\pi x)$ and Skew Tent Map, the *Ionosphere* dataset achieves an F1 score of 0.876. Our method's versatility is further demonstrated with the Random Forest Algorithm, achieving a perfect F1 score of 1.0 on the *Iris* dataset with the Skew Tent and Logistic Map composition and the same score on the *Penguin* dataset using the $sin(\pi x)$ and Skew Tent Map composition. This streamlined approach meets the demand for faster and more efficient classification algorithms, offering reliable performance in data-rich environments.

KEYWORDS

Neurochaos learning
Skew tent map
Logistic map
Tracemean
Composition

INTRODUCTION

In recent years, Artificial Intelligence (AI), particularly machine learning (ML), has seen rapid advancement, significantly improving data analysis and intelligent computing applications (Sarker *et al.* 2021). The digital era is characterised by an abundance of data from several areas, including mobile technology, commerce, social media, and healthcare. Comprehensive analysis of this data and the development of intelligent, automated systems require a profound understanding of AI, especially machine learning. This domain includes many machine learning approaches, including supervised, unsupervised, semi-supervised, and reinforcement learning. Furthermore, deep learning, a subset of machine learning, has exhibited considerable effectiveness in extensive analysis of data (Sarker 2021). However, machine learning models frequently require substantial training, and as the dataset size increases, the computational resources needed for training correspondingly escalate (Niel 2023).

Contrary to prevalent misunderstandings, "Chaos" in mathematics does not denote disorder or confusion (Faure and Korn 2001). The investigation of *Deterministic Chaos* (Devaney 2018) has emerged as a prominent research domain across multiple disciplines. Nonlinear dynamical systems (for continuous flows) with more than two degrees of freedom can demonstrate chaotic behaviour, rendering their long-term evolution uncertain in spite of the dynamics being completely deterministic. For discrete-time nonlinear dynamical systems, chaos is exhibited at 1-dimension itself. Here *Chaos* refers to the unpredictable outcomes (often random-like) from such simple deterministic systems. The human brain is a distinctly nonlinear system (Kowalik *et al.* 1996). In contrast to other systems that often stabilise following transient

Manuscript received: 15 December 2024,
Revised: 17 February 2025,
Accepted: 25 February 2025.

[1]akhilahenryu@am.amrita.edu (**Corresponding author**)
[2]nithin@nias.res.in

states, the brain perpetually shifts between several states. Evidence indicates that chaos exists in numerous biological systems, especially in the brain, where chaotic dynamics are observable in electroencephalogram (EEG) signals. Despite the seemingly random nature of these signals, they possess intrinsic patterns (Aram *et al.* 2017).

Conventional machine learning and deep neural network frameworks are only marginally influenced by the internal workings of the human brain (Harikrishnan and Nagaraj 2020). In (Harikrishnan and Nagaraj 2020), a novel brain-inspired learning system called *Neurochaos Learning* (NL) is proposed for classification tasks. NL basically utilizes chaos at the level of individual neurons, unlike artificial neural networks (ANNs). The proposed learning paradigm comprises of two distinct architectures: (a) ChaosNet, and (b) Chaos-based features or ChaosFEX (CFX) combined with classical machine learning (ML) models. Input data is transmitted to the Feature Extraction block, where properties derived from the chaotic firing of 1-dimensional chaotic Generalized Lüroth Series (GLS) neurons, specifically firing rate, energy, firing time, and entropy, are retrieved and classified either using cosine similarity (ChaosNet) or via machine learning classifiers (CFX+ML). ChaosNet and CFX+ML (Sethi *et al.* 2023) are designed to harness the advantageous characteristics of biological neural networks, stemming from the complex chaotic behaviour of individual neurons, and have demonstrated the ability to perform challenging classification tasks on par with or superior to traditional artificial neural networks, while necessitating significantly fewer training samples. However, a limitation of the proposed algorithm is the presence of hyperparameters, which require significant time for tuning. Additionally, another drawback is that the transformed features in ChaosNet and ChaosFEX exhibit dependency.

The research presented here aims to improve the current Neurochaos Learning architectures by employing compositions of chaotic maps (as neurons in the input layer of NL) rather than one specific map, thus minimising the number of features and hyperparameters while preserving method efficacy. We propose employing four distinct combinations of chaotic maps: (i) Skew Tent (Harikrishnan and Nagaraj 2020) and Logistic Map (AS *et al.* 2023), (ii) Logistic and Skew Tent Map, (iii) Skew Tent and $sin(\pi x)$ (Palacios-Luengas *et al.* 2021), and (iv) $sin(\pi x)$ and Skew Tent Map for feature extraction. The efficacy of the proposed approach is assessed on classification tasks for 10 different datasets: *Iris* (Fisher 1936), *Haberman* (Haberman 1973), *Seeds* (Dua *et al.* 2017), *Statlog* (Dua *et al.* 2017), *Bank* (Gillich and Lohweg 2010), *Cancer* (Street *et al.* 1993), *Ionosphere* (Sigillito *et al.* 1989), *Wine* (Forina *et al.* 1988), *Sonar* (Horst *et al.* 2020), and *Penguin* (Gorman and Sejnowski 1988).

The subsequent sections of the paper are organised as follows: Section 2 presents the properties of the 1D chaotic maps and their compositions used in this study. Section 3 delineates the suggested algorithm. Section 4 presents the findings from the algorithm using various compositions of chaotic maps. Section 5 compares the F1 scores of the proposed algorithm to those of ChaosNet. Ultimately, Section 6 concludes with prospective avenues for further research.

1D CHAOTIC MAPS AND THEIR COMPOSITIONS

Chaotic maps are iterative mathematical functions that exhibit highly sensitive dependence on initial conditions, leading to seemingly random behavior despite being deterministic in nature. In this work, we focus on three well-known 1D chaotic maps: Logistic map, Skew Tent map, and $sin(\pi x)$ map. Each map has distinct characteristics that make it suitable for various applications in chaos theory and feature extraction for machine learning.

In the following subsections, we briefly define these chaotic maps and subsequently introduce the composition of chaotic maps, which plays a crucial role in the algorithm proposed in this study. The Skew Tent Map, $sin(\pi x)$, and Logistic Map are one-dimensional nonlinear dynamic systems characterised by a single degree of freedom. They are extensively examined in chaos theory and have been previously delineated in many studies (Palacios-Luengas *et al.* 2021; AS *et al.* 2023; Nagaraj 2022).

A skew tent map $T_{skew-tent}(x) : [0,1) \rightarrow [0,1)$ is defined as:

$$T_{\text{skew-tent}}(x) = \begin{cases} \frac{x}{b}, & 0 \leq x < b, \\ \frac{1-x}{1-b}, & b \leq x < 1, \end{cases}$$

where $x \in [0,1)$ and $0 < b < 1$. In this work, we consider $b = 0.499$. The graph of $T_{\text{skew-tent}}(x)$ for $b = 0.499$ is illustrated in Figure 1a. It intersects the line $y = x$ at two distinct positions. Consequently, the fixed points are 0 and 0.666 (Kuijpers 2021). Both the fixed points are unstable. If we start with a value slightly greater than zero, the map will push the trajectory away from zero, making $x = 0$ an unstable fixed point. Likewise, the other fixed point, 0.666, is also unstable. Generalised Luröth Series (GLS) maps preserve the Lebesgue measure and exhibit uniform distribution on the interval $[0,1)$ as the invariant distribution (Nagaraj 2022). Every GLS map on the interval [0,1) exhibits ergodicity. Therefore, the skew tent map is also ergodic (Dajani and Kraaikamp 2002). The Lyapunov Exponent for this skew tent map, with a skew value of 0.499, is 0.6931.

The logistic map is defined by the following equation:

$$x_{n+1} = r x_n (1 - x_n),$$

where x_n takes the value in the interval $(0,1)$ and r is the bifurcation parameter which lies in the interval $(0,4]$. For the Logistic Map, we consider the parameter $r = 4$, which results in fully chaotic behavior (Chen *et al.* 2021). The corresponding graph for the Logistic Map with $r = 4$ is shown in Figure 1b. The logistic map with $r = 4$ intersect the line $y = x$ at two distinct points, resulting in two fixed points are 0 and $\frac{3}{4}$. Both the fixed points are unstable. The logistic map with $r = 4$ has an invariant distribution given by: (Ayers and Radunskaya 2024)

$$f(x) = \begin{cases} \frac{1}{x(1-x)} & \text{for } 0 < x < 1, \\ 0 & \text{otherwise.} \end{cases}$$

Also the map is ergodic with a Lyapunov exponent of 0.6724 (Machicao *et al.* 2019; Naanaa 2015).

The $sin(\pi x)$ map on $(0,1)$ is shown in the Figure 1c. It is a simple dynamical system, similar to logistic map, exhibiting complex chaotic behaviour with a lyapunov exponent of 0.6889. Here the fixed points are $x = 0$ and $x = 0.7365$, both of which are unstable (Griffin 2013; Alzaidi *et al.* 2018).

Composition of 1D Chaotic Maps

Let f and g be two functions. Then, by definition, the composition (Muthuvel *et al.* 2000; Suryadi *et al.* 2020) of two functions f and g defined by $fog(x) = f(g(x))$ where g is applied first followed by f. In this work, we study the following compositions of maps:

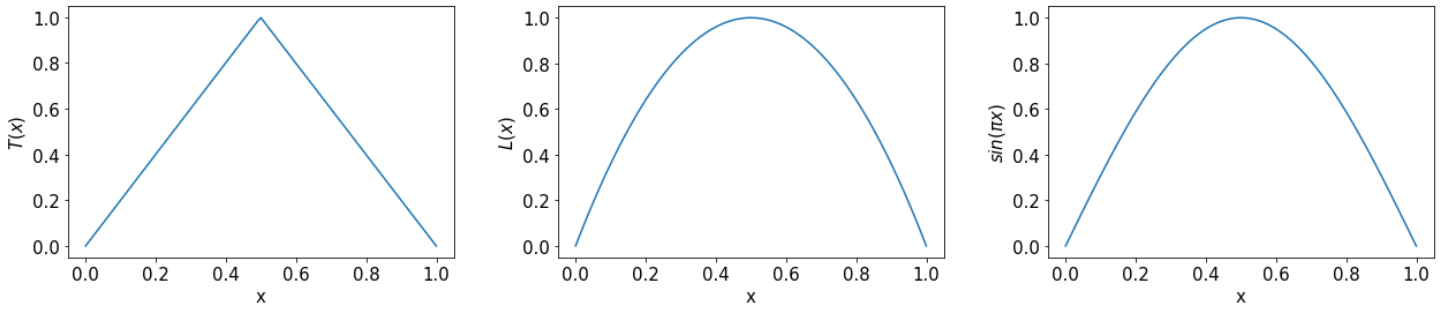

(a) Skew-tent map **(b)** Logistic map **(c)** $sin(\pi x)$ map

Figure 1 1D Chaotic Maps: Skew Tent Map $T(x)$, Logistic Map $L(x)$, $sin(\pi x)$ Map $S(x)$.

- Skew Tent map and Logistic map ($T \circ L$ map)
- Logistic map and Skew Tent map ($L \circ T$ map)
- Skew Tent map and $sin(\pi x)$ ($T \circ S$ map)
- $sin(\pi x)$ and Skew Tent map ($S \circ T$ map)

The composition of these maps are continuous, non-commutative, indicating that the sequence of compositions is distinct. The sequence of applying the Skew Tent Map followed by the Logistic Map yields different outcomes/trajectories when compared to the reverse sequence (Logistic Map followed by the Skew Tent Map). This significantly influences the algorithm's performance across the ten analysed datasets. The $sin(\pi x)$ map exhibits certain similarities to the Logistic Map (Zhu *et al.* 2019). The composition of the Skew Tent Map followed by the $sin(\pi x)$ map also differs from the reverse order ($sin(\pi x)$ map followed by the Skew Tent Map). This distinction is essential for evaluating the impact of various map combinations on the algorithm's efficacy.

The Figure 2 illustrate the compositions of the maps and shows that each composition has four distinct fixed points. To determine the approximate values of fixed points of composition of chaotic maps $f \circ g$, it is enough to compute the values of x such that $(f \circ g)(x) - x = 0$ using *fsolve* function in Python with ten equally spaced guesses in $(0, 1)$ within an error of 10^{-5}. Table 1 summarizes the fixed points, their stability, and Lyapunov exponent values of the composition of chaotic maps. A point x_0 is said to be stable if $|f'(x_0)| < 1$ (Alligood *et al.* 1998). Thus, to evaluate the stability of fixed points, the condition

$$\frac{|f(x+h) - f(x-h)|}{2h} < 1,$$

where $h = 10^{-5}$ is verified.

The Lyapunov exponent $h(x_1)$ (Alligood *et al.* 1998) for a given orbit $x_1, x_2, ...$ is defined by:

$$h(x_1) = \lim_{n \to \infty} \frac{ln|f'(x_1)| + ln|f'(x_2)| + \ldots + ln|f'(x_n)|}{n}.$$

The values of the Lyapunov exponent for $T \circ L$, $L \circ T$, $S \circ T$ and $T \circ S$ are all greater than one, implying that the divergence of nearby trajectories happens at an exponentially fast rate. Here the limiting value for Lyapunov exponent is approximated after $100,000$ iterations. These compositions are highly chaotic and its sensitivity to initial conditions is extreme. The distributions of points in the trajectory generated by the composition of maps (in each of the four cases) with an initial point 0.01 are shown in Figure 3.

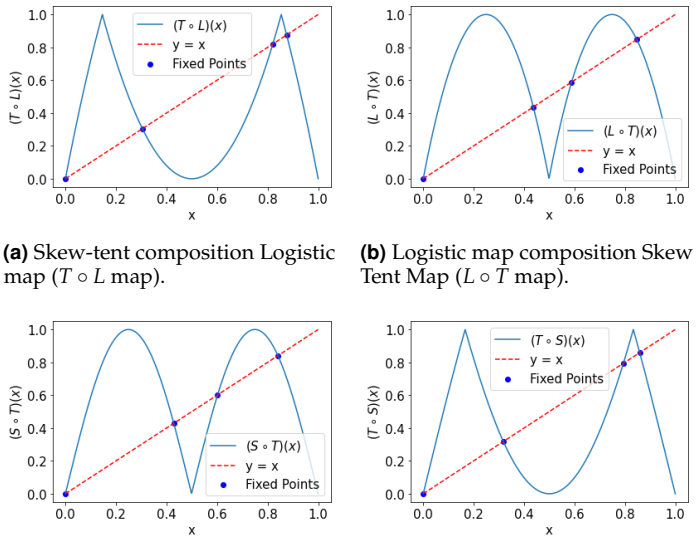

(a) Skew-tent composition Logistic map ($T \circ L$ map). **(b)** Logistic map composition Skew Tent Map ($L \circ T$ map).

(c) $sin(\pi x)$ map composition Skew Tent Map ($S \circ T$ map). **(d)** Skew Tent map composition $sin(\pi x)$ map ($T \circ S$ map).

Figure 2 First return maps and fixed points for the composition of 1D chaotic maps (Skew Tent map, Logistic Map and $sin(\pi x)$).

The following section introduces the modified Neurochaos Learning Algorithm using the composition of chaotic maps - $T \circ L$, $L \circ T$, $S \circ T$, $T \circ S$.

Table 1 Fixed Points, Stability and Lyapunov Exponents of 1D Chaotic Map Compositions

Composition	Fixed Points (approx.)	Stability	Lyap. Exp.
ToL	0.0, 0.3046, 0.8206, 0.8752	Unstable	1.2840
LoT	0.0, 0.4367, 0.5889, 0.8470	Unstable	1.2838
ToS	0.0, 0.3179, 0.8590, 0.7944	Unstable	1.2957
SoT	0.0, 0.6020, 0.4286, 0.8407	Unstable	1.2961

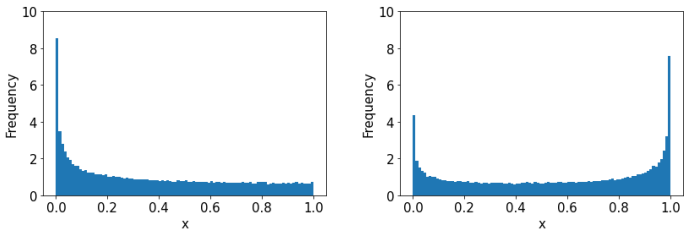

(a) Skew-tent composition Logistic map ($T \circ L$ map).

(b) Logistic map composition Skew Tent Map ($L \circ T$ map).

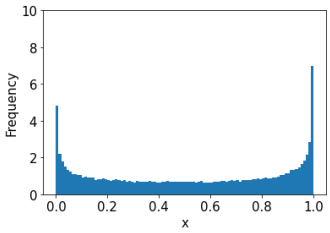

(c) $sin(\pi x)$ map composition Skew Tent Map ($S \circ T$ map).

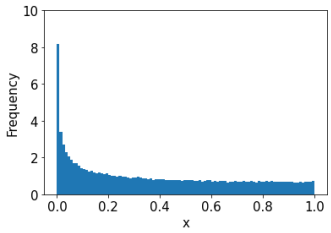

(d) Skew Tent map composition $sin(\pi x)$ map ($T \circ S$ map).

Figure 3 Distribution of points from the trajectories generated by $T \circ L$, $L \circ T$, $S \circ T$ and $T \circ S$ maps.

PROPOSED ALGORITHM

The proposed algorithm in Figure 4 leverages the composition of chaotic maps to enhance the feature extraction process in Neurochaos Learning (Sethi *et al.* 2023; Balakrishnan *et al.* 2019). The motivation behind this approach is to improve the classification performance by reducing the number of hyperparameters and utilising a single feature – the *mean* of the neural trace, which is computationally efficient and robust across various datasets. This section outlines the key steps involved in the algorithm.

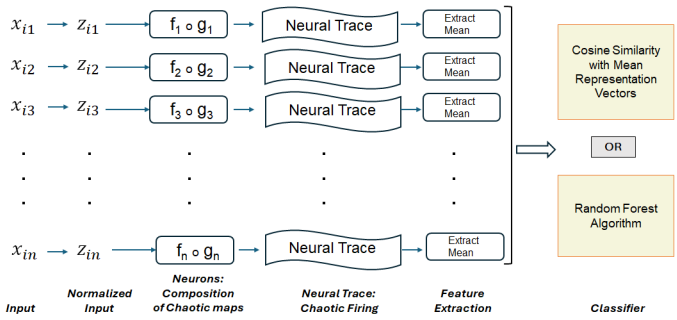

Figure 4 Block diagram depicting the proposed algorithm in this study.

- **Step 1 : Normalisation**
  Consider a dataset of m samples, each with n features, represented as:

  $$\{(x_{11}, x_{12}, \ldots, x_{1n}), (x_{21}, x_{22}, \ldots, x_{2n}), \ldots, (x_{m1}, x_{m2}, \ldots, x_{mn})\}.$$

  Each feature attribute x_{ij} can be normalised using min-max normalisation technique. Specifically, the normalised value z_{ij} can be computed as:

  $$z_{ij} = \frac{x_{ij} - min\{x_{ij} : 1 \leq i \leq m\}}{max\{x_{ij} : 1 \leq i \leq m\} - min\{x_{ij} : 1 \leq i \leq m\}}$$

  for $1 \leq j \leq n$. Thus the resulting normalised dataset is:

  $$\{(z_{11}, z_{12}, \ldots, z_{1n}), (z_{21}, z_{22}, \ldots, z_{2n}), \ldots, (z_{m1}, z_{m2}, \ldots, z_{mn})\}.$$

  This transformation ensures that all features are scaled within the range $[0, 1]$, thereby making them suitable for subsequent steps in the algorithm.

- **Step 2 : Neural Trace Generation**
  For each normalised feature value z_{ij}, a corresponding neural trace is generated by applying a composition of chaotic maps. The generation process begins with an initial neural activity, denoted as q. Here, q serves as a hyperparameter, and its value is tuned between 0.01 to 0.99 with a step value 0.01 during training to optimise performance. The dataset was split with 20% allocated for testing and remaining 80% for training. The chaotic maps are iteratively composed, transforming the initial neural activity based on the value of z_{ij}, to produce a unique neural trace for each feature. Suppose f and g are the chaotic maps and using $f \circ g$ for generating neural trace, the neural trace can be mathematically represented as

  $$N = \{q, f \circ g(q), (f \circ g)^2(q) = f \circ g \circ f \circ g(q), \ldots, (f \circ g)^T(q)\}.$$

  This neural trace (with firing time T) serves as the foundation for the feature extraction process in the subsequent steps of the algorithm.

- **Step 3 : Feature Extraction**
  In the next phase, feature extraction is performed by analysing the generated neural trace corresponding to each z_{ij}. Given n features, we require n instances of the composition of chaotic maps f and g, denoted as $f_1 \circ g_1, f_2 \circ g_2 \ldots, f_n \circ g_n$, corresponding to each $z_{i1}, z_{i2}, \ldots, z_{in}$.

  The neural trace

  $$N_j = \{q, f_j \circ g_j(q), (f_j \circ g_j)^2(q) = f_j \circ g_j \circ f_j \circ g_j(q), \ldots\}$$

  where $j = 1, 2, \ldots, n$, evolves under the influence of the chaotic map composition $f_j \circ g_j$ until it reaches an ϵ-neighborhood of the corresponding stimulus, z_{ij}. For this algorithm, the noise ϵ is set to a value of 0.25, meaning the neural trace halts when its trajectory comes within 0.25 units of the feature z_{ij}. Once this condition is met, the mean value of the neural trace up to this point, t_{ij} is computed. This mean serves as a summary statistic for the chaotic behavior of the neural trace, capturing essential information about the feature z_{ij}. The resulting mean value for each trajectory

  $$\{(t_{i1}, t_{i2}, \ldots, t_{in}) : i = 1, 2, \ldots, m\}$$

  will be utilised in the subsequent classification step. This computation of mean is performed for each feature of each training instance of each class.

- **Step 4 : Classification**
  Once the mean of the neural trace is computed for each z_{ij}, they can be either classified using cosine similarity or Random Forest Algorithm (Breiman 2001).

  1. *Cosine Similarity(Cos) classifier*: In this approach, the transformed features are classified by computing the cosine similarity between the feature vectors and the mean representation

vectors of each class.
Let the given m data samples belongs to k classes.

$$\{(x_{l_1 1}, x_{l_1 2}, \ldots, x_{l_1 n}), (x_{l_2 1}, x_{l_2 2}, \ldots, x_{l_2 n}), \ldots, (x_{l_r 1}, x_{l_r 2}, \ldots, x_{l_r n})\}$$

be the r samples in class l. After normalisation, the extracted data be:

$$\{(t_{l_1 1}, t_{l_1 2}, \ldots, t_{l_1 n}), (t_{l_2 1}, t_{l_2 2}, \ldots, t_{l_2 n}), \ldots, (t_{l_r 1}, t_{l_r 2}, \ldots, t_{l_r n})\}.$$

Then the mean representation vector corresponding to the class l can be defined as:

$$M^{(l)} = \left(\frac{\sum_{i=l_1}^{l_r} t_{i1}}{r}, \frac{\sum_{i=l_1}^{l_r} t_{i2}}{r}, \ldots, \frac{\sum_{i=l_1}^{l_r} t_{in}}{r} \right).$$

In order to classify a particular *test* data instance $X_i = (x_{i1}, x_{i2}, \ldots, x_{in})$, calculate the cosine similarity of extracted feature vector of the data instance $T_i = (t_{i1}, t_{i2}, \ldots, t_{in})$ with the mean representation vectors of each class $\{M^{(1)}, M^{(2)}, \ldots, M^{(l)}, \ldots, M^{(k)}\}$. Cosine similarity is defined as follows :

$$\cos\theta = \frac{M^{(j)} \cdot T_i}{||M^{(j)}||\ ||T_i||}$$

where $j = 1, 2, \ldots, l, \ldots k$. The data instance will belong to the class with least value.

2. *Random Forest (RF) classifier*: Random Forest (Breiman 2001) is a powerful machine learning algorithm that employs technique of *bagging* with numerous decision trees and consolidates their predictions to attain a high degree of classification accuracy. The RF classifier can adeptly manage the non-linear interactions inherent in the chaotic dynamics of the neural trace by utilising the diversity of decision trees. Instead of classifying using cosine similarity, the transformed dataset

$$\{(t_{l_1 1}, t_{l_1 2}, \ldots, t_{l_1 n}), (t_{l_2 1}, t_{l_2 2}, \ldots, t_{l_2 n}), \ldots, (t_{l_r 1}, t_{l_r 2}, \ldots, t_{l_r n})\}$$

is classified using Random Forest Algorithm. The number of estimators for Random Forest Algorithm was optimised through 5-fold cross-validation selecting from the values $1, 10, 100, 1000, 10000$.

While extracting features for classification using Random Forest Algorithm, instead of tuning q value again for neural trace, the value of q tuned for each dataset in Cos Classifier is reused. Thus both Cos and RF classifiers used same values of q, which is indicated in Table 3, Table 4, Table 5 and Table 6. The flowchart (Figure 4) depicts the proposed algorithm. Both methods offer distinct advantages, and the choice between them depends on the specific characteristics of the dataset and the performance requirements of the task.

RESULTS AND ANALYSIS

In this section, we present the F1 Score (Christen *et al.* 2023) results for the proposed algorithm using four different compositions of chaotic maps. The classification was performed on 10 different datasets, and we report the F1 scores for two classification methods: Cosine Similarity and Random Forest (RF). The F1 Score, which balances precision and recall, provides a robust measure of the classifier's performance across varying data characteristics.

Table 2 Description of datasets used in this study.

Dataset	Features	Classes	Samples
Iris	4	3	150
Haberman's Survival	3	2	306
Seeds	7	3	210
Statlog (Heart)	13	2	270
Ionosphere	34	2	351
Bank Note Auth.	4	2	1372
Breast Cancer Wis.	31	2	569
Wine	13	3	178
Penguin	4	3	342
Sonar	60	2	208

The datasets used in this evaluation are as follows: *Iris*, *Haberman*, *Seeds*, *Statlog*, *Ionosphere*, *Bank*, *Breast Cancer*, *Wine*, *Penguin*, and *Sonar*. Table 2 shows the number of features and samples in each dataset used in this study. For each dataset, the F1 scores for both Cosine Similarity and Random Forest classifiers are presented, allowing for a comprehensive comparison of the algorithm's effectiveness across different domains (Sethi *et al.* 2023).

Tables 3 and 4 display the training and testing F1 scores of the proposed Neurochaos Learning algorithm utilising the composition of the Skew Tent Map and the Logistic Map. These tables illustrate the algorithm's performance over the chosen ten unique datasets. Similarly, tables 5 and 6 substitute the Logistic Map with the $sin(\pi x)$ map, which possesses certain dynamical characteristics akin to those of the Logistic Map. The performance of the Neurochaos Learning algorithm is rigorously analysed and compared utilising these compositions of chaotic maps across identical datasets.

The performance of custom Random Forest (RF) algorithms, where features are extracted using various compositions of 1D chaotic maps and subsequently passed to the Random Forest algorithm, was compared against standalone RF algorithm across multiple datasets:

- *Iris*: The composition of the Skew Tent and Logistic Maps (denoted as ToL and LoT) followed by classification using Random Forest resulted in a perfect F1 Score of 1.0, achieving 100% classification accuracy. This demonstrates the powerful synergy between chaotic feature extraction and the RF classifier for this dataset.
- *Penguin*: A similar performance boost was observed when using features from the composition of the $sin(\pi x)$ and Skew Tent Maps (denoted as ToS and SoT) with RF classification, also reaching an F1 Score of 1.0, marking complete accuracy in classifying the *Penguin* dataset.
- *Cancer*: The combination of the Skew Tent and $sin(\pi x)$ maps (ToS) followed by RF classification delivered a notable improvement of 4.79% over standalone RF. Additionally, the composition of the Skew Tent and Logistic Maps (ToL) with RF also exhibited a 3.81% increase in performance.
- *Wine*: Minor yet consistent improvements were observed, with the LoT RF and ToS RF algorithms outperforming stan-

Table 3 Training & Testing F1 scores: $L \circ T$ Map -Based NL Algorithm.

Sl No	Dataset	Initial Neural Activity(q)	F1 Score using Cosine Similarity		F1 Score using Random Forest	
			Training	Testing	Training	Testing
1	*Iris*	0.98	0.912	0.916	0.948	1.000
2	*Haberman*	0.27	0.584	0.569	0.559	0.456
3	*Seeds*	0.78	0.831	0.652	0.889	0.926
4	*Statlog*	0.78	0.810	0.792	0.843	0.774
5	*Bank Note Authentication*	0.28	0.858	0.774	0.938	0.911
6	*Breast Cancer Wisconsin*	0.74	0.931	0.903	0.949	0.918
7	*Ionosphere*	0.75	0.803	0.727	0.923	0.893
8	*Wine*	0.63	0.950	0.862	0.977	0.976
9	*Sonar*	0.45	0.757	0.703	0.818	0.775
10	*Penguin*	0.98	0.957	0.968	0.918	0.920

Table 4 Training & Testing F1 scores: $T \circ L$ Map -Based NL Algorithm.

Sl No	Dataset	Initial Neural Activity (q)	F1 Score using Cosine Similarity		F1 Score using Random Forest	
			Training	Testing	Training	Testing
1	*Iris*	0.98	0.920	0.910	0.946	1.000
2	*Haberman*	0.27	0.594	0.557	0.573	0.483
3	*Seeds*	0.03	0.876	0.783	0.893	0.822
4	*Statlog*	0.23	0.807	0.710	0.842	0.797
5	*Bank Note Authentication*	0.95	0.858	0.836	0.863	0.843
6	*Breast Cancer Wisconsin*	0.54	0.930	0.849	0.952	0.954
7	*Ionosphere*	0.50	0.808	0.691	0.917	0.909
8	*Wine*	0.63	0.957	0.943	0.973	0.968
9	*Sonar*	0.46	0.750	0.734	0.813	0.798
10	*Penguin*	0.25	0.959	0.960	0.911	0.917

dalone RF by 1.04% and 3.73%, respectively. This highlights the advantage of feature extraction using chaotic maps for this dataset.

The custom algorithms using Cosine Similarity classifier (Cos) for classification, after feature extraction from 1D chaotic maps, were also compared against the original ChaosNet algorithm (Sethi *et al.* 2023):

- *Sonar*: ToL Cos and SoT Cos significantly outperformed ChaosNet, showing improvements of 14.15% and 12.80%, respectively. Additionally, ToS Cos exhibited a solid 10.08% increase, underscoring the effectiveness of these map compositions in enhancing classification accuracy for the *Sonar* dataset.
- *Cancer*: The LoT Cos and SoT Cos algorithms outperformed ChaosNet by 6.86% and 9.41%, respectively, indicating their superior performance for this dataset, especially in capturing complex patterns.
- *Penguin*: The performance of LoT Cos and SoT Cos were nearly equivalent to ChaosNet, with only marginal improvements.

Table 5 Training & Testing F1 scores: $T \circ S$ Map -Based NL Algorithm.

Sl No	Dataset	Initial Neural Activity (q)	F1 Score using Cosine Similarity		F1 Score using Random Forest	
			Training	Testing	Training	Testing
1	*Iris*	0.98	0.884	0.916	0.966	0.889
2	*Haberman*	0.28	0.594	0.557	0.546	0.431
3	*Seeds*	0.04	0.898	0.783	0.931	0.902
4	*Statlog*	0.56	0.806	0.671	0.837	0.791
5	*Bank Note Authentication*	0.95	0.852	0.850	0.941	0.911
6	*Breast Cancer Wisconsin*	0.54	0.928	0.849	0.946	0.963
7	*Ionosphere*	0.50	0.808	0.691	0.899	0.876
8	*Wine*	0.63	0.957	0.943	0.973	0.968
9	*Sonar*	0.46	0.755	0.708	0.808	0.798
10	*Penguin*	0.04	0.950	0.965	0.949	1.000

Table 6 Training & Testing F1 scores: $S \circ T$ Map -Based NL Algorithm.

Sl No	Dataset	Initial Neural Activity (q)	F1 Score using Cosine Similarity		F1 Score using Random Forest	
			Training	Testing	Training	Testing
1	*Iris*	0.98	0.894	0.917	0.948	0.928
2	*Haberman*	0.95	0.591	0.490	0.540	0.447
3	*Seeds*	0.04	0.878	0.749	0.915	0.897
4	*Statlog*	0.01	0.811	0.735	0.824	0.810
5	*Bank Note Authentication*	0.28	0.858	0.771	0.924	0.904
6	*Breast Cancer Wisconsin*	0.70	0.927	0.924	0.961	0.901
7	*Ionosphere*	0.76	0.803	0.876	0.873	0.807
8	*Wine*	0.63	0.949	0.888	0.971	0.918
9	*Sonar*	0.46	0.761	0.725	0.813	0.775
10	*Penguin*	0.76	0.954	0.964	0.946	1.000

- *Statlog*: LoT Cos demonstrated superiority over ChaosNet, with a 7.32% improvement. This further emphasizes the strength of the proposed algorithm in specific datasets where chaotic features provide additional discriminative power.
- *Haberman*: In this dataset, LoT Cos showed a modest improvement of 1.61% over ChaosNet, indicating enhanced classification performance even in more challenging datasets.

Table 7 compares the best F1 scores of our proposed algorithm with that of ChaosNet and standalone Random Forest algorithms. Figures 5 and 6 gives a comparison of F1 scores of proposed algorithm with ChaosNet and Random Forest Algorithm on different datasets.

Overall, the analysis highlights that the proposed Neurochaos Learning algorithms using different 1D chaotic map compositions for feature extraction outperform classical stand-alone classifiers like Random Forest and ChaosNet on various datasets. The non-commutative nature of map compositions plays a significant role in the performance variations observed, with different combinations producing distinct improvements depending on the dataset and

Table 7 Comparison of best F1 scores achieved by the proposed algorithms, Random Forest and ChaosNet. 'Cos' stands for Cosine Similarity based classifier used in NL.

Dataset	ChaosNet F1 Score	Standalone RF F1 Score	Best F1 Score -Cos Algorithms	Best F1 Score - Custom RF
Iris	1.000	1.000	0.917 ($S \circ T$ Cos)	1 ($L \circ T$ RF, $T \circ L$ RF)
Haberman	0.560	0.560	0.569 ($L \circ T$ Cos)	0.483 ($T \circ L$ RF)
Seeds	0.845	0.877	0.783 ($T \circ S$ Cos, $T \circ L$ Cos)	0.926($L \circ T$ RF)
Statlog	0.738	0.838	0.792 ($L \circ T$ Cos)	0.810 ($S \circ TRF$)
Bank Note Authentication	0.845	0.974	0.85 ($T \circ S$ Cos)	0.911 ($L \circ T$ RF, $T \circ S$ RF)
Breast Cancer Wisconsin	0.927	0.919	0.924($S \circ T$ Cos)	0.963($T \circ S$ RF)
Ionosphere	0.860	0.909	0.876($S \circ T$ Cos)	0.909($T \circ L$ RF)
Wine	0.976	0.966	0.943 ($T \circ L$ Cos, $T \circ S$ Cos)	0.976 ($L \circ T$ RF)
Sonar	0.643	0.798	0.734 ($T \circ L$ Cos)	0.798($T \circ L$ RF, $T \circ S$ RF)
Penguin	0.964	0.929	0.968($L \circ T$ Cos)	1.000 ($T \circ S$ RF , $S \circ T$ RF)

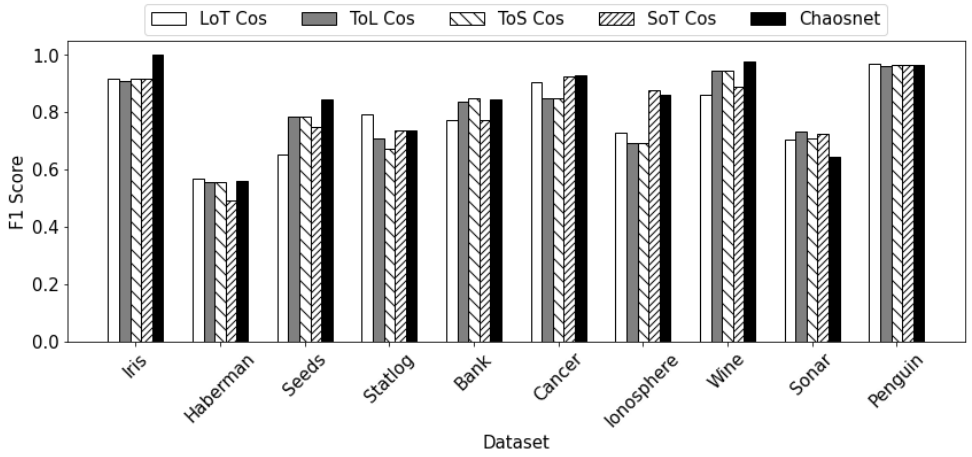

Figure 5 Comparison of F1 scores of Algorithms computed using cosine similarity on different datasets.

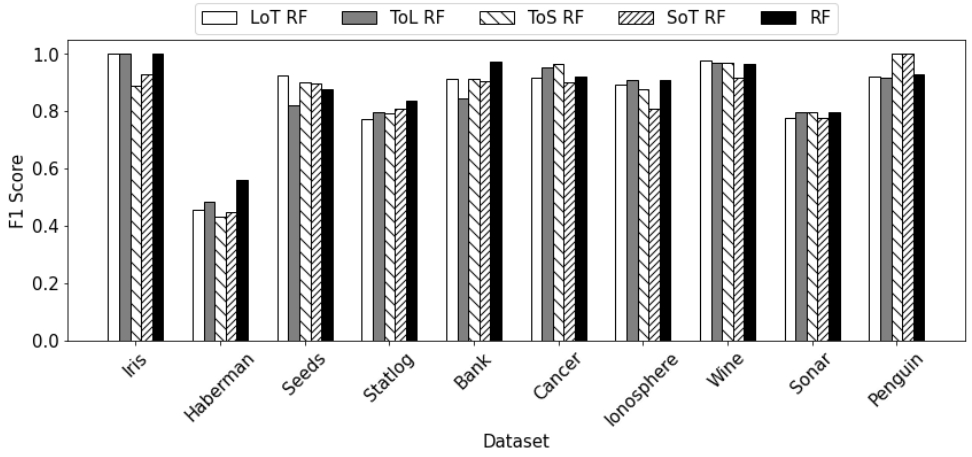

Figure 6 Comparison of F1 scores of custom Random Forest algorithms on different datasets.

classification method used.

CONCLUSION

The results demonstrate the robust performance of the proposed neurochaos-based algorithms on diverse datasets. Across multiple datasets, custom algorithms that use the composition of 1D chaotic maps, such as Skew Tent, Logistic, and $sin(\pi x)$ maps, consistently outperform traditional models like standalone Random Forest and ChaosNet. Notably, the improvements are especially pronounced in datasets such as *Cancer*, *Penguin*, and *Sonar*, indicating that the chaotic map-based feature extraction technique offers substantial advantages in these scenarios. The Lyapunov exponent for each of these composition of 1D chaotic maps is greater than 1.0, and their fixed points are unstable, indicating they are highly chaotic. Building on the promising results of the current study, there are several avenues for future research that can further enhance the performance and applicability of the proposed neurochaos-based algorithms:

- Exploring New Compositions of 1D Chaotic Maps: We plan to investigate different new combinations of 1D chaotic maps to uncover compositions that yield even better F1 scores. The non-commutative nature of these compositions offers a rich space to explore for improving classification results across diverse datasets.
- Application to Varied Datasets: Expanding the analysis to a broader range of datasets, particularly those with more complex or noisy structures, will help assess the generalisability and robustness of the custom algorithms in different real-world scenarios.
- Impact of Chaotic Map Compositions on Performance: A deeper investigation into how different chaotic map compositions affect algorithm performance can reveal valuable insights. Understanding the influence of map properties, such as their sensitivity to initial conditions and chaotic behavior, could lead to optimised feature extraction techniques for specific types of data.
- Incorporating Noise Robustness: Analysing the performance of these algorithms under varying noise levels can offer insights into their stability and resilience. Future work could involve introducing noise into the datasets and observing how different compositions of chaotic maps handle this, with the goal of developing more noise-tolerant algorithms.

These research directions not only offer opportunities to improve the current algorithms but also contribute to advancing the broader field of chaos theory-based machine learning.

Acknowledgments

Nithin Nagaraj would like to acknowledge the financial support of Anusandhan National Research Foundation (ANRF), Department of Science & Technology, Govt. of India (Grant No. TAR/2021/000206) towards this research.

Availability of data and material

Not applicable.

Conflicts of interest

The authors declare that there is no conflict of interest regarding the publication of this paper.

Ethical standard

The authors have no relevant financial or non-financial interests to disclose.

LITERATURE CITED

Alligood, K. T., T. D. Sauer, J. A. Yorke, and D. Chillingworth, 1998 Chaos: an introduction to dynamical systems. SIAM Review **40**: 732–732.

Alzaidi, A. A., M. Ahmad, H. S. Ahmed, and E. A. Solami, 2018 Sine-cosine optimization-based bijective substitution-boxes construction using enhanced dynamics of chaotic map. Complexity **2018**: 9389065.

Aram, Z., S. Jafari, J. Ma, J. C. Sprott, S. Zendehrouh, *et al.*, 2017 Using chaotic artificial neural networks to model memory in the brain. Communications in Nonlinear Science and Numerical Simulation **44**: 449–459.

AS, R. A., N. B. Harikrishnan, and N. Nagaraj, 2023 Analysis of logistic map based neurons in neurochaos learning architectures for data classification. Chaos, Solitons & Fractals **170**: 113347.

Ayers, K. and A. Radunskaya, 2024 Noisy fixed points: Stability of the invariant distribution of the random logistic map. arXiv preprint arXiv:2403.13116 .

Balakrishnan, H. N., A. Kathpalia, S. Saha, and N. Nagaraj, 2019 Chaosnet: A chaos based artificial neural network architecture for classification. Chaos: An Interdisciplinary Journal of Nonlinear Science **29**.

Breiman, L., 2001 Statistics department university of california berkeley, ca 94720. 2001. Random Forests .

Chen, S., S. Feng, W. Fu, and Y. Zhang, 2021 Logistic map: Stability and entrance to chaos. In *Journal of Physics: Conference Series*, volume 2014, p. 012009, IOP Publishing.

Christen, P., D. J. Hand, and N. Kirielle, 2023 A review of the f-measure: its history, properties, criticism, and alternatives. ACM Computing Surveys **56**: 1–24.

Dajani, K. and C. Kraaikamp, 2002 *Ergodic theory of numbers*, volume 29. American Mathematical Soc.

Devaney, R. L., 2018 *A first course in chaotic dynamical systems: theory and experiment*. CRC Press.

Dua, D., C. Graff, *et al.*, 2017 Uci machine learning repository, 2017. URL http://archive. ics. uci. edu/ml **7**: 62.

Faure, P. and H. Korn, 2001 Is there chaos in the brain? i. concepts of nonlinear dynamics and methods of investigation. Comptes Rendus de l'Académie des Sciences-Series III-Sciences de la Vie **324**: 773–793.

Fisher, R. A., 1936 The use of multiple measurements in taxonomic problems. Annals of eugenics **7**: 179–188.

Forina, M., R. Leardi, C. Armanino, S. Lanteri, P. Conti, *et al.*, 1988 Parvus an extendable package of programs for data exploration, classification and correlation .

Gillich, E. and V. Lohweg, 2010 Banknote authentication. 1. Jahreskolloquium Bild. Der Autom pp. 1–8.

Gorman, R. P. and T. J. Sejnowski, 1988 Analysis of hidden units in a layered network trained to classify sonar targets. Neural networks **1**: 75–89.

Griffin, J., 2013 The sine map. Retrieved May **4**: 2018.

Haberman, S. J., 1973 The analysis of residuals in cross-classified tables. Biometrics pp. 205–220.

Harikrishnan, N. and N. Nagaraj, 2020 Neurochaos inspired hybrid machine learning architecture for classification. In *2020 International Conference on Signal Processing and Communications (SPCOM)*, pp. 1–5, IEEE.

Horst, A. M., A. P. Hill, and K. B. Gorman, 2020 palmerpenguins: Palmer archipelago (antarctica) penguin data. r package version 0.1. 0.

Kowalik, Z. J., A. Wróbel, and A. Rydz, 1996 Why does the human brain need to be a nonlinear system? Behavioral and Brain Sciences **19**: 302–303.

Kuijpers, B., 2021 Deciding the point-to-fixed-point problem for skew tent maps on an interval. Journal of Computer and System Sciences **115**: 113–120.

Machicao, J., M. Alves, M. S. Baptista, and O. M. Bruno, 2019 Exploiting ergodicity of the logistic map using deep-zoom to improve security of chaos-based cryptosystems. International Journal of Modern Physics C **30**: 1950033.

Muthuvel, K. *et al.*, 2000 Composition of functions. International Journal of Mathematics and Mathematical Sciences **24**: 213–216.

Naanaa, A., 2015 Fast chaotic optimization algorithm based on spatiotemporal maps for global optimization. Applied Mathematics and Computation **269**: 402–411.

Nagaraj, N., 2022 The unreasonable effectiveness of the chaotic tent map in engineering applications. Chaos Theory and Applications **4**: 197–204.

Niel, O., 2023 A novel algorithm can generate data to train machine learning models in conditions of extreme scarcity of real world data. arXiv preprint arXiv:2305.00987 .

Palacios-Luengas, L., R. Marcelín-Jiménez, E. Rodriguez-Colina, M. Pascoe-Chalke, O. Jiménez-Ramírez, *et al.*, 2021 Function composition from sine function and skew tent map and its application to pseudorandom number generators. Applied Sciences **11**: 5769.

Sarker, I. H., 2021 Machine learning: Algorithms, real-world applications and research directions. SN computer science **2**: 160.

Sarker, I. H., M. H. Furhad, and R. Nowrozy, 2021 Ai-driven cybersecurity: an overview, security intelligence modeling and research directions. SN Computer Science **2**: 173.

Sethi, D., N. Nagaraj, and N. B. Harikrishnan, 2023 Neurochaos feature transformation for machine learning. Integration **90**: 157–162.

Sigillito, V. G., S. P. Wing, L. V. Hutton, and K. B. Baker, 1989 Classification of radar returns from the ionosphere using neural networks. Johns Hopkins APL Technical Digest **10**: 262–266.

Street, W. N., W. H. Wolberg, and O. L. Mangasarian, 1993 Nuclear feature extraction for breast tumor diagnosis. In *Biomedical image processing and biomedical visualization*, volume 1905, pp. 861–870, SPIE.

Suryadi, M., Y. Satria, V. Melvina, L. N. Prawadika, and I. M. Sholihat, 2020 A new chaotic map development through the composition of the ms map and the dyadic transformation map. In *Journal of Physics: Conference Series*, volume 1490, p. 012024, IOP Publishing.

Zhu, S., G. Wang, and C. Zhu, 2019 A secure and fast image encryption scheme based on double chaotic s-boxes. Entropy **21**: 790.

How to cite this article: Henry, A., and Nagaraj, N. Neurochaos Learning for Classification using Composition of Chaotic Maps. *Chaos Theory and Applications*, 7(2), 107-116, 2025.

CHAOS
Theory and Applications
in Applied Sciences and Engineering

e-ISSN: 2687-4539
RESEARCH ARTICLE
Vol.7 / No.2 / 2025 / pp.117-124
https://doi.org/10.51537/chaos.1633880

Analog Circuit Implementation of Fractional-Order Modified Chua's Circuit

Burak Arıcıoğlu [*,β,1]

*Faculty of Technology, Electrical-Electronics Engineering, Sakarya University of Applied Sciences , Serdivan, Türkiye, βBiomedical Technologies Application and Research Center (Biyotam), Sakarya University of Applied Sciences, Serdivan, Türkiye.

ABSTRACT In this paper, the analog circuit implementation of a fractional-order chaotic system is presented. Fractionalization is achieved by replacing integer-order capacitors and inductors with their fractional-order counterparts in Chua's circuit. The paper provides a model for implementing fractional-order capacitors and inductors in the circuit. The results obtained from simulating the fractional-order Chua's circuit are compared with those derived from the Grünwald-Letnikov numerical solution. All results show strong agreement.

KEYWORDS
Chaos
Chaotic systems
Fractional-order systems
Chua's circuit
Circuit realization

INTRODUCTION

Chaos, as a science subject, was introduced by Edward Lorenz (Lorenz 1963). Later, Chua's circuit (Matsumoto 1984) became very important in the advancement of chaos science because it is the simplest autonomous chaotic circuit. In addition, when chaos was first introduced, few mathematical tools were available, so experimental methods were more favourable. In Chua's circuit, obtaining data experimentally is straightforward, which contributed to its widespread attention in the literature (Wu 1987).

In recent years, fractional-order chaos has become a topical subject because fractional-order chaotic systems exhibit richer dynamic behaviour than their integer order counterparts (Sheu *et al.* 2008). Numerous studies in the literature have explored the fractionalization of Chua's circuit. In most of these studies, only the system obtained from Chua's circuit is fractionalized mathematically without analog circuit implementation (Sene 2021; De la Sen *et al.* 2021; Boudjerida *et al.* 2022; Younis *et al.* 2025). Moreover, in some studies, Chua's circuit is fractionalized digitally so that it is implementation is carried out via a microcontroller (Wang *et al.* 2021; Wu *et al.* 2025) or an FPGA (field programable gate array) (Abd El-Maksoud *et al.* 2018; Wu *et al.* 2024; Abd El-Maksoud *et al.* 2019; Taşdemir *et al.* 2025).

Nowadays, there are numerous method implement chaotic system digitally (Emin and Yaz 2024; Kıran 2024; Seyyarer *et al.* 2025). However, in the analog realization, the system may exhibit more chaotic behaviour than in the digital realization because of the finite sampling intervals and precision (Michaels, A. J. 2011). Moreover, the analog circuit components are less complex and therefore much cheaper than digital circuit components.

This study aims to implement and validate an analog fractional-order Chua's circuit using fractional-order capacitors and inductors, comparing its behaviour with numerical simulations based on the Grünwald-Letnikov method. For the circuit implementation, a model for the fractional-order capacitor and inductor is introduced.

The main contribution of this study is the analog implementation of fractionalized Chua's circuit. The other main contribution is implementing fractional-order capacitor and inductor which are employed in many different study fields such as: control (Swain *et al.* 2017), fractional-order oscillators (Ahmad *et al.* 2001), fractional-order filters (Adhikary *et al.* 2016), fractional-order resonators (Adhikary *et al.* 2016), modelling of lithium-ion batteries (Zou, *et al.* 2017), modelling of neural networks (Peasgood *et al.* 2003) and so on.

The organization of the article is as follows. In the second section, the fractional-order operator and the modelling of the fractional-order capacitor and inductor is given. In the next section, fractional-order Chua's circuit are given. In the later section, the circuit implementation of the fractional-order Chua's circuit is presented. Finally, the conclusion is given in the last section.

Manuscript received: 5 February 2025,
Revised: 10 March 2025,
Accepted: 14 April 2025.

[1]baricioglu@subu.edu.tr (**Corresponding author**)

FRACTIONAL-ORDER CAPACITOR AND INDUCTOR

The Riemann–Liouville (RL) definition of fractional-order integrator is

$$ {}_0D_t^{-q} f(t) = \int_0^t \frac{(t-\tau)^{q-1}}{\Gamma(q)} f(\tau) d\tau \tag{1} $$

here q is the fractional-order. For a fractional-order capacitor, the relationship between the voltage and the current is

$$ v_C(t) = \frac{1}{C} {}_0D_t^{-q} i_C(t) = \frac{1}{C} \int_0^t \frac{(t-\tau)^{q-1}}{\Gamma(q)} i_C(\tau) d\tau \tag{2} $$

Here $v_C(t)$ is the voltage across the capacitor and $i_C(t)$ is the current passes through the capacitor. If we take the Laplace transform of Equation 2

$$ V_C(s) = \frac{1}{C} L\{{}_0D_t^{-q} i_c(t)\} = \frac{1}{C} \frac{1}{s^q} I_C(s) \tag{3} $$

From Equation 3 the impedance of the fractional-order capacitor obtained as

$$ Z_C(s) = \frac{V_C(s)}{I_C(s)} = \frac{1}{C} \frac{1}{s^q} \tag{4} $$

The impedance given in Equation 4 cannot be implemented using discrete components. However, its impedance function can be approximated as described in (Charef *et al.* 1992). This approximation is given in Equation 5

$$ \frac{1}{C} \frac{1}{s^q} \cong \frac{1}{C} \frac{1}{p_t^q} \frac{1}{\left(1 + \frac{s}{p_t}\right)^q} \cong \frac{1}{C} \frac{1}{p_t^q} \frac{\prod_{i=0}^{N-1} \left(1 + \frac{s}{z_i}\right)}{\prod_{i=0}^{N} \left(1 + \frac{s}{p_i}\right)} \tag{5} $$

Here C is the capacitance of the fractional-order capacitor, q is the fractional-order, p_t is the corner frequency (alternatively $1/p_t$ is the relaxation time), and z_i, and p_i are the zeros and poles of the approximated impedance function respectively. The value of N in Equation 5 is calculated as (Charef *et al.* 1992)

$$ N = Integer \left(\frac{\log\left(\frac{w_{\max}}{p_0}\right)}{\frac{y}{10q(1-q)}} \right) + 1 \tag{6} $$

Also, the values of the poles and zeros of the approximated impedance function are calculated (Charef *et al.* 1992):

$$ \begin{aligned} p_0 &= p_t 10^{y/20q} \\ z_i &= (10^{y/10q(1-q)})^i 10^{y/10(1-q)} p_0 \\ p_i &= (10^{y/10q(1-q)})^i p_0 \end{aligned} \tag{7} $$

Here y is the maximum error in dB between the actual and the approximated lines. After all the poles and the zeros of the approximated impedance function are calculated, the partial fraction decomposition is performed to the right side of Equation 5.

$$ \frac{1}{C} \frac{1}{p_t^q} \frac{\prod_{n=0}^{N-1} \left(1 + \frac{s}{z_i}\right)}{(s+p_o)(s+p_1)\ldots(s+p_N)} = \frac{r_0}{s+p_0} + \frac{r_1}{s+p_1} + \ldots + \frac{r_N}{s+p_N} \tag{8} $$

As seen in Equation 7, all the poles and zeros are in alternate order, hence all the residues in Equation 8 are positive constants. Because of this, the approximated impedance function can be implemented using passive elements. The simple fractions on the right side of Equation 8 can be easily realized by parallel connected RC elements. The value of the resistors and capacitors is calculated as:

$$ \begin{aligned} C_i &= \frac{1}{r_i} \\ R_i &= \frac{r_i}{p_i} \end{aligned} \tag{9} $$

The approximated impedance for the fractional-order capacitor is given in Figure 1.

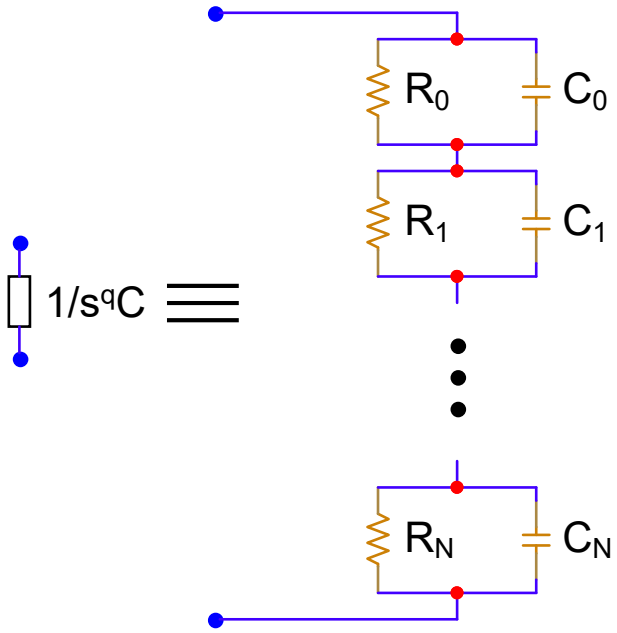

Figure 1 The approximated circuit for the fractional-order capacitor.

For a fractional-order induct-or, the relationship between the voltage and the current is

$$ v_L(t) = L_0 D_t^q i_L(t) = L \frac{1}{\Gamma(1-q)} \frac{d}{dt} \int_a^t \frac{i_L(\tau)}{(t-\tau)^q} d\tau \tag{10} $$

Here $v_L(t)$ is the voltage across the inductor and $i_L(t)$ is the current passes through the inductor. If we take the Laplace transform of Equation 10

$$ V_L(s) = L\, L\{{}_0D_t^q i_L(t)\} = L s^q I_L(s) \tag{11} $$

From Equation 11 the admittance of the fractional-order inductor obtained as

$$ Y_L(s) = \frac{I_L(s)}{V_L(s)} = \frac{1}{L} \frac{1}{s^q} \tag{12} $$

The admittance given in Equation 12 cannot be implemented using discrete components. However, its admittance function can be approximated as described in (Charef *et al.* 1992). This approximation is given in Equation 13

$$ \frac{1}{L} \frac{1}{s^q} \cong \frac{1}{L} \frac{1}{p_t^q} \frac{1}{\left(1 + \frac{s}{p_t}\right)^q} \cong \frac{1}{L} \frac{1}{p_t^q} \frac{\prod_{i=0}^{N-1} \left(1 + \frac{s}{z_i}\right)}{\prod_{i=0}^{N} \left(1 + \frac{s}{p_i}\right)} \tag{13} $$

Here L is the inductance of the fractional-order inductor, q is the fractional-order, p_t is the corner frequency (alternatively $1/p_t$ is the relaxation time), and z_i and p_i are the zeros and poles of the approximated admittance function respectively.

Here the value of N and, z_i, and p_i is calculated using Equation 6 and 7 respectively.

After all the poles and the zeros of the approximated admittance function are calculated, the partial fraction decomposition is performed to the right side of Equation 13.

$$\frac{1}{L}\frac{1}{p_t^q}\frac{\prod_{n=0}^{N-1}\left(1+\frac{s}{z_i}\right)}{(s+p_o)(s+p_1)\ldots(s+p_N)} = \frac{r_0}{s+p_0}+\frac{r_1}{s+p_1}+\ldots+\frac{r_N}{s+p_N} \tag{14}$$

As seen in Equation 7, all the poles and zeros are in alternate order, hence all the residues in Equation 14 are positive constants, too. This enables the implementation of the approximated admittance function using passive elements. The simple fractions on the right side of Equation 14 can be easily realized by series connected RL elements. The value of the resistors and inductors is calculated as:

$$\begin{aligned} L_i &= \frac{1}{r_i} \\ R_i &= \frac{p_i}{r_i} \end{aligned} \tag{15}$$

The approximated admittance for the fractional-order inductor is given in Figure 2.

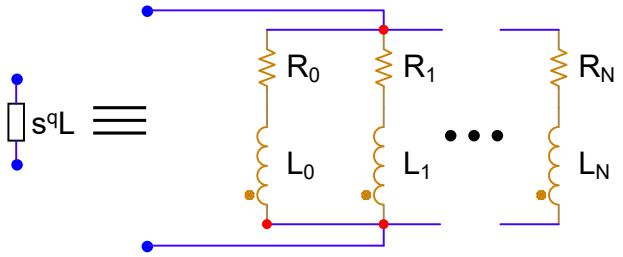

Figure 2 The approximated circuit for the fractional-order inductor.

FRACTIONAL-ORDER CHUA'S CIRCUIT

In this section, fractional-order Chua's circuit analysis is presented. The fractional-order Chua's circuit is given in Figure 3. In the modified version, only the nonlinear resistor (G_N) is changed as proposed by (Tang *et al.* 2003) with respect to the original circuit. In the modified version, the nonlinear resistor contains the $x|x|$ function instead of a piece-wise linear function.

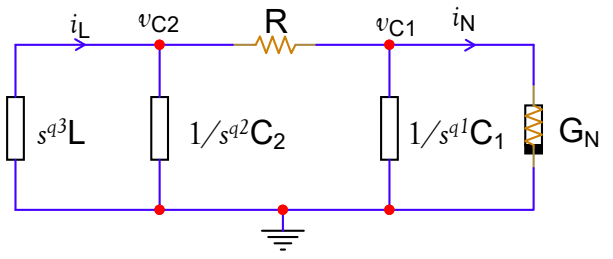

Figure 3 The fractional-order Chua's circuit.

For the modified nonlinear resistor, the voltage and current relationship is given in Equation 16.

$$i_N = g(v_N) = \alpha v_n + \beta v_n|v_n| \tag{16}$$

Here, i_N is the current passes through the nonlinear resistor and v_N is the voltage across the nonlinear resistor. As seen in Equation 16, the current of the nonlinear resistor is a function of the voltage.

If Kirchhoff's current law (KCL) is applied to the nodes v_{C1}, and v_{C2} the following fractional-order differential equation set is obtained.

$$\begin{aligned} C_1\,{}_0D_t^{-q_1}v_{C1} &= -\frac{v_{C1}-v_{C2}}{R} - g(v_{C1}) \\ C_2\,{}_0D_t^{-q_2}v_{C2} &= -\frac{v_{C2}-v_{C1}}{R} + i_L \\ L\,{}_0D_t^{-q_3}i_L &= -v_{C2} \end{aligned} \tag{17}$$

Then Equation 17 can be rewritten as:

$$\begin{aligned} {}_0D_t^{-q_1}v_{C1} &= -\frac{v_{C1}-v_{C2}}{RC_1} - \frac{1}{C_1}g(v_{C1}) \\ {}_0D_t^{-q_2}v_{C2} &= -\frac{v_{C2}-v_{C1}}{RC_2} + \frac{1}{C_2}i_L \\ {}_0D_t^{-q_3}i_L &= -\frac{1}{L}v_{C2} \end{aligned} \tag{18}$$

A fractional-order chaotic system can be obtained from Chua's circuit as in Equation 18. In the fractional-order chaotic system, the state variables are v_{C1}, v_{C2}, and i_L.

To investigate the dynamic behaviour of the fractional-order system, bifurcation diagrams and Lyapunov exponent analysis are carried out (Khan *et al.* 2025). In Fig. 4 bifurcation diagram is plotted with respect to the fractional-order q. In this bifurcation diagram, period doubling route to chaos is observed.

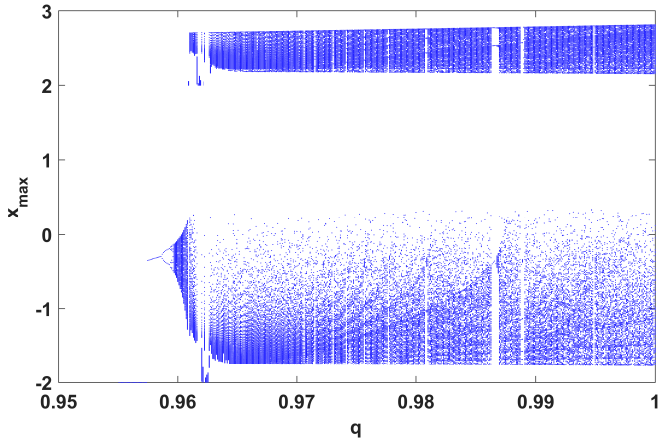

Figure 4 The bifurcation diagram with respect to the fractional-order q for the values of the circuit elements $R = 1, C_1 = 0.1079, C_2 = 1$, and $L = 0.0833$; and the initial conditions $v_{C1} = -1.01, v_{C2} = -0.01$, and $i_L = -0.01$.

Then, the bifurcation diagram is plotted with respect to the resistor R and shown in Fig. 5. In this bifurcation diagram, period doubling and period halving bifurcation is observed.

As a final dynamic analysis, the Lyapunov exponents are plotted and given in Fig. 6. As seen in Fig. 4, 5 and 6 the fractional-order system with given parameter values exhibits chaotic behaviour.

In this section, the numerical calculation of fractional-order Chua's circuit is also presented. For the numerical calculations, the

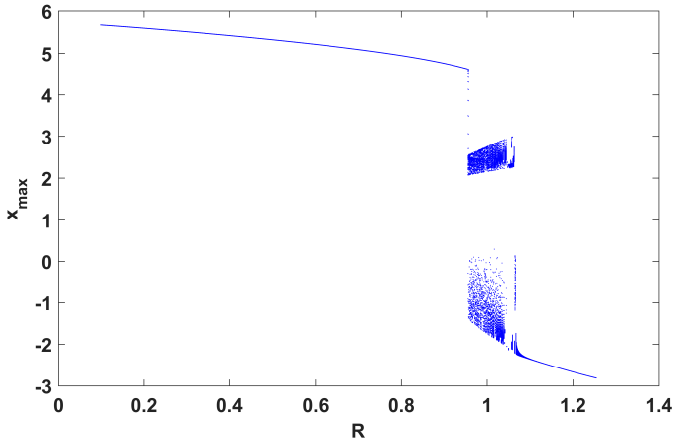

Figure 5 The bifurcation diagram with respect to the resistor R for the fractional-orders $q_1 = 0.96, q_2 = 0.97$, and $q_3 = 0.98$; the values of the circuit elements $C_1 = 0.1079, C_2 = 1$, and $L = 0.0833$; and the initial conditions $v_{C1} = -1.01, v_{C2} = -0.01$, and $i_L = -0.01$.

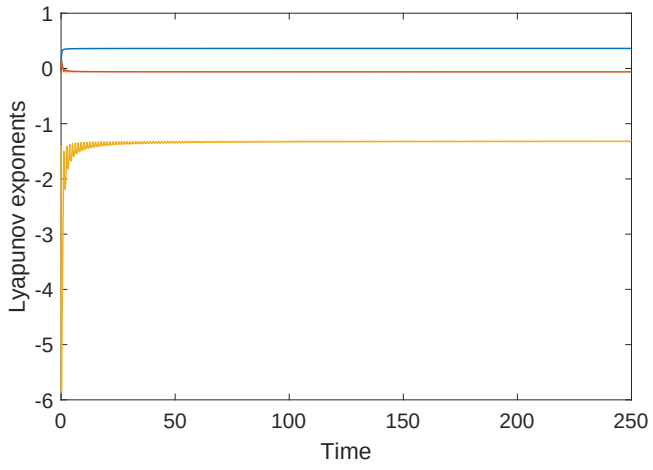

Figure 6 The Lyapunov exponents for the fractional-orders $q_1 = 0.96, q_2 = 0.97$, and $q_3 = 0.98$; the values of the circuit elements $R = 1, C_1 = 0.1079, C_2 = 1$, and $L = 0.0833$; and the initial conditions $v_{C1} = -1.01, v_{C2} = -0.01$, and $i_L = -0.01$.

Grünwald-Letnikov (GL) method is used since the finite difference-based definition of the GL is equivalent to the RL definition (Scherer *et al.* 2011; Chen *et al.* 2019).

Then, the fractional-order Grünwald–Letnikov fractional integral is:

$$ {}_0D_t^{-q} f(t) = \lim_{h \to 0} h^q \sum_{i=0}^{\frac{t}{h}} (-1)^i \binom{-q}{i} f(t - ih) \tag{19} $$

Here $f(t)$ is the differentiable function, q is the fractional-order, h is the step size, and $\binom{-q}{i}$ is the binomial coefficients.

In the numerical calculations the value of $R = 1, C_1 = 0.1079$, $C_2 = 1$, and $L = 0.0833$. Also, the values of parameters $\alpha = -1.5$ and $\beta = 0.25$, the initial conditions are selected as $v_{C1} = -1.01$, $V_{C2} = -0.01$, and $i_L = -0.01$ as given in (Wang *et al.* 2021). The voltage-current relationship graph of the nonlinear resistor is given in Figure 7. And the fractional-orders are selected as $q_1 = 0.96$, $q_2 = 0.97$, and $q_3 = 0.98$.

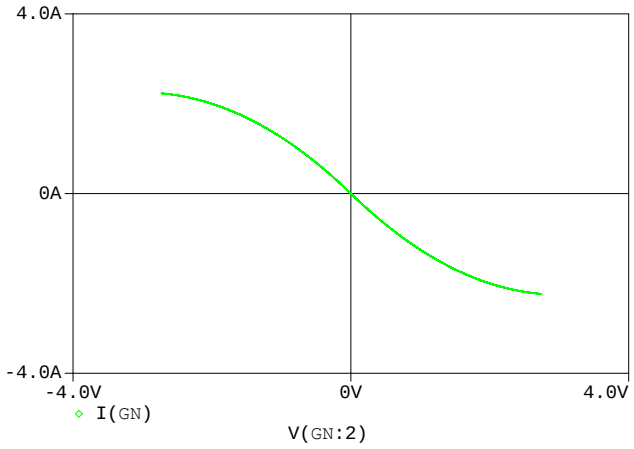

Figure 7 The voltage-current relationship of the nonlinear resistor .

For the given parameter values the fractional-order chaotic system in Equation 18 can be written as

$$ \begin{aligned} {}_0D_t^{-0.96} v_{C1} &= -9.267(v_{C1} - v_{C2}) - 9.267\left(-1.5v_{C1} + 0.25v_{C1}|v_{C1}|\right) \\ {}_0D_t^{-0.97} v_{C2} &= -\left(v_{C2} - v_{C1}\right) + i_L \\ {}_0D_t^{-0.98} i_L &= -12v_{C2} \end{aligned} \tag{20} $$

In Figure 8 the time series, in Figure 9 the phase portraits obtained from the numerical calculation are shown.

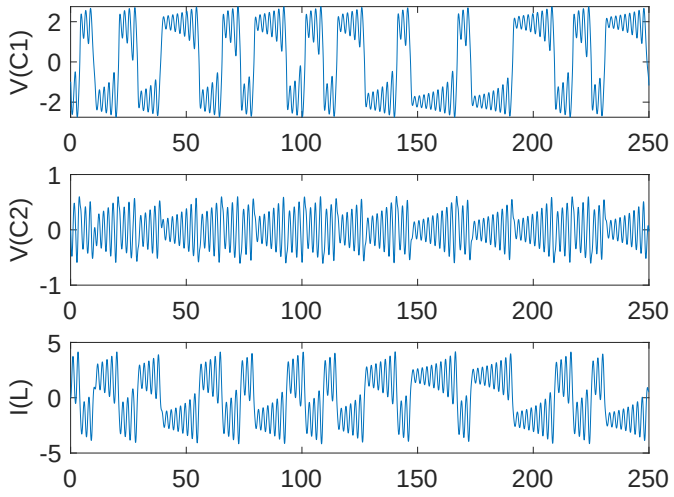

Figure 8 The time series of the fractional-order chaotic system when the fractional-orders $q_1 = 0.96, q_2 = 0.97$, and $q_3 = 0.98$; the values of the circuit elements $R = 1, C_1 = 0.1079, C_2 = 1$, and $L = 0.0833$; and the initial conditions $v_{C1} = -1.01, v_{C2} = -0.01$, and $i_L = -0.01$.

CIRCUIT IMPLEMENTATION

In this section, the circuit implementation of the fractional-order Chua's circuit and its simulation results are presented.

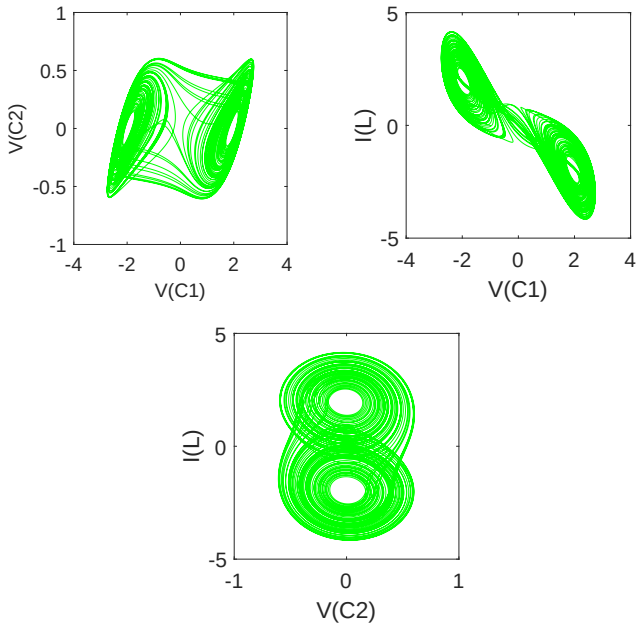

Figure 9 The phase portraits of the fractional-order chaotic system when the fractional-orders $q_1 = 0.96, q_2 = 0.97$, and $q_3 = 0.98$; the values of the circuit elements $R = 1, C_1 = 0.1079, C_2 = 1$, and $L = 0.0833$; and the initial conditions $v_{C1} = -1.01, v_{C2} = -0.01$, and $i_L = -0.01$.

In all the approximated impedance of admittance calculations, the maximum error $y = 0.3$ dB, the corner frequency $p_t = 0.01$rad/sec, and the maximum frequency $\omega_m ax = 100$ rad/sec.

For the fractional-order capacitor C_1 in Figure 3, the fractional-order is selected as $q_1 = 0.96$ and the value of $C_1 = 0.1079$F. For this case, the approximated impedance function has eight poles, and the values of the capacitors and resistors in the approximated impedance function are given in Table 1.

In Figure 10, the approximated and the actual impedance function is given for the frequency range of interest.

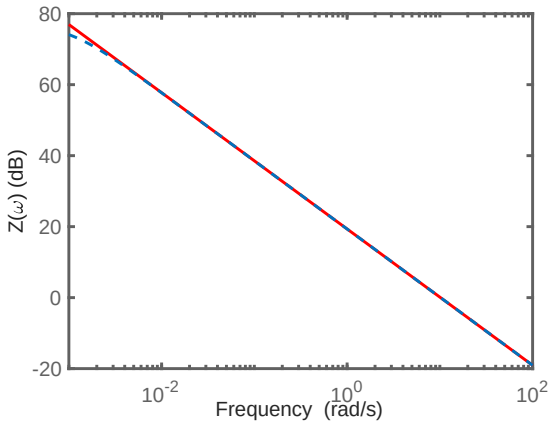

Figure 10 The approximated (blue dash) and the actual (red line) impedance function for the fractional-order capacitor C_1 over the frequency range of 0.001-100 rad/sec.

For the fractional-order capacitor C_2 in Figure 3, the fractional-order is selected as $q_2 = 0.97$ and the value of $C_2 = 1$F. For this case, the approximated impedance function has six poles, and the values of the capacitors and resistors in the approximated impedance function are given in Table 2.

In Figure 11, the approximated and the actual impedance function is given for the frequency range of interest.

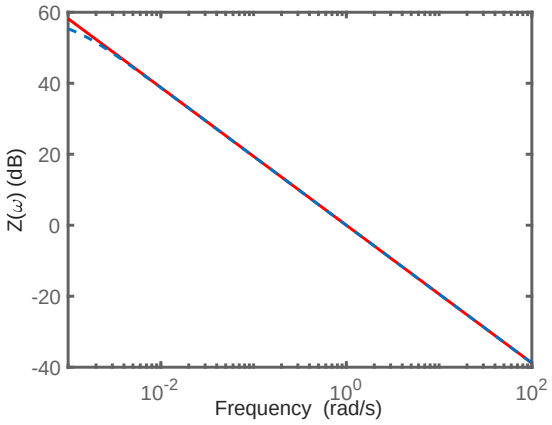

Figure 11 The approximated (blue dash) and the actual (red line) impedance function for the fractional-order capacitor C_2 over the frequency range of 0.001-100 rad/sec.

For the fractional-order inductor L in Figure 3, the fractional-order is selected as $q_3 = 0.98$ and the value of $L = 0.0833$H. For this case, the approximated admittance function has five poles, and the values of the inductors and resistors in the approximated admittance function are given in Table 3.

In Figure 12, the approximated and the actual admittance function is given for the frequency range of interest.

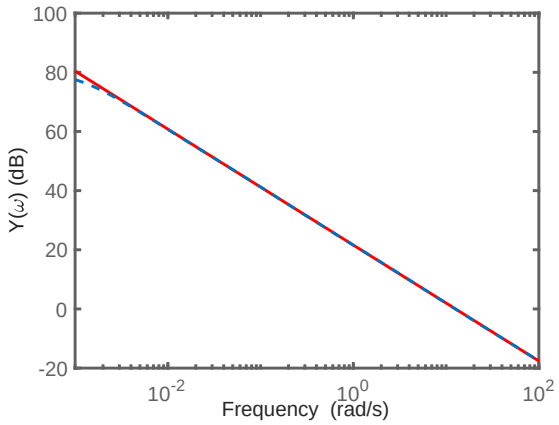

Figure 12 The approximated (blue dash) and the actual (red line) admittance function for the fractional-order inductor L over the frequency range of 0.001-100 rad/sec.

In Figure 13, the complete circuit for the fractional-order Chua's circuit is shown. The nonlinear resistor is modelled with an analog behaviour model (ABM) device in Spice

The time series and the phase portraits obtained from the simulation of the fractional-order Chua's circuit are shown in Figure 14 and 15, respectively.

Table 1 The values of capacitors and resistors for the approximation of fractional-order capacitor C_1 in Figure 3.

n	0	1	2	3	4	5	6	7
C_i(F)	0.140	1.562	1.671	1.588	1.483	1.381	1.282	1.175
$R_i(\Omega)$	6908.38	102.21	15.81	2.75	0.488	0.0867	0.0155	0.0028

Table 2 The values of capacitors and resistors for the approximation of fractional-order capacitor C_2 in Figure 3.

n	0	1	2	3	4	5
C_i(F)	1.197	14.709	14.868	13.947	12.989	12.005
$R_i(\Omega)$	806.10	6.11	0.563	0.0559	0.0056	0.0006

Table 3 The values of capacitors and resistors for the approximation of fractional-order capacitor C_2 in Figure 3.

n	0	1	2	3	4
L_i(H)	0.093	1.230	1.178	1.099	1.022
$R_i(\Omega)$	0.0001	0.043	1.40	44.46	1402.82

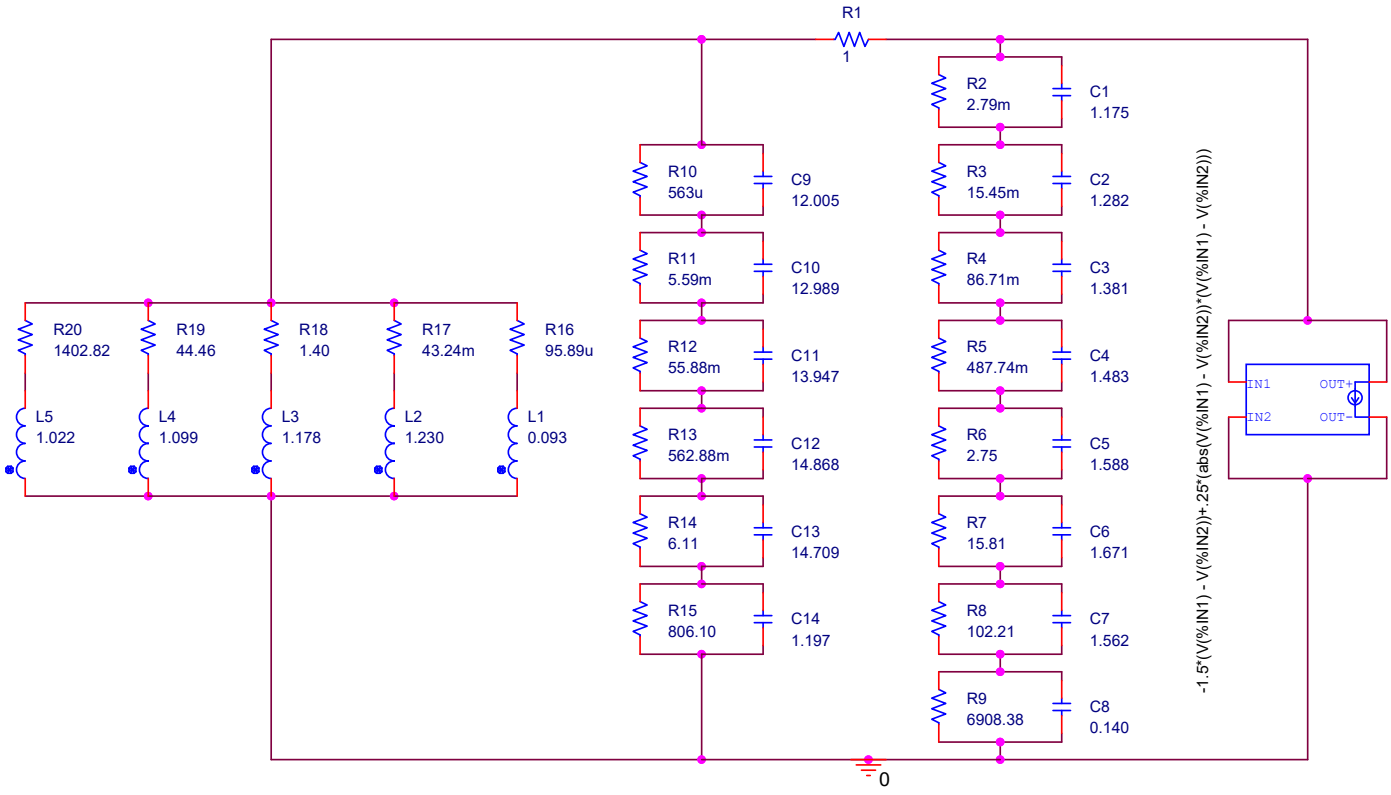

Figure 13 The circuit implementation of the fractional-order Chua's circuit when the fractional-orders $q_1 = 0.96, q_2 = 0.97$, and $q_3 = 0.98$; the values of the circuit elements $R = 1, C_1 = 0.1079, C_2 = 1$, and $L = 0.0833$.

As seen in Figure 8, 9,14, and 15, the time series and the phase portraits obtained from numeric calculation and simulation are very close to each other. This shows that the fractional-order Chua's circuit is realized successfully. In addition, the modelling of fractional-order capacitor, and inductor is accurate enough.

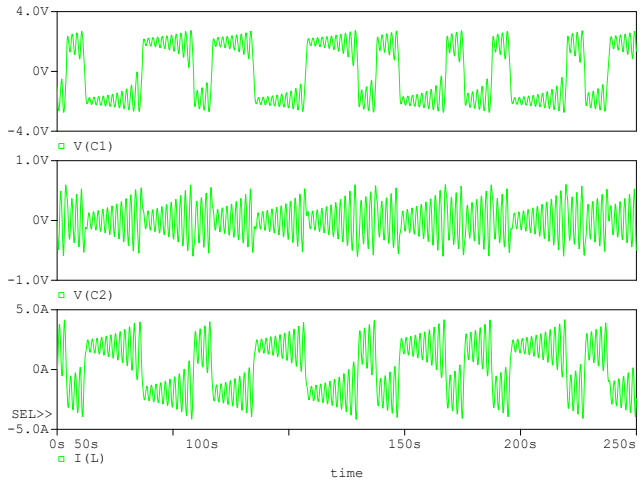

Figure 14 The time series of the fractional-order Chua's circuit when the fractional-orders $q_1 = 0.96, q_2 = 0.97$, and $q_3 = 0.98$; the values of the circuit elements $R = 1, C_1 = 0.1079, C_2 = 1$, and $L = 0.0833$; and the initial conditions $v_{C1} = -1.01, v_{C2} = -0.01$, and $i_L = -0.01$.

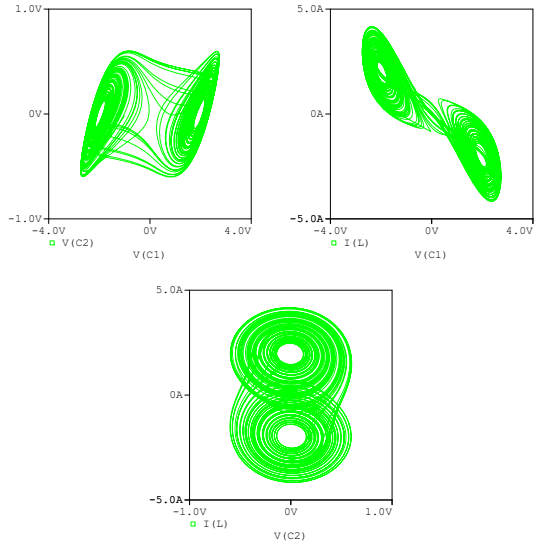

Figure 15 The phase portraits of the fractional-order Chua's circuit when the fractional-orders $q_1 = 0.96, q_2 = 0.97$, and $q_3 = 0.98$; the values of the circuit elements $R = 1, C_1 = 0.1079, C_2 = 1$, and $L = 0.0833$; and the initial conditions $v_{C1} = -1.01, v_{C2} = -0.01$, and $i_L = -0.01$

CONCLUSION

In this study, Chua's circuit is fractionalized by using fractional-order capacitors and an inductor. By applying the circuit analysis to the fractionalized Chua's circuit, a fractional-order chaotic system is obtained and is solved numerically with the GL algorithm. Then, the analog realization of the fractional-order Chua's circuit is successfully implemented. In the paper, it is shown that the numerical and simulation results are in good accordance. This is one of the main contributions of the paper, since in most of the studies Chua's circuit is fractionalized either numerically or digitally. Another contribution is that the paper presents modelling of fractional-order capacitor and inductor. For the presented method to be applicable for the modelling of the fractional-order capacitor and inductor, the fractional-order must vary between 0 and 1($0 < q < 1$). Final remark, there is no direct method for determining the value of maximum error y and the frequency range other than trial and error.

Ethical standard

The author has no relevant financial or non-financial interests to disclose.

Availability of data and material

Not applicable.

Conflicts of interest

The author declares that there is no conflict of interest regarding the publication of this paper.

LITERATURE CITED

Abd El-Maksoud, A. J., A. A. Abd El-Kader, B. G. Hassan, M. A. Abdelhamed, N. G. Rihan, *et al.*, 2018 FPGA implementation of fractional-order Chua's chaotic system. In *2018 7th international conference on modern circuits and systems technologies (MOCAST)*, (pp. 1–4), IEEE.

Abd El-Maksoud, A. J., A. A. Abd El-Kader, B. G. Hassan, N. G. Rihan, M. F. Tolba, *et al.*, 2019 FPGA implementation of sound encryption system based on fractional-order chaotic systems. Microelectronics Journal **90**: 323–335.

Adhikary, A., S. Sen, and K. Biswas, 2016 Practical realization of tunable fractional order parallel resonator and fractional order filters. IEEE Transactions on Circuits and Systems I: Regular Papers **63(8)**: 1142–1151.

Ahmad, W., R. El-Khazali, and A. S. Elwakil, 2001 Fractional-order Wien-bridge oscillator. Electronics Letters **37(18)**: 1110–1112.

Boudjerida, N., M. S. Abdelouahab, R. Lozi, 2022 Modified projective synchronization of fractional-order hyperchaotic memristor-based Chua's circuit. Journal of Innovative Applied Mathematics and Computational Sciences **2(3)**: 69–85.

A. Charef, H. H. Sun, Y. Y. Tsao, and B. Onaral, 1992 Fractal system as represented by singularity function. IEEE Transactions on automatic Control **37(9)**: 1465–1470.

H. Chen, F. Holland, and M. Stynes, 2019 An analysis of the Grünwald-Letnikov scheme for initial-value problems with weakly singular solutions. Applied Numerical Mathematics **139**: 52–61.

De la Sen, M., S. Deniz, and H. Sözen, 2021 A new efficient technique for solving modified Chua's circuit model with a new fractional operator. Advances in Difference Equations **2021**: 1–16.

Emin, B., and M. Yaz, 2024 Digital Implemen-tation of Chaotic Systems Using Nvidia Jetson AGX Orin andCustom DAC Converter. Chaos and Fractals **1(1)**: 38–41.

Khan A., C. Li, Z. Zhang, and X. Cen, 2025 ATwo-memristor-based Chaotic System with Symmetric Bifurcationand Multistability. Chaos and Fractals **2(1)**: 1–7.

Kiran, H. E., 2025 A Novel Chaos-Based Encryp-tion Technique with Parallel Processing Using CUDA for MobilePowerful GPU Control Center. Chaos and Fractals **1(1)**: 6–18.

Lorenz, E. N., 1963 Deterministic nonperiodic flow. Journal of atmospheric sciences **20(2)**: 130–141.

Matsumoto, T., 1984 A chaotic attractor from Chua's circuit. IEEE transactions on circuits and systems **31(12)**: 1055–1058.

Michaels, A. J., 2011 Quantitative comparisons of digital chaotic circuits for use in communications. In *roceedings of the Joint INDS 11 & ISTET 11*, (pp. 1–8), IEEE.

Peasgood, W., L. A. Dissado, C. K. Lam, A. Armstrong, and W. Wood, 2003 A novel electrical model of nerve and muscle using Pspice. Journal of Physics D: Applied Physics **36(4)**: 311.

Scherer, R., S.L. Kalla, Y. Tang, and J. Huang, 2011 The Grünwald-Letnikov method for fractional differential equations. Computers & Mathematics with Applications **62(3)**: 902–917.

Sene, N., 2021 Mathematical views of the fractional Chua's electrical circuit described by the Caputo-Liouville derivative. Revista mexicana de fisica **67(1)**: 91–99.

Seyyarer, E., F. Ayata, and S. Özdem, 2025 The Role of Technological Approaches in Cyber Security of Au-tonomous Vehicles. ADBA Computer Science **2(1)**, 1–6.

Sheu, L. J., H.K. Chen, J. H. Chen, L. M. Tam, W. C. Chen, *et al.*, 2008. Chaos in the Newton–-Leipnik system with fractional order. Chaos, Solitons & Fractals **36(1)**: 98–103.

Swain, S. K., D. Sain, S. K. Mishra, and S. Ghosh, 2017 Real time implementation of fractional order PID controllers for a magnetic levitation plant. AEU-International Journal of Electronics and Communications **78**: 141–156.

Tang, K. S., K. F. Man, G. Q. Zhong, and G. Chen, 2003 Modified Chua's circuit with $x|x|$. Control Theory and Application **20**: 223–227.

Taşdemir, M. F., M. Tuna, and I. Koyuncu, 2025 FPGA-Based Chaotic Oscillator Designs and Performance Analysis. Chaos and Fractals **2(1)**, 8–13.

Wang, J., L. Xiao, K. Rajagopal, A. Akgul, S. Cicek, and B. Aricioglu, 2021 Fractional-order analysis of modified Chua's circuit system with the smooth degree of 3 and its microcontroller-based implementation with analog circuit design. Symmetry **13(2)**: 340.

Wu, C., L. Xiong, and N. Yang, 2024 Modeling and dynamics analysis of a novel fractional-order meminductive multi-stable chaotic circuit and its FPGA implementation. Chaos, Solitons & Fractals **186**: 115222.

Wu, S., 1987 Chua's circuit family. Proceedings of the IEEE **75(8)**: 1022–1032.

Wu, X., K. Hu, S. He, H. Wang, and Z. Zhang, 2025 A fractional-order Chua's system: System model, numerical simulations, hidden dynamics, DSP implementation and voice encryption application. AEU-International Journal of Electronics and Communications 155691.

Younis, M., H. Ahmad, M. Ozturk, and D. Singh, 2025 A novel approach to the convergence analysis of chaotic dynamics in fractional order Chua's attractor model employing fixed points. Alexandria Engineering Journal **110**: 363–375.

Zou, C., X. Hu, S. Dey, L. Zhang, and X. Tang, 2017 Nonlinear fractional-order estimator with guaranteed robustness and stability for lithium-ion batteries. IEEE Transactions on Industrial Electronics **65(7)**: 5951–5961.

How to cite this article: Arıcıoğlu, B. Analog Circuit Implementation of Fractional-Order Modified Chua's Circuit. *Chaos Theory and Applications*, 7(2), 117-124, 2025.

CHAOS
Theory and Applications
in Applied Sciences and Engineering

e-ISSN: 2687-4539
RESEARCH ARTICLE
Vol.7 / No.2 / 2025 / pp.125-137
https://doi.org/10.51537/chaos.1615617

Modeling and Analysis of Nonlinear Chaotic Mechanical Dynamics in Laser Scanning Systems

José A. Núñez-López[*,1], **David Meza-García**[*,2], **Oleg Sergiyenko**[*,3], **Vera Tyrsa**[δ,4], **Julio C. Rodríguez-Quiñonez**[δ,5], **Wendy Flores-Fuentes**[δ,6], **Fernando Lopez-Medina**[*,7], **Cesar Sepulveda-Valdez**[*,8], **J. Fabián Villa-Manriquez**[*,9], **Humberto Andrade-Collazo**[*,10], **Evgeny Burnaev**[α,11], **Svetlana Illarionova**[α,12], **Danilo Cáceres- Hernández**[β,13] **and Ruben Alaniz-Plata**[*,14]

[*]Engineering Institute, Autonomous University of Baja California, Mexicali, Mexico, [δ]Engineering Faculty, Autonomous University of Baja California, Mexicali, Mexico, [α]Skolkovo Institute of Science and Technology (Skoltech), Moscow, Russia, [β]Intelligent Systems Laboratory, Faculty of Electrical Engineering, Technological University of Panama, Panama.

ABSTRACT This paper presents a novel approach to modeling and analyzing chaotic mechanical vibrations in laser scanning systems. The model explicitly incorporates nonlinear friction using the LuGre friction model. Experimental validation demonstrates chaotic behavior manifested in irregular velocity fluctuations. Dominant frequencies and maximum vibration amplitudes were identified under various operational conditions. A maximum disturbance amplitude of 1.65 rad/s² was observed under the most demanding conditions (25 RPS, ±15° inclination). The proposed model was validated experimentally, providing insights into the interplay of chaotic vibrations and nonlinear friction. A robust control strategy was introduced to mitigate these effects. This strategy is supported by Lyapunov stability analysis and computational implementation. The results demonstrate the effectiveness of the control strategy in reducing the negative effects of friction and chaotic vibrations. The findings could benefit precision engineering, nonlinear dynamics research, and machine vision.

KEYWORDS
Chaos theory
Nonlinear dynamics
Friction
Vibrations
Laser scanning

INTRODUCTION

Laser scanners are essential tools in industry, providing precise distance mapping and high-speed image processing capabilities. These systems are widely applied in tasks such as accurate measurements, part identification, and robotic control (Sergiyenko *et al.* 2020). An example is the Technical Vision System (TVS), described in (Lindner 2021), which integrates a laser scanning system utilizing the Dynamic Triangulation measurement method to calculate 3D coordinates within its field of view (FOV). The system employs electric motors to drive both the positioning laser (PL) and the scanning aperture (SA), enabling mapping across the FOV.

Friction is a complex and nonlinear phenomenon arising from the contact between surfaces, significantly affecting the positioning accuracy of mechanical systems (Gohar and Rahnejat 2012). Various models have been proposed over time to describe friction, each with its limitations in capturing all its effects (Canudas de Wit *et al.* 1995; Armstrong-Hélouvry *et al.* 1994; Popov *et al.* 2010). Understanding friction is crucial for designing control laws to mitigate its undesirable effects (Selivanov and Fridman 2023; Marton and Lantos 2007). Friction can be modeled as static or dynamic and is described using algebraic or differential equations (Armstrong-Hélouvry *et al.* 1994).

On the other hand, mechanical vibrations are a nonlinear and complex consequence of motion in mechanical systems (Lazutkin *et al.* 2017). These phenomena can arise from various sources, such as unbalanced forces, external excitations, or interactions be-

Manuscript received: 12 January 2025,
Revised: 18 March 2025,
Accepted: 21 April 2025.

[1]jose.nunez10@uabc.edu.mx
[2]david.meza.garcia@uabc.edu.mx (**Corresponding author**)
[3]srgnk@uabc.edu.mx
[4]vtyrsa@uabc.edu.mx
[5]julio.rodriguez81@uabc.edu.mx
[6]flores.wendy@uabc.edu.mx
[7]fernando.lopez.medina@uabc.edu.mx
[8]cesar.sepulveda@uabc.edu.mx
[9]fabian.manriquez@uabc.edu.mx
[10]humberto.andrade@uabc.edu.mx
[11]e.burnaev@skoltech.ru
[12]s.illarionova@skoltech.ru
[13]danilo.caceres@utp.ac.pa
[14]ruben.alaniz@uabc.edu.mx

tween components, and they significantly impact the stability and precision of positioning systems. Vibrations can exhibit chaotic behavior under certain conditions, further complicating their analysis and control (Zhao *et al.* 2010). While studies on nonlinear vibrations in cantilever beams and structural systems have provided insights into how stiffness and damping variations influence dynamic response (Pany and Rao 2004; Pany 2023; Pany and Rao 2002), in laser scanning systems, such vibrations, coupled with friction effects, can degrade the accuracy of the scanning process rather than geometric anisotropies, leading to errors in positioning and measurement (Liu *et al.* 2021).

This paper focuses on modeling and estimating the chaotic vibrations observed in laser scanning systems, specifically those influenced by frictional forces. By leveraging experimental data from MPU6050 vibration sensors and the open-loop response of the scanning aperture system, authors propose a comprehensive approach to analyze and mitigate these effects. The developed model and its validation through numerical simulations and physical experimentations aim to provide a robust tool for understanding and controlling the intricate dynamics of mechanical vibrations in these applications.

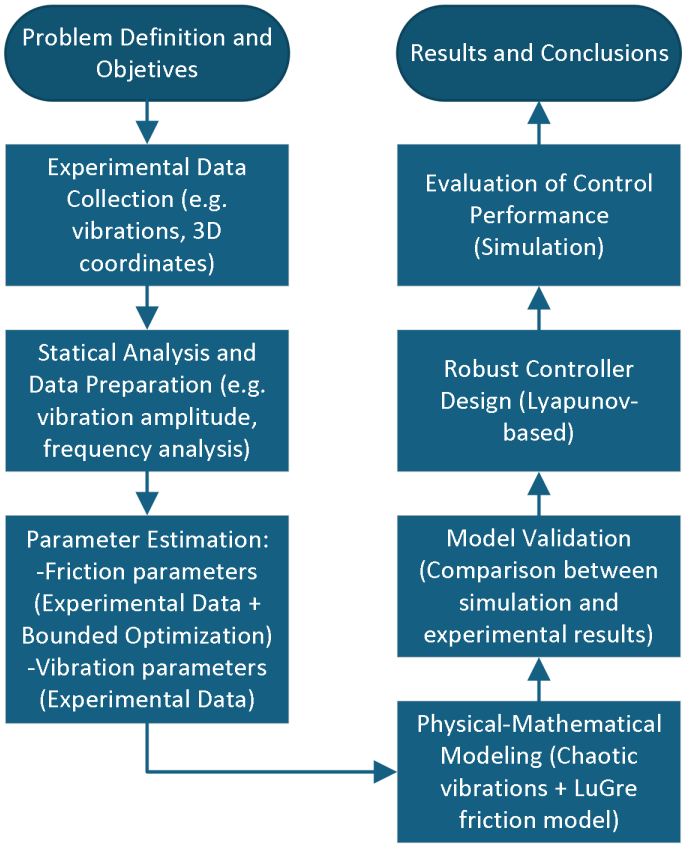

Figure 1 Overall methodology flow chart describing key stages of the research.

The novelty of this research lies in the explicit modeling and control of nonlinear chaotic vibrations coupled with frictional effects in laser scanning actuator subsystems, a topic scarcely addressed in current literature. While existing studies have explored nonlinear dynamics or friction individually, there remains a gap in simultaneously addressing chaotic vibrational disturbances combined with nonlinear friction in laser scanning actuator systems. This paper specifically addresses this gap by integrating the experimental characterization of chaotic vibrations into a robust nonlinear control framework, validated by Lyapunov stability analysis and experimental data.

Figure 1 shows the overall methodology followed in this study, highlighting the integration of experimental measurements, statistical analysis, physical-mathematical modeling, parameter estimation, validation, and robust control design.

TECHNICAL VISION SYSTEM

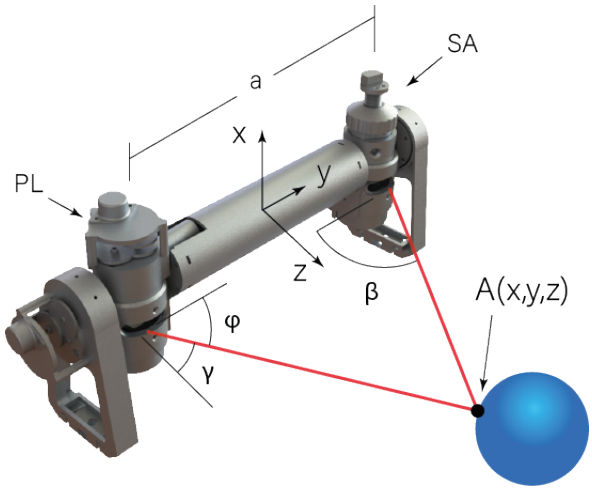

Figure 2 Diagram of the Laser Scanner TVS prototype.

The TVS (Figure 2) prototype was fabricated using PLA plastic filament via 3D printing, selected due to its mechanical properties that are suitable for lightweight robotic applications. Studies have reported the following characteristics for PLA:

- **Yield Strength:** 45 MPa (Al Khawaja *et al.* 2020).
- **Hardness:** Ranging from 55 to 76.33 Shore D in non-planar models (Atef *et al.* 2022).
- **Natural Frequency:** Approximately 214 Hz (Kushwaha *et al.* 2022).

These mechanical properties influence the structural behavior of the TVS, particularly its response to vibrations, which may affect coordinate accuracy. Since this prototype can be integrated into mobile robots or mounted on an optical table, different mechanical constraints may alter its vibrational response (Sergiyenko *et al.* 2020; Sepulveda-Valdez *et al.* 2024; Alaniz-Plata *et al.* 2025).

Dynamic Triangulation Method

The TVS operation is based on the dynamic triangulation method, which enables accurate three-dimensional mapping by combining angularly directed laser beams, reflective surface analysis, and geometric principles. The system is composed of two main subsystems: the Positioning Laser (PL) and the Scanning Aperture (SA). These components work together to capture and process the reflected light from obstacles, ultimately calculating the 3D coordinates of the reflection point with the following equations:

$$x = a\left(\frac{\sin(\varphi)\sin(\beta)}{\sin(\varphi+\beta)}\right) \tag{1}$$

$$y = a\left(\frac{1}{2} - \frac{\cos(\varphi)\sin(\beta)}{\sin(\varphi+\beta)}\right) \tag{2}$$

$$z = a\left(\frac{\cos(\varphi)\sin(\beta)\tan(\gamma)}{\sin(\varphi+\beta)}\right) \tag{3}$$

These equations allow determining a specific point in three-dimensional space (x, y, z) based on the given parameters, such as the angle φ, the angle β, the angle γ, and the value of a. The parameter a represents the fixed baseline distance between the Positioning Laser (PL) and the Scanning Aperture (SA). By varying the angles β and γ, multiple points in space are generated, allowing for the visualization of a broader spatial distribution. This approach is particularly useful for analyzing trajectories, point distributions, or patterns generated by angular variations in three-dimensional systems.

Positioning Laser

The Positioning Laser subsystem (Figure 3) is responsible for accurately directing a laser beam to various points within the environment. It is composed of four main components: a laser emitter, two 45-degree inclined mirrors —one fixed and one movable— and two stepper motors.

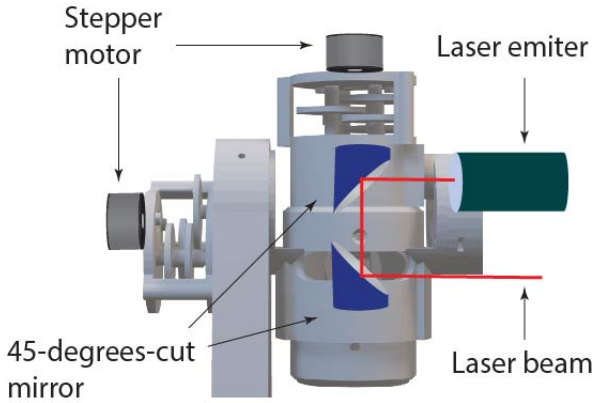

Figure 3 Diagram of the Positioning laser (PL).

The operation begins with the laser emitter generating a laser beam, which is initially directed toward a fixed 45-degree inclined mirror. This mirror redirects the beam orthogonally toward a second rotating mirror. The rotating mirror, mounted on a movable axis, dynamically adjusts the direction of the laser beam with the aid of one of the stepper motors. This motor enables the mirror to be precisely oriented in small increments of angularity, controlling the angle φ.

Furthermore, the second stepper motor controls the movement of the main rod in the TVS, adjusting the angle γ. Together, these angles, φ and γ, determine the location of the laser beam within the FOV, allowing the subsystem to target specific points in the environment as needed.

Scanning Aperture

The Scanning Aperture (Figure 4) is the main component of the TVS, designed to capture and process laser beams reflected off surfaces in the environment. Its key function is to determine the reflection angle, which is used to calculate the three-dimensional coordinates of the reflected points. This system includes a 45° rotating mirror that redirects the beams toward a lens array, which focuses the light onto an optical sensor. The Scanning Aperture subsystem integrates a DC motor as an actuator, which converts electrical energy into mechanical motion to rotate the 45° mirror. This sensor detects the reflected beams and confirms the presence of obstacles, while a zero-position sensor synchronizes these detections with the angular position of the mirror, generating reference pulses during each 360° rotation. The incidence angle β is estimated using the pulses recorded by both sensors, allowing the integration of geometric and temporal information. This design, based on sensor synchronization and the dynamic control of the rotating mirror, ensures quasi-real-time measurements.

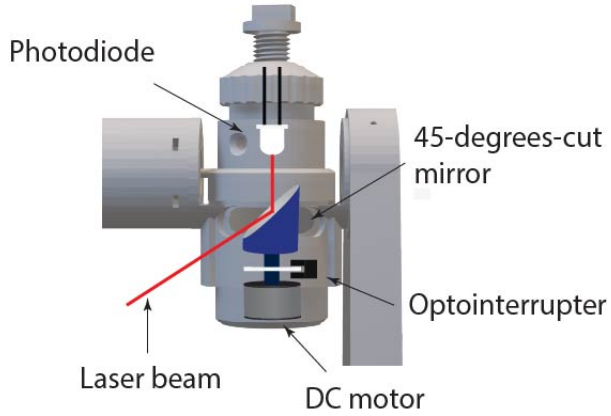

Figure 4 Diagram of the Scanning aperture (SA) subsystem.

MODEL DEVELOPMENT

To address the problem of scanning velocity stability in laser scanning systems, authors consider the dynamics of the DC motor responsible for the scanning aperture. The proposed model integrates both electrical and mechanical behaviors, incorporating the influence of friction and mechanical vibrations.

General Dynamic Model

To address disturbances in the scanning process, the dynamics of the electric drive system can be generalized as:

$$\dot{x}(t) = Ax(t) + Bu(t) + C\rho(t) \tag{4}$$

$$y(t) = Dx(t) \tag{5}$$

where: In this formulation, $x(t) \in \mathbb{R}^n$ is the state vector of dimension n, which includes variables such as angular position, velocity, and current. The control input vector of dimension m is denoted as $u(t) \in \mathbb{R}^m$, while the output vector of dimension l, $y(t) \in \mathbb{R}^l$, represents measurable quantities like the scanning velocity or position. The matrices A, B, C, and D define the system dynamics and coupling terms. The term $\rho(t) \in \mathbb{R}^p$ accounts for external disturbances vector of dimension p, which are assumed to be unknown but bounded. This general description provides the base for analyzing faults and disturbances in the scanning aperture system, enabling robust control.

DC Motor Model

The DC motor drives the scanning aperture and is modeled by the following state-space representation, derived from its electrical and mechanical characteristics:

$$\dot{x}_1(t) = x_2(t) \tag{6}$$

$$\dot{x}_2(t) = -\frac{k_v}{J}x_2(t) + \frac{k_M}{J}x_3(t) \tag{7}$$

$$\dot{x}_3(t) = -\frac{k_b}{L}x_2(t) - \frac{R}{L}x_3(t) + \frac{k_u}{L}u(t) \tag{8}$$

In this model, $x_1(t)$ represents the angular position of the motor output shaft, while $x_2(t)$ denotes the angular velocity at the same point. The variable $x_3(t)$ corresponds to the current flowing through the motor windings, and $u(t)$ represents the input voltage applied to the motor. The parameter J is the combined moment of inertia of the motor and the scanning aperture assembly, which characterizes the system's resistance to changes in rotational speed. The term k_v is the viscous friction coefficient, reflecting the losses due to mechanical friction, and k_M is the torque constant, which relates the motor's torque to the current. The back electromotive force (EMF) constant, k_b, links the angular velocity to the induced voltage in the motor windings. Additionally, R and L are the armature resistance and inductance, respectively, defining the electrical dynamics of the motor, while k_u represents the amplification factor of the input voltage.

Incorporating Nonlinear Effects of Vibrations and Friction

Friction and mechanical vibrations are integral to the system dynamics. Vibrations are modeled as a nonlinear perturbation, potentially exhibiting chaotic behavior, which couples with frictional forces in the following manner:

It is assumed that the motor is influenced by mechanical vibrations, which lead to variations in the velocity of the motor output shaft. These variations, caused by the vibrational disturbances, can be introduced into the model (4) through an unknown function $\Delta_v(t)$, resulting in the following system of equations:

$$\dot{x}_1(t) = x_2(t) \tag{9}$$

$$\dot{x}_2(t) = -\lambda_1 x_2(t) + \lambda_2 x_3(t) - \lambda_3 \tau_f(t) - \Delta_v(t) \tag{10}$$

$$\dot{x}_3(t) = -\lambda_4 x_2(t) - \lambda_5 x_3(t) + \lambda_6 u(t) \tag{11}$$

Table 1 presents the mathematical expressions used to define the system parameters λ_1 to λ_6.The numerical values of the physical parameters involved in these expressions were provided in the 'Characterization and Parameter Estimation' subsection.

Table 1 Mathematical Expressions for System Parameters

Parameter	Mathematical Expression
λ_1	k_v/J
λ_2	k_M/J
λ_3	$1/J$
λ_4	k_b/L
λ_5	R/L
λ_6	k_u/L

where:

- $\tau_f(t)$: Nonlinear frictional torque, modeled as a nonlinear function of velocity and position.
- $\Delta_v(t)$: Perturbation due to mechanical vibrations, derived from experimental data using the MPU6050 sensor.

In this model of the laser scanning system, the function $\Delta_v(t)$ represents the influence of mechanical vibrations, which affects the stability of the electric drive's rotation speed. This instability directly impacts the accuracy of the scanning process. The main objective of the research is to estimate $\Delta_v(t)$ and, if its value exceeds a predefined threshold, to account for it in signal processing to estimate the effects of vibrational disturbances on system performance. These vibrations are inherently random, as captured experimentally using the MPU6050 sensor. Therefore, authors model $\Delta_v(t)$ as:

$$\Delta_v(t) \approx \sigma_v \, dW(t), \tag{12}$$

where:

- σ_v: The amplitude of the stochastic noise, estimated experimentally as the standard deviation of the captured data.
- $dW(t)$: The increment of a Wiener process, representing the random nature of the vibrational disturbances.

In practice, the experimentally captured data serves as a direct approximation of $\Delta_v(t)$, capturing both the amplitude and the randomness of the mechanical vibrations (Kumičák 2004; Banerjee 2021). Therefore, the vibrations measured at the motor base, transmitted to the shaft, induce an additional torque in the mechanical dynamics. Using the experimentally obtained angular acceleration of the vibration, this disturbance torque can be represented as:

$$\tau_v = J\Delta_v(t) \tag{13}$$

where τ_v is the combined moment of inertia of the motor and the scanning aperture assembly. The modeled vibration term τ_v is subject to the upper bound:

$$|\tau_v| \leq \tau_v^{max} \tag{14}$$

where the value $\tau_v^{max} = J\Delta_v^{max}$ denotes the maximum positive value of the modeled vibration torque.

The LuGre friction model, originally proposed in (Canudas de Wit *et al.* 1995), provides an effective framework for approximating the nonlinear dynamics of friction. It assumes the presence of micro-imperfections on the contact surfaces, which are modeled as bristle-like deflections to represent the distributed deformation of asperities. While these micro-imperfections are not directly measured, their existence is inferred and incorporated into the model as a deterministic approximation. This approach has been widely adopted in various applications, including DC motor systems (Núñez-López *et al.* 2023; Wang *et al.* 2016; Freidovich *et al.* 2009).

The nonlinear friction torque is described by:

$$\tau_f(\omega) = \sigma_0 \left(1 - \sigma_1 \frac{|\omega|}{g(\omega)}\right) z \tag{15}$$

In this equation, the internal variable z represents the average deflection of the bristle-like elements at the contact surface. The parameter σ_0 corresponds to the bristle stiffness coefficient, encapsulating the elastic behavior of the asperities, while σ_1 reflects the bristle damping coefficient, accounting for energy dissipation during frictional interactions (Canudas de Wit *et al.* 1995).

The transition from static to dynamic friction, a phenomenon critical to capturing real-world behavior, is modeled through the Stribeck effect (Na *et al.* 2018). This is expressed as:

$$g(\omega) = \tau_c + (\tau_s - \tau_c)e^{-(\omega/v_o)^2} \tag{16}$$

Here, τ_c denotes the Coulomb friction torque, which is independent of velocity, while τ_s represents the stiction torque, describing the peak force required to overcome static friction. The parameter v_o defines the Stribeck velocity threshold.

The LuGre friction model ensures symmetry about the origin (Canudas de Wit *et al.* 1995) and permits adhering to the following upper bound:

$$|\tau_f(\omega)| \leq \tau_s \tag{17}$$

where τ_s represents the maximum static friction torque, serving as an upper limit for the nonlinear frictional behavior. In previous studies (Wang *et al.* 2016; Freidovich *et al.* 2009), this model has been parameterized to suit various applications, highlighting its adaptability in DC motor systems.

Based on experimental data and a review of relevant literature, the authors consider this formulation to provide a reliable theoretical framework. The subsequent section will present the model validation for the specific system under study.

MODEL VALIDATION AND REAL-TIME MEASUREMENT OF VIBRATIONS IN THE TVS LASER SCANNING

Experimental validation of the proposed model was performed using the open-loop response and data from MPU6050 vibration sensors, installed on the aperture and positioner (see Fig.5) of the laser scanning system. The results demonstrate the model's capability to accurately predict the dynamics of the scanning system under various operating conditions.

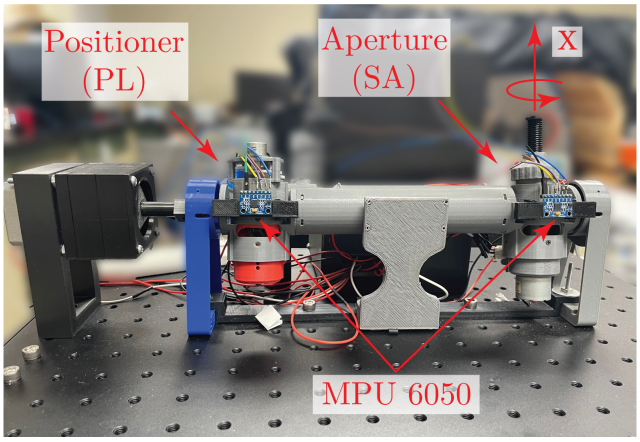

Figure 5 MPU6050 sensor placement on Positioning Laser (PL) and Scanning Aperture (SA) subsystems for vibration data collection.

Prior to experimental data collection, the MPU6050 sensors underwent a standard calibration process to ensure accurate measurement of vibration data. This calibration involved placing each sensor on a flat, vibration-free surface to record baseline (zero-motion) readings, which were then used to offset sensor biases. Subsequently, the sensors were rotated and positioned along known orientations (X, Y, and Z axes) to verify and adjust measurement accuracy for angular velocity and linear acceleration. After this calibration, the sensors were securely mounted on the TVS subsystems to avoid measurement deviations caused by relative motion or misalignment during experiments.

Design of Experiment A

To accurately measure mechanical vibrations at critical points of the TVS laser scanning prototype, two MPU6050 modules were utilized. These modules measure linear acceleration and angular velocity in three dimensions: X, Y, and Z. Each module, equipped with an accelerometer and a gyroscope, was strategically placed at key locations of the prototype: the PL and the SA (see Figure 5). These locations were selected because they contain optoelectronic elements that are susceptible to mechanical vibrations. Care was taken to ensure that both modules were precisely aligned along the X-axis, which is the primary axis of rotation for the scanning aperture's DC motor. The results, summarized in Fig. 6, provide a foundation for further refinement of the control system.

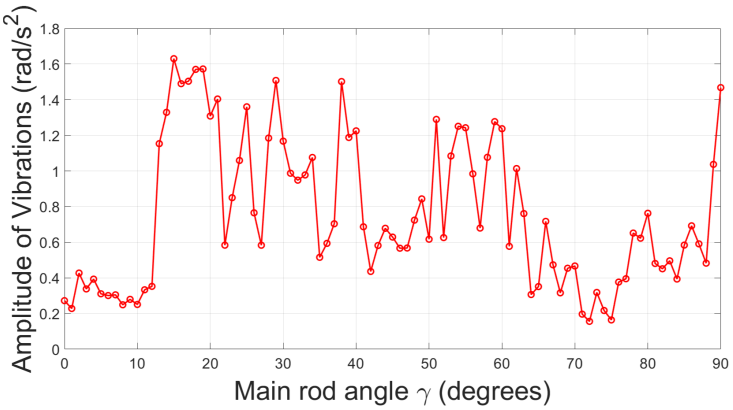

Figure 6 Maximum amplitudes of vibration data (angular acceleration around the X-axis) measured during rotational motion at various angular positions of the main rod of TVS prototype.

Once the sensors were calibrated, they were placed in a fixed position, as shown in Figure 5, from which data collection began. For each angular position, 3000 data points (1000 per axis) were captured over a period of 2 minutes. This procedure was repeated, incrementally increasing the angular position by one degree at a time, until reaching a final position of 90 degrees. By analyzing the data across different angular positions, the dominant frequencies of the vibrations for the SA subsystem were obtained for each rotational speed (RPS) value. These results are summarized in Table 2. Deviations from this trend, such as those around 30 Hz, were not considered in the model, as they likely represent external resonances or higher-order system dynamics beyond the scope of this study.

Table 2 Dominant Frequencies and Corresponding Spectral Amplitudes Captured from Vibration Measurements at Different Rotational Speeds (RPS) for the Scanning Aperture Subsystem

RPS (Hz)	Dominant Frequency (Hz)	Spectral Amplitude (rad/s^2)
15	15.4667	0.0234
20	19.8667	0.0851
25	24.0163	0.2368

Design of Experiment B

In the second experiment, the angles γ and φ were varied within the FOV (as shown in Figures 7, 8 and 9) to analyze their effect on the spatial components, evaluating the system's sensitivity and how vibrations impact the stability and precision of the trajectories. This analysis aims to identify mechanical error sources and their interaction with angular parameters. Specifically, the following angular values were used as reference: For γ, the values were $\gamma_1 = 15^\circ$, $\gamma_0 = 0^\circ$, and $\gamma_2 = -15^\circ$. For φ, the values were $\varphi_1 = 40^\circ$, $\varphi_0 = 60^\circ$, and $\varphi_2 = 80^\circ$. These values facilitated a systematic evaluation of the interaction between angular parameters and the mechanical behavior of the system under varying conditions.

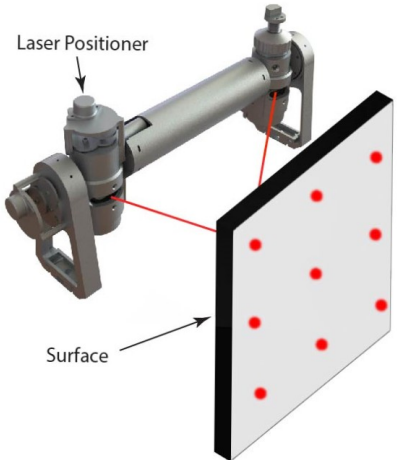

Figure 7 Laser scanning denoting selected targets.

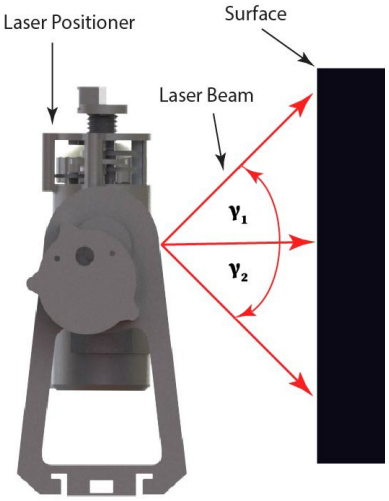

Figure 8 Side view of the TVS prototype denoting selected γ values.

The heat map in Figure 10 illustrates (by color intensity) the maximum vibration amplitude obtained (rad/s^2) observed in each test for the PL and SA subsystems under varying scanning velocities (RPS) and main inclinations of the rod (γ) denoting as red the highest value. The rows represent different values of γ ($-15^\circ, 0^\circ, 15^\circ$), while the columns distinguish between PL and SA subsystems at scanning velocities of 15, 20, and 25 RPS. Higher

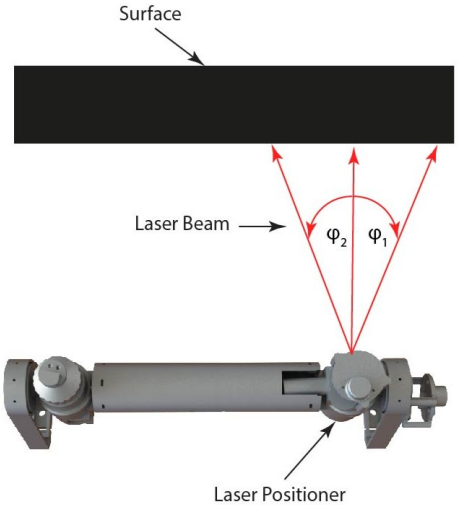

Figure 9 Top view of the TVS prototype denoting selected φ values.

amplitudes, marked in warmer colors, indicate stronger vibration effects, which can be correlated with increased inclination or scanning speed. Based on the experimental results, the maximum disturbance amplitude captured was 1.65 rad/s^2, observed under the highest scanning velocity and inclination conditions. These findings highlight the sensitivity of the system to mechanical vibrations under specific operational conditions.

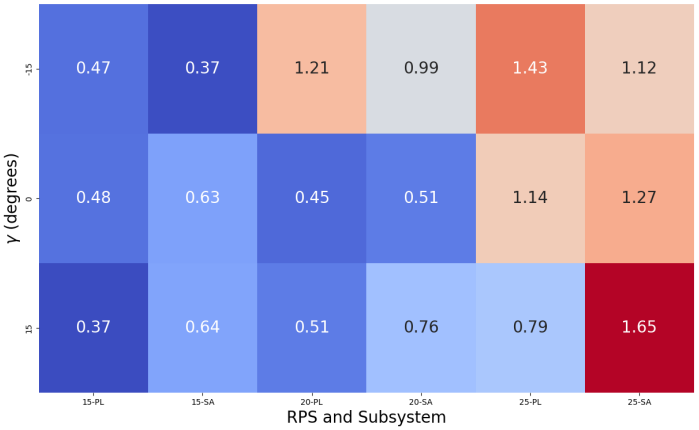

Figure 10 Heatmap depicting maximum vibration amplitudes (in rad/s^2) for PL and SA subsystems, varying main-rod inclination (γ) and scanning velocities (15, 20, 25 RPS). Red indicates higher vibration levels.

By comparing the obtained spectral amplitudes (Table 2) with the maximum amplitudes obtained from the perturbations captured by the sensor (summarized in Figures 10 and 11), it is evident that the spectral amplitudes are significantly smaller. Additionally, as shown in Figure 6, it is evident that, regardless of the value of γ, there is no way to establish a linear or deterministic model for the mechanical vibrations.

This observation suggests that the deterministic component of the vibrational model is negligible, further supporting the validity of the proposed stochastic model for the chaotic mechanical perturbations, as defined in Equation (12). Consequently, this justifies

Table 3 Estimated Parameters for SA

Exp	J	k_v	τ_c	τ_s	σ_0	σ_1	v_o
	$\text{Kg} \cdot \text{m}^2$	$\frac{\text{N·m·s}}{\text{rad}}$	$\text{N} \cdot \text{m}$	$\text{N} \cdot \text{m}$	$\frac{\text{N·m}}{\text{rad}}$	$\frac{\text{N·m·s}}{\text{rad}}$	rad/s
Exp1	3.084×10^{-5}	1.1881×10^{-2}	1.7257×10^{-7}	3.6951×10^{-4}	4.2880×10^{-4}	7.7965×10^{-6}	0.0290
Exp2	6.286×10^{-5}	1.1831×10^{-2}	1.6614×10^{-7}	3.8451×10^{-4}	4.0718×10^{-4}	8.1163×10^{-6}	0.0284
Exp3	7.561×10^{-5}	1.2627×10^{-2}	1.7172×10^{-7}	3.6763×10^{-4}	4.2464×10^{-4}	8.0763×10^{-6}	0.0293
Exp4	6.298×10^{-5}	1.9373×10^{-2}	1.6520×10^{-7}	3.8187×10^{-4}	4.0889×10^{-4}	8.1963×10^{-6}	0.0285
Exp5	6.123×10^{-5}	1.9153×10^{-2}	1.7274×10^{-7}	3.7138×10^{-4}	4.2131×10^{-4}	7.8207×10^{-6}	0.0291
Exp6	6.378×10^{-5}	1.9080×10^{-2}	1.6632×10^{-7}	3.8379×10^{-4}	4.1005×10^{-4}	8.1402×10^{-6}	0.0284
Exp7	6.727×10^{-5}	2.7189×10^{-2}	1.7222×10^{-7}	3.6650×10^{-4}	4.2671×10^{-4}	8.1963×10^{-6}	0.0292
Exp8	6.755×10^{-5}	2.6774×10^{-2}	1.6580×10^{-7}	3.8063×10^{-4}	4.0718×10^{-4}	8.1963×10^{-6}	0.0283
Exp9	6.775×10^{-5}	2.7780×10^{-2}	1.7292×10^{-7}	3.6837×10^{-4}	4.2255×10^{-4}	7.8765×10^{-6}	0.0293

the exclusion of any deterministic term in the formulation of $\Delta_v(t)$.

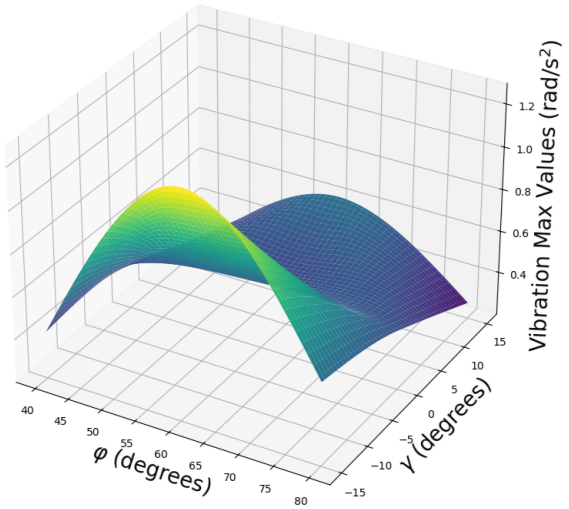

Figure 11 3D Surface representation of maximum vibration amplitudes measured in SA under different conditions of laser positioning.

The selection of experimental parameters was constrained by system limitations. Higher scanning velocities increased outliers in sensor data, reducing reliability, while lower velocities were impractical for real-time navigation and laser scanning. The chosen values balance accuracy and feasibility, ensuring robust data acquisition. Similarly, angles γ and ϕ were set based on field-of-view constraints, detailed in (Alaniz-Plata *et al.* 2025; Sepulveda-Valdez *et al.* 2024).

Characterization and Parameter Estimation

Parameter estimation refers to the process of identifying the dynamical system's constants by minimizing the discrepancy between experimental data and the mathematical model's predictions. Depending on the nature of the parameters and the available data, this can involve direct experimental measurement, statistical analysis, or optimization algorithms. The overall approach typically consists of three main steps:

1. **Mathematical Modeling:** The system's dynamics are described using mathematical equations that characterize the behavior of the system.
2. **Experimentation:** Measurements are obtained from the real system to capture its dynamic behavior.
3. **Data Preparation:** The collected data are refined to match the duration of the simulation time and ensure that the experiment starts at $t = 0$.

According to the recorded experimental data, the stochastic noise parameter σ_v can be parameterized using the maximum ($0.8069\,\text{rad/s}^2$), average ($0.3381\,\text{rad/s}^2$), or minimum ($0.0838\,\text{rad/s}^2$) amplitudes of the observed perturbations. These alternatives provide flexibility for modeling $\Delta_v(t)$, where the maximum ensures an upper-bound estimation, the average represents typical amplitudes, and the minimum reflects an optimistic scenario. It is important to note that this parameterization of chaotic vibrations was based solely on experimental data without relying on an optimization algorithm.

In this study, the parameters associated with frictional effects were estimated using MATLAB's Bounded Design Optimization Tool. Similar to (Núñez-López *et al.* 2023), MATLAB's Parameter Estimation app from the Simulink Design Optimization toolbox was employed, using a bounded nonlinear least-squares algorithm to estimate parameters within predefined limits. Parameter estimation was completed once the optimization tool minimized the error between the model simulation results and the experimental observations (Thenozhi *et al.* 2022).

After conducting a series of experiments at the nine reference points highlighted in Figure 7, the corresponding parameters were estimated and are presented in Table 3.

Throughout the nine experiments, the estimated values of k_M remained consistently close to $8.526 \times 10^{-3}\,\mathrm{N \cdot m/A}$, demonstrating a stable torque constant for the motor under varying conditions. Notice that the authors consider numerically $k_M = k_b$ due to the fact that the motor model assumes no electromagnetic energy losses and that SI units are used ($\mathrm{V \cdot s/rad}$ for k_b). Furthermore, the parameters measured directly for the tested motor were the resistance of the DC armature $R = 11.36\,\Omega$ and the inductance of the armature $L = 1.332 \times 10^{-3}\,\mathrm{H}$. These values are consistent with the motor's electrical dynamics, which were validated during the parameter estimation process.

CONTROL STRATEGY TO MITIGATE MODELED NONLINEAR EFFECTS

To mitigate the modeled nonlinear effects, the control input $u(t)$ is computed using a robust nonlinear control law derived from Lyapunov stability criteria. This control law, explicitly integrated into Equation (11) of the system model, is designed to directly compensate the nonlinear friction torque $\tau_f(t)$ (modeled by the LuGre model) and the stochastic perturbations $\Delta v(t)$. The robust gain G_r used in the control formulation was specifically selected based on the maximum observed friction and vibration values, ensuring that the controller robustly counteracts these disturbances. Achieving stability of the actuator velocity is crucial for accurately determining the incidence angle β, necessary for the precise calculation of 3D coordinates using equations (1), (2), and (3).

Control Law Formulation

To perform a robust nonlinear proportional derivative control, the proposed control law to decrease the negative effect of vibrations is defined as follows:

$$u = -G_p \tanh(\epsilon) - G_d \tanh(\dot{\epsilon}) - G_r \tanh(G_0 \epsilon) \tag{18}$$

where:

- u is the control input.
- ϵ and $\dot{\epsilon}$ are the tracking error and its time derivative, respectively.
- G_p, G_d, G_r are the positive proportional, derivative, and robust gains, respectively.
- G_0 is a sharpness factor enhancing the robustness aspect by strengthening the response as the error ϵ increases.

Mathematically, $\tanh(x)$ saturates to ± 1 as $x \to \pm\infty$, which means:

$$|u| \leq G_p + G_d + G_r \tag{19}$$

ensuring that the maximum possible control input magnitude does not exceed the sum of the gains.

In this formulation, the positioning error ϵ is defined as:

$$\epsilon = \phi - \phi_r \tag{20}$$

where ϕ is the actual position, and ϕ_r is a positive constant reference angular position for the DC motor's shaft of the SA.

As depicted in Figure 12, the reference angle ϕ_r is compared with the actual angle ϕ, generating an error ϵ. The robust controller then computes the control input u to regulate the scanning aperture's velocity by counteracting the nonlinear friction torque $\tau_f(t)$

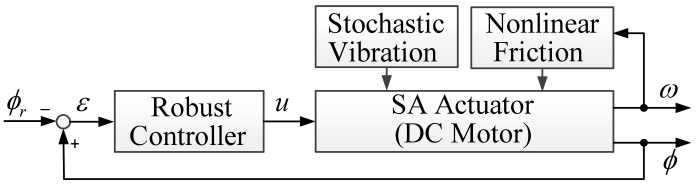

Figure 12 Block diagram illustrating the robust control strategy integrated into the system's model.

and the stochastic vibration term $\Delta v(t)$. This approach ensures that both position and velocity remain bounded, thereby guaranteeing stable operation of the scanning aperture for accurate incidence angle determination.

Lyapunov Stability Analysis

Upon substituting the proposed control law (18) into the motion system's dynamic equation (10), the closed-loop mechanical dynamics are described by:

$$\begin{aligned} J\dot{\omega} = &- \tilde{k}_u G_p \tanh(\epsilon) - \tilde{k}_u G_d \tanh(\dot{\epsilon}) \\ &- \tilde{k}_u G_r \tanh(G_0 \epsilon) - k_v \omega - \tau_f - \tau_v \end{aligned} \tag{21}$$

where J is the system inertia, k_v is the viscous damping coefficient, τ_f, and τ_v represent the nonlinear friction and vibration torques, respectively. Finally, $\tilde{k}_u$ (torque-to-control gain) directly scales the generated torque, simplifying the analysis due to the significantly smaller electrical time constant compared to the mechanical time constant, as observed in similar systems according to the literature (Ogata 2020; Kuczmann 2024).

The proposed control given by (18) ensures global asymptotic positioning stability provided the control gains are chosen to satisfy the constraint given by (19) and the following sufficient conditions:

$$G_p > \frac{G_d}{2} \tag{22}$$

$$G_r \geq \frac{\tau_s + \tau_v}{\tilde{k}_u} \tag{23}$$

To facilitate subsequent analysis, a filtered positioning signal is defined as follows, similar to (Núñez-López *et al.* 2021) and (Zheng *et al.* 2019):

$$\xi = \dot{\epsilon} + \eta tanh(\epsilon) \tag{24}$$

where η is an arbitrarily small positive constant that satisfies the following condition:

$$0 < \eta < \frac{k_v}{J} \tag{25}$$

The open-loop filtered error dynamics are obtained by taking the time derivative of (24):

$$\dot{\xi} = J\dot{\omega} + \eta sech^2(\epsilon)\dot{\epsilon} \tag{26}$$

where $\mathrm{sech}(\cdot)$ is the standard hyperbolic secant function. Multiplying both sides of (26) by J and noting that $\ddot{\epsilon} = \dot{\omega}$ and $\dot{\epsilon} = \omega$ for position control, the equation becomes:

$$J\dot{\xi} = J\dot{\omega} + J\eta sech^2(\epsilon)\omega \tag{27}$$

Substituting $J\dot{\omega}$ from (21) into (27), the resulting expression is:

$$
\begin{aligned}
J\dot{\omega} = &- \tilde{k}_u G_p \tanh(\epsilon) - \tilde{k}_u G_d \tanh(\dot{\epsilon}) \\
&- \tilde{k}_u G_r \tanh(G_0\epsilon) - [k_v - J\eta sech^2(\epsilon)]\omega \\
&- \tau_f - \tau_v
\end{aligned} \tag{28}
$$

The stability proof proceeds using Lyapunov's direct method (Slotine *et al.* 1991). For this purpose, the Lyapunov function candidate is proposed as:

$$
\begin{aligned}
V = &\frac{1}{2}\tilde{J}\tilde{\xi}^2 + \tilde{k}_u[G_p + G_r]\int_0^{\epsilon} tanh(\sigma)\, d\sigma \\
&+ \eta \int_0^{\epsilon} [k_v - \eta J sech^2(\sigma)] tanh(\sigma)\, d\sigma
\end{aligned} \tag{29}
$$

From the property of the standard hyperbolic secant function and the condition (25) on η, it has $k_v - \eta J sech^2(\sigma) \geq k_v - \eta J \geq 0$. Together with the fact that $tanh(\epsilon)\epsilon \geq 0$ for all ϵ, and $tanh(\epsilon)\epsilon = 0$ only for $\epsilon = 0$ it is straightforward to verify that the integral terms are positive and/or semi-positive definite with respect to ϵ.

Taking the time derivative of V along (29) leads to

$$
\begin{aligned}
\dot{V} = &J\tilde{\xi}\dot{\tilde{\xi}} + \tilde{k}_u G_p tanh(\epsilon)\dot{\epsilon} + \tilde{k}_u G_r tanh(\epsilon)\dot{\epsilon} \\
&+ \eta[k_v - \eta J sech^2(\epsilon)] tanh(\epsilon)\dot{\epsilon}
\end{aligned} \tag{30}
$$

After substituting $J\dot{\tilde{\xi}}$ from (28) into (30) using the fact that $\dot{\epsilon} = \omega_o$ for position control, recalling the fact that $-\tau_f(\omega)\omega \leq 0$ from (15) (due to the symmetry about the origin of the model), and $sech^2(\epsilon) \leq 1$ from the property of the hyperbolic secant function, the upper bound for $\dot{V}$ is

$$
\begin{aligned}
\dot{V} \leq &- \tilde{k}_u G_d tanh(\omega)\omega - \tilde{k}_u G_r tanh(G_0\epsilon)\omega - [k_v - \eta J]\omega^2 \\
&- \tau_v\omega - \eta\tilde{k}_u G_p tanh^2(\epsilon) - \eta\tilde{k}_u G_d tanh(\omega) tanh(\epsilon) \\
&- \eta\tilde{k}_u G_r tanh(G_0\epsilon) tanh(\epsilon) - \eta\tau_f tanh(\epsilon) \\
&- \eta\tau_v tanh(\epsilon) + \tilde{k}_u G_r tanh(\epsilon)\omega
\end{aligned} \tag{31}
$$

From the trigonometric property of the hyperbolic tangent function, the following inequality is defined:

$$
-\eta\tilde{k}_u G_d tanh(\omega) tanh(\epsilon) \leq \frac{\eta\tilde{k}_u G_d}{2}[tanh^2(\omega) + tanh^2(\epsilon)] \tag{32}
$$

Using a proposed additional gain condition for G_0 to assure the global asymptotic stability, leading to if $1 \leq G_0$, hence $tanh(\epsilon) \leq tanh(G_0\epsilon)$, and applying the fact $tanh(\omega)\omega \geq tanh^2(\omega)$ from the standard hyperbolic tangent function to (31) leads to:

$$
\begin{aligned}
\dot{V} \leq &- \tilde{k}_u G_d \left[1 - \frac{\eta}{2}\right] tanh^2(\omega) - [k_v - \eta J]\omega^2 - \tau_v^{max}|\omega| \\
&- \eta\left[\tilde{k}_u G_p - \frac{\eta\tilde{k}_u G_d}{2} + \tilde{k}_u G_r - \tau_s - \tau_v^{max}\right] tanh^2(\epsilon)
\end{aligned} \tag{33}
$$

where are used the inequalities (14), (17), (32) and $|tan(\epsilon)| \geq tanh^2(\epsilon)$ from the property of the hyperbolic tangent function.

By the conditions on control gains (22), (23) and (25), the final upper bound for $\dot{V}$ can be written as

$$
\dot{V} \leq -\rho_1 tanh^2(\omega) - \rho_2\omega^2 - \rho_3|\omega| - \rho_4 tanh^2(\epsilon) \tag{34}
$$

where ρ_1, ρ_2, ρ_3, and ρ_4 are some positive constants.

The detailed derivation demonstrates that $\dot{V}$ is negative definite. By applying Barbalat's lemma (Slotine *et al.* 1991), the authors conclude that $\lim_{t\to\infty} \tanh^2(\omega) = 0$, $\lim_{t\to\infty} \omega^2 = 0$, $\lim_{t\to\infty} |\omega| = 0$, and $\lim_{t=\infty} \tanh^2(\epsilon) = 0$, thereby ensuring global asymptotic stability for any initial states $(\phi(0), \omega(0))$.

RESULTS AND DISCUSSION

The purpose of this analysis is to evaluate the effect of mechanical vibrations on the precision of the measured coordinates. Vibrational disturbances can introduce variability in the system, potentially affecting the stability of the scanning process and the accuracy of the spatial measurements. By examining the standard deviations, the authors aim to quantify how the vibrational effects propagate across the different coordinate components.

Figure 13 depicts the open-loop velocity response under multiple operating conditions. The signal exhibits irregular, abrupt, non-periodic fluctuations that suggest a complex, chaotic behavior induced by the synergy of nonlinear friction (modeled by the LuGre approach) and random perturbations, which are represented as stochastic mechanical vibrations in this study. Such chaotic mechanical dynamics negatively affect the system's accuracy because the scanning aperture must maintain as stable a velocity as possible to accurately determine the incidence angle β, which is essential for calculating the 3D coordinates of objects within the field of view using equations (1), (2) and (3). Stochastic angular velocity fluctuations demonstrate a complex dynamic behavior that requires robust control to mitigate performance degradation.

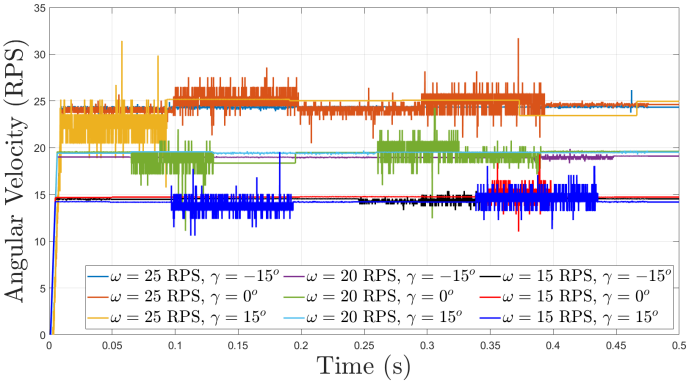

Figure 13 Angular velocity in RPS of the actuator versus time under various operating conditions.

Table 4 presents the experimental uncertainties σ_x, σ_y, and σ_z for the coordinates x, y, and z, respectively, under different inclination angles γ. These uncertainties represent the standard deviation of the coordinate errors, derived from experimental data collected under varying vibrational conditions. From the results in Table 4, it is observed that σ_x and σ_z show a slight decrease as the inclination γ changes from $-15°$ to $15°$. Specifically, σ_x decreases from $2.88056mm$ to $2.58106mm$, while σ_z decreases from $2.00934mm$ to $1.71697mm$. In contrast, σ_y remains consistently smaller in magnitude, with values close to $0.7mm$, except for a notable reduction to $1.6 \times 10^{-2}mm$ when $\gamma = 0°$. As previously established graphically, a numeric relation exists between inclination and vibration characteristics (as shown in Figure 11). This allows the conclusion of the empirical analysis of vibration influence on the measurement uncertainty in a particular case of the presented laser scanner.

These findings suggest that the x- and z-components are moderately affected by changes in inclination, while the y-component exhibits a minimal sensitivity to the vibrational disturbances.

Table 4 Average Experimental Uncertainty (in mm)

γ (Inclination)	σ_x (mm)	σ_y (mm)	σ_z (mm)
$-15°$	2.88	0.77	2.01
$0°$	2.68	0.016	1.82
$15°$	2.58	0.69	1.72

The analysis of the proposed controller's performance was focused exclusively on the x-axis, as detailed in the Model Validation section. This axis was selected due to its primary role in the scanning aperture's rotational dynamics. The computational implementation of the robust control strategy was evaluated based on its ability to mitigate the nonlinear effects of mechanical vibrations and friction. The robust gain, G_r, was particularly chosen to ensure stability under the maximum observed vibrational and frictional disturbances, aligning the control parameters with the experimentally captured data.

To assess the controller's performance under varying gain configurations, metrics such as settling time and maximum overshoot were evaluated for each positioning cycle across a range of angular positions. The parameter ranges employed in these tests are presented in Table 5. The resulting data enabled the identification of an optimal set of control gains that minimized both settling time and overshoot while maintainingthe stable operation of the scanning aperture.

Table 5 Ranges of Proportional, Derivative, Robust Gains, and Reference Positions Employed during the Robust Control Law Evaluation

Parameter	Range of Values
Proportional Gain (G_p)	1.25, 3.78, 6.31
Derivative Gain (G_d)	0.5, 3.11, 8.33
Robust Gain (G_r)	16.33, 18.89, 21.44
Sharpness Factor (G_0)	10, 100, 150
Reference Positions (degrees)	5, 20, 25, 30, 35, 40, 45

The proposed nonlinear control strategy was assessed by measuring the average settling time, maximum overshoot, and final positioning accuracy across various target positions. These results were summarized in and are presented in Table 6.

In Fig. 14, the phase portrait depicts the relationship between angular position (in radians) and angular velocity (in rad/s) for distinct sets of controller gains prior to stabilization at a reference position of 5 degrees. Fig. 15 illustrates the oscillatory behavior of the system's angular position before achieving the desired reference, while Fig. 16 highlights the oscillations in angular velocity during the same interval. The black and red curves exhibit greater oscillatory behavior compared to the blue curve, underscoring the stabilizing effect of the gain G_0. Specifically, the configuration with $G_0 = 10$ (blue curve) achieved the smoothest response and the least overshoot, while the setup with $G_0 = 150$ (black curve) demonstrated the most pronounced oscillations and the longest stabilization time.

Table 6 Summary of Results Obtained under Varying Reference Positions for the Robust Nonlinear Controller

Ref. Position	Average Settling Time	Average Maximum Overshoot
5	0.019139	4.95
20	0.036022	19.98
25	0.041547	24.93
30	0.044959	29.97
35	0.049019	34.92
40	0.053001	39.96
45	0.056768	45.00

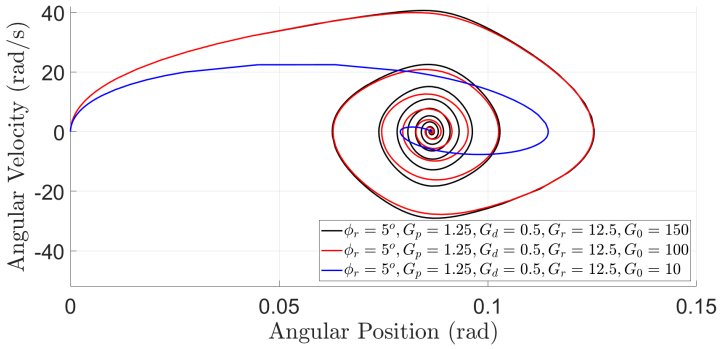

Figure 14 Phase portrait of system's angular position and velocity for different controller constants.

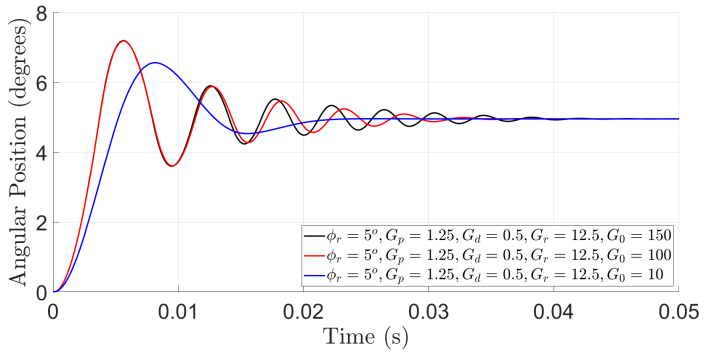

Figure 15 System's position response for different controller constants.

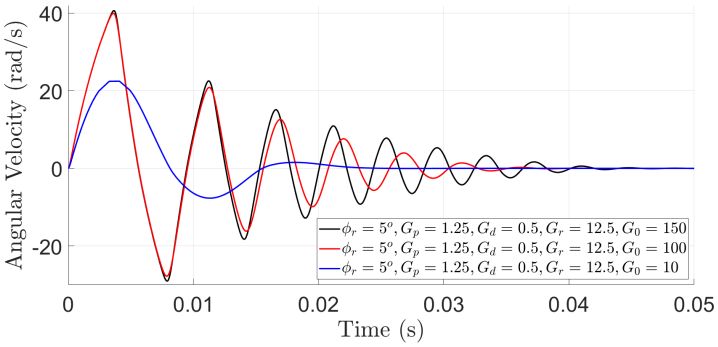

Figure 16 System's velocity response for different controller constants.

The results highlight the effectiveness of the proposed control strategy in maintaining system stability while minimizing the settling time and maximum overshoot. By leveraging the robust gain G_r calibrated to the upper limits of the observed disturbances, the controller demonstrated the ability to ensure smooth operation even under varying dynamic conditions. These findings validate the computational implementation of the control strategy, paving the way for future physical testing and refinement. The Lyapunov stability analysis confirmed the global asymptotic stability of the system, providing theoretical guarantees for the controller's robustness under bounded disturbances.

CONCLUSION

This work developed a physical-mathematical model to describe the mechanical vibrations and nonlinear friction effects in laser scanning systems, integrating both deterministic and stochastic terms that reflect their chaotic nature. Experimental measurements obtained using MPU6050 sensors validated the model, highlighting the significance of random perturbations and their impact on system dynamics.

The findings presented here align with prior studies on nonlinear dynamics in precision systems, particularly regarding the LuGre friction model's effectiveness in capturing nonlinear friction phenomena, as demonstrated in (Canudas de Wit *et al.* 1995; Wang *et al.* 2016; Freidovich *et al.* 2009). However, the distinctive contribution of this work lies in explicitly characterizing and incorporating the chaotic mechanical vibrations measured experimentally into a robust nonlinear control framework. The present study focused on modeling the nonlinear vibrational response of the TVS within typical operational conditions (scanning speeds below 25 RPS) to ensure data acquisition while maintaining realistic performance constraints. Chaotic behavior was explicitly confirmed experimentally through irregular velocity fluctuations at the actuator shaft, with disturbances reaching up to 1.65 rad/s² under demanding conditions (25 RPS, ±15° inclination).

The proposed model not only provides a tool to analyze and understand the inherent complexities of friction and vibration in mechanical systems but also opens opportunities for designing robust control strategies. In this regard, a nonlinear controller based on hyperbolic functions was implemented computationally to mitigate the effects of chaotic perturbations and ensure operational stability. After applying the proposed methodology in the computational implementation, the visualized results suggest a reduction in the negative influence of chaotic signals, leading to a more stable simulated system response. The results demonstrate the effectiveness of this approach, showcasing its potential for high-precision system applications. Future work will aim to implement the proposed control strategy on a physical TVS system prototype, enabling the validation of simulation outcomes under real-world operating conditions.

Limitations of the present study include assumptions made in modeling vibrations as purely stochastic processes, potentially neglecting minor deterministic resonance effects that might influence system behavior. Additionally, the robust control strategy was validated through computational simulations, and its effectiveness under practical implementation constraints, such as actuator saturation or sensor noise, remains to be experimentally verified. The typical operational conditions of TVS to minimize the occurrence of outliers were studied according to previous research (Alaniz-Plata *et al.* 2025; Sepulveda-Valdez *et al.* 2024; Sergiyenko *et al.* 2024). However, further investigation is needed to analyze the effect of material properties on vibrational stability at higher speeds.

APPENDIX

Abbreviations and Symbols

Table 7 Most Relevant Symbols Used in the Manuscript.

Symbol	Description
φ, β, γ	Angles in Dynamic Triangulation Method
a	Fixed distance between PL and SA subsystems
R, L	DC motor armature resistance and inductance
J	Moment of inertia of DC motor and SA assembly
k_M, k_b	DC motor torque constant and back-EMF constant
k_v	Viscous damping friction coefficient of DC motor
τ_s, τ_c	Static friction torque and Coulomb friction torque
σ_0, σ_1	LuGre friction stiffness and damping coefficients
v_o	Stribeck velocity threshold in friction model
σ_v	Standard deviation of experimentally measured stochastic vibration disturbance
G_p, G_d, G_r	Proportional, derivative, and robust control gains
G_0	Sharpness factor enhancing robustness of controller
$\Delta_v(t)$	Stochastic perturbation due to mechanical vibrations
$dW(t)$	Increment of Wiener process
$u(t)$	Control input voltage to DC motor
$\omega(t)$	Angular velocity of DC motor shaft
$\tau_f(t)$	Nonlinear friction torque described by LuGre model
$\tau_v(t)$	Torque induced by mechanical vibrations

Table 8 Most Relevant Abbreviations Used in the Manuscript.

Abbreviation	Description
TVS	Technical Vision System
PL	Positioning Laser
SA	Scanning Aperture
DOF	Degree of Freedom
FOV	Field of View
MPU6050	Inertial Measurement Unit Sensor
RPS	Revolutions per Second

Acknowledgments

This work was supported by the Autonomous University of Baja California.

Availability of data and material

Additional data related to this study are available from the corresponding author upon request.

Conflicts of interest

The authors declare that there is no conflict of interest regarding the publication of this paper.

Ethical standard

The authors have no relevant financial or non-financial interests to disclose.

LITERATURE CITED

Al Khawaja, H., H. Alabdouli, H. Alqaydi, A. Mansour, W. Ahmed, *et al.*, 2020 Investigating the mechanical properties of 3d printed components. In *2020 Advances in Science and Engineering Technology International Conferences (ASET)*, pp. 1–7.

Alaniz-Plata, R., F. Lopez-Medina, O. Sergiyenko, W. Flores-Fuentes, J. C. Rodríguez-Quiñonez, *et al.*, 2025 Extrinsic calibration of complex machine vision system for mobile robot. Integration **102**: 102370.

Armstrong-Hélouvry, B., P. Dupont, and C. C. De Wit, 1994 A survey of models, analysis tools and compensation methods for the control of machines with friction. Automatica **30**: 1083–1138.

Atef, M., A. El-Assal, and M. Magdy, 2022 Analysis of the parameters affecting 3d printed parts for planar and nonplanar models. In *2022 6th International Conference on Robotics and Automation Sciences (ICRAS)*, pp. 224–230.

Banerjee, S., 2021 *Mathematical modeling: models, analysis and applications*. Chapman and Hall/CRC.

Canudas de Wit, C., H. Olsson, K. Astrom, and P. Lischinsky, 1995 A new model for control of systems with friction. IEEE Transactions on Automatic Control **40**: 419–425.

Freidovich, L., A. Robertsson, A. Shiriaev, and R. Johansson, 2009 Lugre-model-based friction compensation. IEEE Transactions on Control Systems Technology **18**: 194–200.

Gohar, R. and H. Rahnejat, 2012 *Fundamentals of Tribology*. London.

Kuczmann, M., 2024 Reviewof dc motor modeling and linear control: Theory with laboratory tests. Electronics **13**: 2225.

Kumičák, J., 2004 Stochastic and deterministic models of noise. In *Advanced Experimental Methods For Noise Research in Nanoscale Electronic Devices*, edited by J. Sikula and M. Levinshtein, pp. 61–68, Dordrecht, Springer Netherlands.

Kushwaha, Y. S., N. S. Hemanth, N. D. Badgayan, and S. K. Sahu, 2022 Free vibration analysis of pla based auxetic metamaterial structural composite using finite element analysis. Materials Today: Proceedings **56**: 1063–1067, First International Conference on Advances in Mechanical Engineering and Material Science.

Lazutkin, G. V., D. P. Davydov, L. A. Varzhitskiy, K. V. Boyarov, and T. V. Volkova, 2017 Non-linear oscillations of mechanical systems with structure damping vibration protection devices. Procedia Engineering **176**: 334–343.

Lindner, L., 2021 *Theoretical method to increase the speed of continuous mapping in a three-dimensional laser scanning system using servomotors control*. Editorial UABC.

Liu, X., W. Tian, J. Yu, and J. Zhao, 2021 Lidar points' bumpy distortion model, displacements and experiments. 2021 5th CAA International Conference on Vehicular Control and Intelligence, CVCI 2021 .

Marton, L. and B. Lantos, 2007 Modeling, Identification, and Compensation of Stick-Slip Friction. IEEE Transactions on Industrial Electronics **54**: 511–521.

Na, J., Q. Chen, and X. Ren, 2018 Chapter 1 - friction dynamics and modeling. In *Adaptive Identification and Control of Uncertain Systems with Non-smooth Dynamics*, edited by J. Na, Q. Chen, and X. Ren, Emerging Methodologies and Applications in Modelling, pp. 11–18, Academic Press.

Núñez-López, J. A., L. Lindner, O. Sergiyenko, J. C. Rodríguez-Quiñonez, W. Flores-Fuentes, *et al.*, 2021 Positioning Improvement for a Laser Scanning System using cSORPD control. In *IECON 2021 – 47th Annual Conference of the IEEE Industrial Electronics Society*, pp. 1–6, Toronto, Canada, ISSN: 2577-1647.

Núñez-López, J. A., O. Sergiyenko, R. Alaniz-Plata, C. Sepulveda-Valdez, O. M. Pérez-Landeros, *et al.*, 2023 Advances in laser positioning of machine vision system and their impact on 3d coordinates measurement. In *IECON 2023- 49th Annual Conference of the IEEE Industrial Electronics Society*, pp. 1–6.

Ogata, K., 2020 *Modern control engineering*.

Pany, C., 2023 Large amplitude free vibrations analysis of prismatic and non-prismatic different tapered cantilever beams. Pamukkale Üniversitesi Mühendislik Bilimleri Dergisi **29**: 370–376.

Pany, C. and G. Rao, 2002 Calculation of non-linear fundamental frequency of a cantilever beam using non-linear stiffness. Journal of sound and vibration **256**: 787–790.

Pany, C. and G. V. Rao, 2004 Large amplitude free vibrations of a uniform spring-hinged beam. Journal of sound and vibration **271**: 1163–1169.

Popov, V. L. *et al.*, 2010 *Contact mechanics and friction*. Springer.

Selivanov, A. and E. Fridman, 2023 Finite-dimensional boundary control of a wave equation with viscous friction and boundary measurements. IEEE Transactions on Automatic Control .

Sepulveda-Valdez, C., O. Sergiyenko, V. Tyrsa, P. Mercorelli, J. C. Rodríguez-Quiñonez, *et al.*, 2024 Mathematical modeling for robot 3d laser scanning in complete darkness environments to advance pipeline inspection. Mathematics **12**.

Sergiyenko, O., R. Alaniz-Plata, W. Flores-Fuentes, J. C. Rodríguez-Quiñonez, J. E. Miranda-Vega, *et al.*, 2024 Multi-view 3d data fusion and patching to reduce shannon entropy in robotic vision. Optics and Lasers in Engineering **177**: 108132.

Sergiyenko, O., W. Flores-Fuentes, and P. Mercorelli, 2020 *Machine vision and navigation*. Springer.

Slotine, J.-J. E., W. Li, *et al.*, 1991 *Applied nonlinear control*, volume 199. Prentice hall Englewood Cliffs, NJ.

Thenozhi, S., A. C. Sánchez, and J. Rodríguez-Reséndiz, 2022 A Contraction Theory-Based Tracking Control Design With Friction Identification and Compensation. IEEE Transactions on Industrial Electronics **69**: 6111–6120.

Wang, X., S. Lin, and S. Wang, 2016 Dynamic friction parameter identification method with lugre model for direct-drive rotary torque motor. Mathematical Problems in Engineering **2016**: 6929457.

Zhao, Q. L., Y. X. Hao, and J. H. Wang, 2010 An application of chaos for vibration control. 2010 International Conference on Mechanic Automation and Control Engineering, MACE2010 pp. 267–270.

Zheng, C., Y. Su, and P. Mercorelli, 2019 Faster Positioning of 1-DOF Mechanical Systems With Friction and Actuator Saturation. Journal of Dynamic Systems, Measurement, and Control **141**.

How to cite this article: Núñez-López, J. A., Meza-García, D., Sergiyenko, O., Tyrsa, V., Rodríguez-Quiñonez, J. C., Flores-Fuentes, W., Lopez-Medina, F., Sepulveda-Valdez, C., Villa-Manriquez, J. F., Andrade-Collazo, H., Burnaev, E., Illarionova, S., Cáceres- Hernández, D., and Alaniz-Plata, R. Modeling and Analysis of Nonlinear Chaotic Mechanical Dynamics in Laser Scanning Systems. *Chaos Theory and Applications*, 7(2), 125-137, 2025.

CHAOS
Theory and Applications
in Applied Sciences and Engineering

e-ISSN: 2687-4539
RESEARCH ARTICLE
Vol.7 / No.2 / 2025 / pp.138-145
https://doi.org/10.51537/chaos.1606633

Managing Chaos: Leadership in Uncertain Environments

Ghayur Ahmad *,1 **and Bassem E. Maamari** *,2
*College of Business Administration, Prince Mohammad Bin Fahd University, Al-Khobar, Saudi Arabia.

ABSTRACT The present study explores the effectiveness of various leadership approaches to improve institutional robustness and flexibility in higher education institutions in Khyber Pakhtunkhwa. This cross-sectional study is based on multiple regression analysis to examine how traditional leadership methods impact chaos management and institutional change readiness in educational organizations. This study examined adaptive, transformational, communicative, empowering, and integrative technological leadership methods. This survey involved 250 faculty members in the region's major universities and used structured questionnaires to quantify the leadership impacts. The findings indicate that the traditional methods of leadership do not enhance institutional robustness on their own. However, the integration of technological innovations into these methods strongly improves their explanatory power, suggesting positive effects on the dependent measures. This demonstrates the significance of technology in the management of leadership in complex learning organizations, particularly in social, political, and economic instability. Moreover, the technological integration of traditional leadership methods in leadership tasks would enhance its potential to provide the basis for reinforcing leadership roles in an institution. The findings revealed that educational administrators should consider technological advancements as a key component in strategic development to promote progress and robustness in educational institutions.

KEYWORDS
Stability
Randomness
Adaptability
Complex system
Chaos

INTRODUCTION

Organizations are able to succeed and flourish when they acquire some fundamental factors of success. One of these pillars for success is efficient management. Despite the widespread belief that financial resources and production facilities are at the core of the success of a firm, corporate history shows evidence that many well sources organizations, with abundant resources and access to financing, have faltered (Adobor *et al.* 2021). The events lead the business community to look into the effect of managing the multiple functional areas of an organization properly, on its success. This concept involves not only tangible assets, but also human talent, as managing is at its core, about leadership and human decision-making activities (Gelgör and Can 2025). This opens the door for analyzing the role of leadership on organizational success. Within this framework, the challenge confronted by organizations revolves around understanding the human ways and processes of thinking and decision-making, both of which are complex and diverse in nature. With such a diverse and complex subject for analysis, it is difficult to properly define human nature's understanding how a person thinks. As a result of these multi-facets, researchers have failed after decades to put forth the best practice framework for managing humans. To date, scientists are still investigating the field of organizational behavior to find answers to these challenges, reporting various new findings, proposing concepts, models and framework that attempt to improve our understanding on people's behavior in workplace (Shufutinsky *et al.* 2020).

The extant literature on leadership and organizational behavior present numerous potential answers to the fundamental challenge in organizations, that is, what are the ideal leadership style and best human behavior at work in a stable work-environment. Knowing that organizations today operate in a more volatile and continuously evolving environment, with change being the only constant at hand. This environment prescribed as chaotic, a situation that ensues at an unexpected turn in time and takes the world by surprise, such as a pandemic. In such an unexpected environment, known as chaos management, the managerial dilemma shifts to a new level, trying to investigate whether chaos can be managed (Uhl-Bien 2021).

The theoretical framework of chaos theory, which posits that within the apparent randomness of complex systems, there are underlying patterns that can be identified and leveraged, underpins this paper. In the dynamic realm of higher education, universities often encounter rapid changes in technology, policy, economic conditions, and societal demands (Bishwas and Sushil 2020). These fluctuations introduce a complexity that can seem chaotic, with Khyber Pakhtunkhwa's unique socio-political environment and educational challenges providing a prime setting for such phenomena. This area, characterized by diverse educational needs and resource variability, serves as an ideal backdrop for exploring how leadership within universities navigates these turbulent conditions.

Manuscript received: 24 December 2024,
Revised: 19 March 2025,
Accepted: 3 May 2025.

[1]gahmad@pmu.edu.sa (**Corresponding author**)
[2]bmaamari@pmu.edu.sa

The study titled "Harnessing Chaos: Evaluating Adaptive Leadership Strategies in Government Sector Higher Education Institutions of Khyber Pakhtunkhwa," i.e., the University of Peshawar and Islamia College University Peshawar, focuses on uncovering the leadership methodologies that enable these institutions not just to cope but to excel amid such uncertainty. This study provides a lens through which the study examines the strategic manoeuvres of university leaders in the study area as they respond to continuous shifts in their operational landscapes.

The application of chaos theory to the management practices of these institutions offers a unique perspective on how adaptive strategies can transform potential disorder into a structured pathway for institutional development and progress. This research investigates the existence, direction and magnitude of the relationship between chaos theory and chaos management on organizational success. It attempts to uncover the needed leadership characteristics and the type of leadership required in times of chaos. The manuscript lays first the foundation of chaos theory and its roots in social sciences, then highlights the relationship between leadership, management science, and the chaos theory, in the attempt to present the most important leadership characteristics in managing chaotic situations or environments.

BASICS OF CHAOS THEORY

Chaos theory, rooted in mathematics and physics, examines complex systems that exhibit sensitive dependence on initial conditions, commonly known as the "butterfly effect." Small changes can lead to significant and unpredictable outcomes, making it relevant to organizational behavior (Lemoine and Richardson 2020). Chaos theory, a fascinating branch of mathematics and physics, deals with the behavior of certain dynamical systems that are highly sensitive to initial conditions, a phenomenon popularly referred to as the "butterfly effect" (Sinha and Sinha 2020). This theory posits that small differences in initial conditions can lead to vastly different outcomes, making long-term predictions for these systems nearly impossible. The origins of chaos theory date back to the late 19th and early 20th centuries, but it gained significant prominence in the 1960s with the pioneering work of Edward Lorenz, whose studies in weather prediction revealed that very small changes in input could drastically alter the weather forecast (Alsharif *et al.* 2021). Chaos theory has since been applied across various fields, including meteorology, engineering, economics, biology, and social science, illustrating its wide-ranging implications (Butkus *et al.* 2023; Dolan *et al.* 2003).

The fundamental principles of chaos theory revolve around the concept of nonlinear dynamical systems, which are systems where the output is not directly proportional to the input. In such systems, simple equations can generate complex behaviors and seemingly random states that are, in fact, deterministic, meaning they follow precise rules, but their sensitivity to initial conditions makes them appear unpredictable and disorderly (Lartey *et al.* 2020). A key characteristic of chaotic systems is what is known as "strange attractors," which are patterns of behavior that can eventually be recognized within the apparent randomness, providing a semblance of structure and predictability in what might initially appear completely random (Kartika and Febriansyah 2021).

Chaos theory challenges traditional notions of predictability and control in complex systems and has profound implications for how we understand and manage processes that are influenced by minute variations (Butkus *et al.* 2024). In the context of organizational leadership, particularly in environments as dynamic as those found in higher education institutions, chaos theory provides a valuable framework for understanding how small policy changes (Taran 2023), leadership decisions, or educational practices can have disproportionately large effects on the institution's future. This sensitivity to initial conditions underscores the importance of meticulous planning and flexible strategy formulation, enabling leaders to harness chaos for innovation and adaptability rather than be overwhelmed by it (De Meyer *et al.* 2002; Yel 2024).

Problem Statement

In the pursuit of understanding how higher education institutions in Khyber Pakhtunkhwa manage chaos, certain leadership strategies stand out as particularly effective. Strategic decision-making enables leaders to constantly be keen on long-range goals as they adjust their planning processes to the changing market conditions. The duty of openness and giving power to the employees keeps the information and decision-making flowing amongst teams and creates flexibility to meet changes. To prevent length, no problems created by constant training in promoting resilience to disruption are raised; however, assurance that an institution can bounce back from unrest quickly is useful in chaotic climates. Besides, relying on procurement represents a critical path to addressing multifaceted contexts because it grows communication as well as analytical skills.

Crisis preparedness, leadership development, and stakeholder engagement are all interlinked as integrated strategies that work hand in hand to guarantee that leadership within these universities survives and flourishes in the face of the inevitable uncertainties of their operating environments. These values entail the incorporation of adaptable, kinetic, and technological leadership in the learning environment to unlock organic procedural transformations into organizational development. The goal of this research is to investigate how higher education institutions in Khyber Pakhtunkhwa manage chaotic and constantly changing contexts, with a focus on the importance of adaptive leadership. Although existing approaches like strategic decision-making, crisis planning, and stakeholder involvement promote adaptation, there is still a considerable gap in applying chaos theory to leadership in this particular scenario.

The primary challenge is a lack of appropriate frameworks for translating chaos theory principles into practical leadership initiatives. In addition to maintaining organizational control and promoting innovation without affecting institutional stability, university administrators have to establish a balance between long-term objectives and short-term adaptation. The study aims to bridge the separation between theory and practice by addressing this gap, thereby providing practical insights for enhancing the effectiveness of leadership in dynamic educational environments.

Objectives of the Study

The goal of this study is to investigate how well-valued universities in the Khyber Pakhtunkhwa province use leadership strategies to manage chaotic environments. We have developed the following objectives to better understand the specific strategies and their impact on institutional resilience and adaptability. The study's distinctiveness is shown by its distinctive application of chaos theory to leadership in higher education, with a particular emphasis on Pakistani universities. Furthermore, the well-described practical contributions underscore the tangible solutions the findings offer to enhance institutional resilience and flexibility. A structured discussion of adaptive leadership models and their theoretical foundations has been added to make the study more academically rigorous. This supports the study's relevance and technical

depth. These contributions provide a valuable framework for university leaders to navigate uncertainty and promote sustainable organizational change (Mandzuk 2024).

1. The aim of this study is to explore the specific leadership strategies that higher education institutions in Khyber Pakhtunkhwa employed to navigate chaotic and uncertain environments in a positive manner.

2. The aim is to analyze the impact of specific strategies on institutional resilience and adaptability to external and internal changes.

3. To compare the leadership approaches of various universities in the region to determine best practices for managing chaos within higher education settings

Research Questions

According to the research objective, the following questions are to be answered in this study.

1. What adaptive leadership strategies are utilized at higher education institutions in Khyber Pakhtunkhwa to manage chaotic conditions?

2. How do these strategies influence the resilience and adaptability of these institutions?

3. How do leadership approaches vary across different universities in Khyber Pakhtunkhwa, and what can be learned from these variations to inform better management of chaos in higher education?

LITERATURE REVIEW

According to (Shahi 2024), the concept of chaos in organizations and, more specifically, in academic contexts, has been the subject of many previous research efforts that address leadership and strategy formulation in organizations as a complex process. As explained by the literature's authors, adaptive leadership provides options needed to manage challenges and risks resulting from chaos. The author also defines adaptive leadership as keeping, altering, reacting to, and learning to flourish in a changing environment. According to (Su *et al.* 2022), this requires leaders to be active in strategic formulation and coordination at the levels of structure building for enhanced organizational adaptability. One suggests that by creating a culture of adaptation and learning, organizations could manage the uncertainties ubiquitous in instances of chaos.

Institutional resilience and adaptability are critical metrics for assessing the effectiveness of leadership strategies in higher education, particularly in environments marked by chaos and uncertainty. Scholarly work in this area, such as that (Zu 2023), highlights the role of strategic human resource management in building resilience, positioning it as essential for an institution's ability to withstand and recover from disruptions. Furthermore, the adaptability of an institution, which refers to its capacity to evolve in response to changing external and internal demands, has been explored through frameworks like adaptive capacity (Khan *et al.* 2024). These studies suggest that the agility with which an institution can modify its functions and structures directly influences its long-term sustainability and effectiveness. This nexus between leadership strategies and institutional outcomes forms a critical area of inquiry, underscoring the importance of leadership in shaping the resilience and adaptive capabilities of educational institutions amid fluctuating circumstances.

According to (Shufutinsky *et al.* 2023), decentralized decision-making allows for quick response and encourages the whole staff to respond quickly to changes and challenges. This approach fits into chaos theory in that it recognizes the stochastic nature of organizations as positive, in contrast to aspiring towards a highly structured system where change cannot happen quickly, as has been discussed earlier. This strategy, however, is highly dependent on the training and delegation of the employees, the aspect that has to be part of the leadership system. In addition, the application of technology in chaos management has also been the subject of debate in the literature.

Technology can also help in the timely sharing of information, in bringing members of a team close together, and in an effective provision of analytical tools capable of being used to identify possible disruption. According to (Hongchai and Weber 2023), technology can assist in simplifying a complex system and increasing the transparency of the processes going on across operations, especially during chaotic conditions where the usual modes of managing cannot hold. What emerges from this integration of technology with adaptive strategies is the ability of leaders to not only cope with but actively harness the intrinsic chaos of the environment to foster growth and adapt change across organizational practices. The concept of leadership within chaotic environments has increasingly been scrutinized in scholarly literature, with numerous studies highlighting various strategies that enhance organizational effectiveness. Leadership strategies are fundamental to navigating the complexities and uncertainties of any dynamic operational landscape.

Nguyen *et al.* (2023) articulate the concept of adaptive leadership, which emphasizes the importance of modifying one's approach to meet the evolving demands of the organization and its environment. Adaptive leaders are proficient in recognizing the nuances of changing circumstances and responding with appropriate strategies that may not have been part of the original planning. This form of leadership is crucial in chaotic environments where predictability is low and the ability to respond to new challenges swiftly can determine organizational survival and success.

Another key strategy identified regarding leadership strategies is transformational leadership, which Sort *et al.* (2023) explored extensively. Transformational leaders inspire and motivate their followers to achieve more than what is usually expected of them, often exceeding their limitations. This strategy is particularly effective in chaotic settings as it fosters an environment of motivation and innovation, driving the organization forward through visionary leadership and strong, personal commitment. Effective communication is paramount in any leadership strategy but becomes critically important in managing chaotic environments. According to (Pratama and Suryosukmono 2024), strategic communication helps in building trust and clarity, which are essential during uncertainty. Leaders who communicate effectively ensure that all members of the organization understand the current challenges and the strategies in place to address them, which helps align the team's efforts toward common goals despite external pressures.

Empowering leadership strategy involves delegating authority and fostering a sense of autonomy among team members (Ribeiro *et al.* 2024) suggest that empowering leaders facilitates an environment where employees feel greater control over their work and are encouraged to take the initiative. This is particularly effective in chaotic scenarios where decision-making must be rapid at multiple organizational levels to respond effectively to evolving situations. Developing organizational resilience is a strategic priority that leaders must cultivate to manage and thrive in chaotic environ-

ments. As (Sánchez and De Batista 2023) explains, resilience in leadership involves the ability to recover from setbacks and the capacity to anticipate disruptions, adapt to new realities, and learn from the process. This strategic foresight is vital for organizations to survive chaotic conditions and emerge more substantial and more adaptable. With the advancement of digital tools, leaders increasingly rely on technology to manage complexity and chaos.

Swierczek (2024) argues that technology can enhance decision-making capabilities, improve communication processes, and facilitate better monitoring of both internal and external environments. The strategic use of technology can help leaders gather real-time data, engage with stakeholders more effectively, and implement strategies swiftly, making it an invaluable tool in chaotic environments. Finally, the ability to lead effectively through crises often seen as the pinnacle of managing chaos is a crucial leadership strategy. 'Crisis leadership' involves not only dealing with the crisis at hand but also preparing the organization for potential future crises. Duarte Alonso *et al.* (2023) note that crisis leadership requires an acute awareness of the challenges and the ability to keep the organization focused and functioning. Leaders who excel in crisis leadership are adept at navigating through uncertainty, making decisive choices, and maintaining morale, which are essential for sustaining the organization through turbulent times.

A significant gap in the current literature can be identified when reviewing the existing literature, which focuses on leadership approaches applied in higher education institutions during volatile and uncertain environments. The majority of studies have looked almost solely to stable and predictable contexts; less effort has been directed to investigating how these leadership behaviors affect institutional change and vulnerability in situations that are experiencing high levels of socio-political and economic transformation, for example, Khyber Pakhtunkhwa. Moreover, a dearth of empirical studies has been conducted about the dissimilar effects of these modes of leadership adoption with specific reference to various universities. This lack of research clearly defines the need to conduct broad research on how certain leadership styles can be well utilized to mitigate havoc hence promoting organizational success within contexts that are relatively under-researched and, therefore, inherently more tumultuous.

Thus, this study seeks to contribute to the existing body of scholarship by providing a comprehensive analysis of the leadership practices that can help improve the resilience and adaptability of the higher education institutions in Khyber Pakhtunkhwa province. While the extant literature investigates adaptive leadership and chaos theory independently, there is inadequate study on their interaction in higher education institutions, notably in Khyber Pakhtunkhwa. This investigation mitigates this disparity by furnishing a structured framework that integrates chaos theory into leadership strategies, thereby providing university leaders with practical insights to improve their adaptability and resilience. This study advances our understanding of how leadership may effectively navigate uncertainty in dynamic academic environments by merging theoretical models with real-world issues. Figure 1 shows the impact of dependent and independent variables.

METHODOLOGY

The implemented methodology for the study "Harnessing Chaos: Evaluating Adaptive Leadership Strategies in Higher Education Institutions of Khyber Pakhtunkhwa" is fundamentally quantitative, aimed at empirically analyzing the impact of leadership strategies on institutional resilience and adaptability. Following the approach outlined by (Tariq *et al.* 2024), the research quantifies attitudes and behaviors related to leadership strategies using numerical data, essential in capturing the nuances of managing chaos in educational settings. Data collection involves administering a structured questionnaire, based on a 5-point Likert scale, to faculty members across selected public sector universities in Peshawar. The questionnaire design is informed by comprehensive literature reviews and preliminary interviews, ensuring that the questions effectively capture the variables of interest—adaptive leadership, transformational leadership, communication strategies, empowering leadership, and technological integration.

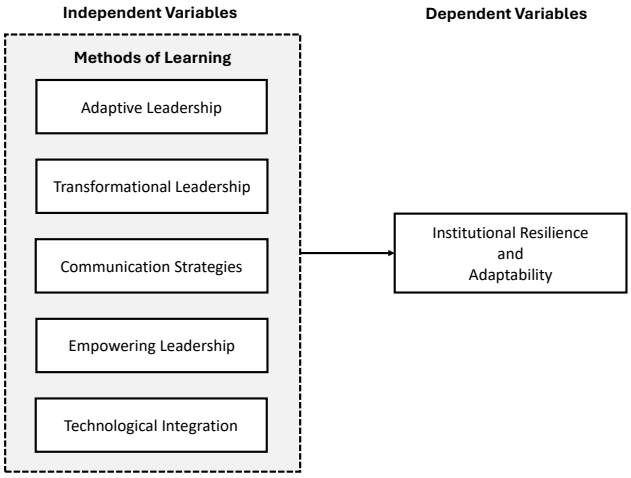

Figure 1 Conceptual Framework

To accommodate a substantial sample, 125 faculty members from each participating university are targeted, employing convenience sampling to facilitate ease of data gathering. The responses are then compiled and statistically analyzed using SPSS to examine the correlations and impacts of the leadership strategies. This analysis includes tests for reliability (Cronbach's alpha), normality (Kolmogorov-Smirnov & Shapiro-Wilk tests), and linearity, alongside regression and correlation tests to ascertain the relationships between the independent variables and the dependent outcomes of resilience and adaptability. The objective is to elucidate how different leadership approaches influence the ability of institutions to navigate and thrive amidst the dynamic challenges of their operational environments.

RESULTS

Demographic analysis of the study respondents reveals that the majority, 164 (65.6 %) participants were males, and 86 respondents (34.4%) as female, out of a total 250 participants. This distribution reflects a male-dominant sample, with females making up just over a third of the survey population. Likewise, regarding the age of the respondents, a majority number of the respondents were in the 21-35 years age group, i.e. 150 individuals or 60% of the total sample were in this age group. This is followed by those aged 36-50 years, who make up 21.2% of the sample with 53 respondents. The youngest group, below 21 years, includes 43 respondents (17.2%), and the smallest group, those above 50 years, consists of only 4 individuals (1.6%). This age distribution suggests a predominantly young to middle-aged demographic, with very few participants in the post-50 age category.

Furthermore, in terms of marital status, the majority of respondents (137 respondents, 54.8%) were married compared to those who were unmarried (113 respondents, 45.2%). The last category

in demographic information is the institutional affiliation of the respondents, which is divided between the University of Peshawar and Islamia College University, with a slightly higher representation from the University of Peshawar, which accounts for 54% of the respondents (135 individuals). In contrast, the respondents who belonged to Islamia College University represent 46% (115 respondents).

Chi-Square

In this study, a comprehensive case processing summary shows that all 250 cases were valid and included in the analysis, with no exclusions due to listwise deletion, ensuring a complete data set for accurate statistical evaluation, explained in Table 1. Similarly, Table 2 describes the reliability statistics revealed a Cronbach's Alpha of .411 across six items, which might suggest a moderate internal consistency within the dataset. Typically, a higher Cronbach's Alpha (above .7) is indicative of better internal consistency, suggesting that the scale used might require review or adjustment to enhance its reliability.

Table 1 Case Processing Summary

	N	%
Cases Valid	250	100.0
Excluded[a]	0	0.0
Total	250	100.0

Listwise deletion based on all variables in the procedure.

Table 2 Reliability Statistics

Cronbach's Alpha	N of Items
0.411	6

Moreover, Table 3 illustrates the Chi-square test to examine the relationship between different leadership strategies and the combined variable of institutional resilience and adaptability to change. The results of the Chi-Square tests indicate significant associations for all the variables tested.

Table 3 Test Statistics

Variable	Chi-Square (df, p)
Adaptive Leadership	164.552 (22, p = 0.000)[a]
Transformational Leadership	113.888 (20, p = 0.000)[b]
Communication Strategies	117.264 (22, p = 0.000)[a]
Empowering Leadership	153.312 (25, p = 0.000)[c]
Technological Integration	148.832 (20, p = 0.000)[b]
Institutional Resilience & Adaptability	144.592 (21, p = 0.000)[d]

[a] Min. expected freq. = 10.9; 0 cells < 5.
[b] Min. expected freq. = 11.9; 0 cells < 5.
[c] Min. expected freq. = 9.6; 0 cells < 5.
[d] Min. expected freq. = 11.4; 0 cells < 5.

In this regard Adaptive Leadership showed a Chi-Square value of 164.552 with 22 degrees of freedom, resulting in a significance level of .000. Likewise, Transformational Leadership registered a Chi-Square value of 113.888 with 20 degrees of freedom, also achieving a significance level of .000. Furthermore, Communication Strategies resulted in a Chi-Square value of 117.264 with 22 degrees of freedom, with a significance of .000. While Empowering Leadership had a Chi-Square value of 153.312 with 25 degrees of freedom, indicating a significance of .000. In this context Technological Integration reflected a Chi-Square of 148.832 with 20 degrees of freedom, also significant at .000. The dependent variable i.e Institutional Resilience & Adaptability to Change, had a Chi-Square value of 144.592 with 21 degrees of freedom and a significance level of .000.

These significant results reveal a statistically significant relationship between the leadership strategies employed and the institutional resilience and adaptability to change in the surveyed universities. This significant association underscores the impact of leadership practices on organizational outcomes in higher education settings. The tests also confirmed that all expected frequencies in the Chi-Square test were adequate, with no cell having expected frequencies less than 5, which supports the robustness of the statistical analysis.

Regression Analysis

The regression analysis is shown in the Model Summary and ANOVA in Table 4 and Table 5 respectively. The regression analysis gives a step-by-step analysis of the impact of intricate leadership approaches on organizational sustainability and flexibility toward change. First, with only Adaptive Leadership in Model 1, the R Square value is approximately equal to .002, this means that Adaptive Leadership is not a strong predictor of the dependent variable.

Table 4 Model Summary

Model	R	R Square	Adjusted R Square	Std. Error of the Estimate
1	0.045[a]	0.002	-0.002	0.06519
2	0.102[b]	0.010	0.002	0.06504
3	0.125[c]	0.016	0.004	0.06500
4	0.148[d]	0.022	0.006	0.06492
5	0.282[e]	0.079	0.061	0.06312

[a] Predictors: (Constant), Adaptive Leadership
[b] Predictors: (Constant), Adaptive + Transformational Leadership
[c] Predictors: (Constant), Adaptive, Transformational, Communication Strategies
[d] Predictors: (Constant), Adaptive, Transformational, Communication, Empowering
[e] Predictors: (Constant), All Above + Technological Integration

The ANOVA table for each of the models does support these conclusions: The F statistic increases significantly in Model 5, indicating the model has overall statistical significance on a p = 0.001 level. Such progressive addition of variables shows a systematic way of integrating different variables of leadership within an organization with Technological Integration being identified as a critical factor. When more predictor variables are introduced in the other models, the R Square value increases thereby implying a consistent enhancement of explaining the variability in institutional resilience and adaptability. Model 2, rather than Model 1, incorporates both Adaptive Leadership and Transformational Leadership, in addition to which the model provides a slightly

Table 5 ANOVA

Model	Source	Sum of Squares	df	Mean Square	F	Sig.
1	Regression	0.002	1	0.002	0.507	0.477[a]
	Residual	1.054	248	0.004		
	Total	1.056	249			
2	Regression	0.011	2	0.005	1.294	0.276[b]
	Residual	1.045	247	0.004		
	Total	1.056	249			
3	Regression	0.017	3	0.006	1.303	0.274[c]
	Residual	1.039	246	0.004		
	Total	1.056	249			
4	Regression	0.023	4	0.006	1.377	0.242[d]
	Residual	1.033	245	0.004		
	Total	1.056	249			
5	Regression	0.084	5	0.017	4.210	0.001[e]
	Residual	0.972	244	0.004		
	Total	1.056	249			

[a] Predictors: Adaptive Leadership
[b] Transformational Leadership
[c] Communication Strategies
[d] Empowering Leadership
[e] Technological Integration
[f] Dependent Variable: Institutional Resilience & Adaptability

Table 6 Regression Coefficients for Leadership Models

Model	Variable	B	SE	Beta	t	Sig.
1	Constant	0.380	0.023		16.858	0.000
	Adaptive Leadership	0.037	0.052	0.045	0.712	0.477
2	Constant	0.403	0.027		14.661	0.000
	Adaptive Leadership	0.106	0.071	0.130	1.504	0.134
	Transformational L.	-0.121	0.084	-0.125	-1.441	0.151
3	Constant	0.379	0.035		10.959	0.000
	Adaptive Leadership	0.102	0.071	0.125	1.445	0.150
	Transformational L.	-0.125	0.084	-0.128	-1.481	0.140
	Communication S.	0.066	0.057	0.073	1.148	0.252
4	Constant	0.399	0.038		10.495	0.000
	Adaptive Leadership	0.104	0.071	0.127	1.468	0.143
	Transformational L.	-0.126	0.084	-0.129	-1.493	0.137
	Communication S.	0.077	0.058	0.085	1.324	0.187
	Empowering Leadership	-0.068	0.054	-0.081	-1.261	0.208
5	Constant	0.308	0.044		7.077	0.000
	Adaptive Leadership	0.084	0.069	0.103	1.224	0.222
	Transformational L.	-0.081	0.083	-0.083	-0.985	0.326
	Communication S.	0.051	0.057	0.056	0.891	0.374
	Empowering Leadership	-0.104	0.053	-0.123	-1.951	0.052
	Technological Integration	0.266	0.068	0.248	3.902	0.000

Dependent Variable: Institutional Resilience & Adaptability to Change

better fit (R Square = .010). However, the values of significance of these predictors indicate that in this stage none of them could influence the dataset significantly when both predictors were used in a model. Communication Strategies is added to the analysis with Model 3, in addition to the previous predictors, thus raising the R Square to .016, with no significant individual impacts of the predictors.

The trend continues with Model 4 where Empowering Leadership is added and the R Square upgraded to .022. These additions, however, fail to attain statistical significance as the individual predictors indicate that the effect sizes of these variables are likely small or whose combined explanatory value is compromised by multicollinearity as a result of the addition of more variables without necessarily improving the model's fit. Model 5 shows significant enhancement from the previous models with Technological Integration added alongside all the leadership approaches outlined above. This model yields an R^2 equal to .079 and an Adjusted R^2 equal to .061 of the total variances and the latter tells us that this model accounts for 6.1% of institutional resilience and adaptability, net of the number of predictors tested. Out of the lot, Technological Integration has the highest correlation to the dependent variable whereby $t = 3.902$ and $p = 0.0001$.

Table 6, the coefficients table gives a model-by-model description of the significance of each of the variables used in the analysis. As with the case of Technological Integration, positive and strong coefficient indicates a good relationship of the variable with resilience and adaptiveness of the institutional setting, while negative and insignificant coefficients of Empowering Leadership and Transformational Leadership were observed. These finer-grained

Table 7 Excluded Variables from Regression Models

Model	Variable	Beta In	t	Sig.	Partial	Tolerance
1	Transformational L.	-0.125[a]	-1.441	0.151	-0.091	0.537
	Communication S.	0.070[a]	1.096	0.274	0.070	0.990
	Empowering L.	-0.068[a]	-1.068	0.286	-0.068	0.999
	Technological Int.	0.240[a]	3.896	0.000	0.241	1.000
2	Communication S.	0.073[b]	1.148	0.252	0.073	0.989
	Empowering L.	-0.068[b]	-1.075	0.283	-0.068	0.999
	Technological Int.	0.232[b]	3.734	0.000	0.232	0.983
3	Empowering L.	-0.081[c]	-1.261	0.208	-0.080	0.977
	Technological Int.	0.227[c]	3.599	0.000	0.224	0.963
4	Technological Int.	0.248[d]	3.902	0.000	0.242	0.934

[a] Model: Constant, Adaptive Leadership
[b] Transformational Leadership
[c] Communication Strategies
[d] Empowering Leadership
[e] Dependent Variable: Institutional Resilience & Adaptability

data suggest that some leadership practices probably improve institutional flexibility and resiliency more or less directly, while others probably work in subtler or potentially fewer positive ways.

CONCLUSION

The study focused on investigating the effects of diversified leadership behaviors on adopting institutional resilience in the higher education context of Khyber Pakhtunkhwa, using regression analysis on quantitative data to examine the moderating link between leadership behaviors and organizational performance. The study shows that despite the previous suggestions that adaptive, transformational, communication, and empowering leadership styles have a significant impact on organizations, these leadership styles did not display significant independent effects in defining institutional resilience and flexibility. Still, the addition of technological integration as a leadership strategy was a significant advancement over the previous models. Integration of technology was found to be a meaningful predictor with positive impacts on institutional responsiveness and flexibility.

This implies that when higher education institutions are experiencing change and operating in uncertain environments, there is a need to integrate technology into leadership processes strategically. Aside from improving the ability to learn and prepare for adversity, it also helps strengthen the resiliency of the institution against threats. This research underscores the importance of leadership in the educational sector to adopt tech-savvy tactics to navigate and orchestrate their operating environments proactively to enhance institutional performance and sustainability. This study underscores the significance of diverse leadership styles and technological integration in fostering institutional resilience, but it also highlights certain limitations that require attention. Despite its value, quantitative data is the primary source of the research, which may not fully convey the complex nature of leadership dynamics in higher education.

Future research could include qualitative observations to provide a deeper understanding of leadership flexibility. Furthermore, this study only focuses on institutions in Khyber Pakhtunkhwa, Pakistan and expanding its scope to other locations could enhance its generalizability. Further research might examine the long-term effects of technology-driven leadership methods on institutional sustainability and other moderating variables that may affect higher education leadership resilience and adaptability.

Ethical standard

The authors have no relevant financial or non-financial interests to disclose.

Availability of data and material

Not applicable.

Conflicts of interest

The authors declare that there is no conflict of interest regarding the publication of this paper.

LITERATURE CITED

Adobor, H., W. P. K. Darbi, and O. B. O. Damoah, 2021 Strategy in the era of "swans": the role of strategic leadership under uncertainty and unpredictability. Journal of Strategy and Management .

Alsharif, H. Z. H., T. Shu, B. Obrenovic, D. Godinic, A. Alhujailli, *et al.*, 2021 Impact of entrepreneurial leadership and bricolage on job security and sustainable economic performance: An empirical study of croatian companies during covid-19 pandemic. Sustainability **13**: 11958.

Bishwas, S. K. and Sushil, 2020 Environmental uncertainty, leadership and organisation culture as predictors of strategic knowledge management and flexibility. International Journal of Knowledge Management Studies **11**: 393–407.

Butkus, M., G. Schiuma, I. Bartuševičienė, O. G. Rakauskiene, L. Volodzkiene, *et al.*, 2023 The impact of organizational resilience on the quality of public services: Application of structural equation modeling. Equilibrium. Quarterly Journal of Economics and Economic Policy **18**: 461–489.

Butkus, M., G. Schiuma, I. Bartuseviciene, L. Volodzkiene, O. G. Rakauskiene, *et al.*, 2024 Modelling organisational resilience of public sector organisations to navigate complexity: empirical insights from lithuania. Journal of Economic Interaction and Coordination pp. 1–27.

De Meyer, A., C. H. Loch, and M. T. Pich, 2002 Managing project uncertainty: from variation to chaos. MIT Sloan management review **43**: 60.

Dolan, S. L., S. Garcia, and A. Auerbach, 2003 Understanding and managing chaos in organisations. International journal of management **20**: 23–35.

Duarte Alonso, A., O. T. K. Vu, S. K. Kok, and M. O'Shea, 2023 Adapting to dynamic business environments: a comparative study of family and non-family firms operating in western australia. Management Research Review **46**: 755–775.

Gelgör, E. and S. P. Can, 2025 Decision making in bank personnel selection using the analytical hierarchy process. Information Technology in Economics and Business **2**: 12–17.

Hongchai, D. M. and C. M. Weber, 2023 Leadership for technology management in a volatile, uncertain, complex, and ambiguous (vuca) world: a review of the literature and a research agenda. In *2023 Portland international conference on management of engineering and technology (PICMET)*, pp. 1–23, IEEE.

Kartika, I. T. and H. Febriansyah, 2021 Leading and navigating chaotic situation: How leadership through resiliency play a role in the process of responding to emerging new situation induced by novel coronavirus outbreak. no. August pp. 11–13.

Khan, H. S. u. d., M. S. Chughtai, Z. Ma, M. Li, and D. He, 2024 Adaptive leadership and safety citizenship behaviors in pakistan: the roles of readiness to change, psychosocial safety climate, and proactive personality. Frontiers in Public Health **11**: 1298428.

Lartey, F. M. *et al.*, 2020 Chaos, complexity, and contingency theories: a comparative analysis and application to the 21st century organization. Journal of Business Administration Research **9**: 44–51.

Lemoine, P. A. and M. D. Richardson, 2020 Planning for higher education institutions: Chaos and the covid-19 pandemic. Educational Planning **27**: 43–57.

Mandzuk, D., 2024 On the edge of chaos: how the deans at one canadian university have managed to lead in the face of the pandemic and other sources of uncertainty and complexity. Journal of Higher Education Policy and Management **46**: 18–31.

Nguyen, T., L. Hallo, N. Chileshe, and N. H. Nguyen, 2023 Towards

a sustainable integrated management approach to uncertainty surrounding covid-19. Systems Research and Behavioral Science **40**: 819–835.

Pratama, D. R. and G. Suryosukmono, 2024 The influence of motivation, authentic leadership, and organizational culture on employee performance in the south bengkulu health office. SENTRALISASI **13**: 83–96.

Ribeiro, M. F., C. G. d. Costa, and F. R. Ramos, 2024 Exploring purpose-driven leadership: Theoretical foundations, mechanisms, and impacts in organizational context. Administrative Sciences **14**: 148.

Sánchez, M. A. and M. De Batista, 2023 Business continuity for times of vulnerability: Empirical evidence. Journal of Contingencies and Crisis Management **31**: 431–440.

Shahi, S. G., 2024 Navigating uncertainty: How leaders can empower employees in times of crisis. In *Energy Crisis and Its Impact on Global Business*, pp. 238–255, IGI Global.

Shufutinsky, A., D. DePorres, B. Long, and J. R. Sibel, 2020 Shock leadership development for the modern era of pandemic management and preparedness. International Journal of Organizational Innovation **13**.

Shufutinsky, A., B. Long, J. R. Sibel, and B. B. H. Shufutinsky, 2023 Shock leader mindfulness: An essential element for leading organizations through crises. In *The Routledge Companion to Leadership and Change*, pp. 203–218, Routledge.

Sinha, D. and S. Sinha, 2020 Managing in a vuca world: Possibilities and pitfalls. Journal of Technology Management for Growing Economies **11**: 17–21.

Sort, J. C., R. V. Turcan, and Y. Taran, 2023 De-internationalisation, re-internationalisation and business model innovation: Exploring the intersection. Journal of Business Models **11**: 77–96.

Su, R., B. Obrenovic, J. Du, D. Godinic, and A. Khudaykulov, 2022 Covid-19 pandemic implications for corporate sustainability and society: A literature review. International Journal of Environmental Research and Public Health **19**: 1592.

Swierczek, A., 2024 Driven by supply chain ambidexterity. substitutable and complementary effects of supply chain emergence and control on triadic relational performance. Journal of Purchasing and Supply Management **30**: 100894.

Taran, Y., 2023 The challenge of authentic leadership in a volatile, uncertain, complex and ambiguous business environment. In *The Emerald Handbook of Authentic Leadership*, pp. 125–144, Emerald Publishing Limited.

Tariq, R., Y. Wang, and K. F. Latif, 2024 The impact of entrepreneurial leadership on the project success: the mediating role of knowledge-oriented dynamic capabilities. Journal of Enterprise Information Management **37**: 1016–1043.

Uhl-Bien, M., 2021 Complexity leadership and followership: Changed leadership in a changed world. Journal of Change Management **21**: 144–162.

Yel, H., 2024 The effect of school principals' quantum leadership behavior on organizational uncertainty. In *New Perspectives for Leadership after the COVID-19 Pandemic*, pp. 127–148, Apple Academic Press.

Zu, L., 2023 Overcoming sustainability challenges: The role of responsible management and leadership. In *Responsible Management and Taoism, Volume 1: Managing Responsibly for Sustainable Business Development in the VUCA World*, pp. 111–131, Emerald Publishing Limited.

How to cite this article: Ahmad, G., and Maamari, B. E. Managing Chaos: Leadership in Uncertain Environments. *Chaos Theory and Applications*, 7(2), 138-145, 2025.

CHAOS
Theory and Applications
in Applied Sciences and Engineering

e-ISSN: 2687-4539
RESEARCH ARTICLE
Vol.7 / No.2 / 2025 / pp.146-153
https://doi.org/10.51537/chaos.1643191

Frequency Chaos Game Method and Fractals Show Evolutionary Relationships of the PRKN Gene in Primates

Rodrigo Perez-Gala [*,1], **Yordy S. Cangrejo-Useda** [α,2], **Camila V. Castillo-Lopez** [α,3], **Maria J. Sanchez-Manjarrez** [α,4], **Cristian E. Cadena-Caballero** [α,5], **Francisco Martinez-Perez** [α,β,σ,6] **and Fernando Ramirez-Alatriste** [*,7]

*Maestría en Ciencias de la Complejidad, Universidad Autónoma de la Ciudad de México Campus Del Valle, Ciudad de México, 03100, México, [α] Laboratorio de Genómica Celular Aplicada (LGCA), Grupo de Investigación en Cómputo Avanzado y a Gran Escala (CAGE), Universidad Industrial de Santander, Bucaramanga, Santander, 680006, Colombia, [β] Grupo de Investigación, en Microbiología y Genética. Universidad Industrial de Santander, Bucaramanga, Santander, 680006, Colombia, [σ] Centro de Supercomputación y Cálculo Científico de la Universidad Industrial de Santander – (SC3UIS) Universidad Industrial de Santander, Bucaramanga, Santander, 680006, Colombia.

ABSTRACT The Chaos Game Representation (CGR) algorithm and its frequency-based optimization, the Frequency Chaos Game Representation (FCGR), offer alignment-free methods for analyzing DNA sequences through fractal geometry. This study investigates the evolutionary relationships of the *PRKN* gene in primates using FCGR, exploring his capacity to reveal phylogenetic signals. We applied FCGR to *PRKN* gene sequences from 16 primate species, calculating nucleotide frequencies and generating fractal representations. Phylogenetic relationships were inferred from fractal similarity and compared to established phylogenies and Shannon entropy was employed to correlate sequence organization with fractal patterns. Results demonstrate that FCGR effectively captures evolutionary relationships of the *PRKN* gene, yielding phylogenetic clustering consistent with conventional methods. The fractal patterns and their relation to Shannon entropy reveal structural organization within the *PRKN* gene sequence, independent of sequence length. This alignment-free, fractal-based approach offers a rapid and informative tool for studying genetic evolution, with potential applications in understanding primate phylogeny and neurodegenerative disorders linked to *PRKN*.

KEYWORDS
Chaos game representation
Frequency chaos game representation
Fractals
Phylogeny
PRKN gene
Primates
Evolutionary relationships

INTRODUCTION

Complex systems science provides a powerful framework for understanding biological organization across multiple scales, from molecules to ecosystems (Siegenfeld and Bar-Yam 2020). While a universal definition remains elusive, complex systems are characterized by large ensembles of interacting elements, spontaneous self-organization, and emergent non-trivial structures that cannot be predicted solely from individual components (Mitchell and Newman 2002). Within this paradigm, fractal geometry, the study of self-similar patterns at different scales, offers a unique lens for examining biological complexity (Retnaningsih 2024). Fractals, characterized by self-similarity, fractional dimensions, and iterative generation, are observed both geometrically and statistically in nature (Chatterjee and Yilmaz 1992; Kantelhardt 2008), and increasingly recognized as inherent properties of biological sequences and evolutionary processes (Saeed 2020).

The Chaos Game Representation (CGR) is a prime example of applying fractal concepts to DNA sequence analysis. CGR transforms nucleotide sequences into fractal images, notably the Sierpiński triangle, by iteratively mapping sequence elements to defined vertices in a geometric space (Barnsley 1988). This method, when applied to DNA, generates a 'Sierpiński carpet'-like fractal, visually encoding sequence-specific patterns (Jeffrey 1990). To enhance the analysis of large DNA sequences, the Frequency Chaos

Manuscript received: 20 February 2025,
Revised: 28 May 2025,
Accepted: 30 May 2025.

[1]galagro35@gmail.com
[2]stivencu2411@gmail.com
[3]taini0623@gmail.com
[4]mariasanchezmanjarres@gmail.com
[5]cadena.9605@gmail.com
[6]fjmartin@uis.edu.co
[7]fernando.ramirez@uacm.edu.mx (**Corresponding author**)

Game Representation (FCGR) was developed. FCGR utilizes k-mer frequencies to generate fractals, offering a more generalized and computationally efficient approach for analyzing long genomic regions (Bai-lin *et al.* 2000; Deschavanne *et al.* 1999). These fractal-based methods offer a graphical representation of global sequence properties (Löchel and Heider 2021) and have proven effective in phylogenetic analysis without sequence alignment, even for megabase-sized genomes (Jeffrey 1990; Bai-lin *et al.* 2000; Deschavanne *et al.* 1999). Furthermore, fractal structure can be quantitatively linked to Shannon entropy (Allen *et al.* 2009), a measure of information content or disorder within a sequence. By quantifying entropy, we can assess the information distribution and identify recurring patterns reflected in fractal formation (Allen *et al.* 2009), providing insights into the intrinsic organization of genetic information as a complex system (Mouchet and Mouillot 2010).

The study of complex patterns in biology has been explored across various disciplines, including physiology through chaos theory (Boubaker 2024), as well as in genetic networks exhibiting chaotic behavior (Kozlovska and Sadyrbaev 2024) and in cryptographic applications where dynamic DNA coding based on chaos enhances image encryption security (Patidar and Kaur 2024). Building upon these principles, this study examines the *Parkin RBR E3 Ubiquitin Protein Ligase* (*PRKN*) gene, a particularly relevant candidate for fractal analysis due to its inherent complexity. *PRKN* is the second largest gene in the human genome (Tanaka 2020), conserved across diverse species including primates (Marín *et al.* 2004), and characterized by a large size (1.3 Mbp in primates) with extensive intronic regions exceeding exon size (Munk *et al.* 2021). The encoded protein contains multiple conserved domains, including an N-terminal ubiquitin-like domain and C-terminal RING/IBR/RING finger motifs (Wang *et al.* 2023), and is involved in critical cellular processes such as protein ubiquitination and mitophagy (Leduc-Gaudet *et al.* 2022; Wang *et al.* 2023). Dysfunction of *PRKN* is strongly implicated in neurodegenerative disorders, particularly early-onset Parkinson's disease and autosomal recessive juvenile Parkinsonism (Ahmad *et al.* 2023; Olszewska *et al.* 2022). Given its complex structure, conserved evolutionary history, and functional significance, we hypothesize that the *PRKN* gene exhibits a discernible "fractal organization" reflecting its evolutionary trajectory. This fractal organization, visualized through FCGR and CGR, could provide a novel alignment-free approach to infer phylogenetic relationships among primates based on the *PRKN* gene.

Therefore, this study aims to: (1) calculate nucleotide frequencies and generate fractal representations of the *PRKN* gene in 16 primate species using FCGR and CGR; (2) construct a phylogeny based on fractal similarity; (3) explore the relationship between Shannon entropy and fractal patterns in *PRKN* sequences; and (4) compare the fractal-based phylogeny with established primate phylogenies. We hypothesize that FCGR and CGR will effectively reveal evolutionary relationships of the *PRKN* gene in primates, offering a rapid and alignment-free method for phylogenetic inference and providing insights into the complex organization and evolution of this critical gene.

MATERIALS AND METHODS

Database Construction and Nucleotide Frequency Calculation

***PRKN* Gene Sequence Retrieval:** *PRKN* gene sequences from 16 primate species were retrieved from the 'Primate *PRKN* gene database' (Cangrejo-Useda *et al.* 2025). Species included: *Homo sapiens*, *Gorilla gorilla gorilla*, *Pan paniscus*, *Pan troglodytes*, *Pongo abelii*, *Pongo pygmaeus*, *Macaca fascicularis*, *Macaca mulatta*, *Macaca thibetana thibetana*, *Rhinopithecus roxellana*, *Trachypithecus francoisi*, *Nomascus leucogenys*, *Symphalangus syndactylus*, *Microcebus murinus*, *Callithrix jacchus* and *Lemur catta*. These 16 species were selected to represent a broad phylogenetic range within primates, based on data availability and the existing literature on primate genomics. The database itself was curated by (Cangrejo-Useda *et al.* 2025) using the NCBI GenBank records. For each species, the longest available sequence annotated as the complete *PRKN* gene (including introns and exons) was selected. The selection of the longest available complete gene sequence aimed to ensure the inclusion of as much of the gene's architecture, including potential regulatory regions within introns, as possible for comprehensive fractal analysis. Sequence accession numbers are provided in (Cangrejo-Useda *et al.* 2025).

Sequence Cleaning and Nucleotide Frequency Analysis: To ensure analysis of only nucleotide sequences, identification tags, spaces, and any non-nucleotide characters were removed from each *PRKN* gene sequence using the Code FASTA SEQUENCE CLEANER program (GITHUB of the Complexity Science Group: Chaos, Fractals, Nature Applications (CSFANA) (Rodrigo-Gala 2025). This program verifies and cleans nucleic acid sequences downloaded from databases. The Code Nucleotide Relative Frequency Visualizer program (NRFV) ((CSFANA) (Rodrigo-Gala 2025)) was then used to calculate the total and relative frequency of each nucleotide (Adenine, Thymine, Guanine, Cytosine) for each *PRKN* gene sequence. These frequencies were used for subsequent fractal frequencies analysis.

Chaos Game Representation (CGR) and Frequency Chaos Game Representation (FCGR) Fractal Generation

Algorithm Description: Sierpiński Carpet fractals were generated using the 'Chaos Game' algorithm, implemented for *PRKN* gene sequences with the DNA Frequency Fractal Generator program (DFFG) ((CSFANA)(Rodrigo-Gala 2025)). The DFFG program is based on the work of (Allen *et al.* 2009) and (Cabrera-Becerril and Rayón 2025), and implements the frequency version of CGR as proposed by (Deschavanne *et al.* 1999), modified from the original Jeffrey method (Jeffrey 1990).

Fundamentally, CGR is a graphical method that translates a primary sequence (like DNA) into a two-dimensional fractal pattern. For DNA, each nucleotide (A, T, G, C) is assigned to a corner of a square. Starting from the center of the square, subsequent points are plotted iteratively: for each nucleotide in the sequence, a new point is plotted halfway between the previous point and the corner corresponding to the current nucleotide. This iterative process reveals underlying patterns in the sequence composition. The Frequency Chaos Game Representation (FCGR) builds upon CGR by focusing on the frequencies of k-mers (short nucleotide subsequences of length k). Instead of plotting individual points, FCGR divides the square into a grid where each cell corresponds to a specific k-mer. The intensity or color of each cell then represents the frequency of that k-mer in the sequence. This provides a quantitative and visual representation of the k-mer distribution, forming a characteristic 'Sierpiński carpet'-like fractal that reflects global sequence patterns

The FCGR algorithm operates by assigning each of the four DNA nucleotides (A, T, G, C) to a vertex of a unit square. For a given DNA sequence, the algorithm iteratively plots points within the square. The first point is typically placed at the center of the square. Subsequent points are generated by the following steps:

(a) $K = 1 - mer$

G	C
A	T

(b) $K = 2 - mer$

GG	GC	CG	CC
GA	GT	CA	CT
AG	AC	TG	TC
AA	AT	TA	TT

(c) $K = 3 - mer$

GGG	GGC	GCG	GCC	CGG	CGC	CCG	CCC
GGA	GGT	GCA	GCT	CGA	CGT	CCA	CCT
GAG	GAC	GTG	GTC	CAG	CAC	CTG	CTC
GAA	GAT	GTA	GTT	CAA	CAT	CTA	CTT
AGG	AGC	ACG	ACC	TGG	TGC	TCG	TCC
AGA	AGT	ACA	ACT	TGA	TGT	TCA	TCT
AAG	AAC	ATG	ATC	TAG	TAC	TTG	TTC
AAA	AAT	ATA	ATT	TAA	TAT	TTA	TTT

Figure 1 The configuration of string counters for K values ranging from 1 to 3 within squares of identical dimensions.

1. **Read the next nucleotide** in the DNA sequence. 2. **Identify the vertex** corresponding to that nucleotide (e.g., A=top-left, T=top-right, C=bottom-left, G=bottom-right). 3. **Calculate the midpoint** between the current point and the vertex identified in step 2. 4. **Plot a new point** at this midpoint. 5. **Repeat steps 1-4** for the entire DNA sequence.

In FCGR, instead of plotting each point individually, the algorithm calculates the frequency of k-mers (sequences of length k) within the DNA sequence. This frequency matrix is then used to generate a grayscale image representing the fractal. Higher k-mer frequencies are represented by darker pixels, and lower frequencies by lighter pixels, creating the Sierpiński carpet fractal pattern.

k-mer Size and Fractal Resolution: To determine the appropriate fractal resolution and pattern complexity, k-mer sizes ranging from 3 to 11 nucleotides were tested. A k-mer size of 7 nucleotides was chosen for the final analysis as it provided optimal resolution of recursive patterns and sufficient detail in the fractal images without excessive image darkening observed at larger k-mer sizes (≤ 8). Larger k-mer sizes resulted in overly dense fractals that obscured pattern visualization, while smaller k-mer sizes lacked the complexity to effectively differentiate sequences. Furthermore, the quadrant position in the fractals proposed by (Bai-lin *et al.* 2000) was used to construct fractals showed in Figure 1.

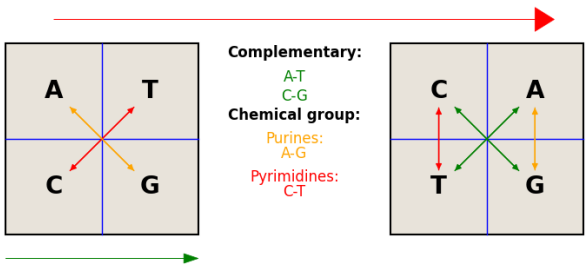

Figure 2 Quadrants arrangements to fractals construction. (a) Default parameters, (b) quadrant adjustment.

Quadrant Adjustment for Fractal Symmetry: To optimize fractal symmetry and definition, two quadrant arrangements for nucleotide assignment within the unit square were tested (Figure 2). The default arrangement (Figure 2a) placed Adenine-Thymine in the upper quadrants and Guanine-Cytosine in the lower quadrants. An alternative arrangement (Figure 2b) was tested, swapping to Cytosine-Adenine in the upper and Thymine-Guanine in the lower quadrants. The arrangement in Figure 2b, with complementary bases arranged diagonally and chemical groups (purines and pyrimidines) placed vertically, was chosen for improved visual symmetry and pattern clarity in the generated fractals.

Analysis of Fractal Images and Matrices

Occurrence frequency and composition of nucleotide k-mers for PRKN gene fractals in primates: The reading and counting of combinations for nucleotide k-mers of the *PRKN* gene from primates were generated with the **DFFG** program, to obtain the nucleotide occurrence frequency of each possible k-mer combination. The result was visualized in a grouped manner based on the number of occurrences and in descending order with the K-mer **Frequency-Clustering (KFC) and K-mer Frequency-Rank Plot (KFRP) programs** (CSFANA)(Rodrigo-Gala 2025).

The fractals generated by DFFG were verified using the **DNA Chaos Game Algorithm program (DCGA)** (CSFANA)(Rodrigo-Gala 2025). In this way, the fractal images of the *PRKN* gene in primates were verified.

Comparative Analysis of Frequency Matrices: The DFFG program also generates a frequency matrix representing the k-mer counts for each sequence. To analyze differences between these numerical matrices, the Numerical Matrix Difference Analyzer program (NMDA) ((CSFANA)(Rodrigo-Gala 2025) was employed. NMDA calculates the absolute percentage difference between corresponding cells in two matrices. For a set of matrices $M_1, M_2, ..., M_n$, the difference matrix Δ_i for each matrix M_i compared to all other matrices M_j ($j \neq i$) is calculated as:

$$\Delta_i = \{|M_i - M_j| \quad | \quad j \neq i\}, \quad \text{for} \quad i = 1, 2, ..., n. \tag{1}$$

The average percentage difference across all comparisons was used as a measure of matrix dissimilarity.

Phylogenetic Analysis and Dendrogram Construction

Phylogenetic Tree Construction: For comparison with fractal-based analyses, a phylogenetic tree of the *PRKN* gene was constructed using standard phylogenetic methods. Gene sequences were aligned using the Lamassemble program (Frith *et al.* 2021) with default parameters. *Mus musculus PRKN* gene sequence was used as an outgroup to root the tree. Phylogenetic analyses were performed using the CIPRES Science Gateway online platform (Miller *et al.* 2015). Maximum likelihood phylogenetic reconstruction was performed using IQ-Tree V.2.1.2 (Minh *et al.* 2020) with branch support assessed by ultra-bootstrap (Hoang *et al.* 2018) and SH-aLRT (Anisimova *et al.* 2011) with 1000 replicates each. The GTR+G substitution model was selected using jModelTest 2 (Darriba *et al.* 2012) based on the corrected Akaike information criterion (AICc).

Dendrogram Construction from Fractal Matrices: To visualize relationships based on fractal matrix similarity, dendrograms were constructed using the Similarity Dendrogram program (SimDendro) (CSFANA)(Rodrigo-Gala 2025). SimDendro calculates the Euclidean distance between frequency matrices and generates a similarity dendrogram. The cophenetic correlation coefficient was calculated to assess the fit between the dendrogram and the original distance matrix.

Shannon Entropy Calculation:

Shannon entropy ($H(X)$) for each *PRKN* gene sequence was calculated using the Shannon Entropy Calculator and Visualizer program (SECV) ((CSFANA)(Rodrigo-Gala 2025)) using the formula:

$$H(X) = -\sum_{i=1}^{n} P(x_i) \cdot \log_2 P(x_i) \tag{2}$$

where $P(x_i)$ is the frequency of each nucleotide (x_i) in the sequence, and $n = 4$ (for A, T, G, C). SECV calculates Shannon entropy and generates a ranked list and graph of entropies for all input sequences.

RESULTS

Primates *PRKN* gene nucleotide characterization

Consistent with previous reports (Cangrejo-Useda *et al.* 2025), the *PRKN* gene exhibited a conserved size of approximately 1,300,000 base pairs across the 16 primate species analyzed. Exceptions were observed in *Microcebus murinus* and *Lemur catta*, which displayed smaller sequence sizes, potentially due to intron/exon modifications or deletions (Supplementary Material 1).

The nucleotide composition analysis of the *PRKN* gene revealed an enrichment of adenine-thymine (A-T) compared to cytosine-guanine (C-G) pairs across all species. This pattern aligns with Chargaff's principle of base pair complementarity (Vischer and Chargaff 1948) but highlights a specific A-T enrichment in primate *PRKN* sequences. While *M. murinus* and *L. catta* exhibited similar overall patterns, the relative nucleotide frequencies were more balanced in *M. murinus*, potentially reflecting its reduced gene size. In contrast, *L. catta* displayed the highest A-T percentage among all species (supplementary material 1). These structural variations participate in the functional characteristics of the *PRKN* gene (Benisty *et al.* 2023) and could be related to the gene expansion and structure (Brovkina *et al.* 2023) .

Chaos Game Representation and Sierpiński Carpet Fractals

Nine fractal images, that corresponded to k-mer sizes from 3 to 11, were generated for each species (Supplementary Material 2). Recursive patterns emerged only for k-mer sizes of 7 to 11, with optimal resolution observed at $7-mers$ (Fig. 3). Larger k-mer sizes (≥ 8) resulted in image darkening, hindering pattern visualization. The fractal images for $7-mers$ displayed asymmetric, grid-like patterns dominated by black and navy-blue squares, reflecting low k-mer presence, particularly for combinations with high C-G content (Supplementary Material 2).

Distinct differences in fractal coloration were observed for *Callithrix jacchus*, *L. catta*, and *M. murinus*. These species exhibited red-dominated quadrants, indicative of altered k-mer distribution. The fractals of *M. murinus* lacked defined patterns, attributed to its reduced sequence size and balanced nucleotide proportions. Meanwhile, the fractals of *L. catta* and *C. jacchus* suggested an influence

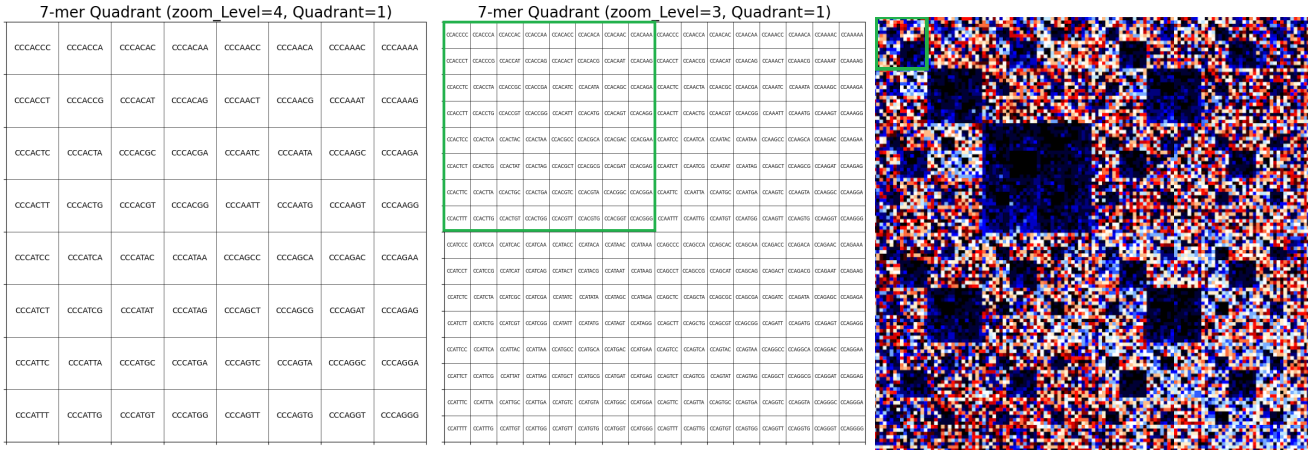

(a) zoom level = 4 **(b)** zoom level= 3 **(c)** without zoom

Figure 3 Visualization of 7-mers at different zoom levels and quadrants. (a) shows a more detailed area with zoom level = 4, where the matrix is divided into 16 parts per side, displaying a specific quadrant. (b) has zoom level = 3, dividing the matrix into 8 parts per side and showing the same quadrant at a larger scale. (c) displays the full matrix without zoom, allowing for structural comparisons at different scales. (illustrates the composition of the fractal.).

of tandem repeats within the *PRKN* gene on k-mer distribution (Sievers *et al.* 2021).

Adjusting the nucleotide arrangement in fractals (e.g., guanine-adenine and thymine-cytosine quadrants) maintained overall patterns but shifted the location of large squares, further validating the robustness of the methodology (Fig. 2, Supplementary Material 2).

Frequency and Composition of 7-Mer

Analysis of $7-mer$ frequencies revealed a total of 16,384 unique $7-mer$ combinations. Across most species, A/T-rich $7-mers$ occurred more frequently than G/C-rich $7-mers$. However, *Microcebus murinus*, *Callithrix jacchus*, and *Lemur catta* deviated from this trend, exhibiting comparable frequencies of GC-rich and AT-rich $7-mers$ (Quantitative data provided in Supplementary Material 1 and 2). This suggests a shift in k-mer frequency distribution in these species.

This k-mer distribution has showed similarities in the presence of short tandem repeats not only between animals but in the entire eukarya domain, as reported by (Sievers *et al.* 2021), and is higly related with the presence of transposable elements (Farré *et al.* 2011; Sievers *et al.* 2021), structures that may be content in the *PRKN* introns and explained: the AT enrichment in the gene and provides a possible explanation of the gene evolution and growth (Boissinot 2022; Sievers *et al.* 2021).

Quantitative Comparison of Fractal Images and Matrices

With the CGR and FCGR methodologies, the fractal images for the *PRKN* gene sequences confirmed regions of low and high k-mer density (Supplementary Material 4 and 5). The observed patterns were consistent across species, supporting the validity of the analytical approach. Additionally, dendrograms constructed from Euclidean distance matrices revealed clustering patterns that aligned closely with established phylogenies based on *PRKN* gene sequences and a known primate phylogeny (Makova *et al.* 2024; Duda and Zrzavý 2013).

Phylogenetic Relationships from Fractal Analysis and Comparison to Known Phylogeny

Dendrograms constructed from Euclidean distances of frequency matrices (SimDendro) using $7-mer$ data (Figure 4b, 4c, 4d) showed phylogenetic clustering largely consistent with established primate phylogenies (Makova *et al.* 2024; Duda and Zrzavý 2013) (Supplementary Material 6). Dendrograms without outgroup root-

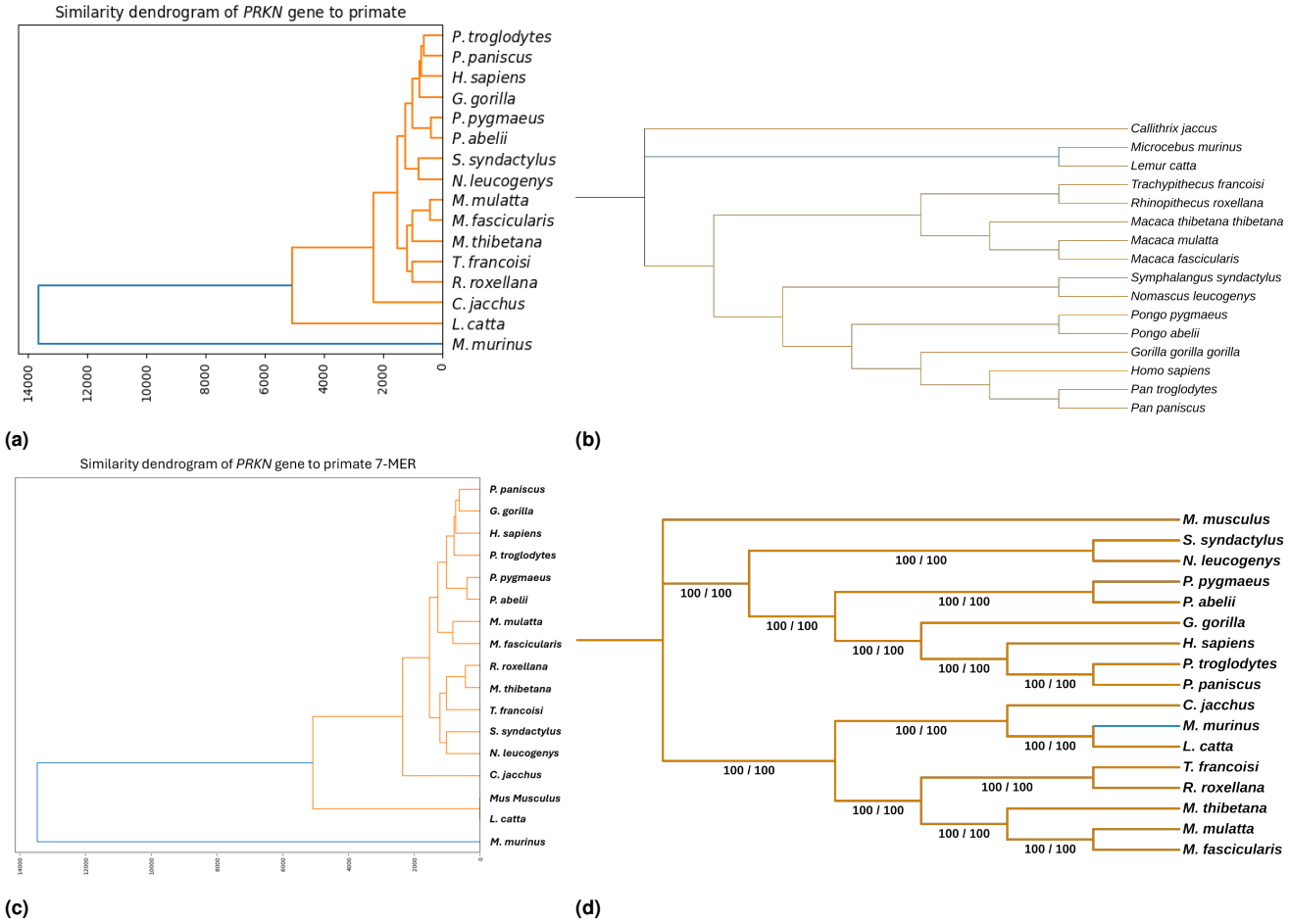

Figure 4 *PRKN* primates gene dendograms and phylogenies. Dendograms were generated with 7-mers and phylogenies were constructed with maximun likelihood aproximation. (a) and (b) corresponded to analisys without outgroup; and (c)-(d) included *M. musculus* as outgroup and rooted the phylogeny. (b) phylogeny was rooted by default. Numbers in phylogenies represents the bootstraps values for each node. Colors in branches indicate the species clustering similarities in dendograms respect to phylogenies. Exceptions were founded in (c) and (d), with diferent clustering to *M. murinus*.

ing (Figure 4a) clearly separated Hominoidea and Cercopithecoidea superfamilies. Inclusion of *Mus musculus* as an outgroup (Figure 4b, 4c) rooted the dendrogram and placed *Microcebus murinus* and *Lemur catta* as distinct outgroups to the main primate cluster, although the exact placement of *Microcebus murinus* varied depending on analysis parameters (Figure 4c, 4d). The cophenetic correlation coefficient for the dendrograms was consistently high (≥ 0.90), indicating a good fit between the dendrogram and the original distance matrix. Phylogenetic trees constructed using maximum likelihood (IQ-Tree) (Figure 4b, 4c, 4d) largely mirrored the topology of the fractal-based dendrograms, further supporting the phylogenetic signal captured by FCGR.

These results are consistent with previously reported *PRKN* Primate gene phylogeny (Cangrejo-Useda *et al.* 2025), which showed similar cluster of species. This suggests that fractal-based analyses capture meaningful evolutionary signals without the need for alignment. It is noteworthy that those phylogenetical reconstruction did not represented the evolutionary history of Primate species, but generates similar patterns, which suggest a strong conservation in this gene.

However, the inclusion of *PRKN* sequence of *M. musculus* in the dendogram construction, showed a different cluster in primates species, and suggested *M. murinus* as outgroup. This could be due to differences in gene size, which indicates the high influence of the sequence size in the dendogram construction. Despite this, the clustering of species without *M. musculus*, showed similarities respect to the *PRKN* phylogeny constructed with the standard protocol but in a reduced cost in time and computer requeriments, that reflects de accuracy of the method proposed here.

Shannon Entropy of *PRKN* Gene Sequences

Shannon entropy values for *PRKN* gene sequences ranged from 1.96 (*Lemur catta*) to 1.99 (*Microcebus murinus*), with an average of 1.97 for the other 14 species (Quantitative data provided in Supplementary Material 5). Lower Shannon entropy in *Lemur catta* correlated with more uniform, less complex fractal patterns. Conversely, higher entropy in *Microcebus murinus* corresponded to more diffuse, less defined fractal patterns. Overall, a trend was observed: species with lower Shannon entropy tended to exhibit more structured and visually distinct fractal patterns, while higher entropy correlated with less defined fractal structures, suggesting an inverse relationship between sequence randomness (entropy) and fractal pattern organization.

The high entropy in *M. murinus* could be related with its sequence size, however, it is difficult to determined the fidelity of the sequence, based in the gene physiology, its pattern of expression and the diffucult to access to genetic information of the species (Ahmad *et al.* 2023; Tanaka 2020). However, was possible to construct a dendogram similar to the phylogeny stablished to *PRKN* gene.

DISCUSSION

This study demonstrates the effectiveness of Frequency Chaos Game Representation (FCGR) and Chaos Game Representation (CGR) methods for analyzing evolutionary relationships of the *PRKN* gene in primates through fractal geometry. Our results show that FCGR, an alignment-free approach, successfully captures phylogenetic signals within *PRKN* gene sequences, yielding phylogenetic clustering largely congruent with established primate phylogenies derived from traditional alignment-based methods (Makova *et al.* 2024; Duda and Zrzavý 2013). This congruence is supported by both visual inspection of fractal patterns, quantitative analysis of fractal image and matrix differences, and dendrogram construction based on fractal similarity.

Advantages and Limitations of FCGR for Phylogenetic Analysis

FCGR offers several advantages for phylogenetic analysis, particularly for long DNA sequences like the *PRKN* gene. Being alignment-free, FCGR circumvents the computational cost and potential biases associated with multiple sequence alignment, a significant bottleneck for large-scale genomic datasets. FCGR provides a holistic, global view of sequence organization, capturing patterns that might be missed by alignment-based methods focused on local sequence similarity. The graphical fractal representation facilitates visual comparison of complex sequence patterns across species. However, FCGR also has limitations. As an alignment-free method, it may lack the fine-grained resolution of alignment-based methods for detecting subtle evolutionary differences at the nucleotide level. The choice of k-mer size is crucial and can influence the resulting fractal patterns and phylogenetic inference. Further research is needed to optimize k-mer size selection and explore the sensitivity of FCGR to different evolutionary scenarios.

Sequence Size Influence and *Microcebus murinus* Placement

The placement of *Microcebus murinus* as an outgroup in fractal-based dendrograms, and its variable positioning depending on analysis parameters, raises interesting questions. While consistent with the use of *Mus musculus* as an outgroup in the phylogenetic tree, the smaller sequence size of *Microcebus murinus PRKN* gene compared to other primates might influence fractal pattern generation and dendrogram placement. Smaller sequences may generate less complex or less defined fractal patterns, potentially affecting distance calculations and clustering. Future studies could investigate methods to normalize fractal analysis for sequence length variations, or explore the use of sliding window FCGR approaches to analyze sub-regions of the *PRKN* gene and assess regional variations in fractal patterns and phylogenetic signal.

PRKN Gene Fractal Organization, Entropy, and Evolution

The observed relationship between Shannon entropy and fractal patterns suggests a link between sequence organization and fractal structure in the *PRKN* gene. Lower Shannon entropy, indicative of less random nucleotide distribution, tended to correlate with more structured and visually distinct fractal patterns. Conversely, higher entropy correlated with less defined fractals. This suggests that regions of lower sequence entropy within the *PRKN* gene may contribute disproportionately to the formation of defined fractal patterns, potentially reflecting functionally important or evolutionarily conserved regions. For instance, the extensive intronic regions of the PRKN gene, which vastly exceed exon size, are known to harbor regulatory elements and reflect evolutionary history. The distinct fractal patterns observed could be influenced by the composition and organization of these introns, which might vary less in conserved functional regions, leading to lower entropy and more defined fractal sub-structures. Conversely, regions with higher mutation rates or less functional constraint might exhibit higher entropy and less defined fractal patterns. The observed AT-richness of the PRKN gene (as noted in Results) could also contribute to specific fractal signatures, as AT-rich regions often have different structural properties and evolutionary dynamics than GC-rich regions. While this study does not directly link fractal patterns to specific functional domains of the PRKN protein or its role in neurodegenerative disorders, future research could investigate the fractal organization of exons and introns separately

and explore correlations between fractal patterns, entropy profiles, and known functional elements within the PRKN gene. Furthermore, given PRKN's implication in Parkinson's disease, exploring whether disease-associated mutations or variants alter these fractal signatures could offer novel insights into genotype-phenotype correlations or even serve as a basis for computational diagnostic approaches. The alignment-free nature of FCGR makes it particularly suited for analyzing such large and complex genes where traditional alignment methods can be challenging. While this study does not directly link fractal patterns to specific functional domains of the *PRKN* protein, future research could investigate the fractal organization of exons and introns separately and explore correlations between fractal patterns, entropy profiles, and known functional elements within the *PRKN* gene. Furthermore, investigating how selection pressures and evolutionary events shape the fractal organization of genes like *PRKN* could provide novel insights into the evolution of gene structure and function.

Limitations and Future Directions

This study provides a preliminary investigation into the application of FCGR and CGR for primate *PRKN* gene phylogeny. Limitations include the use of a single gene (*PRKN*) and a limited number of primate species. Further studies should expand the analysis to include additional genes and a broader taxonomic sampling of primates and other mammals. Exploring the application of FCGR to other types of genomic data, such as non-coding regions or whole genomes, could further demonstrate the versatility of this approach. Developing more sophisticated quantitative metrics for characterizing fractal patterns beyond entry-by-entry differences could also enhance the analytical power of FCGR. Future research could also explore the biological significance of the observed fractal patterns and their relationship to gene function, regulation, and evolutionary adaptation.

CONCLUSION

The Frequency Chaos Game Representation (FCGR) method, and its base algorithm CGR, provide a valuable alignment-free approach for analyzing evolutionary relationships of the *PRKN* gene in primates. FCGR effectively captures phylogenetic signals, yielding dendrograms largely congruent with established phylogenies. The study highlights the potential of fractal geometry and FCGR as a rapid and informative tool for phylogenetic inference, particularly for long DNA sequences, and provides novel insights into the complex organization and evolution of the *PRKN* gene. Further research is warranted to explore the full potential of fractal-based methods in genomics and evolutionary biology, and to investigate the biological significance of fractal patterns in gene sequences.

Acknowledgments

This work was supported by Maestria en Ciencas de la Complejidad from the Universidad Autonoma de la Ciudad de Mexico, Campus Colonia del Valle, Mexico; by the Complexity Science Group: Chaos, Fractals, Nature Applications from the Universidad Autonoma de la Ciudad de Mexico. Moreover, by a research stay granted by the Universidad Industrial de Santander by resolution 558 of October 20, 2023, and for the Grupo de Investigación en Computo Avanzado y a Gran Escala (CAGE) from Centro de Supercomputacion y Calculo Cientifico of the Universidad Industrial de Santander.

Ethical standard

The authors have no relevant financial or non-financial interests to disclose.

Availability of data and material

Supplementary material can be found in (Perez-Gala *et al.* 2025).

Conflicts of interest

The authors declare that there is no conflict of interest regarding the publication of this paper.

LITERATURE CITED

Ahmad, A., D. Nkosi, and M. A. Iqbal, 2023 Park2 microdeletion or duplications have been implicated in different neurological disorders including early onset parkinson disease. Genes **14**: 600.

Allen, B., M. Kon, and Y. Bar-Yam, 2009 A new phylogenetic diversity measure generalizing the shannon index and its application to phyllostomid bats. The American Naturalist **174**: 236–243.

Anisimova, M., M. Gil, J. F. Dufayard, C. Dessimoz, and O. Gascuel, 2011 Survey of branch support methods demonstrates accuracy, power, and robustness of fast likelihood-based approximation schemes. Systematic biology **60**: 685–699.

Bai-lin, H., L. H.C., and Z. Shu-yu, 2000 Fractals related to long dna sequences and complete genomes. Chaos, Solitons & Fractals **11**: 825–836.

Barnsley, M. F., 1988 *Fractals Everywhere*. Academic Press, San Diego.

Benisty, H., X. Hernandez-Alias, M. Weber, M. Anglada-Girotto, F. Mantica, *et al.*, 2023 Genes enriched in a/t-ending codons are co-regulated and conserved across mammals. Cell systems **14**: 312–323.e3.

Boissinot, S., 2022 On the base composition of transposable elements. International Journal of Molecular Sciences **23**.

Boubaker, O., 2024 Chaos in physiological control systems: Health or disease? Chaos Theory and Applications **6**: 1–12.

Brovkina, M., M. Chapman, M. Holding, *et al.*, 2023 Emergence and influence of sequence bias in evolutionarily malleable, mammalian tandem arrays. BMC Biology **21**.

Cabrera-Becerril, A. and U. Rayón, 2025 Chaos-game_pygame.ipynb. Accedido: 16 de enero de 2025.

Cangrejo-Useda, Y. S., R. Perez-Gala, L. M. Vera-Cala, C. Barrios-Hernandez, E. P. Ardila-Sandoval, *et al.*, 2025 Prkn gene introns in families from order primates show common open reading frames.

Chatterjee, S. and M. R. Yilmaz, 1992 Chaos, fractals and statistics. Statistical Science **7**: 49–68.

Darriba, D., G. L. Taboada, R. Doallo, and D. Posada, 2012 jmodeltest 2: more models, new heuristics and parallel computing. Nature Methods 2012 9:8 **9**: 772–772.

Deschavanne, P. J., A. Giron, J. Vilain, G. Fagot, and B. Fertil, 1999 Genomic signature: characterization and classification of species assessed by chaos game representation of sequences. Molecular Biology and Evolution **16**: 1391–1399.

Duda, P. and J. Zrzavý, 2013 Evolution of life history and behavior in hominidae: Towards phylogenetic reconstruction of the chimpanzee–human last common ancestor. Journal of Human Evolution **65**: 424–446.

Farré, M., M. Bosch, F. López-Giráldez, M. Ponsà, and A. Ruiz-Herrera, 2011 Assessing the role of tandem repeats in shaping the genomic architecture of great apes. PLOS ONE **6**: 1–12.

Frith, M. C., S. Mitsuhashi, and K. Katoh, 2021 lamassemble: Multiple alignment and consensus sequence of long reads. Methods in molecular biology (Clifton, N.J.) **2231**: 135–145.
Hoang, D. T., O. Chernomor, A. V. Haeseler, B. Q. Minh, and L. S. Vinh, 2018 Ufboot2: Improving the ultrafast bootstrap approximation. Molecular biology and evolution **35**: 518–522.
Jeffrey, H. J., 1990 Chaos game representation of gene structure. Nucleic Acids Research **18**: 2163–2170.
Kantelhardt, J. W., 2008 Fractal and multifractal time series. Physics Reports **808**: 1–43.
Kozlovska, O. and F. Sadyrbaev, 2024 In search of chaos in genetic systems. Chaos Theory and Applications **6**: 13–18.
Leduc-Gaudet, J. P., S. N. Hussain, and G. Gouspillou, 2022 Parkin: a potential target to promote healthy ageing. The Journal of Physiology **600**: 3405–3421.
Löchel, H. F. and D. Heider, 2021 Chaos game representation and its applications in bioinformatics. Chaos **19**: 6263–6271.
Makova, K., B. Pickett, R. Harris, and et al., 2024 The complete sequence and comparative analysis of ape sex chromosomes. Nature **630**: 401–411.
Marín, I., J. I. Lucas, A. C. Gradilla, and A. Ferrús, 2004 Parkin and relatives: the rbr family of ubiquitin ligases. Physiological Genomics **17**: 253–263.
Miller, M. A., T. Schwartz, B. E. Pickett, S. He, E. B. Klem, *et al.*, 2015 A restful api for access to phylogenetic tools via the cipres science gateway. Evolutionary bioinformatics online **11**: 43–48.
Minh, B. Q., H. A. Schmidt, O. Chernomor, D. Schrempf, M. D. Woodhams, *et al.*, 2020 Iq-tree 2: New models and efficient methods for phylogenetic inference in the genomic era. Molecular biology and evolution **37**: 1530–1534.
Mitchell, M. and M. Newman, 2002 Complex systems theory and evolution. In *Encyclopedia of evolution*, edited by M. Pagel, pp. 1–5, Oxford University Press, New York, NY.
Mouchet, M. A. and D. Mouillot, 2010 Decomposing phylogenetic entropy into α, β and γ components. Biology Letters **6**: 665–668.
Munk, S. H., V. Voutsinos, and V. H. Oestergaard, 2021 Large intronic deletion of the fragile site gene prkn dramatically lowers its fragility without impacting gene expression. Frontiers in Genetics **12**.
Olszewska, D. A., A. McCarthy, A. I. Soto-Beasley, *et al.*, 2022 Parkin, pink1, and dj1 analysis in early-onset parkinson's disease in ireland. Irish Journal of Medical Science **191**: 901–907.
Patidar, V. and G. Kaur, 2024 Lossless image encryption using robust chaos-based dynamic dna coding, xoring and complementing. Chaos Theory and Applications **6**: 13–18.
Perez-Gala, R., Y. S. Cangrejo-Useda, C. V. Castillo-Lopez, M. J. Sanchez-Manjarres, C. E. Cadena-Caballero, *et al.*, 2025 Frequency chaos game method and fractals show evolutionary relationships of the prkn gene in primates.
Retnaningsih, R., 2024 Fractal geometry, fibonacci numbers, golden ratios, and pascal triangles as designs. The Journal of Academic Science **1**: 51–66.
Rodrigo-Gala, 2025 Complexity-science-group-chaos-fractals-nature-aplications. GitHub repository.
Saeed, M., 2020 Fractal genomics of sod1 evolution. Immunogenetics **72**: 439–445.
Siegenfeld, A. F. and Y. Bar-Yam, 2020 An introduction to complex systems science and its applications. Complexity **2020**: 6105872.
Sievers, A., L. Sauer, M. Hausmann, and G. Hildenbrand, 2021 Eukaryotic genomes show strong evolutionary conservation of k-mer composition and correlation contributions between introns and intergenic regions. Genes **12**.
Tanaka, K., 2020 The pink1-parkin axis: An overview. Neuroscience Research **159**: 9–15.
Vischer, E. and E. Chargaff, 1948 The composition of the pentose nucleic acids of yeast and pancreas. Journal of Biological Chemistry **176**: 715–734.
Wang, X. S., T. R. Cotton, S. J. Trevelyan, *et al.*, 2023 The unifying catalytic mechanism of the ring-between-ring e3 ubiquitin ligase family. Nature Communications **14**: 14.

How to cite this article: Perez-Gala, R., Cangrejo-Useda, Y. S., Castillo-Lopez, C. V., Sanchez-Manjarres, M., Cadena-Caballero, C. E., Martinez-Perez, F., and Ramirez-Alatriste, F. Frequency Chaos Game Method and Fractals Show Evolutionary Relationships of the PRKN Gene in Primates. *Chaos Theory and Applications*, 7(2), 146-153, 2025.

CHAOS
Theory and Applications
in Applied Sciences and Engineering

e-ISSN: 2687-4539
RESEARCH ARTICLE
Vol.7 / No.2 / 2025 / pp.154-165
https://doi.org/10.51537/chaos.1588198

A Chaos-Causality Approach to Principled Pruning of Dense Neural Networks

Rajan Sahu [*,1], **Shivam Chadha** [α,2], **Archana Mathur** [β,3], **Nithin Nagaraj** [§,4] **and Snehanshu Saha** [γ,5]

[*]Dept. of CSIS, Birla Institute of Technology and Sciences Pilani, Pilani, India, [α]Dept. of Mathematics, BITS Pilani KK Birla Goa Campus, Goa, India, [β]Dept. of Artificial Intelligence and Data Science, Nitte Meenakshi Institute of Technology (NMIT), Bangalore, India, [§]Complex Systems Programme, National Institute of Advanced Studies, Bangalore, India, [γ]Dept. of CSIS and APPCAIR, BITS Pilani KK Birla Goa Campus, Goa, India.

ABSTRACT Reducing the size of a neural network (pruning) by removing weights without impacting its performance is an important problem for resource-constrained devices. In the past, pruning was typically accomplished by ranking or penalizing weights based on criteria like magnitude and removing low-ranked weights before retraining the remaining ones. Pruning strategies also involve removing neurons from the network to achieve the desired reduction in network size. We formulate pruning as an optimization problem to minimize misclassifications by selecting specific weights. We have introduced the concept of chaos in learning (Lyapunov Exponents) through weight updates and used causality-based investigations to identify the causal weight connections responsible for misclassification. Two architectures are proposed in the current work - Lyapunov Exponent Granger Causality driven Fully Trained Network (LEGCNet-FT) and Lyapunov Exponent Granger Causality driven Partially Trained Network (LEGCNet-PT). The proposed methodology gauges causality between weight-specific Lyapunov Exponents (LEs) and misclassification, facilitating the identification of weights for pruning in the network. The performance of both the dense and pruned neural networks is evaluated using accuracy, F1 scores, FLOPS, and percentage pruned. It is observed that, using LEGCNet-PT/LEGCNet-FT, a dense over-parameterized network can be pruned without compromising accuracy, F1 score, or other performance metrics. Additionally, the sparse networks are trained with fewer epochs and fewer FLOPs than their dense counterparts across all datasets. Our methods are compared with random and magnitude pruning and observed that the pruned network maintains the original performance while retaining feature explainability. Feature explainability is investigated using SHAP and WeightWatchers. The SHAP values computed for the proposed pruning architecture, as well as for the baselines (random and magnitude), indicate that feature importance is maintained in LEGCNet-PT and LEGCNet-FT when compared to the dense network. WeightWatchers results reveal that the network layers are well-trained.

KEYWORDS
Chaos
Granger causality
Neural networks
Lyapunov exponent
Weight pruning

INTRODUCTION

Designing a neural network architecture is critical to developing neural networks for various Artificial Intelligence (AI) tasks, particularly in deep learning. AI, or Artificial Intelligence, refers to the simulation of human intelligence in machines designed to perform tasks typically requiring human cognition. These tasks include learning, problem-solving, reasoning, and understanding natural language. AI systems use algorithms and data to improve their performance over time, often becoming more efficient with experience.

One of the fundamental challenges in designing neural networks is finding the right balance between model complexity and sample size, which can significantly impact the network's performance. In general, a larger network with more parameters (overparameterized) can potentially learn more complex functions and patterns from the data (Prandi *et al.* 2017). However, larger networks may also be prone to overfitting. On the other hand, smaller networks with fewer parameters may not have enough capacity to learn complex relationships in the data. This can lead to underfitting. Therefore, the challenge in network architecture design is to find the right balance between model complexity and sample size, so that the network can learn to generalize well to new, unseen data. In this context, over-parameterized networks (Zou *et al.* 2018; Mohapatra *et al.* 2022) have become increasingly popular in the deep learning era due to their ability to achieve high expressivity and potentially better generalization performance (Shen *et al.* 2019). The idea is to increase the number of parameters in the network beyond what is strictly necessary to fit the training data and remarkable generalization to test data. Pruning techniques should reduce the number of parameters in a neural network without compromising its accuracy.

Manuscript received: 21 November 2024,
Revised: 24 February 2025,
Accepted: 27 March 2025.

[1]f20190572p@alumni.bits-pilani.ac.in
[2]f20190704g@alumni.bits-pilani.ac.in
[3]archana.mathur@nmit.ac.in (**Corresponding author**)
[4]nithin@nias.res.in
[5]scibase.snehanshu@gmail.com

It is important to ponder why we do not simply train a smaller network from scratch to make training more efficient. The reason is that the architectures obtained after pruning are typically more challenging to train from scratch (Liu *et al.* 2018), and they often result in lower accuracy compared to the original networks. Therefore, while standard pruning techniques can effectively reduce the size and energy consumption of a network, it does not necessarily lead to a more efficient training process.

BACKGROUND AND PROBLEM STATEMENT

Neural network pruning has two main goals to achieve - one being the reduction of model size and the other being a consequence of the former - improved inference efficiency. Traditional pruning methods such as random pruning (Mittal *et al.* 2018b,a) or magnitude-based pruning (Lee *et al.* 2020; Saleem *et al.* 2024) inherently incorporate a form of regularization that could potentially affect or hinder the natural course of learning dynamics of a model. Even though empirically the methods seem to work well, we are interested in a principled approach of pruning that takes the model's task performance into account. Random pruning removes weights in a stochastic manner. Magnitude-based pruning removes weights based on their absolute values, assuming a certain relationship between the magnitude of weights and contribution in the final model performance (Medhat *et al.* 2023). These methods fundamentally don't operate under a static or predefined criterion that does not dynamically adapt to the model's learning trajectory. A key limitation of these approaches is that they impose pruning decisions as an implicit form of regularization rather than integrating pruning dynamically into the optimization process itself.

We pose a broad *Research Question* here: Is there a principled approach to pruning overparameterized, dense neural networks to a reasonably good sparse approximation such that performance is not compromised and explainability is retained? It is well known that dense neural network training and particularly weight updates via SGD have some element of chaos (Zhang *et al.* 2021; Herrmann *et al.* 2022). We expect that, between the successive weight updates due to SGD and miss-classification, there is some observed causality and non-causal weights (parameters) can be pruned, leading to a sparse network i.e. some weight updates cause a reduction in network (training) loss and some do not! Can we train a dense network till a few epochs to derive a pruned architecture for the derivative to run for the remaining epochs and produce performance metrics in the $\epsilon-$ball of the original, dense network? Does this sparse network also train well, verified with Shapley (Lundberg and Lee 2017) and WeightWatcher (*WW*) (Martin *et al.* 2020) tests? Specifically, we contribute to the following:

- Present a unique and unifying framework on chaos and causality for deep network pruning. The unifying framework uses Lyapunov Exponent (LE) (Kondo *et al.* 2021) and Granger causality (GC) (Granger 1969) tandem.
- Propose novel pruning architectures, Lyapunov Exponent Granger Causality driven Fully Trained Network (LEGCNet-FT) and Lyapunov Exponent Granger Causality driven Partially Trained Network (LEGCNet-PT).
- LEGCNet-FT and LEGCNet-PT compare very well in performance and other baselines, Random (Liu *et al.* 2022) and Magnitude based (Li *et al.* 2018) pruning techniques.
- Establish feature consistency of LEGCNet-FT and LEGCNet-PT in explainability.
- Verify empirically that the proposed architectures for pruning are not over-trained and obviously not overparameterized but can still generalize well, on diverse data sets while saving FLOPs (FLoating-point OPeration). We accomplish this via the *WW* test.

We approach pruning as a constrained optimization problem rather than a strict regularization step. Instead of focusing purely on reducing network size, we ensure that pruning decisions adhere to model performance, directly accounting for accuracy and fewer epochs. Using Lyapunov Exponents (LE) and Granger Causality (GC), we identify non-causal weights parameters that do not significantly contribute to loss minimization and selectively remove them. Unlike traditional methods that prune weights based on static criteria, our approach dynamically adapts pruning decisions based on learning dynamics. Our LEGCNet-FT (Fully Trained) and LEGCNet-PT (Partially Trained) frameworks validate this approach. LEGCNet-FT performs pruning after full training, while LEGCNet-PT identifies and removes non-causal weights early in training, significantly reducing computational overhead without compromising accuracy. This adaptive strategy ensures that pruning is an integral part of optimization rather than an afterthought.

The remainder of the paper is organized to present the key methodologies used to develop the pruning technique, followed by a detailed experimental setup and strong empirical evidence of the proposed technique in contrast to the baselines. In summary, we propose pruning techniques, *LEGCNet-FT and LEGCNet-PT* which perform at par with the dense, unpruned architecture and the existing pruning baselines. *In methods like magnitude/random pruning, the choice of percentage pruning for a specific dataset or network is often arbitrary and difficult to select. Our method gives a natural threshold for weight pruning, unlike random, magnitude, and other pruning methods. While maintaining consistent performance, these techniques also help reduce epochs to converge and FLOPs to compute while maintaining feature consistency with their dense counterparts and ensuring proper training across layers validated via WW statistics.*

We claim the following:

- Non-causal weights are identified as the ones which do not impact the accuracy and therefore must be removed from the fully connected network. Such a pruned network performs as well as the dense counterpart, retains the feature explainablity of the dense sibling.
- *Why is feature consistency IN SHAP (explainability test) important for pruned networks?*.
- Such a pruned network satisfies the network health diagnostic test (Weightwatcher (*WW*)) and also incurs reduced floating point operations (FLOPs). Additionally, the stable equilibrium in the loss landscape can be obtained if we can construct a suitable Lyapunov (Energy) function. The motivation for pruning is strongly tied to the health diagnostic tests for DNNs, *WW* in particular. This is because it is possible to establish all layers of a DNN to be correctly trained and therefore not contribute to the generalization gap. This indicates some induced, implicit self-regularization via pruning. Therefore, favorable *WW* Statistics is a strong indicator of the pruned network's spectral distribution being heavy-tailed i.e. the pruned network is correctly trained. This establishes the validity of the pruning mechanism proposed in the paper.

The technical motivation behind our claims is sourced from a diverse set of questions- Why chaos? Does Chaos helps learning and can we support it with experimental results? Do we expect causality between 2 time series sequences weight and loss series? Does it

satisfy the lottery ticket hypothesis by deriving a pruned network by deleting no-causal weights? Wiener-Granger causality is based on the principle that "predictability implies causation". We believe that causality, as estimated by Granger causality, is in any case not to be treated as actual causality, but only an indication of predictability of one time series with the incorporation of information from another time series. This type of predictability also means a kind of redundancy of information and hence informs and justifies the pruning to be carried out. With this view of pruning (of redundant connections) in mind, we need only a reasonable measure of estimating such redundancies in the connections. For this purpose, Granger causality is sufficient. More sophisticated methods such as Transfer Entropy, Compression-Complexity Causality could be tried out in future versions of this work.

It should be noted that the mere use of statistical measures such as correlation or mutual information does not suffice as they lack the directionality of information flow, which is provided by causality measures such as Granger causality and others. The direction of the flow of information is important since we are interested in knowing which connections influence misclassification errors and which ones do not so that pruning can be done appropriately. As per Judea Pearl's ladder of causation, associations (correlations) are at the first rung of the ladder and measures such as Granger causality are at a higher rung. This is a unified view of statistical correlations and causation - seen to be at different levels of measures of information flow (or influence). Chaos, causality, and the manifestation of the Lottery Ticket Hypothesis are the key motivations behind our proposed pruning mechanism.

Chaos and Causality

One way to address the issue of explainability in AI/machine learning is to seek causal explanations for choices made in the learning process. Conversely, a learning process that incorporates choices made out of causal considerations is easier to explain and interpret. This is the motivation behind using causality-based criteria for the choice of what to prune (or not prune) in this study. To this end, we employ Granger Causality (GC) (Granger 1969), one of the earliest and nearly model-free causality testing between two processes (or measurements/time series).

The principle of pruning that is causally informed is formulated as follows. Those connections (weights) in the learning network that do not causally impact the loss are chosen for pruning. To determine the causal impact of a particular connection to the loss, we perform GC between the windowed LE of the weight time series for that connection and the classification accuracy. The rationale behind this is the intuition that the chaotic signature of weight updates supports learning. Biological inspiration for chaotic signatures as a marker for learning is the empirical fact that neurons in the human brain exhibit chaos (Faure and Korn 2001; Korn and Faure 2003) at all spatiotemporal scales. Starting from single neurons to coupled neurons to a network of neurons to different areas of the brain, chaos has been found to be ubiquitous to the brain (Korn and Faure 2003).

Chaotic systems are known to exhibit a wide range of patterns (periodic, quasi-periodic, and non-periodic behaviors), are very robust to noise, and enable efficient information transmission (Nagaraj and Vaidya 2009), processing/computation (Ditto and Sinha 2015), (Kuo 2005) and classification (Balakrishnan *et al.* 2019). There is also some evidence to suggest that weak chaos is likely to aid learning (Sprott 2013). Thus our choice of testing causal strength between LE (a value > 0 is a marker of chaos) and classification accuracy as a criterion for pruning to yield sparse subnetworks that capture the learning of the task at hand.

Gradient Descent and Low Dimensional Chaos

Is the process of updating weights in backpropagation via Gradient Descent chaotic? Is there an alternative interpretation of the minima in the weight landscape via low-dimensional chaos? The weight update in SGD is written as $w_{i+1} \leftarrow w_i - \eta_i \nabla_w f(w_i)$ may be thought of as a discretization to the first order ODE: $w'(t) = -\nabla_w f(w_i)$. The minimizer of the SGD is therefore conceived as a stable equilibrium of the ODE. That is, the minimum, w^* can be thought of as a fixed point to the iterates $w_{i+1} = G(\eta_i, w_i) \equiv w^* = G(\eta_i, w^*)$.

Empirical evidence of chaos in backpropagation: We performed a series of experiments on different datasets to check Sensitive Dependence On Initial Conditions (SDIC) for weight initialization, on a single hidden layer neural network. The weight initialization matrix W_{ij} followed Gaussian distribution $(W_{ij} \sim N(0, \sigma^2))$. We recorded two sets of executions - one with initial weight $w_{11} : w_{ij} \forall i \in 1..h, \forall j \in 1..n$, where n, h are the number of input and hidden neurons - and another, with infinitesimal perturbation $(w_{11} + \delta)$ keeping other parameters same. Each time, the network was trained via gradient descent, and weight series were recorded. The method was repeated for the second weight connection $w_{ij}, i = 1, j = 2$. Later, the Lyapunov Exponents (LE) were computed using the TISEAN package (Hegger *et al.* 1998) on the recorded weight series to measure the perturbed trajectory due to initial perturbation δ. We observed positive LE which marked the presence of some chaotic behavior in gradient descent.

In other words, to introduce perturbation in our experiments, we initialize the weights of the dense neural network and run the experiment under normal conditions. Once a baseline is established, we induce a controlled perturbation on a single weight connection. Specifically for a given weight, we introduce a small perturbation modifying it to the original weight, added with an infinitesimally small value before we start training the model. For example, a weight w0 is initialized to w0=2.0 in the first run, and after adding a small perturbation, w0=2.0001, we rerun the backpropagation capturing the weight updates each time. The purpose of this perturbation is to analyse the sensitivity of the model to slight alterations and observe how these changes propagate through the learning process. We try to investigate if the learning process is chaotic. The computation of Lyapunov exponents and their positive values confirms the presence of weak chaos during backpropagation.

Lottery ticket hypothesis

The "lottery ticket hypothesis" (Frankle and Carbin 2018) is a concept in neural network pruning that suggests that within a dense and over-parameterized neural network, there exist sparse subnetworks that can be trained to perform just as well as the original dense network. Any fully connected feed-forward network $f^d(x; \phi)$, with initial parameters ϕ when trained on a training set D, f^d achieves a test accuracy a and error e at iteration j. Our work LEGCNet, validates the lottery ticket hypothesis by finding the "winning ticket", m, to construct the sparse network, f^s such that $acc^s \geq a$ and $j^s < j$ where $\|\phi\| \gg \|m\|$.

MATERIALS AND METHODS

Dense Neural network - Let f^d be a dense neural network of depth l and width h defined as

$$f^d(x) = W_i^d \sigma_i(W_{i-1}^d \sigma_i(...W_1^d(x))) \tag{1}$$

where W_i^d is the weight matrix for layer i such that $i \in 1..l$.
Sparse Neural Network - Let f^s be sparse neural network of the same architecture as f^d, with depth l and width h.
Two approaches: LEGCNet-FT and LEGCNet-PT - To validate the working of LEGCNet, we divided the method into two discrete approaches. In one approach, the entire training weight series is used for computing LEs, testing GC, and for the identification of causal weights. Essentially, the dense network is trained till convergence and the approach is called LEGCNet-Full Train (LEGCNet-FT). In the second approach, LEGCNet-PT, the network is trained only till certain epochs (10% of the total iterates) and these few weight updates are used for identifying the causal weights.

Granger causality as a tool

We have used popular model-free/ data-driven methods such as Wiener-Granger Causality or G-causality. Granger causality or G-causality works on the principle of modeling the two processes X and Y as auto-regressive processes. Specifically, to determine if '*Y G-causes X*', the two models considered are:

$$X(t) = \sum_{\tau=1}^{\infty} (p_\tau X(t-\tau)) + \sum_{\tau=1}^{\infty} (r_\tau Y(t-\tau)) + \varepsilon_c, \tag{2}$$

$$X(t) = \sum_{\tau=1}^{\infty} (q_\tau X(t-\tau)) + \varepsilon, \tag{3}$$

where t stands for time, p_τ, q_τ, r_τ are coefficients at a time lag of τ and $\varepsilon_c, \varepsilon$ are error terms. Covariance stationarity is assumed for both X and Y. Whether Y G-causes X (or not) can be predicted by the measure known as F-statistic which is the log ratio of the prediction error variances:

$$F_{Y \to X} = \ln \frac{var(\varepsilon)}{var(\varepsilon_c)}. \tag{4}$$

If the model represented by equation (2) is a better model for $X(t)$ than equation (3), then $\text{var}(\varepsilon_c) < \text{var}(\varepsilon)$ and $F_{Y \to X} > 0$, suggesting that *Y Granger causes X*. Even though G-causality uses the notion of autoregressive models for the variables, the generic nature of this modeling with minimal assumptions about the underlying mechanisms makes it a popular choice in a wide range of disciplines.

Lyapunov exponents as a tool

In dynamical systems, Lyapunov exponents are used to measure the rate of divergence of infinitesimally close trajectories, and they are an important tool for characterizing the behavior of chaotic systems. In a chaotic system, even small differences in initial conditions can lead to large differences in the behavior of the system over time. Lyapunov exponents provide a way to quantify sensitivity to initial conditions, and they can be used to predict the long-term behavior of a system. Systems with positive Lyapunov exponents are considered to be chaotic, while systems with negative Lyapunov exponents are stable and predictable. The magnitude of the Lyapunov exponents provides information about the rate of divergence or convergence of close trajectories, and this can be used to study the dynamics of neural network training (via gradient descent) in a quantitative way. It's worth noting that the Lyapunov exponent is a sensitive measure of chaos and requires careful numerical computation.
A differential equation defining a continuous-time smooth dynamical system in n dimensions is given as $\dot{x} = f(x)$ where $f : U- > R^n$ is a continuous function and $x(t) \in R^n$ is a state variable at time t. A map $f : U- > R^n$ defines a discrete-time smooth dynamical system in n-dimensions, as $x_{t+1} = f(x_t)$ where x_t is the state of the system at time t. Let there be two points x_0 and $x_0 + \delta_0$ which are separated by a small vector δ at t=0. At time t, the rate of separation of the two neighboring points, as they travel in a chaotic region, is given as $|\delta_t| \approx |\delta_0| e^{\lambda t}$ where λ is the LE, δ_0 is the difference between the two trajectories at t=0 and δ_t is the difference at t=t. The λ is calculated as

$$\lambda_{f(x)} = \lim_{\delta_0 \to 0} \lim_{n \to \infty} \left\{ \frac{1}{n} ln \frac{|\delta_t|}{|\delta_0|} \right\} \tag{5}$$

Different methods exist for calculating the Lyapunov exponent, such as the Wolf algorithm (Wolf *et al.* 1985) or the Rosenstein method (Rosenstein *et al.* 1993), which have specific considerations depending on the system being studied.

Windowed Weight Updates

Consider a neural network with n inputs and r outputs, p hidden layers of h neurons, and, the input vector denoted as $x \in R^n$, The network when trained by SGD generates a sequence of weight updates represented by $w^{ji} = \left[w_0^{ji}, w_1^{ji}, ..., w_s^{ji}, ..., w_S^{ji} \right]$ where w_s^{ji} is the weight of the ith neuron of the input layer and the jth neuron of the hidden layer at the sth iteration. Considering, the weights being collected for the initial few epochs, the weight iterates for the hidden layer and output layer are $W_h = \left\{ w^{ji} \right\}, W_o = \left\{ w^{kj} \right\} \quad \forall i \in \{1,..,n\}, \forall j \in \{1,..,m\}, \forall k \in \{1,..,r\}$ An infinitesimal perturbation δ_0 is introduced in the initial weight w^{11}, given as $w^{11\delta_0} = w^{11} + \delta_0$, keeping other parameters - weights (initialization), learning rate, optimizer, and loss function- same. The network is then retrained with the perturbed weight, and the weight updates are recorded again as $W_h^{\delta_0} = \left\{ w^{ji\delta_0} \right\}, W_o^{\delta_0} = \left\{ w^{kj\delta_0} \right\} \quad \forall i \in \{1,..,n\}, \forall j \in \{1,..,m\}, \forall k \in \{1,..,r\}$ A difference series obtained by subtracting perturbed weights from initial weights is $\delta W_h = \left\{ \delta w^{ji} \right\}, \delta W_o = \left\{ \delta w^{kj} \right\} \quad \forall i \in \{1,..,n\}, \forall j \in \{1,..,m\}, \forall k \in \{1,..,r\}$. We divide the weight series δw^{ji} into D windows, $w^{ji} = \bigcup_{l=1}^{D} w^{ji(l)}$, and compute the LEs of all the windowed-weight trajectories. The series of the LE λ of the windowed-weight trajectories $w^{ji(D)}$ are represented using the notation $\left\{ \lambda^{ji\{1\}}, \lambda^{ji\{2\}}, ..., \lambda^{ji\{D\}} \right\}$. Additionally, we record the accuracy at every window during training $\forall l \in 1, \ldots, D$, captured for weights at $w^{ji(l)}$ and $w^{kj(l)}, \forall i \in \{1,..,n\}, \forall j \in \{1,..,m\}, \forall k \in \{1,..,r\}$. After computing the series of windowed-Lyapunov exponents and corresponding *wls*, we test the Granger Causality (GC) between them. The F-statistics of the two series are computed, and the p-value is measured to check whether the windowed-Lyapunov exponents "Granger-caused" the loss, *wls*. If so, then this reveals that certain weight connections are causing the loss, and they are pruned from the network. Hence, the weights that resulted in Lyapunov exponents "Granger-causing" the loss, are chosen for pruning. Before checking the GC, we confirmed that the series is stationary.

Approximation capability of LEGCNet

The approximation capability of LEGCNet is explored here, that a sparse network, f^s, and dense network, f^d are ϵ close to each other if the activation function used in the network satisfies the Lipschitz property . We have theoretically established that the AF sigmoid is Lipschitz (Lemma 1) and showed the sparse network LEGCNet, approximates the dense counterpart.

The motivation of the theoretical analysis is taken from (Qian and Klabjan 2021) which states that the approximation abilities of dense and sparse networks are ϵ close only if an activation function is L1 Lipschitz. The main theorem and lemma in this section build that the LEGCNet pruned network (f^s) is ϵ-close to f^d with probability 1-δ (Qian and Klabjan 2021). Consider f^d to be a dense neural network in Figure 1 defined as

$$f^d(x) = W_i^d \sigma_i(W_{i-1}^d \sigma_i(...W_1^d(x))) \tag{6}$$

where W_i^d is the weight matrix for layer i such that $i \in 1..l$ and $h_i > h_0, h_i > h_l, \forall i \in 1...(l-1)$. We assume that for network in (6), σ_i is L_i-Lipschitz and weight matrix W_i^d is initialized from uniform distribution $U[\frac{-K}{\sqrt{max(h_i,h_{i-1})}}, \frac{K}{\sqrt{max(h_i,h_{i-1})}}]$, for some constant K.

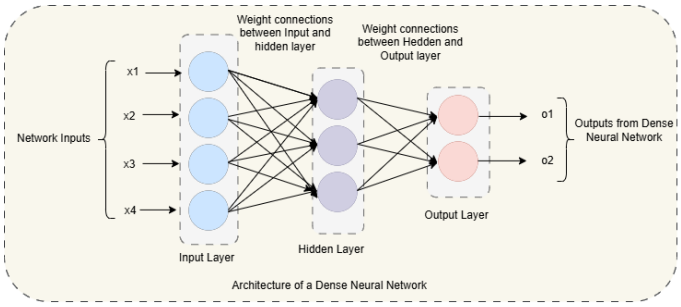

Figure 1 Dense Neural Network

Theorem 0.1. *(Approximation Capability of the Sparse Network) Let* $\epsilon > 0$, $\delta > 0$, $\alpha \in (0,1)$ *such that the, for some constants* K_1, K_2, K_3, K_4, K_5,

$$h \geqslant max\left\{K_1^{\frac{1}{\alpha}}, \left(\frac{K_2}{\epsilon}\right)^{\frac{1}{\alpha}}, \left(\frac{K_3}{\delta}\right)^{\frac{1}{\alpha}}, K_4 + K_5 log\left(\frac{1}{\delta}\right)\right\}$$

then sparse network f^s *obtained from LEGCNet by the mask m, and pruning the weights* $W_i^d, \forall i \in 1...l$ *is* ϵ*-close to* f^d*, with the probability* $(1-\delta)$*, i.e.*

$$\sup_{x \in B_{d0}} \left\| f^s(x) - f^d(x) \right\|_2 \leq \epsilon$$

Remark: Lipschitz property of the activation functions (Saha *et al.* 2020) is a necessary condition to validate the approximation capability of the proposed sparse network. We have used *sigmoid activation* in the sparsely trained/pruned network.

Lemma 0.2. *Sigmoid activation is Lipschitz.*

Proof: If a function $f(x)$ is Lipschitz continuous, then: $\|f(x) - f(y)\| \leq K\|x-y\| \equiv \|f'(x)\| \leq K$. If $K < 1, f$ is a contraction map as well. We know that Sigmoid, $\sigma(x) = \frac{1}{1+e^{-x}}$; and $\|\sigma'\| = \|\sigma(x)(1-\sigma(x))\|$. It's easy to follow that : $\|\sigma(x)(1-\sigma(x))\| \leq \|\sigma(x)\| \|1-\sigma(x)\| \leq C_1, C_2$. Since $0 \leq C_1, C_2 \leq 1$, $C_1 * C_2 = \delta \leq 1$. Hence sigmoid is Lipschitz.

Methodology Overview

Our methodology in Figure 2 gauges causality between weight-specific Lyapunov Exponents (LEs) and misclassification, facilitating the identification of weights for pruning and retention in the network. In the initial step, we train an MLP and record the weights at the end of each iteration (single forward and backward pass), resulting in a time series of weights for the entire training batch. In the first round of training, the weight series is saved for all the weight connections. We introduce a small perturbation in one weight connection and train the network for the second time. Inducing a perturbation is done to discover the chaotic behavior of a NN by investigating the SDIC of the network (the initial conditions - initial weights). After the second round of training, a difference series is computed for all the weight connections.

This process gives insight into changes observed in weight trajectories after introducing a small perturbation to one weight connection. This step captures the impact of the perturbation on the entire network's weights. Once the difference series is obtained, we divide the series into K partitions to obtain the LEs on each partition for every connection. The LEs are then investigated further by computing their causality with misclassification. If, for a particular connection, the causality is established, we infer that the connection hinders learning. The process is repeated for all connections. The causal ones are saved and the non-causal ones become candidates for pruning.

Our pruning method was developed as follows. Initially, we trained a simple Multi-layer Perceptron (MLP) on a given dataset. Throughout the training process, we recorded the weights at each iteration, resulting in a time series of weight values. These weight time series were subsequently utilized to estimate the LE, a measure of chaotic behavior, using the TISEAN package in conjunction with MATLAB scripts. This estimation was performed using a sliding window approach, generating a time series of LEs.

By combining the time series of Lyapunov exponents and the model accuracies obtained at the end of each window, we employed a Granger causality module to investigate whether the weights had a causal relationship with the model's accuracy. This analysis determined whether specific weights "Granger caused" the accuracy. Based on our experiments, the time series of LEs consistently exhibited positive values, indicating the presence of chaotic elements in the weight time series. Consequently, our study focused on understanding whether these weights Granger caused the model's accuracy. Any weights that did not demonstrate this causal relationship were pruned before conducting subsequent model runs (code will be shared on request).

These findings and our pruning methodology contribute to a better understanding of the relationship between weights and model accuracy, enhancing the efficiency and performance of future training iterations. The complete implementation details and code will be shared on request.

EXPERIMENTAL SETUP

In our study, we employed Python3.10 and Matlab R2022a to conduct experiments on a single hidden layer neural network on various datasets. Our experiments were conducted on a Ryzen 9 3900XT Desktop Processor with 32GB RAM and 1TB HDD. During training, we stored the weight updates for every connection in CSV files. We assumed a window size of 200 iterates and computed the LE for each weight connection on every window. Further, we calculated the training and test accuracy on every window, to capture the misclassification rates. Thus, we obtained a sequence of windowed LEs and windowed accuracies for every connection.

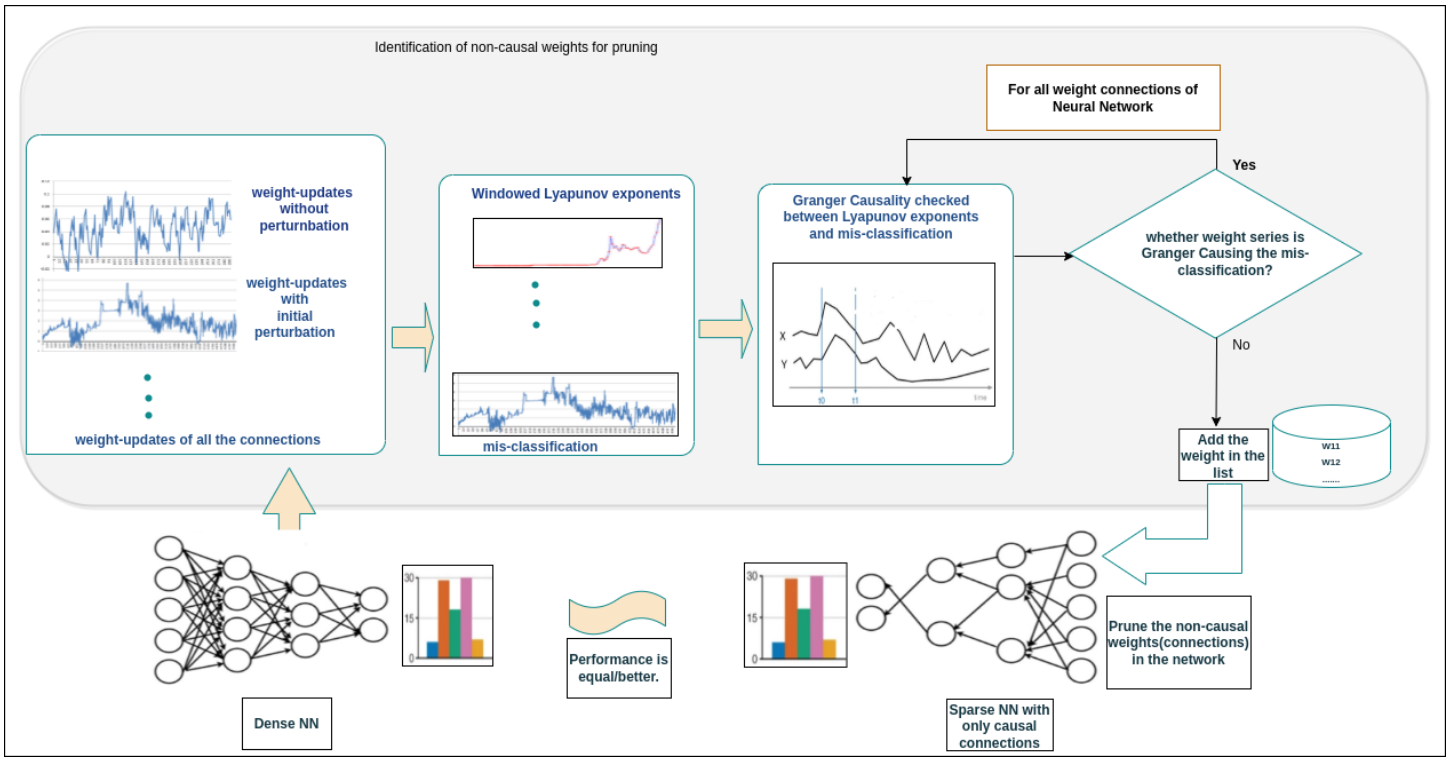

Figure 2 Weights pruned via LEGCNet method for selecting connections in sparse neural network

We then computed the GC between the windowed LEs and the misclassification rate to identify weight connections that Granger caused misclassification.

In the process of pruning the network, we removed the connections for which the LEs were found to Granger cause misclassification. After pruning, we reran the experiment by keeping the same initial weights, optimizers, and other hyperparameters as the unpruned network. We extended the work on seven different datasets and recorded the epochs and accuracies of the pruned network. Interestingly, we observed that the accuracies of the sparse network exceeded those of the dense network. We have used seven datasets - Cancer, Titanic, Banknote, Iris, Iris (3 features), Vowel and MNIST. The datasets we used for experiments are tabular datasets stored as CSV files.

The file contains features as well as class labels associated with the problem(classification) at hand. The features are fed as input to the neural network and the output labels are provided as classes or categories of each corresponding dataset. The code base of a neural network fetches the input and output explicitly. The information about the inputs/outputs (features/labels) of the dense neural network is related to the precise dataset in use and this is publicly available on the UCI Machine learning repository.

In our study, we conducted experiments in two parts. In the first part, we trained the neural network until convergence (LEGCNet-FT) in Figure 3 and computed windowed-LEs for each weight connection as well as windowed accuracies. We then computed the GC and pruned the network by removing connections that were found to cause misclassification. In the second part of the experiment, we trained the network only for a few epochs (LEGCNet-PT) in Figure 4 and used these initial weight updates to compute windowed LEs and accuracies, repeating the same procedure as in the first part of the experiment. Finally, we compared the performance of the pruned network (LEGCNet-FT and LEGCNet-PT) to that of the original network. The results of all these experiments were recorded and presented in tables. The code will be shared on request.

RESULTS AND DISCUSSION

We ran the experiments on seven tabular datasets - Cancer, Titanic, Banknote, Iris, Iris (3 features) Vowel and MNIST. The datasets were divided into 80:20 train-test split and the code was run five times, each maintaining different network initialization. The best results from every initialization are reported in Tables 1 and 2. Table 1 is the comparison of the performance of Dense and LEGCNet-FT. We present the description of table columns.

FLOPs - DN are the Flops needed for training the Dense network, FLOPs - LEGCNet-FT - FLOPs consumed for training the LEGNet-FT network, Non causal Weights - those weights which were found non-causal in Dense Network; Epochs are the epochs needed for Dense and LEGCNet-FT, Accuracy and F1 scores are shown for Dense and LEGCNet-FT. The column percentage pruned (fraction of parameters removed *100) shows the weight connections removed from the dense network.

We compared the FLOPs, % pruned (fraction of parameters removed *100), accuracy, f1-scores, and epochs for all methods (dense, LEGCNet-FT and LEGCNet-PT). Table 1 shows the performance comparison of dense network and LEGCNet-FT. Remarkably, LEGCNet-FT achieves notable reductions in FLOPs without compromising accuracy. Furthermore, LEGCNet-FT converges significantly faster consuming a few epochs compared to the dense network. Specifically, for the Titanic, Vowel, and Cancer datasets, LEGCNet-FT achieves convergence in just half the number of epochs required by the dense network. Nonetheless, both network achieves a similar level of performance without significant differences, thus validating the lottery ticket hypothesis. Table 2 demonstrates the performance of LEGCNet-PT. It shows that

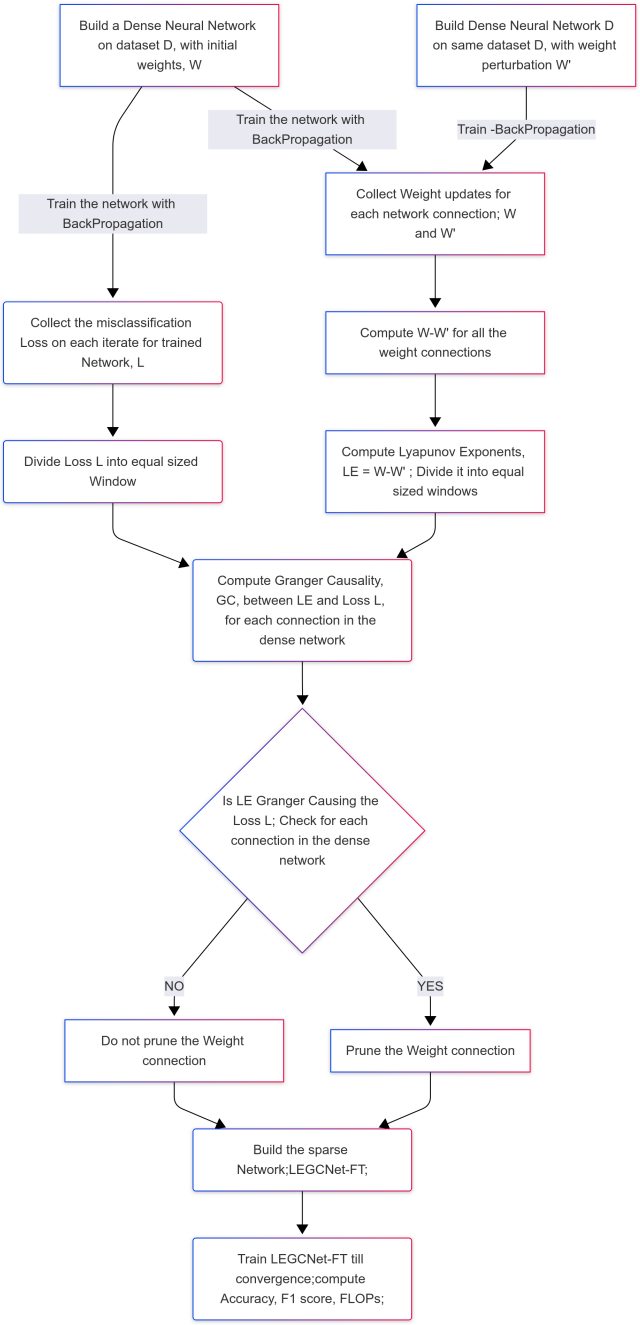

Figure 3 Flowchart for LEGCNet-FT

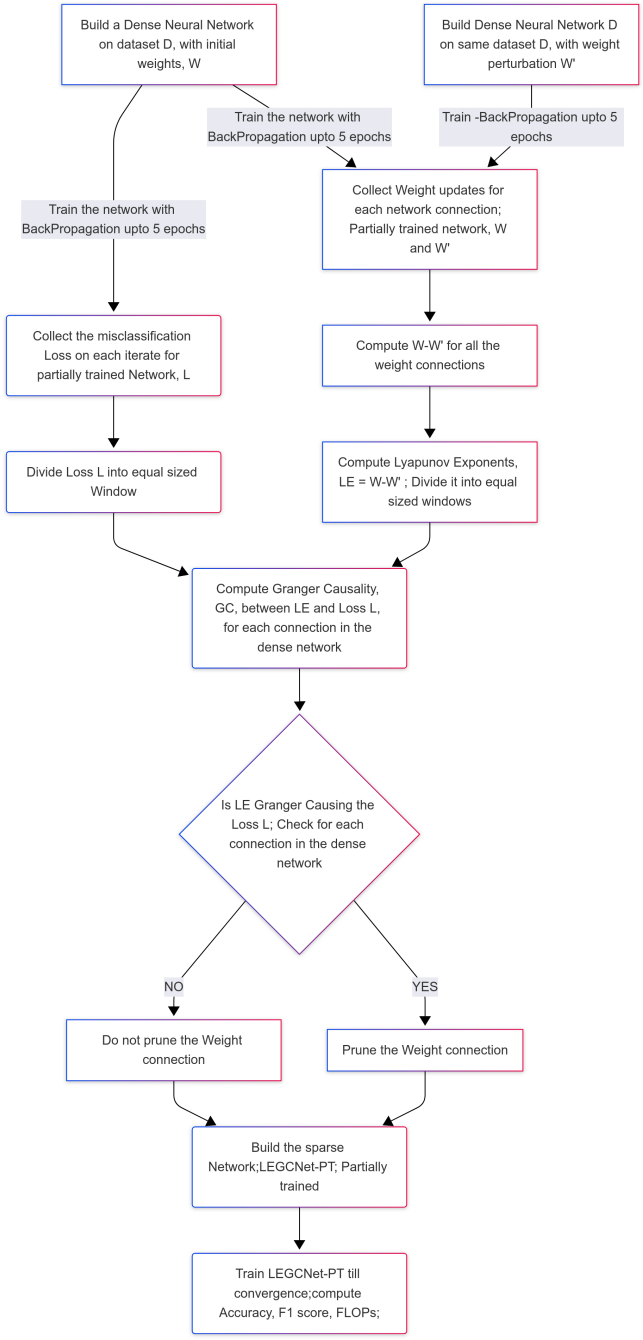

Figure 4 Flowchart for LEGCNet-PT

LEGCNet-PT performs at par with its counterpart, in terms of convergence speed, FLOPs, accuracy, and F1 scores.

We utilized two diagnostic tools, *namely WW and SHAP*. The *WW* validates the compliance of our architecture, as reflected in the Table 3 and Figure 5 plotted for MNIST. *WW* is a powerful open-source diagnostic tool designed for analyzing Deep Neural Networks (DNN). without requiring access to training or test data. It leverages cutting-edge research on the underlying principles of deep learning, specifically the Theory of Heavy-Tailed Self-Regularization (HT-SR).

Drawing inspiration from various fields such as Random Matrix Theory (RMT), Statistical Mechanics, and Strongly Correlated Systems, WeightWatcher provides valuable insights into the inner workings of DNNs and sheds light on why deep learning proves to be effective.

WW analyzes each layer by plotting the empirical spectral distribution (ESD), which represents the histogram of eigenvalues from the layer's correlation matrix. Additionally, it fits the tail of the ESD to a (truncated) power law and presents these fitted distributions on separate axes. This visualization approach provides a clear representation of the eigenvalue distribution and highlights the presence of heavy-tailed behavior in the network's layers. In general, the ESDs observed in the best layers of high-performing DNNs can often be effectively modeled using a Power Law (PL) function. The PL exponents, denoted as alpha, tend to be closer to 2.0 in these cases indicating a heavy-tailed behavior in the layer's

Table 1 Comparison of Dense Networks (DN) and Sparse Networks using LEGCNet-Fully Trained (FT) across datasets. Accuracies and F1-scores are reported on the test set.

Dataset (hidden)	FLOPs DN	FLOPs FT	Non-causal	Epochs DN	Epochs FT	Acc. DN	Acc. FT	F1 DN	F1 FT	% Pruned
Cancer (6)	60	54	6	70	38	0.8759	0.8686	0.8656	0.8570	10.00
Titanic (8)	56	52	4	43	20	0.7225	0.7177	0.6948	0.6843	7.14
Banknote (8)	40	36	4	9	7	0.9018	0.8909	0.9016	0.8906	10.00
Iris (6)	42	40	2	182	166	0.9000	0.9000	0.9124	0.9419	4.76
Iris (3f) (6)	36	26	10	139	126	0.9000	0.9000	0.9330	0.9040	27.78
Vowel (4)	36	34	2	36	14	0.7462	0.7538	0.7307	0.7400	5.56
MNIST (50, 30)	41000	40861	139	27	30	0.9121	0.9165	0.8669	0.8781	0.34

Table 2 Comparison of Sparse Networks where causality is derived from two training strategies: full training (LEGCNet-FT) and partial training (LEGCNet-PT). Iris 3f refers to the Iris dataset with 3 features. *Epochs** indicates the number of epochs used to compute non-causal weights in LEGCNet-PT.

Dataset (*Epochs**)	FLOPs FT	FLOPs PT	Epochs FT	Epochs PT	Acc. FT	Acc. PT	F1 FT	F1 PT	% Pruned
Cancer (12)	54	42	38	24	0.8686	0.8759	0.8570	0.8643	30.00
Titanic (3)	52	29	20	36	0.7177	0.7249	0.6843	0.6969	48.21
Banknote (2)	36	37	7	6	0.8909	0.8945	0.8906	0.8943	7.50
Iris (20)	40	40	166	173	0.9000	0.9000	0.9419	0.9124	4.76
Iris 3f (20)	26	28	126	135	0.9000	0.9333	0.9040	0.9330	22.22
Vowel (5)	34	28	14	20	0.7538	0.7538	0.7400	0.7441	22.22
MNIST (5)	40861	40867	30	29	0.9165	0.9152	0.8781	0.8408	0.32

Table 3 Comparison of Random and Magnitude-based pruning strategies on sparse networks (SN).

Dataset	Epochs	Acc. Rand	Acc. Mag	F1 Rand	F1 Mag
Cancer	42	0.8759	0.8905	0.8656	0.8814
Titanic	35	0.7201	0.7201	0.6842	0.6906
Banknote	6	0.8945	0.9018	0.8943	0.9015
Iris	179	0.9000	0.9000	0.9124	0.9124
Iris (3f)	160	0.9000	0.9333	0.9330	0.9330
Vowel	28	0.7462	0.7462	0.7229	0.7307
MNIST	31	0.9119	0.9121	0.8627	0.8669

Table 4 WeightWatcher summary for models trained with the same initialization on MNIST.

Model	Layer 1 (784–50)		Layer 2 (50–30)		Layer 3 (30–10)	
	α	α_w	α	α_w	α	α_w
Dense	2.19	1.63	1.51	1.88	1.94	2.76
LEGCNet-FT	2.24	1.64	1.51	1.83	2.29	3.20
LEGCNet-PT	2.19	1.71	1.51	1.85	2.73	3.87
Random	2.30	1.53	1.70	1.95	2.00	2.84
Magnitude	2.19	1.63	1.55	1.85	1.96	2.78

correlation matrix. *WW* offers several layer metrics to assess the distinction between well-trained and well-correlated layers from the Marchenko-Pastur (MP) random bulk distribution. By analyzing these metrics, *WW* provides insights into the randomness and heavy-tailed nature of layer distributions. The alpha lies between 2.0 and 6.0 on every layer (Table 4). The ESD plots of the three types of training (dense, LEGCNet-PT, LEGCNet-FT) manifest a heavy-tailed distribution of eigenvalues on each layer indicating the layers are well-trained (Figure 5). A careful observation at Figure 5 reveals the following: ESD plot of a layer, where the orange spike on the far right is the tell-tale clue; it's called a Correlation Trap (LeCun *et al.* 1990). A Correlation Trap refers to a situation where the empirical spectral distributions (ESDs) of the actual (green) and random (red) distributions appear remarkably similar, except for a small correlation shelf located just to the right of 0. In the random ESD (red), the largest eigenvalue (orange) is noticeably positioned further to the right and is separated from the majority of the ESD's bulk. This phenomenon indicates the presence of strong correlations in the layer, which can potentially affect the overall behavior and performance of the network. Figure 5 is the case of well-trained layers. Layers have an overlap of random and original ones when they have not been trained properly because they look almost random, with only a little bit of information present. And the information the layer learned may even be spurious. This is the case of a well-trained layer.

SHAP (SHapley Additive exPlanations) is a game-theoretic technique utilized to provide explanations for the output of machine learning models. By connecting optimal credit allocation with local explanations, SHAP employs the well-established Shapley

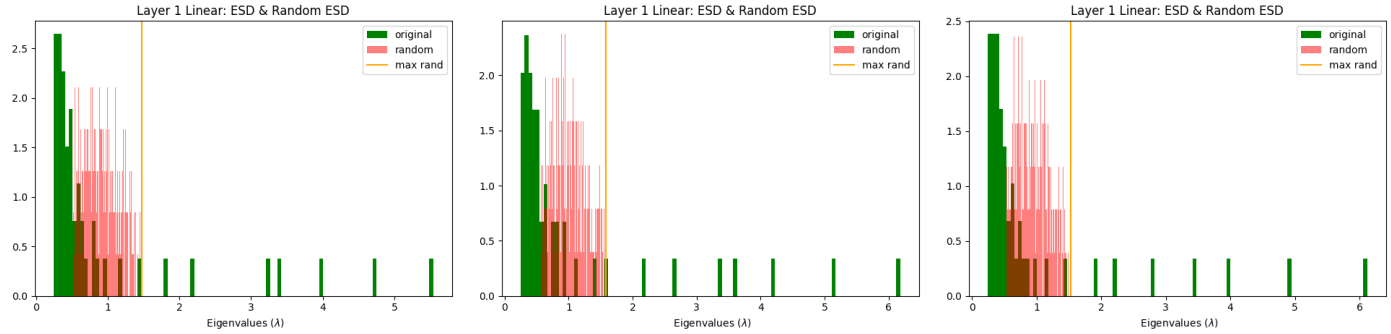

Figure 5 *WW* plots for dense and LEGCNet-FT, and LEGCNet-PT networks on MNIST data (layer 1), Plots reveal the correct training of the proposed architectures. WW plots of MNIST for random and magnitude pruning are available in Appendix

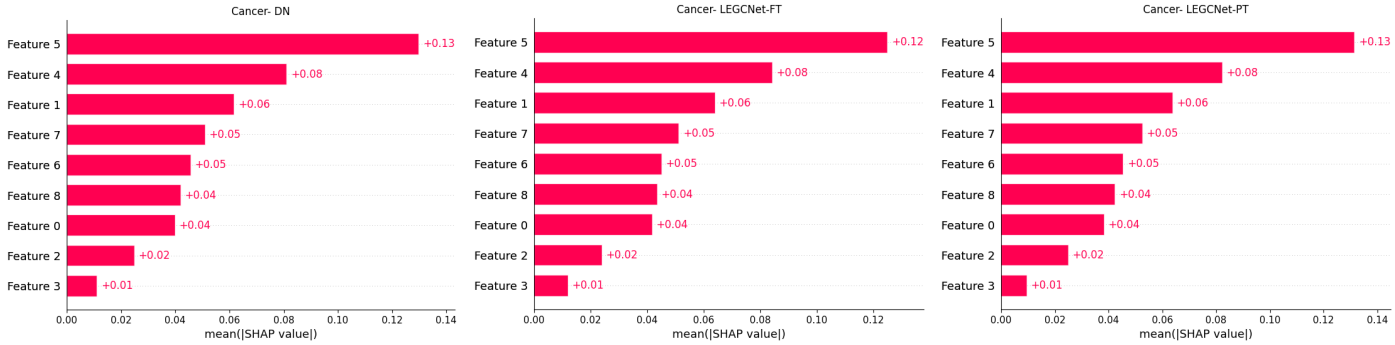

Figure 6 Shap values and feature importance computed on Cancer dataset (Banknote and Titanic plots can be seen in Appendix) for all three models - Dense Network, LEGCNet-FT and LEGCNet-PT; the feature importance for the dense network is the same as LEGCNet-FT and LEGCNet-PT

values from game theory and their related extensions. SHAP enables a comprehensive understanding of the contributions made by different features in the model's output, facilitating insightful explanations for its decision-making process. If a network is pruned according to some underlying principles, then the consistency in feature explainability is maintained before and after pruning i.e. the features that explain the outcome before pruning (fully connected, dense network) remain consistent on the pruned network.

The SHAP values computed for the proposed pruning architecture as well as for the baselines - random and magnitude - indicate that the feature importance is maintained in LEGCNet-PT and LEGCNet-FT when compared with dense (Figure 6). However, the baseline pruning methods (random, magnitude pruning) could not maintain the feature consistency as seen in the SHAP plots. Though magnitude pruning shows feature consistency for Cancer, banknote, and Titanic datasets, the random pruning could not (please refer Appendix file for these plots).

Unlike the current baselines, the percentage of pruned weights in the proposed work is significantly less. This is because only the non-causal weights are pruned, weights that play no role in impacting the loss/accuracy. LEGCNet ensures a mechanism to check which weights to prune and which ones to keep by measuring the causality between the LEs of weights and misclassification. Whether the pruned weights are large in number or small, is guided by connections that contribute to the training. Additionally, if the network is not overparameterized, the methodology righteously removes those connections that do not contribute during training. We argue that the proposed strategy is efficient and accurate, with the additional benefit of passing network fitting and explainability tests, in addition to satisfying the lottery ticket hypothesis (Tables 1 and 2 Experimental section.). One of the other salient features of LEGCNet is that, unlike other pruning methods, it does not need the dense network to be trained for the entire cycle of epochs to identify pruning candidates. Rather, such candidates are detected after a few initial epochs so that the retraining can start immediately. This is reflected in reduced FLOPs without compromising key performance indicators (Tables 1, 2). Notably, our architecture is validated for correct training via *WW* Statistics as detailed in the diagnostic section previously. We discuss more on our findings from these experiments.

How do our results align with the Lottery ticket hypothesis? Our work validates the lottery ticket hypothesis empirically, by showing the comparable (and sometimes better) performance of LEGCNet-PT and LEGCNet-FT as against dense architecture, as reflected in the Tables 1 and 2 in the Experimental section. The pruned network not only gets trained with lesser epochs than the dense, but it also uses lesser FLOPs to achieve this performance.

Is our architecture Validated for correct training via WW Statistics? As detailed in the WeightWatcher section previously, we have conducted a thorough examination of our pruning method's impact on neural network training, validating that it maintains the network's capability to encode accurate representations from the data, akin to the method without pruning. However, it is important to acknowledge that some skepticism may arise concerning the results presented in the table. Notably, we observed that the middle layer consistently exhibited signs of undertraining, irrespective of whether pruning was applied or not. This phenomenon can be at-

tributed to the architecture's design, where the first layer, due to its significantly higher number of interactions, encodes a substantial portion of the information, leaving the middle layer comparatively underutilized in terms of information encoding. Moreover, the final layer efficiently captures the essential information required for accurate classification, which has been frequently observed in deep-layer neural networks with a roughly uniform node count of around 30 nodes per layer (except the first and last layers).

It is crucial to emphasize that our primary focus in this investigation was on the effects of pruning, rather than achieving perfect classification performance. The benchmark accuracy served as an indicative measure of model performance, while the underlying motivation centered around the observation that ESD (Eigenvalue Spacing Distribution) plots do not align precisely with those of random matrices. In conclusion, while the middle layer's undertraining may raise concerns, the core contribution of this study lies in demonstrating that our pruning method effectively retains the neural network's ability to encode meaningful representations from the data, ensuring that essential information is preserved while achieving a desirable balance between accuracy and interpretability. These insights serve to shed light on the intricate interplay between pruning and neural network architectures.

How do the proposed method and architectures produce consistent feature explainability, in contrast with baseline pruning architectures? The experimental results demonstrated that the proposed pruning method exhibits notable advantages in maintaining feature importance compared to the traditional random and magnitude pruning methods. The feature consistency remained relatively stable after employing the proposed pruning technique, which was not the case for the other two methods. For random pruning, we observed that pruning 40% of the weights led to satisfactory accuracy levels for the respective datasets. Similarly, magnitude pruning, with a 25% pruning threshold based on weight magnitudes, yielded comparable benchmark accuracies. The SHAP plots provided critical insights into the behavior of feature importance during pruning. In the case of random and magnitude pruning, significant fluctuations in feature importance were evident after pruning. These fluctuations could potentially hinder the interpretability of the underlying model. However, our proposed pruning method demonstrated remarkable resilience in preserving feature importance, with minimal perturbations observed in SHAP plot patterns enabling a more interpretable and transparent pruned model. By selectively targeting weights based on a novel criterion, the proposed method ensures that crucial features are retained, thus For mission-critical tasks on edge devices such as predicting power consumption of applications (Alavani *et al.* 2023) or forecasting real-time blood glucose prediction, feature explainability on pruned networks is critical as it helps determine accurate prediction when dimensionality is a curse. *How is our method doing in comparison with baseline pruning methods?* The overall performance of our methods, when compared with the dense and baselines, shows that the Chaos-Causality framework consumes fewer epochs and fewer FLOPs (Tables 1, 2) to train the sparse network without compromising the accuracy and F1-score thus validating the Lottery ticket hypothesis. When compared with dense networks, LEGCNet-PT and LEGCNET-FT needed lesser training epochs on 6 out of 7 datasets, while the accuracy remained at par across all methods.

CONCLUSION

The main idea is to decide on a weight connection in the dense neural network, whether it should 'be pruned or not to be pruned', and this decision is governed by the presence or absence of the causal relationship between the Lyapunov exponent and the misclassification loss during the neural network training (backpropagation) for the specific connection. If the causality is established between them, it is pruned otherwise it remains unchanged during the backpropagation. Once pruned, we investigate whether the pruned network performs well or becomes worse compared with its dense counterpart. To validate this, we train the sparse network till convergence and compare its performance.

Tables 1 and 2 show that comparison. We compared the FLOPs, percentage pruned (fraction of parameters removed *100), accuracy, f1-scores, and epochs for all methods (dense, LEGCNet-FT and LEGCNet-PT). Table 1 shows the performance comparison of dense network and LEGCNet-FT. Remarkably, LEGCNet-FT achieves notable reductions in FLOPs without compromising accuracy. Furthermore, LEGCNet-FT converges significantly faster consuming a few epochs compared to the dense network. Specifically, for the Titanic, Vowel, and Cancer datasets, LEGCNet-FT achieves convergence in just half the number of epochs required by the dense network. Nonetheless, both networks achieve a similar performance level without significant differences, thus validating the lottery ticket hypothesis. Table 2 demonstrates the performance of LEGCNet-PT. It shows that LEGCNet-PT performs at par with its counterpart, in terms of convergence speed, FLOPs, accuracy, and F1 scores.

In conclusion, we emphasize that our primary focus in this investigation was on the effects of pruning, rather than achieving perfect classification performance. In the past, pruning was typically accomplished by ranking or penalizing weights based on criteria like magnitude and removing low-ranked weights before retraining the remaining ones. We formulate pruning as an optimization problem to minimize misclassifications by selecting specific weights. To pick these weights, we have introduced the concept of chaos in learning (Lyapunov Exponents) through weight updates and have used causality-based investigation to identify those causal weight connections responsible for misclassification. We proposed two architectures - Lyapunov Exponent Granger Causality driven Fully Trained Network (LEGCNet-FT) and Lyapunov Exponent Granger Causality driven Partially Trained Network (LEGCNet-PT). We compared three distinct pruning techniques: random pruning, magnitude pruning, and our pruning approach. Overall, the experimental outcomes validate the superiority of the proposed pruning method. The findings hold great promise for further advancements in network optimization and model explainability. We demonstrated that:

- By incorporating Lyapunov exponent (LE) values from weight updates and verifying the causality of LE with accuracy, one can identify certain weights in a dense network that do not significantly contribute to improving accuracy or diminishing misclassification
- Pruning these unnecessary (noncausal) weights results in a subnetwork that can achieve the same or sometimes better validation accuracy as the original dense network.
- The sub-network, once pruned, and trained from the start (offline pruning) with the same initialization as the dense network, achieves comparable, and sometimes better, training speed while reaching the same validation accuracy.
- The subnetwork, LEGCNet-PT, after pruning, does not require further tuning to match the performance of the original dense

network.

- By using LEGCNet-PT,/LEGCNet-FT to prune the weight connections, a dense over-parameterised network determines weight connections to be pruned without compromising on accuracy/F1 score or any other performance metrics.
- When compared with the classical methods like random pruning and magnitude pruning we observe that our methods perform at par and sometimes better in terms of classification accuracy on all datasets.
- The accuracy comparison of dense networks and sparse networks (using LEGCNet-PT, LEGCNet-FT) reveals that the sparse networks perform better.
- We also found via experiments that the sparse networks were trained on lesser epochs and fewer FLOPs than their dense counterpart on all datasets.
- By using SHAP, we showed that a dense network when pruned using LEGCNet-PT/LEGCNet-FT demonstrates remarkable resilience in preserving feature importance, and enables a more interpretable and transparent pruned model.

Our pruning approach is yet to be tested on baseline architectures (Resnet, Densenet), and Large Language Models and savings in carbon emission need to be computed.

Acknowledgments

Archana Mathur and Nithin Nagaraj would like to thank SERB-TARE for supporting the work under Grants TAR/2021/000206. Snehanshu Saha would like to thank the Anuradha and Prashanth Palakurthi Center for Artificial Intelligence Research (APPCAIR), SERB SURE-DST (SUR/2022/001965), ANRF-CRG (CRG/2023/003210), and the DBT-Builder project (BT/INF/22/SP42543/2021), Govt. of India for partial support.

Ethical standard

The authors have no relevant financial or non-financial interests to disclose.

Availability of data and material

Not applicable.

Conflicts of interest

The authors declare that there is no conflict of interest with respect to the publication of this article.

LITERATURE CITED

Alavani, G., J. Desai, S. Saha, and S. Sarkar, 2023 Program analysis and machine learning based approach to predict power consumption of cuda kernel. ACM Transactions on Modeling and Performance Evaluation of Computing Systems .

Balakrishnan, H. N., A. Kathpalia, S. Saha, and N. Nagaraj, 2019 Chaosnet: A chaos based artificial neural network architecture for classification. Chaos: An Interdisciplinary Journal of Nonlinear Science **29**.

Ditto, W. L. and S. Sinha, 2015 Exploiting chaos for applications. Chaos: An Interdisciplinary Journal of Nonlinear Science **25**.

Faure, P. and H. Korn, 2001 Is there chaos in the brain? i. concepts of nonlinear dynamics and methods of investigation. Comptes Rendus de l'Académie des Sciences-Series III-Sciences de la Vie **324**: 773–793.

Frankle, J. and M. Carbin, 2018 The lottery ticket hypothesis: Finding sparse, trainable neural networks. ICLR 2019 .

Granger, C. W., 1969 Investigating causal relations by econometric models and cross-spectral methods. Econometrica: journal of the Econometric Society pp. 424–438.

Hegger, R., H. Kantz, and T. Schreiber, 1998 Practical implementation of nonlinear time series methods: The tisean package. Chaos **9 2**: 413–435.

Herrmann, L. M., M. Granz, and T. Landgraf, 2022 Chaotic dynamics are intrinsic to neural network training with sgd. In *Neural Information Processing Systems*.

Kondo, M., S. Sunada, and T. Niiyama, 2021 Lyapunov exponent analysis for multilayer neural networks. Nonlinear Theory and Its Applications, IEICE .

Korn, H. and P. Faure, 2003 Is there chaos in the brain? ii. experimental evidence and related models. Comptes rendus biologies **326**: 787–840.

Kuo, D., 2005 Chaos and its computing paradigm. IEEE Potentials **24**: 13–15.

LeCun, Y., I. Kanter, and S. A. Solla, 1990 Second order properties of error surfaces: Learning time and generalization. In *NIPS 1990*.

Lee, J., S. Park, S. Mo, S. Ahn, and J. Shin, 2020 Layer-adaptive sparsity for the magnitude-based pruning. In *International Conference on Learning Representations*.

Li, G., C. Qian, C. Jiang, X. Lu, and K. Tang, 2018 Optimization based layer-wise magnitude-based pruning for dnn compression. In *International Joint Conference on Artificial Intelligence*.

Liu, S., T. Chen, X. Chen, L. Shen, D. C. Mocanu, *et al.*, 2022 The unreasonable effectiveness of random pruning: Return of the most naive baseline for sparse training. In *The Tenth International Conference on Learning Representations, ICLR 2022, Virtual Event, April 25-29, 2022*, OpenReview.net.

Liu, Z., M. Sun, T. Zhou, G. Huang, and T. Darrell, 2018 Rethinking the value of network pruning. ArXiv **abs/1810.05270**.

Lundberg, S. M. and S.-I. Lee, 2017 A unified approach to interpreting model predictions. Red Hook, NY, USA, Curran Associates Inc.

Martin, C. H., T. Peng, and M. W. Mahoney, 2020 Predicting trends in the quality of state-of-the-art neural networks without access to training or testing data. Nature Communications **12**.

Medhat, S., H. Abdel-Galil, A. E. Aboutabl, and H. Saleh, 2023 Iterative magnitude pruning-based light-version of alexnet for skin cancer classification. Neural Computing and Applications pp. 1–16.

Mittal, D., S. Bhardwaj, M. M. Khapra, and B. Ravindran, 2018a Recovering from random pruning: On the plasticity of deep convolutional neural networks. 2018 IEEE Winter Conference on Applications of Computer Vision (WACV) pp. 848–857.

Mittal, D., S. Bhardwaj, M. M. Khapra, and B. Ravindran, 2018b Studying the plasticity in deep convolutional neural networks using random pruning. Machine Vision and Applications **30**: 203 – 216.

Mohapatra, R., S. Saha, C. A. C. Coello, A. Bhattacharya, S. S. Dhavala, *et al.*, 2022 Adaswarm: Augmenting gradient-based optimizers in deep learning with swarm intelligence. IEEE Transactions on Emerging Topics in Computational Intelligence **6**: 329–340.

Nagaraj, N. and P. G. Vaidya, 2009 Multiplexing of discrete chaotic signals in presence of noise. Chaos: An Interdisciplinary Journal of Nonlinear Science **19**.

Prandi, C., S. Mirri, S. Ferretti, and P. Salomoni, 2017 On the need of trustworthy sensing and crowdsourcing for urban accessibility in smart city. ACM Trans. Internet Technol. **18**.

Qian, X.-Y. and D. Klabjan, 2021 A probabilistic approach to neural network pruning. In *International Conference on Machine Learning*.

Rosenstein, M. T., J. J. Collins, and C. J. D. Luca, 1993 A practical method for calculating largest lyapunov exponents from small data sets. Physica D: Nonlinear Phenomena **65**: 117–134.

Saha, S., N. Nagaraj, A. Mathur, R. Yedida, and S. H. R, 2020 Evolution of novel activation functions in neural network training for astronomy data: habitability classification of exoplanets. The European Physical Journal. Special Topics **229**: 2629 – 2738.

Saleem, T. J., R. Ahuja, S. Prasad, and B. Lall, 2024 Insights into the lottery ticket hypothesis and iterative magnitude pruning. ArXiv **abs/2403.15022**.

Shen, Z., H. Yang, and S. Zhang, 2019 Nonlinear approximation via compositions. Neural networks : the official journal of the International Neural Network Society **119**: 74–84.

Sprott, J., 2013 Is chaos good for learning. Nonlinear dynamics, psychology, and life sciences **17**: 223–232.

Wolf, A., J. Swift, H. L. Swinney, and J. A. Vastano, 1985 Determining lyapunov exponents from a time series. Physica D: Nonlinear Phenomena **16**: 285–317.

Zhang, L., L. Feng, K. Chen, and C. H. Lai, 2021 Edge of chaos as a guiding principle for modern neural network training. ArXiv **abs/2107.09437**.

Zou, D., Y. Cao, D. Zhou, and Q. Gu, 2018 Stochastic gradient descent optimizes over-parameterized deep relu networks.

How to cite this article: Sahu, R., Chadha, S., Mathur, A., Nagaraj, N. and Saha, S. A Chaos-Causality Approach to Principled Pruning of Dense Neural Networks. *Chaos Theory and Applications*, 7(2), 154-165, 2025.

CHAOS
Theory and Applications
in Applied Sciences and Engineering

e-ISSN: 2687-4539
RESEARCH ARTICLE
Vol.7 / No.2 / 2025 / pp.166-176
https://doi.org/10.51537/chaos.1626298

A New Model Proposal for a Paradigm Shift for Strategic Management in the Context of Chaos Theory

Büşra Yiğitol [*,1] **and Mustafa Atilla Arıcıoğlu** [α,2]

[*]Necmettin Erbakan University, Faculty of Aviation and Space Sciences, Civil Aviation Management, Köyceğiz Campus, 42090, Meram, Konya, Türkiye,
[α]Necmettin Erbakan University, Faculty of Political Science, Business Administration and Management, Köyceğiz Campus, 42090, Meram, Konya, Türkiye.

ABSTRACT

The 21st-century business world is characterized by a multitude of dynamics, which are evolving at an unprecedented pace. Many academic studies have analyzed this volatile business environment using the concepts of chaos and complexity. In such an unpredictable context, planning for the future has become increasingly challenging. Strategic management, as a process, plays a crucial role in enabling managers to assess the organization's position, identify opportunities arising from environmental changes, and evaluate both internal and external factors. Consequently, it embodies a structure that is inherently sensitive to environmental changes. The turbulent and chaotic nature of contemporary environmental conditions necessitates a paradigm shift in the strategic management process. Chaos theory, which emphasizes the unpredictability and interconnectedness of systems, offers a valuable lens to understand and explain the dynamics driving this shift. This study proposes an alternative model for the strategic management process, aiming to enhance its adaptability to rapid and unpredictable environmental changes by integrating the principles of chaos theory.

KEYWORDS

Chaos theory
Strategic Management
Strategic management process model

INTRODUCTION

Many concepts such as time, flexibility, questioning of existence, making sense of goals, existence and harmony of the environment, consistency and internal control, leadership, are considered to understand and create strategy. In particular, the movement and change of the environment persuade managers and organizations to go beyond the meaning and existence of concepts and re-question them for the formation and execution of strategy. Especially since the mid-1700s, the pace of industrial and economic development has been growing geometrically with the reflection of inventions and discoveries on production, capitalism, and companies. This opens up the formation and execution of the strategy, which is the guide of the future, to discussion. In the last century, the rediscovery of man, the decisive presence of communication, the expansion of the domain of technology, and the re-awareness of culture have led to a more critical questioning of strategic changes. Especially the remarkable spread of global integration after 1989, companies relocating to new areas of sovereignty through network relations, and multipolarity exercises make it necessary to consider strategy and the management of the process in the context of new paradigms (Galambos 2005; Guillory 2007; Miles and Snow 2010; Smith *et al.* 2017).

In other words, the two basic questions asked by Drucker (1954), titled

- What is our job?
- And what should happen?

must find new answers and solutions within the framework of this change.

The new geography that emerged with the last great war in the twentieth century, traces left by the oil/energy and financial crises that continue to create an uninterrupted impact from the past to the future, contributions of the bipolar world to the war industry and resource distribution, problems in resource management of countries governed by coups and civil wars, and the redefinition of the values of living spaces all describe a difficult period in terms of how companies are managed. Difficulties have increased even more since the beginning of the 1990s. While strong crises are now affecting the whole world by emerging with short time intervals and high fluctuations, chaos has begun to be used as

Manuscript received: 24 January 2025,
Revised: 30 May 2025,
Accepted: 10 June 2025.

[1]b.bozal89@gmail.com (**Corresponding author**)
[2]maaricioglu@gmail.com

a method and approach in learning and managing crises. In the twenty-first century, the world is witnessing new and deeper shifts, and in this context, it becomes necessary to reconsider strategy and the concepts that make up strategy. This requirement is a priority for all institutions and organizations involved in strategic planning, but especially for companies spread all over the world. In other words, the strategy, along with its existing components, implementation tools, and methods, seems to need a paradigm shift.

In this study, we first focused on the traditional meaning of the concept of strategy in the literature and then determined the existence of variables foreseen for change, revealing how the strategy evolved in response to the paradigm change. At this point, the existence of chaos is discussed to understand and manage the paradigm shift. In the last part of the study, the validity and meaning of the paradigm shift in strategy for managers and organizations were investigated. For the research, interviews with senior managers of global companies operating in Türkiye, and senior managers of Turkish companies operating globally, were conducted and measured using the qualitative method.

A DISCUSSION ON CHANGE IN STRATEGIC MANAGEMENT

The concept of strategy, which refers to the Latin word startum, stands out as the most frequently used concept in the comprehensive planning and direction of every operation carried out between the parties during war and peacetime (Freedman 2018; Earle 2015; Akad 2001). According to Chandler (1962), who was very careful and courageous about the inclusion of strategy in the field of business management, strategy is the determination of a company's long-term goals, objectives, and field of activity, and allocating the resources necessary for these actions.

The definitions diversify as strategy intersects with management or begins to be used for management. Hunger and Wheelen (2003) underline a common assessment. According to them, strategic management refers to managerial decisions and actions, which determine the future performance of the business. Nutt and Backoff (1987) state that strategic management requires short-term, sequential, and consistent solutions for long-term problems while maintaining organizational integrity. De Bono (1996) argues that strategic management is a mental process and attitude towards being superior to competition. Drucker (1999) states that strategic management is answering the questions, "What is our job and what should it be?" and anticipating the future consequences of the decisions that can be made in line with the determined goals and objectives.

According to Hamel and Prahalad (1989), the intention emerges with the three basic characteristics of direction, discovery, and destiny, and expresses a certain perspective on the long-term market or competitive position that one hopes to build within ten years. While Mintzberg (1987) defines strategy as Plan, Pattern, Position, Perspective, and Ploy, strategic management is the concept of identification, implementation, and management of the strategies that managers carry out to achieve organizational goals and objectives. According to Mintzberg, the features that the strategic management process should have are: to be carried out consciously, to preserve the model, which plays an important role in establishing order between the internal and external environments, to be sustainable, to be unique, clear, and simple, and to be fully formulated before implementation (Mintzberg 1990).

In the light of this information, it becomes clear that strategic management should have the following points;

- explain the ontological justification,
- long-term planning related to short and medium term,
- the ability to act consistently with planning,
- integrity and consistency of action,
- a control covering the entire process,
- understanding the environment and managing environmental awareness,
- the existence of a competitive ability,
- the ability to use intuition,
- having a mind that gives importance to the minds of others,
- ultimately learning sustainability,

The elements of this intersection cluster are parallel to the historical development of the strategic management process. As shown in Figure 1, these elements are connected to the historical process.

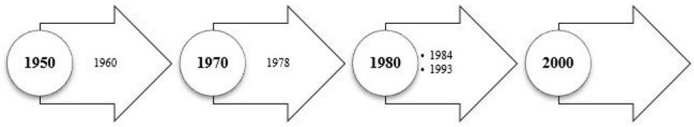

Figure 1 Historical development of strategic management (created by the author)

Figure 1 conveys the development of the strategic management process, which started in the 1960s, both in its current and future forms. In this context, while the debate initiated by Peter Drucker on "what the purpose of businesses is and what it should be" is evaluated from a strategy perspective focused on organization and management (Drucker 1942), Selznick (1957) emphasizes the distinctive features of organizations and the necessity of harmonizing the resources of organizations with environmental demands and expectations. Chandler (1962) emphasizes that the organizational structure should follow the strategy adopted by the business. Therefore, he defines strategic management as determining the long-term goals of businesses and allocating the resources the business has to achieve these goals. By combining the ideas of Drucker and Chandler, Andrews made evaluations from a more holistic perspective, including what the business of the enterprise should be, its goals and resources (Ansoff 1965).

Ansoff (1965), who is considered to be the founder of corporate strategy, approached the idea of strategic management in a more product-and market-focused manner. He stated that the basic nature of the current and future business is determined by product and market activities. While Mintzberg focuses on the strategy formation process in his work *Patterns in Strategy Formation* Mintzberg (1978), Porter (1985) considers the structure-strategy and performance paradigm as a remarkable strategic approach. de Bono (2000) emphasized that the ability to compete alone is not enough; it is necessary to go beyond competition, being supra-competitive, and create value monopolies. Most importantly, being supra-competitive is a mental attitude.

Porter (1985) expresses a mental attitude of superiority over the competition, which is foundational, whereas positional superiority in a business sense is defined as achieving this superiority through lower costs or differentiation from competitors. According to Prahalad and Hamel (1990), core competence, which is the main element that a strategy must include, can be defined as "a harmonious combination of multiple resources and skills that differentiates a firm in the market" and is therefore the basis of companies' competitiveness. In all the approaches listed above and those that will be discussed further, the effort to build the future by using time and knowledge as well as technology can be explained ontologically.

This new situation that emerged towards the end of the twentieth century and its use as a justification for the twenty-first century has prompted a review of the relations. Organizational and managerial systems, like economic and political systems, cause hardening in the vessels of the organism and cause it to lose its vitality due to the changes experienced over time (Fukuyama 2002). The metaphor of blood vessels hardening and losing their vitality points out the dysfunctionality of existing systems and highlights the necessity to adapt to the emergence of new systems. Due to the recent developments in the world, it becomes clear that current approaches in the organizational and managerial field require discussion and new approaches to be addressed.

If we were to discuss the change using the literature under headings, we could list the following elements.

- Change in the concept of Time:In the words of Dedyukhina, present time refers to any time period, regardless of day or night. Technology compresses time (Dedyukhina 2017). Smart factories, houses, buildings, cryptocurrency markets that do not close, and social media platforms that facilitate digital communication are technologies that destroy people's perception of time and create a new, altered consciousness regarding time in our current century. Information and digital technologies disconnect objects from their local, cultural, historical, and geographical meanings; past, future, and present are transmitted within the same message, erasing the perception of time, and the concept of simultaneity emerges. The change of order in the relationship between past, future, and present, that is, the validity of disorder, brings about the indifferentiation of time (Castells 2008).

- Collaborative structures gaining ımportance:It is stated that organizations are considered to be innovative forms characterized by flexibility and adaptation because of their more chaotic environments (Dijksterhuis *et al.* 1999). This situation highlights new forms of relationship and existence. These new forms support less hierarchy. Focusing on core competencies enables businesses to gain competitive advantage and respond to customer needs faster (Kabue and Kilika 2016). At this point in competition, many factors such as the speed of product and service implementation, differentiating aspects, and the availability of personal demand and product personalization opportunities propel businesses into a new realm. The interconnection of all systems within an intelligent and global network reveals the necessity of a brand new economic system (Rifkin 2015). Therefore, in terms of current reasons, the connection and interaction with the external environment need to be changed (Jacobides 2021).

- Economy, trade, and political uncertainty in the New World Order:The existence of a global economy is revealed by examining the scope of the impact of the economic crises. Today, economic crises initiated by the world's central authorities are affecting the economies of many countries and causing bottlenecks. For example, the 2008 crisis is regarded as a global crisis caused by the collapse of the American mortgage market (Alantar 2008). Globalization, which emerged as a paradigm at the end of the 20th century, describes a technology-oriented unified globe that McLuhan metaphorizes as the "Global Village" (Mcluhan and Powers 2020). These unification efforts are not only social or cultural, but also have political and ecological consequences (Dirlik 2012). As a matter of fact, according to Frase (Frase 2018), companies, which are the new actors of globalization, have to create different scenarios about the future, consider the possibility of each scenario coming true, and keep themselves ready.

- The change that emerged with Industry 4.0, when the definitions of technology and its effects on the business world are evaluated, brings Schumpeter's concept of creative destruction to mind. The most striking example of the concept of creative destruction is Industry 4.0, which has been discussed frequently in recent literature. Industry 4.0, first put forward in Germany in 2011, has resonated in many areas since then (Roblek *et al.* 2016; Vaidya *et al.* 2018; Xu *et al.* 2018; Yang and Gu 2021). With digitalization, collaborative shared resources have increased. It is predicted that this system will be the dominant economic paradigm in the world.

- Changing human resource: The supreme role of man over nature, in the words of Julian Huxley, "his role, whether he wants it or not, is to be the leader of the evolutionary process on Earth, and his task is to manage and direct it in the direction of general development" (Peccei 2013). It creates a new classification of society in which the role of people today is in managing and directing. This society is described as the smart society, Society 5.0, which came into prominence especially with the Industry 4.0 technological transformation (Fukuyama 2018). The society characterized by the notion of "Smart Society" is introduced as a smart society philosophy that will manage technological power correctly and promises a life worthy of humanity (Onday 2019; Arıcıoğlu *et al.* 2020). This life interacts with culture and suggests the rediscovery of humanity. In their studies, several authors also bring to light discussions on how this transformation affects culture (Harvey 1990; Smith 1990; Barber 1996; Ritzer 1998; Lieber and Weisberg 2002; Dirlik 2009). The arguments presented suggest that the change encompasses more than just the world economy and the increase in trade across national borders. In an age of uncertainty, where constant change is experienced, managers need both their previous experiences and something different from what has been done. Anticipating and dealing with the unexpected require a different managerial mentality. The COVID-19 epidemic can be considered the most current example of the subject. The global pandemic has created new norms and made uncertainty more noticeable for managers. Due to the daily changes affecting the activities of businesses, the decision-making process that responds to this rapid

change has become as important as the decision itself (Naidoo 2020).

- Global temperatures are increasing every year, and the global warming trend is occurring much faster than past experiences (National Geographic 2021). Due to a number of events that have global consequences, such as acid rain, oil pollution, depletion of water resources, fluorocarbon propellants, radiation leaks, toxic waste, and infectious diseases, national borders become less relevant and countries become ecologically interdependent (Barber 1996). The interdependence of every country in the world on environmental issues has led to the emergence of market-based mechanisms for emission reduction and the formation of a new market. This emissions trading system, defined as the carbon market, is the cornerstone of the policy to combat climate change and the main tool used to effectively reduce greenhouse gas emissions and their associated costs (European Commission 2021).

What has summarized above is not only related to the environment, which is generally recognized. It also emphasizes how new situations and complexities should be managed. In other words, the birth of a new era leads to an understanding of the naturalness of chaos, not order. In this context, it is necessary to discover a learning method while updating perspectives through it.

LEVERAGING THE EXISTENCE OF THE CHAOS APPROACH TO DISCOVER AND MANAGE CHANGE IN STRATEGIC MANAGEMENT

Contrary to Classical physics, which models the universe as a "continuity," Quantum theory has revealed that both light and energy exhibit discontinuity (Norton 1993). Thus, it was discovered that the quantum mechanical laws governing the behavior of atoms and their components are apparently probabilistic, meaning that only the probability of something allows prediction. This discovery shows us that the universe and reality are no longer concepts that work like a clock, and that events in real life are complex and do not proceed in a linear flow (Açıkalın 2015). Therefore, unpredictability now prevails, and the traditional understanding of science is replaced by a new understanding of science that defines itself in terms of quantum, chaos and complexity. The nature of the new science includes non-linear chaotic systems. Chaos theory deals with phenomena that are difficult to predict, in contrast to the more predictable phenomena addressed by traditional science (Straussfogel and Schilling 2009).

According to Kellert (1992), chaos theory is the qualitative study of unsteady aperiodic behavior in deterministic nonlinear dynamical systems. So it can be said that it deals with nonlinear phenomena that are virtually impossible to predict or control, such as turbulence, weather, the stock market, and our brain waves. The literature on chaos theory is enriched by the studies of meteorologists, biologists, and even social scientists. The common output of researchers in this huge literature is that experiments show that nature has unpredictable behavior and that these create some random and complex patterns that are not compatible with linear calculations and formulas (Namaki 2018).

Chaotic systems are characteristically sensitive to initial conditions (Straussfogel and Schilling 2009). One of the most important clues to understanding chaos is the term "Butterfly effect," which is used for the phenomenon of sensitive dependence on initial conditions, and this is illustrated by the saying "If a butterfly flaps its wings in China, there will be a hurricane in Texas" (Stewart 1990). In this way, Lorenz not only discovered chaos with his butterfly effect theory, but also determined its key mechanism (Halpern 2018). In a way, he brought the theory, put forward by Poincaré, at the level of scientific philosophy to the level of quantitative science (Ruelle 1990). Another name that made important contributions to the theory is Lev D. Landau (Landau 1944). Landau explains the turbulence situation as follows: If a certain number of modes of a fluid affected by an external force are motionless, smooth flow occurs; if a single mode is in motion, periodic flow; if more than one mode is in motion, irregular flow; and if many modes are in motion, turbulence occurs (Ruelle 2006). Another characteristic related to chaos theory is strange attractors. The 'strange attractor' described by Ruelle and Takens was described by Lorenz in 1963.

As can be seen, chaos theory focuses on unpredictability in events and behavior. Natural living systems and organizations are also much more complex than mechanical ones. Organizations consist of many integrated subsystems. Many dynamics, including external and internal conditions, organizational culture, leadership styles, teams and people in teams, and people's personality traits, can change the course of the organization and reshape the process (Harris 2022). The complexity of business organizations is further increased by many micro and macro factors, such as personality diversity among organizational members, the complex nature of operations, changes in interpersonal relationships, ever-changing macroeconomic variables, and the policy environment. In this context, Thietart and Forgues (1995) argue that organizations are "nonlinear dynamic systems subject to forces of stability and forces of instability that push them towards chaos."

Applying chaos theory to organizational behavior allows theorists to take a step back from the management of daily activities and understand how organizations function as unified systems. In this context, Tom Peters first stated in the 1980s that managers should be prepared for environmental and technological changes. Peters offers a strategy to help companies cope with the uncertainty of competitive markets and states that the focus should be on customer sensitivity, rapid innovation, empowering staff, and most importantly, learning to work in a changing environment (Peters 1987). 21st century realities confirm Peters' analysis by making the deficiency in these tools more evident.

The organizational system of companies that expand rapidly in the 21st century is becoming more complex and unpredictable, and this causes existing theories to be inadequate in explaining the system. Traditional hierarchy-based approaches exclude this complexity, and explain business organizations as logical entities. However, it looks at the nature of contemporary business organizations from multiple perspectives using new approaches (Llora and Cordero 2016). Companies, vendors, and suppliers are in constant interaction with each other due to direct or indirect competition. According to Levy (1994), all interactions in which companies participate are strategic in the sense that one company's decisions take into account the expected reactions of others. Therefore, institutional macro, and micro actions will be interdependent. In chaos theory, small disturbances in a company multiply non-linearly over time. As a result, every action can affect other companies. Traditional strategy concepts and paradigms suggest that small changes in parameters upset the balance and require a corresponding renewal.

Chaos theory contradicts this concept. Additionally, chaos theory forces us to analyze how small changes can have enormous consequences. In other words, chaos theory does not explain every variable affecting the organization, but emphasizes that balance will be restored, and chaos inherently leads to order. In other

words, what managers must accept is that in complex systems, planning and control, before action, cannot solve everything. Additionally, managers need to learn how to manage the change process (Morgan 1997).

In recent years, we have come across many examples confirming this thesis. For example, Industry 4.0 technologies and the digital transformation process propel businesses to a very different dimension. While technologies such as the Internet of Things (IoT), cyber-physical systems (CPS), smart manufacturing, smart factories, cloud computing, cognitive computing, and artificial intelligence cause changes in business processes, they also create uncertainty and confusion for the industry of the future (Majocco *et al.* 2024). The direction and severity of this transformation are not clear in terms of its details and consequences. Another example is the pandemic process. The pandemic has shown companies the change in the global climate, the economic interdependence among countries, what technological changes mean for the activities of businesses, and the vulnerability of human-based production processes.

The ongoing crisis since 2020 is still felt in the business world. This situation further increases the uncertainty and complexity of the business world (Sharma *et al.* 2020). Another ongoing example is the Russia-Ukraine war that broke out in 2022. It reveals the process of the war and its resulting effects of this war between the two countries on other countries, and their global economic dependency. The dependency on raw materials and energy is becoming more evident. As can be seen, Industry 4.0, the pandemic, and the Russia-Ukraine war reveal disorder in the business world.

Chaos theory explains how businesses can navigate this disorder. While chaos theory involves the effort to understand and define the environment, it also brings with it the effort to define and understand the organization (Arıcıoğlu and Berk 2022). The underlying premise of chaos theory is the belief that there is disorder within order. In other words, while there is disorder at lower levels in a system, there is order throughout the system. Chaos theory views a company as a self-organizing living system that allows its employees and management to adapt and develop to environmental changes (Smith 2011). The key to survival for organizations is to develop rules that can keep an organization operating "on the edge of chaos," as in natural systems (Stacey *et al.* 2000; Arıcıoğlu and Berk 2022).

PARADIGM SHIFT IN THE STRATEGIC MANAGEMENT PROCESS

The strategic management process shows the steps taken by managers and organizations in planning, formulating, implementing the strategy, and creating new plans and practices through feedback. While Hunger and Wheelen (2003) define a process through environmental scanning, formulation, implementation, and control, Hofer and Schendel (1978) evaluate the strategy process as a seven-stage process. Steiner (1969) explains the stages of the strategy management process in six steps in his book *Top Management Planning*. Nutt and Backoff (1987) discussed the process in six stages.

According to the design school called "The Basic Design School Model" by Mintzberg, which includes founders such as Andrews, Selznick and Chandler, the main steps of the strategic management process are: external evaluation, internal evaluation, formation of strategic options, evaluation and strategy selection, and strategy implementation (Mintzberg 1990). Bryson and Alston (2004) evaluate the strategic management process as comprising six stages. According to Morden (2007), the strategic management process is a four-stage process.

When evaluating the approaches and models in the literature:

1. The strategic management process is commonly seen as a five-stage model: *Goal Definition & Strategist Selection, Environmental Analysis, Organizational Direction, Implementation, Control* (see Figure 2).
2. The process follows a deterministic, sequential mechanism, where each step depends on the completion of the previous one.
3. External environmental factors are considered beyond the company's influence or control.
4. Errors in the process can only be addressed by relating them to the output of the previous stage or through interventions made during the process.
5. Time is typically measured in long-term values like 5 or 10 years, which include considerations for operational strategies.
6. The methods and tools used are standardized and fixed throughout the analysis and control stages.

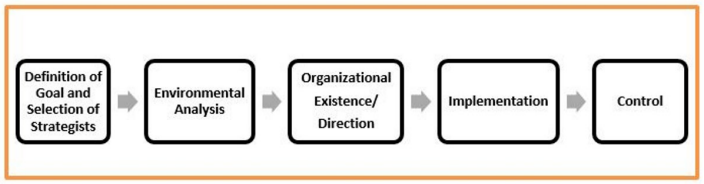

Figure 2 The five-stage strategic management process

In summary, the strategic management paradigm focuses on aligning organizations with their environment to gain a competitive advantage (Bain & Company 2018). As changes arise, fundamental concepts governing this relationship must be re-evaluated, signaling a paradigm shift. This shift can be explained through the theses of Kuhn and Feyerabend and , where scientific theories are debated in terms of their relative or universal nature. In other words, the claim of incommensurability of scientific theories is criticized by many philosophers of science. The basis of these criticisms is the debate about whether knowledge is relative depending on time, place, society, culture, historical period, conceptual framework, personal tendencies, beliefs, or whether it is possible to reveal absolute and universal knowledge independently of these issues. The introduction of an innovative and previously unknown definition, the assertion of new values, or a new style of presentation, understanding, or approach is also described as a paradigm. Feyerabend argued that the move from Newtonian to Einsteinian physics was driven by practicality, not accuracy.

This study highlights the need for a new paradigm in strategic management, as current theories fail to address present realities. The required paradigm shift involves both structural and process changes, with the process aspect addressing abnormalities that current paradigms cannot explain. Structurally, it calls for a redesign of the strategic management process.

The history of strategic management shows that each era developed its own approach based on its context. Today, these approaches face validity issues. The dynamics highlighted in this

study reveal that current strategic management processes are inadequate and require new experiences. This calls for a flexible and adaptable structure, emphasizing a proactive rather than reactive approach. The strategic management process is now designed in a cyclical, multidimensional relationship (see Figure 3), providing the flexibility and dynamism needed for today's environment. In this structure, all steps, especially strategic awareness, interact continuously, driving dynamism. Redesigning the process in response to changing conditions requires up-to-date information from the environment at each step. Businesses must maintain both strategic awareness and leverage insights from other stages of the process. The dynamics in Figure 3 reflect the need for this new approach, reshaping the strategic management process.

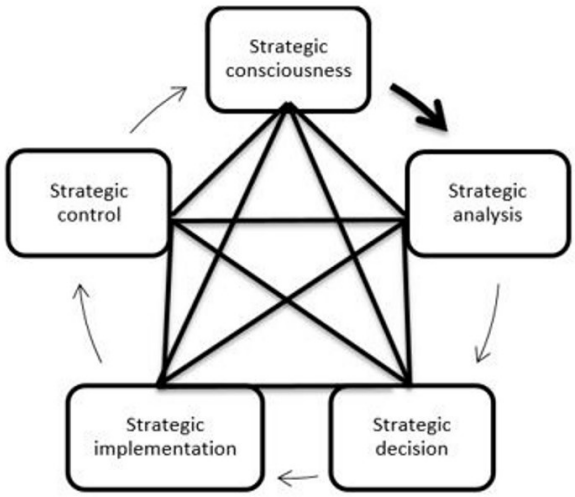

Figure 3 The new strategic management process

The structural form of the strategic management process needs a paradigm shift. The structure and process should be dynamic, as shown in the figure. A dynamic structure is a structure that can easily adapt to change and affect change. The conjunction of the age we live in requires a proactive approach rather than a reactive process, as explained in detail above.

METHODOLOGY

Sample and Data Collection

This study employed qualitative research methods, with a focus on content analysis. Qualitative research aims to explore and understand the meaning individuals or groups attribute to social or human problems (Creswell and Creswell 2018). It involves open-ended questions, data collected in natural settings, inductive analysis, and the researcher's interpretation of the data. Content analysis, a tool used in qualitative research, measures the presence and associations of specific words, themes, or concepts in data. Data for this study were gathered through semi-structured interviews, each lasting 45 to 90 minutes. The interviews, conducted online between April 1 and July 31, 2022, were recorded and transcribed. As shown in Table 1, a total of nineteen administrators constitute the study group of the research.

The participants were informed to ensure a better understanding of the concepts, and the consistency of their answers. In line with the events explained by the participants, different questions were asked according to the situation, and the data were obtained reliably.

Table 1 The sample of research

Participant No	Sector	Position
K1	Energy	Sales Manager
K2	Food	R&D Manager
K3	NGO	Head of Overseas Org.
K4	Consultancy	Business Partner
K5	Food	General Manager
K6	Software	Partner & Manager
K7	Software	Partner & Manager
K8	Paper	Executive
K9	Petrochemical	Deputy General Manager
K10	Software	Partner & Manager
K11	Automotive	Factory Manager
K12	Automotive	Production Manager
K13	Electronics	R&D Manager
K14	Food	Production Manager
K15	Iron & Steel	Executive
K16	Food	Production Manager
K17	Food	Executive
K18	Automotive	Executive
K19	Energy	Sales Manager

DATA ANALYSIS AND RESULT

Hierarchical code-sub code

In this study, we defined the hierarchical code-sub code structure. According to the results of hierarchical code-sub code sections, the environmental changes in the 21st century world are summarized in Table 2.

Environmental change awareness has six different subcategories and a total of fifteen codes related to these categories. In Table 2. , the frequencies of all codes related to environmental change awareness and the distributions of these codes are shown. In the category of environmental change awareness, the subcategory, which is expressed as "Technological Change", comes to the fore. This is followed by the categories of "New World Order", "Change of Human Quality", "Collaborative Structuring", "Change in the Concept of Time". The least mentioned environmental change theme was 'changes in the ecosystem'. Therefore, 19 of the interviewed managers evaluated technological changes as a priority environmental factor in the context of strategic management. In environmental changes category, participants usually expressed such as the following sample quotes:

"The nineties were a period when technology was less pervasive than it is today. Today, technology is used extensively. I would say this is the biggest difference." (K6)

"Now, due to the impact of technology, the concepts of digital consumer manager concepts dominate in the business world. Now we see that people are increasingly becoming digital consumers." (K7)

Table 2 Environmental Change Awareness – Hierarchical Code Subdivision Model

Theme	Code Frequency
Technological Changes	1270
New World Order	742
Multipolarity	173
Trade	334
Economic Dependency	336
Political and Political Relations	165
Globalization	360
Company Sizes	76
Time Concept Change	336
Change of Meaning of Time	26
Planning Period	140
Flexible Planning	191
Collaborative Structure	427
Importance of Collaborative Structure	148
Cooperation in SMEs	21
Digital Platforms	289
Human Quality Change	452
Consumer	235
Worker	226
Executive	228
Change in Ecosystem	191

Code-sub code

The model for the code sub-code section related to the chaos theory category examined within the scope of the research is presented in Table 3. According to the code-subcode model, chaos theory has four different subcodes.

Table 3 Chaos Theory – Code and Subcode Model

Theme	Code Frequency
Turbulence	372
Strange Attractors	420
Interaction	52
Butterfly Effect	73

Table 3 shows the frequencies and distributions of all codes related to chaos theory. In the chaos category, the sub-code which is expressed as "strange attractors" stands out. This code is followed by the 'turbulence, 'butterfly effect, 'mutual interaction' codes, respectively. According to these findings, the criteria of strange attractors (420) and turbulence (372) are at the forefront of the basic elements that shape chaos theory. Therefore, according to these findings, it can be said that the basic elements that shape the chaos theory are the factors that are coded as strange attractors, disrupting a linear process and are difficult to predict. The second factor is the turbulence code, which also expresses the gradual shortening of the foresight ability. The number of interaction codes is the lowest among all code categories. This code expresses the interaction between the parts that make up a system. The code was mentioned the least by the managers in the research. In chaos theory category, participants usually expressed such as the following sample quotes:

"We have all witnessed major changes in companies, especially in the 21st century. The world has become a very dynamic and changeable environment. So where is this going? They refer to it as turbulence or chaos theory. Unpredictability, uncertainty, feedback, I know, the butterfly effect, etc." (K4)

"There is a constantly changing structure. This shows that there is a somewhat dynamic structure involved. The occurrence of such consecutive crises as pandemics, wars, and economic crises is an indication that businesses live in a chaotic environment." (K7)

Table 4 presents a code-subcode section model for the strategic management process of all managers examined within the scope of the research. According to the code-subcode model, there are five different subcodes of the strategic management process.

Table 4 Strategic Management Process – Code and Subcode Model

Theme	Code Frequency
Strategic Awareness	857
Strategic Analysis	809
Strategic Decision	803
Strategic Implementation	657
Strategic Control	638

Table 4 shows the frequencies of all codes related to the strategic management process and the distribution of these codes. In the category of strategic management process, the sub-code, which is expressed as "strategic consciousness", is highlighted. This code is followed by "strategic analysis", "strategic decision", "strategic control", and "strategic implementation" codes, respectively. According to these findings, although strategic consciousness (857) is at the forefront of the basic elements that shape the strategic management process, every other element is equally important for the process. In the strategic management category, participants usually expressed thoughts similar to the following sample quotes:

"What we call the big picture is this: it is the ability to make connections between different events in different parts of the world. This is a strategic awareness." (K4)

"Businesses should follow environmental changes. They should consciously execute their strategies with the information they have obtained." (K2)

In this study, participants usually described the strategic management process as a cyclical and multifaceted interrelationship that supports the organization-environment relationship. In strategic management category, participants usually expressed such as the following sample quotes:

"Each step of the strategic management process is important, and it must be carried out interactively. Consciousness must be present at every stage of the process. Environmental analysis

Themes	Chaos	Interaction	Turbulence	Strange attractors	Butterfly effect	Strategic management process	Strategic awareness	Strategic analysis	Strategic decision	Strategic implementation	Strategic control	Total
Environmental change awareness	619	33	213	396	49	850	659	611	643	497	507	5077
Technological Changes	323	15	134	204	13	445	353	299	268	208	207	2469
New world order	213	29	57	135	43	265	187	194	219	158	159	1659
Multipolarity	23	5	13	12	5	66	44	51	46	34	34	333
Trade	109	9	26	84	16	167	115	124	135	96	98	979
Economic Dependency	152	20	33	97	33	142	102	115	119	91	93	997
Political and Political Relations	42	8	16	26	7	86	55	66	64	45	45	460
Globalization	108	17	37	62	26	163	112	122	129	92	94	962
Company Sizes	4	3	4	2	2	33	16	21	20	12	12	129
Time Concept Change	94	6	65	29	7	148	100	106	135	96	106	892
Change of Meaning of Time	5	1	3	3	1	2	1	1	2	1	1	21
Flexible Planning	50	1	30	21	2	109	74	82	98	72	81	620
Planning Period	36	1	30	7	1	50	30	30	48	30	33	296
Collaborative Structure	108	9	20	89	8	107	90	94	90	81	82	778
Cooperation in SMEs	1	1	1	1	1	8	6	5	7	5	5	41
Importance of Collaborative Structure	19	1	2	18	2	34	29	32	29	27	27	220
Digital Platforms	89	3	10	81	3	75	62	68	62	57	58	568
Human Quality Change	87	9	23	67	6	85	69	68	58	51	50	573
Consumer	54	4	14	43	2	46	31	39	31	26	26	316
Worker	36	4	12	26	2	63	49	51	43	39	38	363
Executive	29	4	11	20	2	62	47	49	39	35	34	332
Change in Ecosystem	34	8	13	20	7	120	102	109	106	96	96	711
Chaos	0	52	372	420	72	259	184	183	199	144	149	2034
Interaction	52	0	29	24	28	13	10	12	13	9	9	199
Turbulence	372	29	0	45	24	113	74	79	81	58	62	937
Strange Attractors	420	24	45	0	25	148	111	104	121	87	88	1173
Butterfly Effect	72	28	24	25	0	16	11	13	15	11	11	226
Total	3151	324	1237	1957	387	3675	2723	2728	2820	2158	2205	23385

Figure 4 Relational analyses results

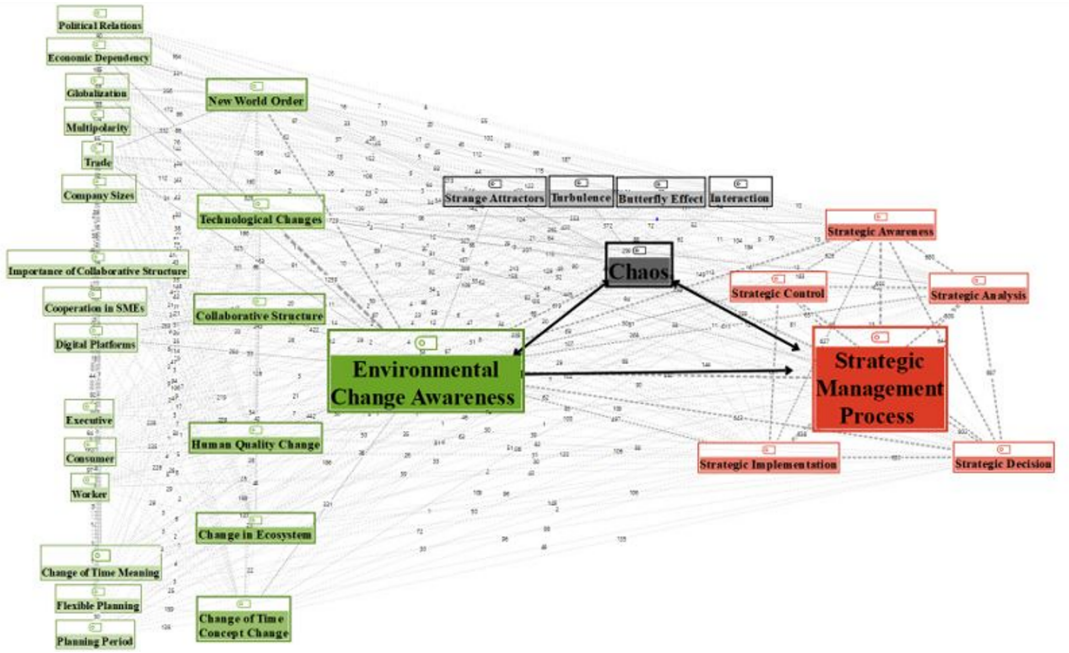

Figure 5 Code co-occurrence model

must be constantly revised. There is so much change happening." (K2)

"I agree that the strategic management process should be a cyclical and multifaceted interrelated ." (K6)

"Considering the environmental changes of the strategic management process, I think that such things and practices should be cyclical." (K10)

"Such a period also shows us that the strategy should be flexible." Regarding this, the process should be carried out cyclically with consciousness and awareness." (K12)

Relational analysis

Relational analysis results are summarized in Figure 4. The color tones in the relationship matrix express the frequency of the codes' relationship . Relational analyses reveal that environmental change awareness is related to both chaos theory and the strategic management process.

Code co-occurrence analysis

Figure 5 presents the "Code Co-occurrence Model," which visualizes the co-occurrence of codes as a network. Line width in the model represents the strength of relationships between variables the thicker the line, the greater the coding overlap between two variables. Although all variables are related, the model highlights clusters where environmental change awareness and chaos

strongly connect to the strategic management process. Similarly, technological changes, strange attractors, and the new world order form another cluster linked to strategic management. Additionally, the model identifies key factors driving environmental change awareness, and chaos.

CONCLUSION

At the end of the 20th century, strategic management and the organization-environment relationship underwent significant changes (Arıcıoğlu and Berk 2022). Factors such as technology, globalization, pandemics, wars, and climate change have created an uncertain and chaotic world, rendering traditional approaches insufficient. Chaos theory has become an increasingly important tool in understanding the modern business environment. The unpredictability and dynamic nature of today's business world can be explained through the fundamental principles of chaos theory. This theory suggests adopting an adaptive approach to strategic management, emphasizing that small changes in the business environment can lead to significant impacts. In competitive conditions, chaos theory enables businesses to continuously analyze their environments, develop flexible strategies against rapid changes, and seize opportunities within uncertainties. This study examines paradigm shifts in strategic management by considering environmental changes and chaos theory, presenting an alternative model. The study contributes uniquely to the literature with its subject, findings, qualitative methods, and multivariate analysis.

The findings of the study reveal that participants emphasized the chaotic nature of competition and the need for new business models and management tools in the business world. In the context of a chaotic environment, technological changes were found to drive new business models and competition, making changes in management tools inevitable. Since the last quarter of the 20th century, the world has witnessed the rapid spread of information and communication technologies (ICT), leading to significant changes and structural transformations (Lechman and Marszk 2019). The impact of technology is also related to the subprocesses of strategic management. In the analysis of code relationships conducted in the study, the technological dimension was found to be associated with processes such as strategic awareness, strategic analysis, strategic decision-making, strategic implementation, and strategic control. Additionally, changes in human behaviors, particularly consumers and employees adapting to digital processes, were highlighted as critical components of the strategic process.

Collaborative structuring has emerged as another important trend that businesses have adopted, especially in chaotic business environments. Collaboration creates a system in which even small enterprises can generate significant changes. In a chaotic environment, collaboration can provide businesses with a competitive advantage. This is because it enables companies with different areas of expertise to come together to develop innovative products and services, share risks to cope with uncertainties more effectively, facilitate access to new markets, and support their growth on a global scale.

The concept of time has also undergone changes, leading to a need for more flexible planning. Supported by chaos theory, the study highlights the unpredictable nature of today's business environment and emphasizes the necessity of strategic adaptation. In an environment where competitive conditions constantly change, businesses' ability to adapt to these dynamic variables becomes more comprehensible through the flexibility and adaptability framework offered by chaos theory. The need for different timeframes in strategic plans compared to previous periods, alongside the requirement for flexibility and dynamic revisions in planning processes, has been highlighted. Expressions related to this theme were organized, which resulted in subcodes such as "changes in the meaning of time," "planning periods," and "flexible planning. Participants emphasized the importance of strategic awareness and analysis. The findings suggest that in a chaotic world, new approaches are essential for managing the organization-environment relationship. The proposed model is structured as a cyclical and multidirectional process that accommodates sudden changes and allows for continuous environmental analysis. Future studies may examine these shifts in an international context or use quantitative research methods to gain broader insights.

This study involved interviews with senior executives from both national and international companies in Turkey. Future studies may expand the research by focusing on foreign companies, providing global support for the study results. Additionally, this study exclusively utilized qualitative research methods. In future research, the topic could be explored using quantitative research methods or a mixed-methods approach to obtain more comprehensive results and contribute to the strategic management literature. Considering that the pace of environmental change may vary across sectors, future studies could focus on conducting more sector-specific research.

Ethical standard

The authors have no relevant financial or non-financial interests to disclose.

Availability of data and material

Not applicable.

Conflicts of interest

The authors declare that there is no conflict of interest regarding the publication of this paper.

LITERATURE CITED

Akad, M. T., 2001 *Strateji Üzerine*. Kastaş Yayınları.

Alantar, Z., 2008 Küresel kriz ve etkileri. Ekonomik Yaklaşım .

Ansoff, H. I., 1965 *Corporate strategy: An analytic approach to business policy for growth and expansion*. McGraw-Hill.

Arıcıoğlu, M. A. and O. N. Berk, 2022 A comparative proposal on learning the chaos to understand the environment. Chaos Theory and Applications **84**: 19–25.

Arıcıoğlu, M. A., B. Yiğitol, and A. Yılmaz, 2020 Endüstri 4.0 üzerine yöntem ve literatür çalışması: Türkiye'deki lisansüstü tez çalışmaları. Erciyes Üniversitesi İktisadi ve İdari Bilimler Fakültesi Dergisi pp. 293–324.

Açıkalın, N., 2015 *Leadership in Chaos: Angela Merkel and European Union*. Example Publisher, İstanbul.

Bain & Company, 2018 Management tools: Core competencies. https://www.bain.com/insights/management-tools-core-competencies/, Retrieved from Bain & Company website.

Barber, B., 1996 *Jihad vs. McWorld: How Globalism and Tribalism Are Reshaping the World*. Ballantine Books.

Bryson, J. M. and F. K. Alston, 2004 *Creating and Implementing Your Strategic Plan: A Workbook for Public and Nonprofit Organizations*, volume 1. John Wiley & Sons.

Castells, M., 2008 *Enformasyon Çağı Ekonomi, Toplum ve Kültür Cilt-1: Ağ*. İstanbul Bilgi Üniversitesi Yayınları.

Chandler, A. D., 1962 *Strategy and Structure: Chapters in the History of the Industrial Enterprise*. MIT Press.

Creswell, J. W. and J. D. Creswell, 2018 *Research Design: Qualitative, Quantitative, and Mixed Methods Approaches*. Sage Publications, fifth edition.

De Bono, E., 1996 *Rekabet Üstü*. Remzi Kitabevi, Çev. O. Özel.

de Bono, E., 2000 *New Thinking for the New Millennium*. Viking Penguin, London, Supra-competitive thinking and value monopolies.

Dedyukhina, A., 2017 Homo distractus: Fight for your choices and identity in the digital age. https://thriveglobal.com/stories/how-technology-changes-our-perception-of-time/, Accessed: 2021-11-01.

Dijksterhuis, M. S., F. A. J. Van den Bosch, and H. W. Volberda, 1999 Where do new organizational forms come from? management logics as a source of coevolution. Organization Science **10**: 569–582.

Dirlik, A., 2009 *Kriz, kimlik ve siyaset: Küreselleşme yazıları*. İletişim Yayınları.

Dirlik, A., 2012 *Küreselleşmenin sonu mu?*. Ayrıntı Yayınları.

Drucker, P. F., 1942 *The Future of Industrial Man: A Conservative Approach*. The John Day Company.

Drucker, P. F., 1954 *The Practice of Management*. Harper Business.

Drucker, P. F., 1999 *Management Challenges for the 21st Century*. HarperBusiness.

Earle, E. M., 2015 *Modern Stratejinin Ustaları*. Doruk Yayınevi.

European Commission, 2021 Eu emissions trading system (eu ets). https://ec.europa.eu/clima/policies/ets_en, Accessed: 2025-07-18.

Frase, P., 2018 *Dört Gelecek: Kapitalizmden Sonra Hayat*. Koç Üniversitesi Yayınları, Translated work.

Freedman, L., 2018 *Strateji*. Alfa Tarih Yayıncılık, Translated work.

Fukuyama, F., 2002 *Tarihin Sonu mu?*. Vadi Yayınları.

Fukuyama, M., 2018 Society 5.0: Aiming for a new human-centered society. Japan Spotlight **27**: 47–50.

Galambos, L., 2005 Recasting the organizational synthesis: Structure and process in the twentieth and twenty-first centuries. Business History Review **79**: 1–38.

Guillory, W. A., 2007 The futureperfect organization: Leadership for the twenty-first century–part i. Industrial and Commercial Training **39**: 52–58.

Halpern, P., 2018 Chaos theory, the butterfly effect, and the computer glitch that started it all. https://www.forbes.com/sites/startswithabang/2018/02/13, Accessed: 2022-04-01.

Hamel, G. and C. K. Prahalad, 1989 Strategic intent. Harvard Business Review **63**: 63–76.

Harris, G., 2022 Chaos theory of organizations. In *Global Encyclopedia of Public Administration, Public Policy, and Governance*, edited by A. Farazmand, Springer, Cham.

Harvey, D., 1990 *The Condition of Postmodernity*, volume 14. Blackwell.

Hofer, C. W. and D. Schendel, 1978 *Strategy Formulation: Analytical Concepts*. West Publishing.

Hunger, J. D. and T. L. Wheelen, 2003 *Essentials of Strategic Management*. Prentice Hall, fourth edition.

Jacobides, M. G., 2021 Building ecosystems: From "what" to "how.". https://www.youtube.com/watch?v=Mt7xwpHdb8o, Accessed: 2025-07-18.

Kabue, L. W. and J. M. Kilika, 2016 Firm resources, core competencies and sustainable competitive advantage: An integrative theoretical framework. Journal of Management and Strategy **7**: 98–108.

Kellert, S. H., 1992 A philosophical evaluation of the chaos theory "revolution.". In *Proceedings of the Biennial Meeting of the Philosophy of Science Association*, volume 2, pp. 33–49.

Landau, L. D., 1944 On the problem of turbulence. Doklady Akademii Nauk SSSR **44**: 339–342.

Lechman, E. and A. Marszk, 2019 *ICT-driven Economic and Financial Development: Analyses of European Countries*. Academic Press.

Levy, D., 1994 Chaos theory and strategy: Theory, application, and managerial implications. Strategic Management Journal **15**: 167–178.

Lieber, R. J. and R. E. Weisberg, 2002 Globalization, culture, and identities in crisis. International Journal of Politics, Culture, and Society **16**: 273–296.

Llora, M. B. and J. F. Cordero, 2016 Using chaos theory as a framework to explain the nature of complexity in contemporary organizations. Revista Economía y Política **12**: 39–56.

Majocco, P., P. Mosch, and R. Obermaier, 2024 Digital transformation under uncertainty–market value effects of early industry 4.0 innovation projects. Procedia Computer Science **232**: 232–241.

Mcluhan, M. and B. R. Powers, 2020 *Global Köy: 21. Yüzyılda Yeryüzü Yaşamında ve Medyada Meydana Gelecek Dönüşümler*. Scala Yayıncılık.

Miles, R. E. and C. C. Snow, 2010 Organizational strategy, structure, and process. Academy of Management Review **3**: 546–562.

Mintzberg, H., 1978 Patterns in strategy formation. Management Science **24**: 934–948.

Mintzberg, H., 1987 The strategy concept i: Five ps for strategy. California Management Review **30**: 11–24.

Mintzberg, H., 1990 The design school: Reconsidering the basic premises of strategic management. Strategic Management Journal **11**: 171–195.

Morden, T., 2007 *Principles of Strategic Management*. Ashgate Publishing Limited.

Morgan, G., 1997 *Images of Organization*. Sage Publications.

Naidoo, E., 2020 7 successful battle strategies to beat covid-19. https://hbswk.hbs.edu/item/7-winning-war-strategies-to-beat-covid-19, Harvard Business School Working Knowledge.

Namaki, Z., 2018 The application of chaos management theories in organization. International Journal of Management Technology **5**: 39–45.

National Geographic, 2021 Global warming. https://www.nationalgeographic.org/encyclopedia/global-warming/.

Norton, J. D., 1993 The determination of theory by evidence: The case for quantum discontinuity, 1900–1915. Synthese **97**: 1–31.

Nutt, P. C. and R. W. Backoff, 1987 A strategic management process for public and third-sector organizations. Journal of the American Planning Association **53**: 44–57.

Onday, O., 2019 Japan's society 5.0: Going beyond industry 4.0. Business and Economics Journal **10**: 2–7.

Peccei, A., 2013 *The Human Quality*. Elsevier.

Peters, T., 1987 *Thriving on Chaos: Handbook for a Management Revolution*. Harper Paperbacks.

Porter, M. E., 1985 *Competitive Advantage: Creating and Sustaining Superior Performance*. The Free Press.

Prahalad, C. K. and G. Hamel, 1990 The core competence of the corporation. Harvard Business Review pp. 79–91.

Rifkin, J., 2015 *Nesnelerin İnterneti ve İşbirliği Çağı*. Optimist Yayınları.

Ritzer, G., 1998 *Toplumun McDonaldlaştırılması*. Ayrıntı Yayınları, Translated by Ş. Süer Kaya.

Roblek, V., M. Meško, and A. Krapež, 2016 A complex view of industry 4.0. SAGE Open **6**.

Ruelle, D., 1990 The claude bernard lecture, 1989. deterministic chaos: The science and the fiction. Proceedings of the Royal Society A: Mathematical, Physical and Engineering Sciences **427**:

241–248.
Ruelle, D., 2006 Turbulence, strange attractors, and chaos. Notices of the AMS **53**: 572–579.
Selznick, P., 1957 *Leadership in Administration: A Sociological Interpretation*. Row, Peterson and Company.
Sharma, P., T. Y. Leung, R. P. Kingshott, N. S. Davcik, and S. Cardinali, 2020 Managing uncertainty during a global pandemic: An international business perspective. Journal of Business Research **116**: 188–192.
Smith, A. D., 1990 Towards a global culture? Theory, Culture & Society **7**: 171–191.
Smith, A. D., 2011 Chaos theory and recessional business environments: Case studies of operational health of service and manufacturing organisations. International Journal of Services and Operations Management **8**: 191–221.
Smith, J., S. Plummer, and M. M. Hughes, 2017 Transnational social movements and changing organizational fields in the late twentieth and early twenty-first centuries. Global Networks **17**: 3–22.
Stacey, R. D., D. Griffin, and P. Shaw, 2000 *Complexity and Management: Fad or Radical Challenge to Systems Thinking?*. Psychology Press.
Steiner, G. A., 1969 *Top Management Planning*. Macmillan.
Stewart, I., 1990 *Does God Play Dice: The Mathematics of Chaos*. Basil Blackwell.
Straussfogel, D. and C. V. Schilling, 2009 Entropy debt: A link to sustainability? In *Proceedings of the 53rd Annual Meeting of the ISSS-2009, Brisbane, Australia*.
Thietart, R. and B. Forgues, 1995 Chaos theory and organization. Organization Science **6**: 19–31.
Vaidya, S., P. Ambad, and S. Bhosle, 2018 Industry 4.0–a glimpse. Procedia Manufacturing **20**: 233–238.
Xu, L. D., E. L. Xu, and L. Li, 2018 Industry 4.0: State of the art and future trends. International Journal of Production Research **56**: 2941–2962.
Yang, F. and S. Gu, 2021 Industry 4.0, a revolution that requires technology and national strategies. Complex & Intelligent Systems pp. 1–15.

How to cite this article: Yiğitol, B., and Arıcıoğlu, M. A. A New Model Proposal for a Paradigm Shift for Strategic Management in the Context of Chaos Theory. *Chaos Theory and Applications*, 7(2), 166-176, 2025.

CHAOS
Theory and Applications
in Applied Sciences and Engineering

e-ISSN: 2687-4539
RESEARCH ARTICLE
Vol.7 / No.2 / 2025 / pp.177-185
https://doi.org/10.51537/chaos.1621022

Analysis of Chaotic Systems in the Generation of Random Phases for Amplitude Holograms

Héctor Eduardo Gilardi Velázquez [§,1] **and Maria-Luisa Cruz** [α,2]

[§]Facultad de Ingeniería, Universidad Panamericana. Josemaría Escrivá de Balaguer 101, Aguascalientes, Aguascalientes, 20296, Mexico, [α]Universidad Panamericana. Facultad de Ingeniería. Álvaro del Portillo 49, Zapopan, Jalisco, 45010, México.

ABSTRACT In recent decades, there has been great interest in the development of applications of chaotic systems in cryptographic systems and communication systems due to their non-periodic and long-term unpredictable nature. In this work, the properties of different chaotic systems, both continuous and discrete in time, are analyzed for the generation of pseudo-random phases practical for holography. The different types of dynamics generated by different systems are analyzed using bifurcation diagrams, transition from chaos to periodic orbits and equilibrium points, as well as two methodologies to construct the phase (Cartesian and polar). Our results shows a better performance in discrete-time systems by generating smooth transitions in the formed patterns and avoiding the generation of artifacts in the holograms, given the wider range of parameters in which the system is stable.

KEYWORDS
Logistic map
Random phase
Chaotic system
Multistability
PWL system
Bifurcation
Holography

INTRODUCTION

Chaos is a phenomenon that is commonly found in nature in different areas as weather climate, dynamics in the solar system, celestial bodies, and population growth in ecology and human studies and physical experiments of electrical circuits, lasers, chemical reactions, fluid dynamics, mechanical systems, and magneto-mechanical devices (Echenausía-Monroy *et al.* 2024). Then, chaotic models can help to simulate these experiments accurately. Also, Chaos has many interesting applications in the development of electrical devices and communication systems, processing information, and communication devices. This is due to the rich behavior of chaotic signals and easy implementations.

Communication and signal processing applications of chaos were established after the chaos synchronization and chaos control theories in 1990. Today, we find many applications of quasi-random sequence generation as, communication channels modeling using chaos, chaotic cryptography, digital image encoding, and chaotic transport phenomena in complex networks (Kocarev *et al.* 2009). An interesting phenomena where the chaos can be found is the light behavior, including applications as holography. Holography is the technique for recording and manipulating a whole wavefront of light. There are several applications of holography; one of them is the development of holographic tridimensional displays Blanche (2021) using computer-generated holograms (CGH). In CGH, a two-dimensional random pattern is necessary to diffuse the energy in the 2-dimensional field. Given that one of the main applications of chaotic systems is the creation of parametric pseudo-random sequences, we proposed using a chaotic system to generate a parametrized 2-dimensional random pattern that increases the hologram quality. In Cruz and Gilardi-Velázquez (2024), we presented the preliminary results of a random phase generated by a chaotic system applied to amplitude-encoded Fourier holograms(AE-FH).

Our proposal aims to analyze the relation between the chaotic system characteristics and the quality of computer-generated holograms. First, we review some important concepts of chaotic systems. The chaotic systems have a strong, sensitive dependence on initial conditions, are similar to random phenomena, and have a continuous broad-band power spectrum. The stable behaviors that can be found in non-linear dynamical systems are: equilibrium points, periodic orbits, and chaotic attractors, quasi-periodic behavior, and the coexistence of attractors (multistability) (Ott 2002; Diaz-gonzalez *et al.* 2022).

The sensibility to changes of the system parameters may or may not lead to changes in the system behavior, and the influence of external disturbances can lead to destabilization of the system or uncontrolled behaviors. These points where parameter values lead

Manuscript received: 16 January 2025,
Revised: 10 March 2025,
Accepted: 11 April 2025.

[1]hgilardi@up.edu.mx (**Corresponding author**)
[2]mlcruz@up.edu.mx

to this type of behavior are called the *tipping point* (Echenausía-Monroy *et al.* 2024). These points are commonly studied by the bifurcation points because the tipping point refers to dynamic behavior. Bifurcation points can describe different behavior changes as stability in equilibrium points, modification on frequency response, and transitions from chaotic to periodic behavior (Rial *et al.* 2004; Jiang *et al.* 2019). The parameter changes in a complex system are crucial to identifying the changes in the system behavior, principally when the global stability or a segmentation of its basin of attraction. These behavior changes can reveal the occurrence of multistability (Gilardi-Velázquez *et al.* 2018; Echenausía-Monroy *et al.* 2020; Njitacke *et al.* 2020). The multistability phenomenon has been exposed in many areas as optical illusions, chemical reactions, and physical phenomena such as the pendulum. Multistability is caused by the existence of multiple basins of attraction. For a given systems parameters, the dynamics may converge to a set of different stable attractors (equilibrium points, periodic orbit, chaotic attractor), which only depend on initial conditions, i.e., for a small change in the initial condition, the trajectories converge to another different set.

For applying correctly a chaotic system in a specific phenomena analysis, it is necessary to find the relation between the phenomena characteristics and the chaotic system properties. In recent years, many articles have been published dealing with chaos-based cryptographic systems (Platas-Garza *et al.* 2021; Munir *et al.* 2021; Razaq *et al.* 2021; Cassal-Quiroga and Campos-Cantón 2020; Cassal-Quiroga *et al.* 2022), i.e., due to the relationship that exists between the properties of chaotic systems and cryptographic properties. In Alvarez and Li (2006), the relationship between these properties is given, e.g., confusion is related to ergodicity, diffusion property is related to sensitivity to initial conditions, and deterministic dynamics is related to deterministic pseudo-randomness. A pseudo-random number generator is a deterministic method commonly generated via nonlinear maps to produce a small set of "random" numbers. This set depends on an initial condition called the seed, which creates a larger set of random-looking numbers called pseudo-random numbers.

Chaotic maps and cryptographic algorithms have similar properties: sensitivity to initial conditions and parameter changes, random-like behavior, and unstable periodic orbits with long periods (Cassal-Quiroga and Campos-Cantón 2020). Approaches based on discrete-time systems (maps) have been widely used in the last decade to generate pseudo-random sequences for block and stream cipher systems (Gotz *et al.* 1997; Mazloom and Eftekhari-Moghadam 2009; Patidar and Kaur 2023). More recently, the scientific community has begun implementing continuous-time systems as cryptosystems; see (Čelikovskỳ and Lynnyk 2012; Khan *et al.* 2013) and references therein. Then, it is important to find which of these two system types is the more advantageous for generating a 2D random pattern for hologram generation.

Next, we review the basic concepts of holography for understanding the use of chaotic systems in computer-generated holograms. A hologram records all the light information in a wavefront generated by a 3D object: amplitude and phase. Contrary to a photograph, which only records the amplitude information. The amplitude represents the light intensity on each object point. Meanwhile, the phase includes information about the object surface. When a hologram is illuminated, a copy of the original object wavefront is generated (Goodman 2005). That is, the light from the hologram looks like it is coming out from the 3D object. When a wavefront light illuminates an object, each point reflects the light waves in several directions; that is why we can observe the object from different points of view. A hologram records all the information from the light coming from the object, including the light intensity and direction. This phenomenon allows recording several points of view of the object in one hologram. Then, in the reconstruction step, a hologram can regenerate all the light rays or waves reflected by the object, and the object recorded in the hologram can be viewed from different angles (Wakunami *et al.* 2013), Figure 1.

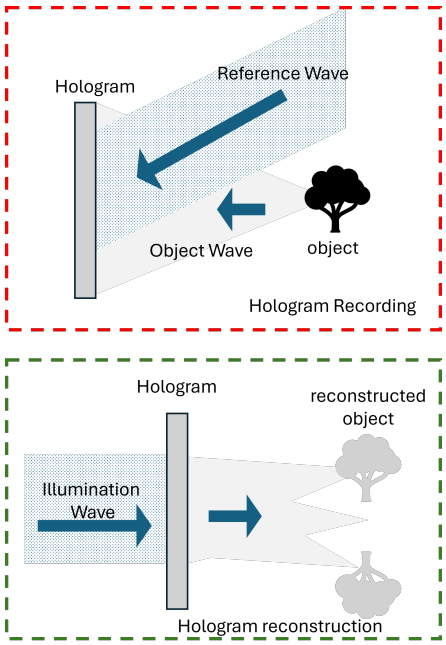

Figure 1 Optical recording and reconstruction of an amplitude hologram.

First, the holograms were recorded in holographic glass plates, using several optical components (Hariharan 1996). Today, the hologram research is focused on computer-generated hologram, where the whole hologram generation process is done by computer simulation (Dallas 2006) and the reconstruction is achieved using spatial light modulators (SLM) or digital micromirror devices (DMD) (Shimobaba and Ito 2019).

Technically, a hologram is an interference pattern, or sum, between two wavefronts, the object and the reference wavefronts. Each wavefront includes amplitude and phase information, represented as a complex number. The holograms can be displayed as amplitude or phase functions (Shimobaba and Ito 2019). Phase-only holograms (POH) are highly used due to their high energy efficiency in object reconstruction. However, the spatial light modulators required to display POH are very expensive. Meanwhile, the amplitude holograms present low energy efficiency but can be displayed in micromirror devices at low prices. There are several configurations for hologram generation. However, the simplest one is the Fourier setup (Goodman 2005). Only one Fourier transform (FT) is applied to the object wavefront to generate the hologram, whereas other configurations require two or more FTs. Nevertheless, the FT of images presents a high concentration of energy in the low frequencies and low energy in the middle and high frequencies. This distribution affects the hologram quality. Consequently, a random phase is added to uniformly distribute the energy in the hologram, especially in Fourier amplitude holograms.

As a result of this addition, a speckle noise is also introduced in the reconstructed object (Lee *et al.* 2022).

Several methods have been proposed to mitigate the effects of random phases in hologram generation. These methods follow different approaches, looking for phase optimization. Even when there are a great variety of approaches to reduce the speckle noise in holography, as far we know, the use of chaotic systems has not been studied previously for this application. Chaotic systems has been applied in criptography but not for controlling the speckle noise in computer-generated holograms.

Our study proposes using the chaotic system parameters to control the randomness in the random pattern used to create the random phase. Previous works have controlled the randomness (He *et al.* 2021) using several band filters in the frequency domain. For each band filter, applying at least two Fast Fourier transforms (FFT) is necessary, and a minimum of 4 filters are used. This makes a total of 8 FFT operations. Our method only requires two FFTs, due to the randomness being controlled by the chaotic function. In our proposal, the dynamics of the functions are controlled by bifurcation parameters to create a two-dimensional pattern with radially varying randomness, which helps to modify the information dispersion within the hologram. In this way, reducing the speckle noise inherent in the reconstructed image is possible when a random phase is used.

The remainder of the work is divided in the following sections: Section 2 presents the theory for the hologram generation used in this work. Section three is dedicated to describing the chaotic systems used, particularly, two chaotic systems are chosen based on piecewise linear systems which are capable of showing bistability, periodic orbits and stable equilibrium points. Likewise, logistic mapping is considered, which has been widely studied in the literature. In the next section, we explain in detail how to generate the random phase using the chaotic function. after that, we present the results for the selected chaotic systems. In the results section, the two methodologies used to generate the random phases and the respective generated holograms are shown. In addition, the viability of the properties of the systems used as well as the methodologies are discussed. Finally, conclusions are established in the last section.

HOLOGRAPHY

The first holograms were recorded and displayed in optical labs, requiring several specialized components and equipment. However, with the rapid spread of computers and the increment of resources such as memory and computing velocity, computer-generated holograms (CGH) have gained significant interest in holography. A CGH is an image that represents the hologram and is generated with the computer simulation of a mathematical model of an optical setup. After that, the CGH can be displayed in an SLM and illuminated by a LASER to reconstruct the 3D object image. In this work, we use amplitude Fourier holograms, where the hologram is defined as:

$$\begin{aligned} H(u,v) =& |U_o(u,v)|^2 + |U_r(u,v)|^2 \\ &+ 2|U_o(u,v)||U_r(u,v)|cos(\phi_o(u,v) - phi_r(u,v)) \end{aligned} \tag{1}$$

where $u_o(x,y) = |O(x,y)|exp^{i\phi_o(x,y)}$ represents the object wavefront, and $u_r(x,y) = |R(x,y)|exp^{i\phi_r(x,y)}$ the reference wave. And $U_o(u,v) = \mathbb{F}\{u_o(x,y)\}, U_r(u,v) = \mathbb{F}\{u_r(x,y)\}$. In the Figure 2 we show a diagram with the generation and reconstruction process of an amplitude CGH. The traditional method sets the random phase $\phi_o(x,y)$ to a 2D matrix filled with random numbers.

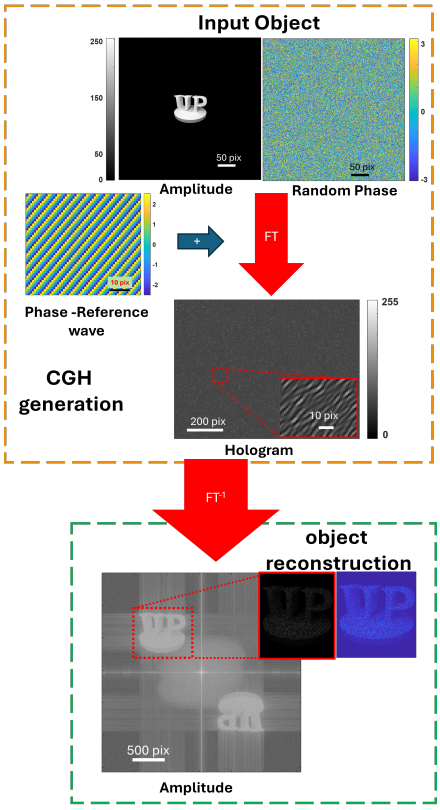

Figure 2 Computer-generated hologram generation process.

In this work, we replace this phase with the phase generated by the chaotic map. The hologram reconstruction is simulated by applying a Fourier transform to $H(u,v)$. In the optical lab, the FT is achieved by analyzing the light wavefront in the focus plane of a convergent lens.

CHAOTIC SYSTEMS

The system that are considered in this work are those called switched or piecewise sytems. Consider a nth-order piecewise system defined as follows (Echenausía-Monroy *et al.* 2024):

$$\dot{\boldsymbol{X}}(t) = f(\boldsymbol{X},t) + \boldsymbol{b}_h,\ x \in \Omega_h, h = 1,2,\ldots,l, \tag{2}$$

where t is the time variable and which can evolve continuously or discretely, $f(\boldsymbol{X},t)$ is a function $f : \mathbb{R}^n \to \mathbb{R}^n$, $\boldsymbol{X}$ is the state vector, $\boldsymbol{b}_h \in \mathbb{R}^n$ is commutation function of system variables, and defined as constant vectors with $h = 1,2,\ldots,l$. Furthermore, $\Omega_1,\ldots,\Omega_l$ denote a polytopic partition of the state space, such that $\bigcap_{h=1}^{l} \Omega_1 = \mathbb{R}^n$ and $\Omega_h \bigcap (\Omega_m)^0 = \emptyset$.

Square chaotic system

The first system that is proposed to be used to generate random phases is a chaotic system which generates spirals in two dimensions and is capable of transitioning from bistability to monostability. The main advantage is that it allows generating chaotic sequences in different ranges of values according to the bifurcation parameter in the range for which system stability is guaranteed (Gilardi-Velázquez *et al.* 2020). The system is described as follows:

$$\dot{\mathbf{x}} = \begin{cases} A_1\mathbf{x} + B_1, & \text{if} \quad x_1 + x_3 < 0 \text{ and } -x_1 + x_3 < 0; \\ A_2\mathbf{x} + B_2, & \text{if} \quad x_1 + x_3 \geq 0 \text{ and } -x_1 + x_3 \leq 0; \\ A_2\mathbf{x} + B_4, & \text{if} \quad x_1 + x_3 > 0 \text{ and } -x_1 + x_3 > 0; \\ A_1\mathbf{x} + B_3, & \text{otherwise;} \end{cases} \tag{3}$$

with A_1 and A_2 given by

$$A_1 = \begin{pmatrix} -0.2 & 4.0 & 0 \\ -4.0 & -0.2_1 & 0 \\ 0 & 0 & 0.2 \end{pmatrix}, A_2 = \begin{pmatrix} -0.25 & 0 & 0 \\ 0 & 0.15 & -4.0 \\ 0 & 4.0 & 0.15, \end{pmatrix}, \tag{4}$$

and B_i with $i = 1, \ldots, 4$ given by:

$$B_1 = -B_4 = \begin{pmatrix} 0.1 \\ 2 \\ 0.3 \end{pmatrix} - k \begin{pmatrix} 0.2 \\ 4 \\ 0.2 \end{pmatrix} \text{ and} \tag{5}$$

$$B_2 = -B_3 = \begin{pmatrix} 0.35 \\ -2 \\ 0.075 \end{pmatrix} - k \begin{pmatrix} 0.25 \\ -4 \\ 0.15 \end{pmatrix}, \tag{6}$$

Considering these values, the system show bistability i.e. presents two stable chaotic attractors due to its heteroclinic orbits. Figure 3 (b) shows the bistable attractor for $k = 0.0$, and for $k = 0.5$ the system behavior is displayed as a quadruple-scroll attractor with square shape for which reason it is called *square chaotic attractor* Figure 3 (a).

For $k = 0.5$, The heteroclinic orbits, responsible for generating the chaotic dynamics, come together at the point $(0, 0, 0)^T$, resulting in the union of the unstable manifolds with the stable manifold. For $k = 0.5$ the system is monostable, i.e. if the initial condition belongs to the basin of attraction, then the trajectory converges to the attractor, if not the solution diverges. Figure 3 (b) shown one of the bistable chaotic attractor for $k = 0$ and initial condition $\mathbf{x}(0) = (0.8, 0.2, -0.8)^T$ onto the plane (x_1, x_3), for this case the attractor formed depends on the attraction basin on which the initial condition belongs (see the reference (Gilardi-Velázquez *et al.* 2020). In Figure 3 (c), the bifurcation diagram for k is shown, in which you can see how as its value increases, the range of values generated in the time series decreases until a single point is generated. This type of pattern is what we seek to use to generate random phases through different types or ranges of disorder in the time series, moving from chaos to periodic orbits, and finally equilibrium.

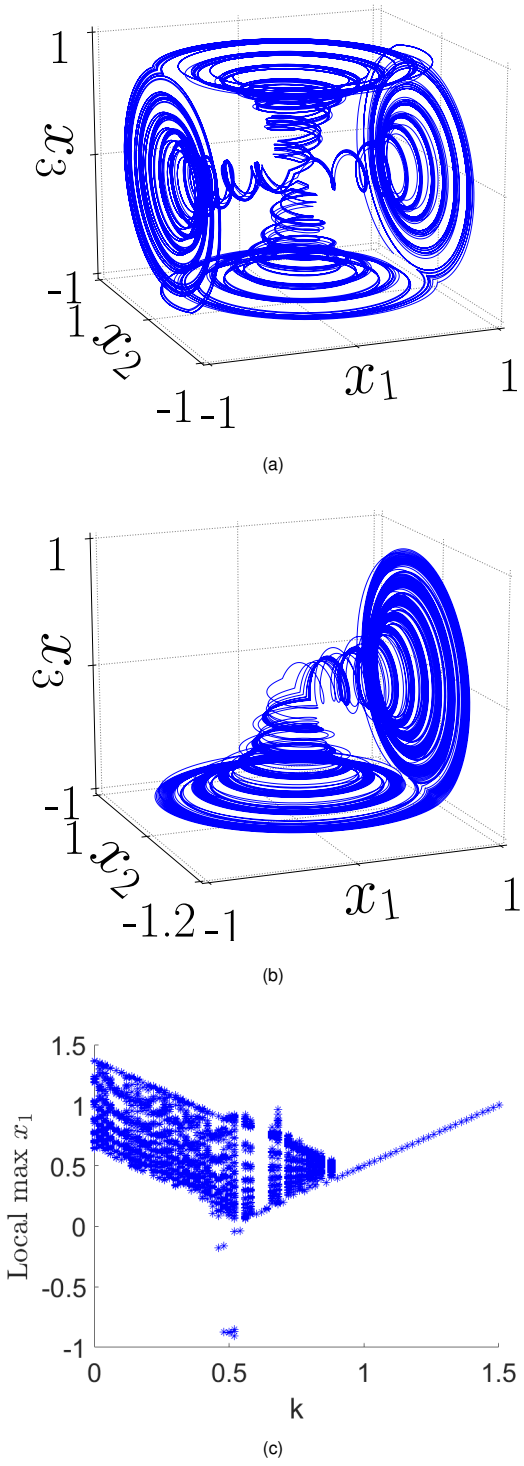

Figure 3 Attractor generated by Eq. (3) for (a)$k = 0.5$ the square attractor, (b) for $k = 0.0$ the bistable attractor and (c) bifurcation diagram for local maximum versus k.

PWL Jerk based system

Consider a nonlinear dynamical system based on the jerk equation defined via affine linear systems given by the round function Gilardi-Velázquez *et al.* (2017) which is defined as follows:

$$\begin{aligned} \dot{x} &= v, \\ \dot{v} &= z, \\ \dot{z} &= -a_1 x - a_2 v - a_3 z - a_4(x), \end{aligned} \tag{7}$$

where $a_i \in \mathbb{R}$ are the system parameters, with $i = 1,2,3$, and $a_4(x) \in \mathbb{R}$ represents the piecewise function.
The parameter a_4 is defined as follows:

$$a_4(x) = c_1 * round(x/c_2), \tag{8}$$

where $c_1, c_2 \in \mathbb{R}$ are parameters. The function is defined as follows:

$$round(x) = \begin{cases} \lceil x - 1/2 \rceil, \text{ para } x < 0; \\ \lfloor x + 1/2 \rfloor, \text{ para } x \geq 0. \end{cases} \tag{9}$$

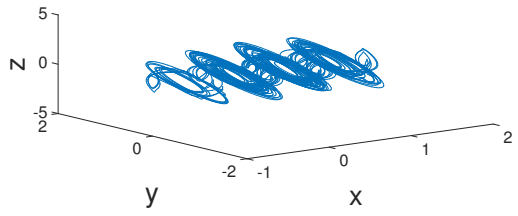

(a)

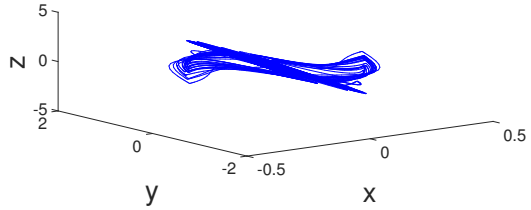

(b)

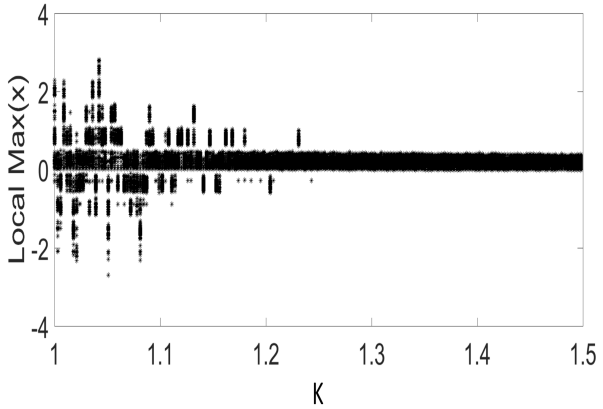

(c)

Figure 4 Attractor generated by Eq. (10) and Eq. (11) for $\alpha_1 = 10.5$, $\alpha_2 = 7$; $\alpha_3 = 0.7$ seen in the multi-scroll (a) for $K = 1.0$ and (b) the multistable scroll in phase space for $K = 1.3$ and (c) bifurcation diagram for local maximum versus K.

In (Gilardi-Velázquez *et al.* 2017), is shown that the system (7) (for $a_1 = 10.5$, $a_2 = 7$, $a_3 = 0.7$) exhibits monostable and multistable scroll attractors by the changes in the bifurcation parameter K. The parameter K is a positive constant which guarantees stability in the range $K \in [1, 1.5]$ (Gilardi-Velázquez *et al.* 2017), responsible for modifying the location of stable and unstable manifolds and allowing the transition from monostability of the multiscroll attractor to multistability of single-scroll attractors. The is described by:

$$\dot{X} = A(K)X + B * a_4(x) \tag{10}$$

with

$$\mathbf{A}(K) = \begin{pmatrix} 0 & 1 & 0 \\ 0 & 0 & 1 \\ Ka_1 & Ka_2 & Ka_3 \end{pmatrix}, \quad B = \begin{pmatrix} 0 \\ 0 \\ 1 \end{pmatrix} \tag{11}$$

It is possible to see the changes in the system behavior according to parameter K by solving numerically the system, where the system transit from the generation of a stable five-scroll attractor Figure 4 (a) for $K = 1$, to a single-scroll attractor which only oscillate around one equilibrium of the system. In order to observe the changes in dynamics Figure 4(c), show the local maxima with respect to the parameter K are shown, where the starting point of the multistable dynamics is $1.15 \leq \mu \leq 2.2$. For $\mu \geq 2.2$, all the oscillating dynamics disappear and converge to the equilibrium point.

Logistic Piecewise map

The logistic map is a discrete-time demographic model analogous to the logistic equation firstly created by Pierre Francois Verhulst, May (1987) is who present the discrete version of the differential equation of the logistic equation being one of the most famous discrete dynamical systems, the logistic map, which is defined as follows:

$$f_\alpha(x) = \alpha x(1 - x), \tag{12}$$

where x is the system variable and α is the bifurcation parameter of the system. The use of a single parameter was possible because the logistic map was normalized and then extended to, $f_\alpha : [-0.5, 1.5] \to [-0.5, 1.5]$ Figure 5 (a), for the bifurcation parameter $\alpha \in [-2, 4]$ and $x_0 \in [-0.5, 1.5]$ (Cassal-Quiroga and Campos-Cantón 2020).

In (Cassal-Quiroga *et al.* 2022) the authors introduce a PWS system based on the logistic map; multiplied by sign function, which allows to extend the domain of logistic map and by defining a switching law, the system can transit from monostability to display bistability. The discrete piecewise dynamical system is given as follow:

$$f_\alpha(x_i) = \begin{cases} -\alpha x_i(1 + x_i), & \text{for } x_i \leq 0, \\ \alpha x_i(-1 + x_i), & \text{for } x_i > 0, \end{cases} \tag{13}$$

where x_i is the system variable, and $\alpha \in \Re$ is the system parameter. The logistic mapping-based piecewise map: $f_\alpha : [-1, 1] \to [-1, 1]$, for $\alpha \in [-4, 4]$ and $x_0 \in [-1, 1]$. In Figure 5 (a) is show the bifurcation diagram for the Logistic Map defined by Eq. (12). In Figure 5 (b) The bifurcation diagram is shown for the modified logistic map Eq. (13), where bistability can be differentiated by the colors red and black, as well as the ranges of values that the map takes depending on the bifurcation parameter, and in Figure 5 (c), an example of bistable behavior is showed via the CobWeb diagram for α= 3.6.

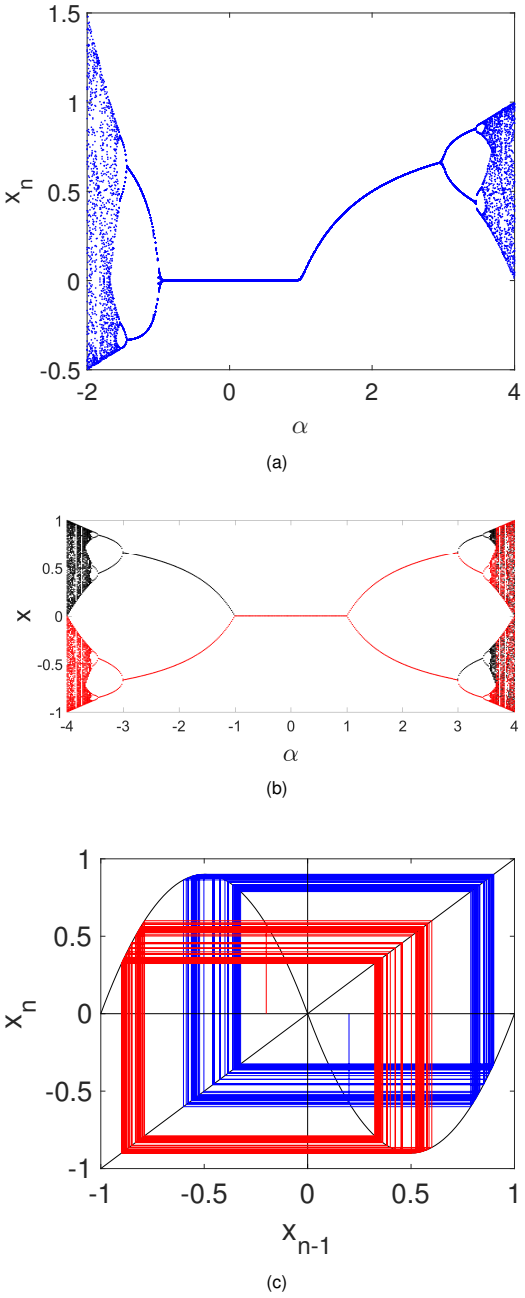

Figure 5 (a) Bifurcation diagram of logistic map Eq. (12), (b) Bifurcation diagram of modified logistic map Eq. (14), (c) CobWeb diagram for Eq. (14) and $\alpha = 3.6$ showing the bistable behavior.

SIMULATED EXPERIMENTS

The FFT of images presents a high concentration of energy in the low frequencies and low energy in the middle and high frequencies. This distribution affects the hologram quality. We seek to generate random phases where, in the center of the phase, there is a high degree of randomness, and as we move away from the center, the disorder decreases until uniformity is reached.

Random phase generation: cartesian coordinates

As a first instance, pseudo-random phases are generated by what we call Cartesian coordinates, i.e., the pattern is generated by constructing a matrix P(i,j), which is traversed by increasing the column and row index order. In addition, we define three regions within the matrix employing circles where these entries are filled by the consecutive values of a time series obtained for three different values of the branch parameter of each system.

Phases and holograms analysis: The Figure 6 shows the patterns generated with the system 3 for $k = 0.5$, $k = 0.2$, $k = 0.0$, Figure 6 (c) the system 10 for $k = 1.0$, $k = 1.2$, $k = 1.3$, and in figure 6 (e) the system 13 for $\alpha = 4.0$, $\alpha = 3.8$, $\alpha = 3.6$. Respectively, the figures 6(b)(d)(f) show the respective holograms formed with the phases of each chaotic system according as is depicted in Figure7, in which the appearance of speckle noise can be observed, with Figure (b) being the one with the greatest noise, and the (f) in which the least noise is presented. Since the system 3 is the one that presents the most abrupt changes in dynamics, there is so much noise in the hologram, which is why this system was discarded as useful. Additionally, as can be seen in the generated phases, horizontal and vertical patterns are observed, these being responsible for the appearance of speckle noise, and since what is sought is to gradually decrease the degree of randomness in the random phase in a radial manner, as a second instance, it is constructed in what we call polar coordinates.

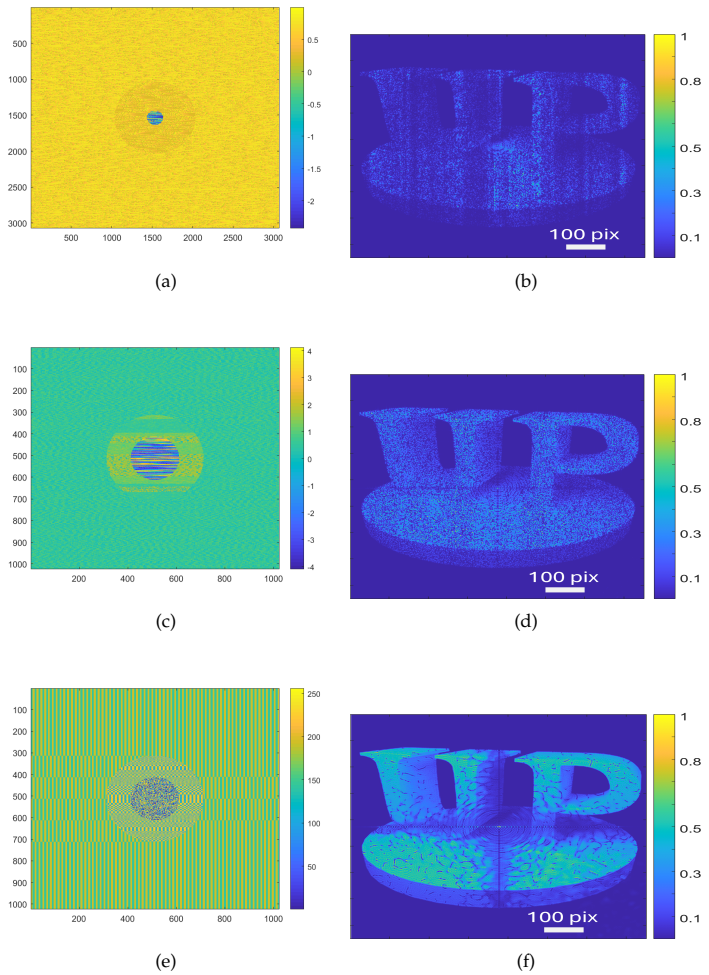

Figure 6 (a,c,e) phase in cartesians coordinates, (b,d,f) corresponding holograms using (a,c,e)

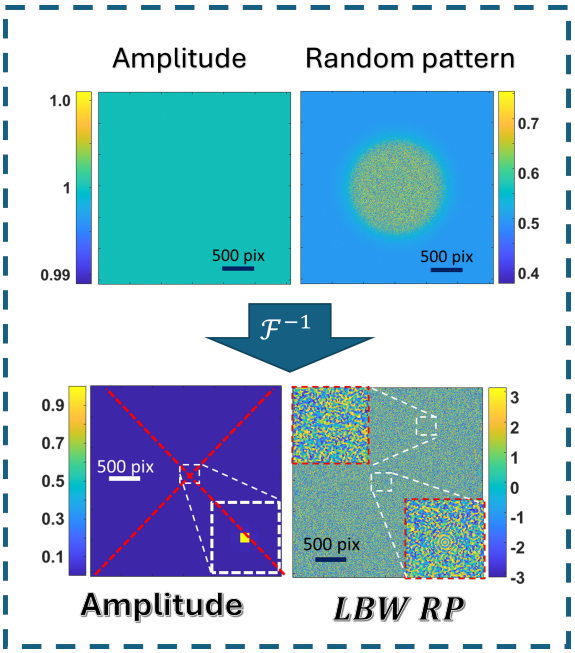

Figure 7 Generation of the LBW random phase, using the chaotic map function.

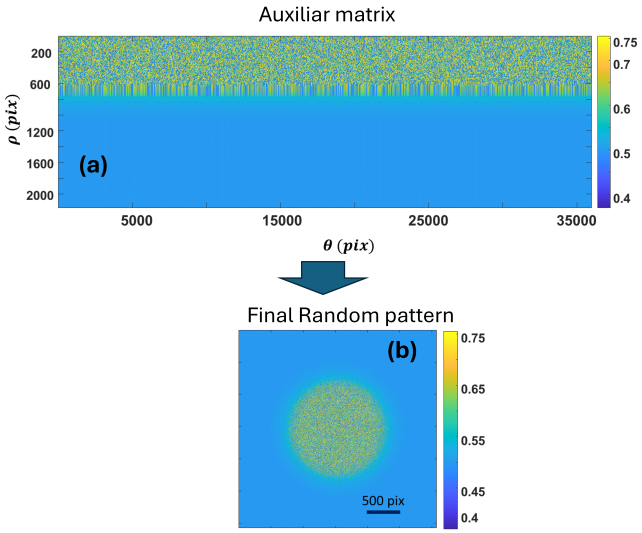

Figure 8 Random pattern generation polar-cartesian coordinates.

Random phase generation: polar coordinates

To avoid overwriting values in the random pattern, we create a secondary pattern in polar coordinates represented by a 2D matrix, $Ap(\rho,\theta)$, whose indexes represent the polar coordinates radial and angular, respectively. ρ and θ vary in the vertical and horizontal direction, respectively, Figure 8(a). Ap has a size of $N_\theta \times M_\rho$ pixels. Where $N_\theta = 360/\Delta_\theta$ and $M_\rho = r_{max}/\Delta_\rho$, and Δ_θ and Δ_ρ are the desired resolutions for the angular and radial coordinates, respectively. Finally, r_{max} is the maximum radius in the hologram field in pixels. That is, if the hologram has $N \times M$ pixels, $r_{max} = \sqrt{(M/2)^2 + (N/2)^2}$.

Phases and hologram analysis: For the system 10, the pattern is constructed by constructing a matrix Ap(ρ,θ) in increasing column-row order, in addition to defining three regions within the matrix by means of circles here defined by ρ where these entries are filled by the consecutive values of a time series obtained for the same three different values $k = 1.0, k = 1.2, k = 1.3$, The generated phase is shown in Figure 9 (a) in which radial patterns are observed, in Figure 9 (b) the hologram formed with this phase is shown, in which the relationship of the Spekle noise related to the radial patterns of the phase can be observed.

Finally, in order to gradually reduce the randomness along the radial axis, we consider a modification to the logistic map where the bifurcation parameter changes as a function of the radial position of the random phase linearly in a range of $\alpha \in [2.9, 4]$

$$f_\alpha(x_i,\rho) = \begin{cases} -\alpha(\rho)x_i(1+x_i), & \text{for } x_i \leq 0, \\ \alpha(\rho)x_i(-1+x_i), & \text{for } x_i > 0, \end{cases} \tag{14}$$

For system 14, the pattern is constructed by constructing a matrix Ap(ρ,θ) in increasing column-row order, these entries are filled by the consecutive values of a time series obtained for the evolution of the bifurcation parameter $\alpha \in [2.9, 4]$ starting for $\rho = 0$ with $\alpha = 4$, and decreasing its value linearly to 2.9 as ρ increases. Figure 9 (c) in which radial patterns are not observed, in Figure 9 (d) the hologram formed with this phase is shown, in which the relationship of the Spekle noise related to the radial patterns of the phase is not observed. These artifacts in the results are generated by the transitions between the different dynamics generated by the mapping do not have abrupt changes, and because the generation of the elements in the time series in the mappings is not continuous.

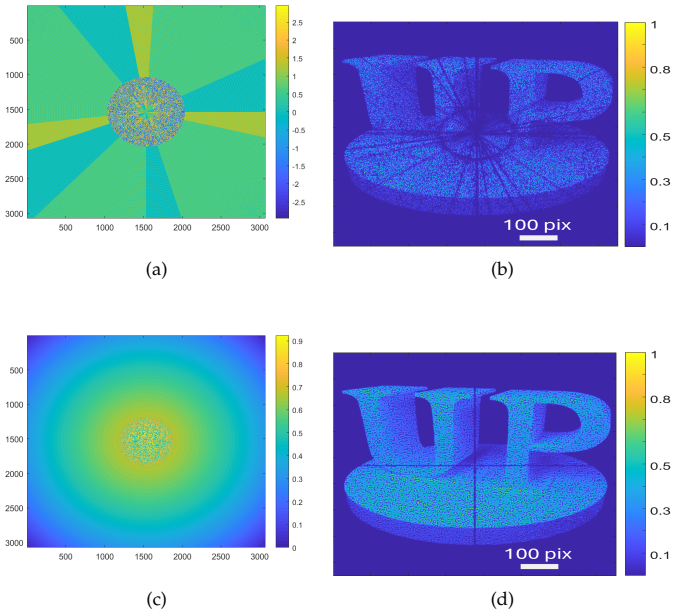

Figure 9 (a,c) phase in polar coordinates, (b,d) corresponding holograms using (a,c)

CONCLUSION

In this work, random phases for amplitude-encoded Fourier holograms based on chaotic systems were generated. Three chaotic systems capable of showing different behaviors, such as multistability, monostability, and periodic orbits, were compared considering two in continuous time and one in discrete time, and two different methodologies for generating the random phase. Our analysis showed that the most suitable systems have smooth changes in their dynamics with respect to the bifurcation parameter, as well as a greater range in parameter values for dynamic transitions, it was shown that discrete systems can offer better results than continuous-time systems because the transitions in the dynamics associated with their bifurcation parameter are smooth. In addition to the two methodologies analyzed, it was observed that the construction of the phases in a radial form helps to reduce the artifacts in the holograms which were generated by the transitions between the different dynamics, moreover with the polar construction giving better results due to the nature of the holograms. Furthermore, this study opens avenues for developing optimal algorithms to generate random phases using different functions for the bifurcation parameter variation and implementing these phases in different hologram types, such as phase-only holograms, which present better energy efficiency. This would also allow for a deeper investigation into the impact of parameter variations on statistical properties of random phases in holography.

Acknowledgments

This work was done with the support of Universidad Panamericana, with the fund "Fondo Fomento a la Investigacion 2023" under the project UP-CI-2023-GDL-11-ING.

Availability of data and material

The data used to support the findings of the study are included within the article.

Ethical standard

The authors have no relevant financial or non-financial interests to disclose.

Conflicts of interest

The authors declare that there is no conflict of interest regarding the publication of this paper.

LITERATURE CITED

Alvarez, G. and S. Li, 2006 Some basic cryptographic requirements for chaos-based cryptosystems. International journal of bifurcation and chaos **16**: 2129–2151.

Blanche, P.-A., 2021 Holography, and the future of 3d display. Light: Advanced Manufacturing **2**: 446–459.

Cassal-Quiroga, B., A. Ruiz-Silva, and E. Campos-Cantón, 2022 Generation of dynamical s-boxes via lag time chaotic series for cryptosystems. In *Complex Systems and Their Applications: Second International Conference (EDIESCA 2021)*, pp. 61–83, Springer.

Cassal-Quiroga, B. B. and E. Campos-Cantón, 2020 Generation of dynamical s-boxes for block ciphers via extended logistic map. Mathematical Problems in Engineering **2020**: 1–12.

Čelikovskỳ, S. and V. Lynnyk, 2012 Desynchronization chaos shift keying method based on the error second derivative and its security analysis. International Journal of Bifurcation and Chaos **22**: 1250231.

Cruz, M.-L. and H. Gilardi-Velázquez, 2024 Speckle noise reduction, in amplitude holograms, using a limited-bandwidth random phase generated by a chaotic map. In *Digital Holography and Three-Dimensional Imaging*, pp. W1B–2, Optica Publishing Group.

Dallas, W. J., 2006 Computer-generated holograms. Digital Holography and Three-Dimensional Display: Principles and Applications pp. 1–49.

Diaz-gonzalez, E., A. Guerra-lópez, B. A. Hernandez, and E. Campos, 2022 Generation of multistability through unstable systems. Chaos Theory and Applications **4**: 234–240.

Echenausía-Monroy, J., R. Cuesta-garcía, H. Gilardi-velázquez, S. S. Muni, and J. Alvarez-gallegos, 2024 Predicting tipping points in a family of pwl systems: Detecting multistability via linear operators properties. Chaos Theory and Applications **6**: 73–82.

Echenausía-Monroy, J. L., G. Huerta-Cuellar, R. Jaimes-Reátegui, J. H. García-López, V. Aboites, *et al.*, 2020 Multistability emergence through fractional-order-derivatives in a pwl multi-scroll system. Electronics **9**: 880.

Gilardi-Velázquez, H. E., R. d. J. Escalante-González, and E. Campos-Cantón, 2018 Bistable behavior via switching dissipative systems with unstable dynamics and its electronic design. IFAC-PapersOnLine **51**: 502–507.

Gilardi-Velázquez, H. E., R. J. Escalante-González, and E. Campos, 2020 Emergence of a square chaotic attractor through the collision of heteroclinic orbits. The European Physical Journal Special Topics **229**: 1351–1360.

Gilardi-Velázquez, H. E., L. Ontañón-García, D. G. Hurtado-Rodriguez, and E. Campos-Cantón, 2017 Multistability in piecewise linear systems versus eigenspectra variation and round function. International Journal of Bifurcation and Chaos **27**: 1730031.

Goodman, J. W., 2005 *Introduction to Fourier optics*. Roberts and Company publishers.

Gotz, M., K. Kelber, and W. Schwarz, 1997 Discrete-time chaotic encryption systems. i. statistical design approach. IEEE Transactions on Circuits and Systems I: Fundamental Theory and Applications **44**: 963–970.

Hariharan, P., 1996 *Optical Holography: Principles, techniques and applications*. Cambridge University Press.

He, Z., X. Sui, H. Zhang, G. Jin, and L. Cao, 2021 Frequency-based optimized random phase for computer-generated holographic display. Applied Optics **60**: A145–A154.

Jiang, J., A. Hastings, and Y.-C. Lai, 2019 Harnessing tipping points in complex ecological networks. Journal of the Royal Society Interface **16**: 20190345.

Khan, M., T. Shah, H. Mahmood, and M. A. Gondal, 2013 An efficient method for the construction of block cipher with multi-chaotic systems. Nonlinear Dynamics **71**: 489–492.

Kocarev, L., Z. Galias, and S. Lian, 2009 *Intelligent computing based on chaos*, volume 184. Springer.

Lee, B., D. Kim, S. Lee, C. Chen, and B. Lee, 2022 High-contrast, speckle-free, true 3d holography via binary cgh optimization. Scientific reports **12**: 2811.

May, R. M., 1987 Chaos and the dynamics of biological populations. Proceedings of the Royal Society of London. A. Mathematical and Physical Sciences **413**: 27–44.

Mazloom, S. and A. M. Eftekhari-Moghadam, 2009 Color image encryption based on coupled nonlinear chaotic map. Chaos, Solitons & Fractals **42**: 1745–1754.

Munir, N., M. Khan, T. Shah, A. S. Alanazi, and I. Hussain, 2021 Cryptanalysis of nonlinear confusion component based encryp-

tion algorithm. Integration **79**: 41–47.
Njıtacke, Z., T. Fozin, L. K. Kengne, G. Leutcho, E. M. Kengne, *et al.*, 2020 Multistability and its annihilation in the chua's oscillator with piecewise-linear nonlinearity. Chaos Theory and Applications **2**: 77–89.
Ott, E., 2002 *Chaos in dynamical systems*. Cambridge university press.
Patidar, V. and G. Kaur, 2023 Lossless image encryption using robust chaos-based dynamic dna coding, xoring and complementing. Chaos Theory and Applications **5**: 178–187.
Platas-Garza, M., E. Zambrano-Serrano, J. Rodríguez-Cruz, and C. Posadas-Castillo, 2021 Implementation of an encrypted-compressed image wireless transmission scheme based on chaotic fractional-order systems. Chinese Journal of Physics **71**: 22–37.
Razaq, A., Iqra, M. Ahmad, M. A. Yousaf, and S. Masood, 2021 A novel finite rings based algebraic scheme of evolving secure s-boxes for images encryption. Multimedia Tools and Applications **80**: 20191–20215.
Rial, J. A., R. A. Pielke, M. Beniston, M. Claussen, J. Canadell, *et al.*, 2004 Nonlinearities, feedbacks and critical thresholds within the earth's climate system. Climatic change **65**: 11–38.
Shimobaba, T. and T. Ito, 2019 *Computer Holography: Acceleration Algorithms and Hardware Implementations*. CRC press.
Wakunami, K., H. Yamashita, and M. Yamaguchi, 2013 Occlusion culling for computer generated hologram based on ray-wavefront conversion. Optics express **21**: 21811–21822.

How to cite this article: Gilardi Velázquez, H. E., and Cruz, M. Analysis of Chaotic Systems in the Generation of Random Phases for Amplitude Holograms. *Chaos Theory and Applications*, 7(2), 177-185, 2025.